

**Brain Network Dynamics in Goal-Directed  
Motor Precision Tasks in Laboratory and  
Real-World Settings**

by

Michael Schubert





**UNIVERSITÄT PADERBORN**  
*Die Universität der Informationsgesellschaft*

# **Brain Network Dynamics in Goal-Directed Motor Precision Tasks in Laboratory and Real-World Settings**

Dissertation

for the academic degree of

Doctor rerum medicinalium

(Dr. rer. medic.)

by

MICHAEL SCHUBERT

2015

Principle supervisor:  
Prof. Dr. rer. medic. Jochen Baumeister

Paderborn, April 27, 2015



# Declaration of Authorship

I declare that the work presented here is, to the best of my knowledge and belief, original and the result of my own investigations, except as acknowledged, and has not been submitted, either in part or whole, for a degree at this or any other University. Formulations and ideas taken from other sources are cited as such. This work has not been published.

Furthermore, I declare to have read and accepted the PhD regulations (in German: Promotionsordnung) no. 50 / 12 (11/12/2012) of the Faculty of Sciences, University of Paderborn.

# Abstract

Precise goal-directed movements are important in everyday life and crucial in sports. In order to execute such movements, cortical brain areas form a functional network. Besides the localization and activity of individual areas, the most important variable to describe a network is the information flow, defined as effective connectivity, between its components.

This work aims to map brain network dynamics of sensorimotor control during goal-directed movement by means of localization, activity and event-related causality.

This is done by using electroencephalography during a targeted precision task in the laboratory and during golf putting on the outside green. Based on source reconstructed signals, dipole localization and time-frequency decomposition are used to identify task-related brain areas. Subsequently, autoregressive models are fitted to the source signals to estimate event-related causality relative to movement onsets utilizing the concept of Granger causality.

For the precision task in the laboratory, anterior cingulate cortex, as well as motor, sensory and parietal areas were identified as task-related. Event-related causality is mainly found between frontal and motor areas within 1.5 s before and 1 s after the movement. The results indicate processes of attentional control, sensorimotor information integration and performance monitoring.

Brain network dynamics can be analyzed by means of localization, activity and connectivity during the execution of precise goal-directed movements. Future studies will have to show how these dynamics are modulated by e.g. performance, skill level or fatigue. Findings from the measurements on the putting green add to currently discussed methodological problems in mobile functional brain imaging and emphasizes the need for further research in this direction.

# Zusammenfassung

In Alltag und Sport ist die Präzision zielgerichteter Bewegungen von hoher Bedeutung. Die Kontrolle dieser Bewegungen wird durch Netzwerke kortikaler Hirnregionen vermittelt. Neben der Lokalisation und Aktivität der Regionen gilt der Informationsfluss zwischen diesen als der wichtigste Netzwerkparameter.

Ziel der vorliegenden Arbeit ist es, sensomotorische Kontrollprozesse bei zielgerichteter Bewegung bezüglich Lokalisation der beteiligten Hirnregionen, ihrer Aktivität und ereigniskorrelierten Kausalität abzubilden.

Hierzu wurde das Elektroenzephalogramm während einer zielgerichteten Präzisionsaufgabe im Labor sowie während des Puttens auf dem Golfplatz abgeleitet. Auf Basis rekonstruierter Quellensignale wurden testrelevant Hirnregionen mittels Dipollokalisierung und Zeit-Frequenzanalyse identifiziert. Durch Anpassung autoregressiver Modelle wurde dann die ereigniskorrelierte Kausalität in Relation zum Bewegungsbeginn nach dem Prinzip der Granger-Kausalität geschätzt.

Für die Präzisionsaufgabe im Labor wurden anteriorer cingulärer Cortex sowie motorische, sensorische, und parietale Areale als testrelevant identifiziert. Ereigniskorrelierte Kausalität ist im Wesentlichen zwischen frontalen und motorischen Arealen zu beobachten. Diese Ergebnisse deuten auf das Abbild kortikaler Prozesse der Aufmerksamkeitskontrolle, sensomotorischen Informationsverarbeitung und Bewegungsevaluation hin.

Netzwerke können in ihrer Lokalisation, Aktivität und Konnektivität während der Ausführung zielgerichteter Präzisionsaufgaben analysiert werden. Zukünftige Arbeiten werden zeigen, wie Einflussfaktoren (z.B. Ermüdung oder Verletzungen) auf die Bewegungspräzision modulierend auf diese Netzwerkdynamiken wirken. Erkenntnisse aus den Messungen auf dem Golfplatz tragen zu aktuell diskutierten Problematiken in der mobilen funktionellen Hirnbildgebung bei.

# Table of contents

|  |             |
|--|-------------|
| <b>Abstract</b>  | <b>vi</b>   |
| <b>Zusammenfassung</b>   | <b>vii</b>  |
| <b>Table of contents</b>   | <b>x</b>    |
| <b>List of figures</b>   | <b>xii</b>  |
| <b>List of tables</b>  | <b>xiii</b> |
| <b>List of abbreviations</b>                                       | <b>xvi</b>  |
| <b>1 Introduction</b>  | <b>1</b>    |
| <b>2 Sensorimotor control and goal-directed movements</b>          | <b>5</b>    |
| 2.1 A model of sensorimotor control . . . . .                      | 5           |
| 2.2 Neuroanatomy in sensorimotor control . . . . .                 | 8           |
| 2.3 The sequential processing of goal-directed movements . . . . . | 12          |
| 2.4 Brain network dynamics in sensorimotor control . . . . .       | 15          |
| <b>3 Measuring network dynamics in sensorimotor control</b>        | <b>17</b>   |
| 3.1 Choice of method . . . . .                                     | 17          |
| 3.2 Electroencephalography - a brief overview . . . . .            | 20          |
| 3.3 From channel to source space by ICA . . . . .                  | 24          |
| 3.3.1 The principle of ICA . . . . .                               | 25          |
| 3.3.2 Application to the EEG . . . . .                             | 26          |
| 3.3.3 Source localization of equivalent single dipoles . . . . .   | 31          |
| 3.3.4 Component identification . . . . .                           | 31          |
| 3.3.5 Component clustering . . . . .                               | 34          |
| 3.4 Brain activity measures . . . . .                              | 34          |
| 3.5 Brain connectivity measures . . . . .                          | 36          |
| 3.5.1 Structural connectivity . . . . .                            | 37          |
| 3.5.2 Functional connectivity . . . . .                            | 37          |

|          |  |           |
|----------|--|-----------|
| 3.5.3    | Effective connectivity . . . . .   | 38        |
| 3.5.4    | Estimating effective connectivity - Application to the EEG                           | 40        |
| <b>4</b> | <b>Applying brain network measures in sports and exercise</b>                        | <b>45</b> |
| 4.1      | Methodological challenges . . . . .  | 45        |
| 4.1.1    | Challenges in data acquisition . . . . .   | 46        |
| 4.1.2    | Suitable movements . . . . .   | 48        |
| 4.2      | Current state of research . . . . .  | 49        |
| 4.2.1    | Measures of brain dynamics in motor precision tasks in controlled settings . . . . . | 49        |
| 4.2.2    | Measures of complex movements in real-world settings . . . . .                       | 54        |
| 4.3      | Summary and Research Deficit . . . . .   | 55        |
| <b>5</b> | <b>Research strategy and specific aims</b>   | <b>57</b> |
| <b>6</b> | <b>Methods</b>   | <b>61</b> |
| 6.1      | Force pulse study . . . . .  | 61        |
| 6.1.1    | Subject characteristics . . . . .  | 62        |
| 6.1.2    | Task setup . . . . .   | 63        |
| 6.1.3    | Task procedure . . . . .   | 63        |
| 6.1.4    | Data acquisition and event processing . . . . .                                      | 65        |
| 6.2      | Golf putt study . . . . .  | 68        |
| 6.2.1    | Subject characteristics . . . . .  | 68        |
| 6.2.2    | Task setup . . . . .   | 69        |
| 6.2.3    | Task procedure . . . . .   | 70        |
| 6.2.4    | Data acquisition and event processing . . . . .                                      | 72        |
| 6.3      | Signal processing . . . . .  | 74        |
| 6.3.1    | ICA and ERSP specific processing . . . . .   | 76        |
| 6.3.2    | Effective connectivity and ERC specific processing . . . . .                         | 80        |
| 6.4      | Statistical procedures . . . . .   | 82        |
| 6.4.1    | Task performance and psychometric measures . . . . .                                 | 82        |
| 6.4.2    | EEG data . . . . .   | 83        |
| <b>7</b> | <b>Results</b>   | <b>85</b> |
| 7.1      | Force pulse study . . . . .  | 85        |
| 7.1.1    | Precondition measures . . . . .  | 85        |
| 7.1.2    | Network localization . . . . .   | 87        |
| 7.1.3    | Network activity . . . . .   | 92        |
| 7.1.4    | Network connectivity . . . . .   | 94        |
| 7.2      | Golf putt study . . . . .  | 100       |
| 7.2.1    | Precondition measures . . . . .  | 100       |
| 7.2.2    | Network localization . . . . .   | 101       |
| 7.2.3    | Network activity . . . . .   | 104       |
| 7.3      | Summary . . . . .  | 105       |

|   |            |
|---|------------|
| <b>8 Discussion</b>   | <b>107</b> |
| 8.1 Force pulse study . . . . .   | 107        |
| 8.1.1 Precondition measures . . . . .   | 108        |
| 8.1.2 Network localization . . . . .  | 109        |
| 8.1.3 Network activity . . . . .  | 112        |
| 8.1.4 Network connectivity . . . . .  | 116        |
| 8.1.5 Limitations . . . . .   | 119        |
| 8.1.6 Concluding the specific aims . . . . .  | 120        |
| 8.2 Golf putt study . . . . .   | 122        |
| 8.2.1 Precondition measures . . . . .   | 123        |
| 8.2.2 Network localization . . . . .  | 125        |
| 8.2.3 Network activity . . . . .  | 127        |
| 8.2.4 Limitations . . . . .   | 128        |
| 8.2.5 Concluding the specific aims . . . . .  | 129        |
| <b>9 Conclusion</b>   | <b>131</b> |
| <b>10 Prospects</b>   | <b>135</b> |
| 10.1 Methodological future work . . . . .   | 135        |
| 10.2 Towards the application of effective connectivity measures in sports<br>and exercise . . . . . | 138        |
| <b>References</b>   | <b>141</b> |
| <b>Appendix</b>   | <b>161</b> |
| <b>A Major axes of the CNS</b>  | <b>161</b> |
| <b>B Model validation and connectivity estimation</b>   | <b>163</b> |
| B.1 Force pulse study: Model validation results . . . . .   | 163        |
| B.2 Force pulse study: Additional ERC results force pulse study . . .                               | 168        |
| <b>C Questionnaires</b>   | <b>172</b> |
| C.1 Anthropometric forms . . . . .  | 172        |
| C.2 The Edinburgh-Inventory - German translation . . . . .  | 179        |
| C.3 The strait anxiety test X1 (STAI-X1) . . . . .  | 181        |
| C.4 Visual Analogue Scale . . . . .   | 182        |
| <b>D Spec sheets</b>  | <b>183</b> |
| D.1 Force transducer - Soemer - Load cell 1022 . . . . .  | 184        |
| D.2 Force transducer - Soemer - digitizing unit LDU 68.1 . . . . .                                  | 186        |
| D.3 Accelerometer - Analog Devices - ADXL330 . . . . .  | 188        |
| D.4 EEG amplifier - Neuroscan - Synamps RT . . . . .  | 190        |
| D.5 Channel locations - Neuroscan - QuickCap64 . . . . .  | 193        |

# List of Figures

|      |  |    |
|------|--|----|
| 2.1  | Model of sensorimotor control . . . . .                            | 6  |
| 2.2  | Major lobes of the human cerebral cortex . . . . .                 | 10 |
| 2.3  | Areas of the neocortex . . . . .                                   | 11 |
| 2.4  | Dorsal and ventral stream of the cortex . . . . .                  | 13 |
| 3.1  | Comparison of brain imaging methods . . . . .                      | 19 |
| 3.2  | Principle EEG origin and recording . . . . .                       | 21 |
| 3.3  | The international 10-20 electrode positioning system . . . . .     | 22 |
| 3.4  | Typical frequency bands of the human EEG . . . . .                 | 24 |
| 3.5  | The cocktail party-problem . . . . .                               | 26 |
| 3.6  | Comparison of ICA algorithms . . . . .                             | 30 |
| 3.7  | Exemplary ERSP image . . . . .                                     | 36 |
| 3.8  | Adaptive MVAR (AMVAR) modeling . . . . .                           | 42 |
| 6.1  | Force pulse study: Operation of force transducer . . . . .         | 63 |
| 6.2  | Force pulse study: Trial sequence . . . . .                        | 65 |
| 6.3  | Force pulse study: Principle data acquisition setup. . . . .       | 66 |
| 6.4  | Force pulse study: Force transducer blueprint . . . . .            | 67 |
| 6.5  | Empirical probabilities of holing out over putt distance . . . . . | 69 |
| 6.6  | Golf putt study: Task setup . . . . .                              | 70 |
| 6.7  | Golf putt study: Putter-head with ADLX330 accelerometer . . . . .  | 73 |
| 6.8  | Golf putt study: Acceleration profiles of swing patterns . . . . . | 74 |
| 6.9  | EEG signal processing pipeline . . . . .                           | 75 |
| 6.10 | Properties of an independent component . . . . .                   | 79 |
| 7.1  | Force pulse study: Task performance . . . . .                      | 86 |
| 7.2  | Force pulse study: Equivalent cluster dipoles . . . . .            | 89 |
| 7.3  | Force pulse study: Cluster ERSP . . . . .                          | 91 |
| 7.4  | Force pulse study: Cluster theta ERD/S . . . . .                   | 92 |
| 7.5  | Force pulse study: Cluster alpha ERD/S . . . . .                   | 93 |
| 7.6  | Force pulse study: Cluster beta ERD/S . . . . .                    | 94 |
| 7.7  | Force pulse study: Time-frequency connectivity grid . . . . .      | 95 |
| 7.8  | Force pulse study: Cluster theta ERC. . . . .                      | 96 |
| 7.9  | Force pulse study: Cluster alpha ERC . . . . .                     | 98 |

|  |     |
|--|-----|
| 7.10 Force pulse study: Cluster beta ERC . . . . .         | 99  |
| 7.11 Golf putt study: Task performance . . . . .           | 101 |
| 7.12 Golf putt study: Equivalent cluster dipoles . . . . . | 103 |
| 7.13 Golf putt study: Cluster ERSP . . . . .               | 104 |



# List of Tables

|     |   |     |
|-----|---|-----|
| 6.1 | Force pulse study: Anthropometric description of subjects . . . . . | 62  |
| 6.2 | Golf putt study: Anthropometric description of subjects . . . . .   | 69  |
| 7.1 | Force pulse study: Identified independent components . . . . .      | 87  |
| 7.2 | Golf putt study: Identified independent components . . . . .        | 102 |

# List of abbreviations

|        |   |
|--------|---|
| 2DG    | 2-Deoxyglucose                                  |
| ACC    | Anterior cingulate cortex                       |
| ACF    | Autocorrelation function                        |
| AMICA  | Adaptive mixture independent component analysis |
| AMVAR  | Adaptive multivariate autoregressive            |
| BA     | Brodman area                                    |
| BEM    | Boundary element model                          |
| BH-FDR | Benjamini-Hochberg false detection rate         |
| BOLD   | Blood oxygenation level dependent               |
| BP     | Bereitschaftspotential                          |
| BSS    | Blind source separation                         |
| CAR    | Common average reference                        |
| CNS    | Central nervous system                          |
| CSF    | Cerebrospinal fluid                             |
| DBN    | Dynamic Bayesian network                        |
| DCM    | Dynamic causal modeling                         |
| DLPFC  | Dorsolateral prefrontal cortex                  |
| DMN    | Default mode network                            |
| DTI    | Diffusion tensor imaging                        |
| DTF    | Directed transfer function                      |
| DWI    | Diffusion weighted imaging                      |
| ECG    | Electrocardiography                             |
| EEG    | Electroencephalography                          |
| EOG    | Electrooculography                              |
| EMG    | Electromyography                                |
| EPSP   | Excitatory postsynaptic potential               |
| ERC    | Event-related causality                         |
| ERCoh  | Event-related coherence                         |
| ERD/S  | Event-related (de-)synchronization              |
| ERN    | Error-related negativity                        |
| ERP    | Event-related potential                         |
| ERSP   | Event-related spectral perturbation             |
| FDG    | Fluorodeoxyglucose                              |
| FDR    | False detection rate                            |

---

|       |   |
|-------|---|
| FFT   | Fast Fourier transformation             |
| FIR   | Finite impulse response                 |
| fMRI  | functional magnetic resonance imaging   |
| fNIRS | functional near infrared spectroscopy   |
| FPGA  | Field programmable gate array           |
| FWER  | Familywise error rates                  |
| GCM   | Granger causality mapping               |
| GCI   | Granger causality index                 |
| ICA   | Independent component analysis          |
| IC    | Independent component                   |
| IPS   | Intraparietal sulcus                    |
| IPSP  | Inhibitory postsynaptic potential       |
| IMA   | Left motor area                         |
| IS2   | Left secondary somatosensory area       |
| M1    | Primary motor area                      |
| MEG   | Magnetoencephalography                  |
| MLS   | Multivariate least squares              |
| MNI   | Montreal neurological institute         |
| MoBI  | Mobile Brain/Body imaging               |
| MPA   | Measure projection analysis             |
| MU    | Motor Unit                              |
| MVAR  | Multivariate autoregressive             |
| MVC   | Maximum voluntary contraction           |
| PC    | Percent consistency                     |
| PCA   | Principal component analysis            |
| PDC   | Partial directed Coherence              |
| PET   | Positron emission tomography            |
| PFC   | Prefrontal cortex                       |
| PGA   | Professional Golfers' Association       |
| PMA   | Premotor area                           |
| PMBR  | Post movement beta rebound              |
| PPC   | Posterior parietal cortex               |
| rMA   | Right motor area                        |
| rS2   | Right secondary somatosensory area      |
| ROI   | Region of interest                      |
| rPDC  | renormalized partial directed coherence |
| rPPC  | Right posterior parietal cortex         |
| RSN   | Resting state networks                  |
| rv    | Residual variance                       |
| S1    | Primary somatosensory area              |
| S2    | Secondary somatosensory area            |
| SI    | Stability index                         |
| SIFT  | Source information flow toolbox         |
| SMA   | Supplementary motor area                |

|         |   |
|---------|---|
| SNR     | Signal to noise ration                      |
| SQUID   | Superconducting quantum interference device |
| STAI-X1 | Strait anxiety test X1                      |
| TE      | Transfer entropy                            |
| tfICA   | Time-frequency ICA                          |
| V1      | Primary visual cortex                       |
| VAR     | Variate autoregression                      |
| VAS     | Visual analogue scale                       |

# 1 Introduction

Together with conscious thought and perception, goal-directed action is considered one of the highest functions of the human brain and is important for daily life activities and exceptionally crucial for the performance in sports and exercise (Saper et al., 2000; Urbin et al., 2011). A precise execution of these movements relies on central control mechanisms allocated in the brain (Baumeister, 2013). When impaired, imprecise movement control can lead to the inability of resolving daily tasks, like reaching and grasping objects. In sports, imprecise goal-directed movements, such as a basketball throw or penalty kick in soccer, can compromise the athlete's performance with possible game-changing consequences. Consequently, restrictions in daily living and loss of performance in sports may reduce one's quality of life. Causes for impaired ability to perform precise goal-directed movements in sports include injuries (Baumeister et al., 2011) and fatigue (Baumeister et al., 2012a). To study the effect these causes have on the central control mechanisms, the first step is to apply methods that map the corresponding brain processes. The following studies will use these methods to gain a mechanistic understanding of the underlying processes during the control of goal-directed movements. Ultimately, this knowledge can help to optimize strategies to enhance or regain performance, as well as for the prevention or treatment of injuries (Baumeister, 2013).

One example of goal-directed movements in sports can be observed on the golf course, whereby the golfer attempts to putt the ball in the hole. This is done on the so-called green with a putter, a club that allows low-speed strokes. During movement planning, information about the extrapersonal space, such as the distance to the hole or slope and friction of the green, as well as information about intrapersonal space such as motion, position, force, and tension of limbs and joints is gathered. This information is then integrated and processed in the brain to generate an adequate motor command (Kandel & Hudspeth, 2013). The resulting coordinated sequence of muscle activation creates a complex movement pattern, leading to the putting stroke (Baumeister, 2013). The putter head then

produces an impact on the ball, which rolls towards the hole depending on the force of impact, direction and spin. Both, successful and non-successful attempts are then monitored through sensory feedback and are used for the optimization of future motor behavior of this kind (Ullsperger et al., 2014).

Functions of movement planning, execution and monitoring are allocated to anatomically distinct brain structures, which play a central role in the so-called sensorimotor control of goal-directed movements and form a functional brain network comprising parts of the prefrontal, motor, somatosensory and parietal cortex as well as subcortical structures (Bear et al., 2007). Although the locations and functional engagement of individual brain structures in goal-directed movement tasks is well described, the mechanisms for sensorimotor control that lead to precise goal-directed movements in sports and exercise are yet not fully understood.

This disparity arises because the description of the anatomical location and functional engagement of each individual brain structure is not sufficient to analyze them as a network. In fact, the most important variable to describe a network is proposed to be its connectivity properties (Varela et al., 2001). The analysis of anatomical and functional brain networks is known as the study of brain connectivity. Especially the brain effective connectivity, which is defined as the directed information flow between distinct brain areas, is believed to add valuable information towards a mechanistic understanding of brain processes (Sporns, 2011). Recent approaches in computational neuroscience now allow the investigation of the effective connectivity of brain networks with possible application in identifying mechanisms underlying the control of goal-directed movements.

This work aims to map the brain network dynamics of sensorimotor control processes during the execution of precise goal-directed movements. This requires the identification of engaged brain areas by their individual localizations, activity patterns, as well as the effective connectivity amongst them. Given the high relevance for application to sports and exercise research, the goal is to do this under the most realistic conditions possible, while still providing a controlled setting for measurements.

Golf putting has been shown to be suitable to study sensorimotor control processes even on the outside putting green using electroencephalography (EEG) (Reinecke et al., 2011). However, before attempting to map brain network dynamics during such a complex movement and in a naturalistic setting, which might be challenging regarding high quality data acquisition, knowledge about applying these measures during less complex goal-directed movements would still be conducive to understanding the brain dynamics of controlled actions. This is typically done using simple movements or key aspects of the more complex movement in a controlled environment. In this regard, Urbin et al. highlights the

---

inherent demand of ballistic force generation in simple motor tasks on the one hand and multi-joint motor performance on the other (Urbin et al., 2011). Urbin even emphasizes the study of simple force pulse generation as invaluable to analyze more complex multi-joint movements (Urbin et al., 2011).

In golf putting, the impact force that is transmitted onto the ball is key to reach the hole. Hence, precise ballistic force generation in a laboratory motor task could be used to transfer this aspect of the golf putt into a simpler single joint movement. Moreover, this can be beneficial to determine the methodological course of action for analyzing data from real-world measurements.

The time scale on which motor behavior happens is within the range of milliseconds, and hence requires the observation of brain network dynamics with sufficient time resolution (Sporns, 2013). High-density EEG allows recording the electric brain activity, mainly generated by neurons in the cerebral cortex (the outer part of the brain), with sufficient temporal resolution, while being lightweight and flexible enough to measure in various settings (Baumeister, 2013). The surface electrodes of EEG capture summed neuronal activity from underlying brain areas with a spatial resolution within the range of centimeters. Due to electric conductivity of the brain, bone and skin, the signal in each electrode consists of unknown mixture of distributed neuronal activity (Nunez & Srinivasan, 2006). Additionally, EEG is especially prone to artifacts related to movements (Thompson et al., 2008). Blind source separation approaches (BSS) offer a data driven method to spatially filter the data to address these problems. The independent component analysis (ICA) is one technique to separate true brain activity from noise or artifactual content and thereby increases the signal to noise ratio (SNR) and spatial resolution of EEG signals (Makeig et al., 1996). This can be very useful when dealing with recordings of lower quality as shown by Gwin, Gramann, and Makeig (2010), who were able to separate brain source activity from movement related artifacts during walking and even running on a treadmill. The ICA returns so-called independent components (ICs) from which the equivalent dipole locations can be estimated (Delorme et al., 2012). The 3D coordinates of each dipole represent a probabilistic estimate of the source signal's origin in the brain. The frequency content of the oscillatory activity of brain sources is known to be space and time dependent for different tasks (Amzica & Lopes da Silva, 2012). Time-frequency analysis can be used to decompose the signal in its spectral properties, so that frequency specific dynamics can be analyzed for each localized brain area. Once identified as task-related by their localization and time-frequency characteristics, these brain areas are defined as the components of a functional network, also referred to as nodes. The effective connectivity can be measured by causal dependencies amongst the nodes. Following the concept of Granger-causality, causal dependency exists when the prediction error of one node's activity is higher compared to the prediction error when including another node's time series (K. Friston et al., 2012; Granger, 1969). A review by Bressler et al. states this approach is 'a valuable adjunct to

more traditional interventional approaches<sup>1</sup> and as 'extremely informative' when applied to non-invasive recorded human EEG data (Bressler & Seth, 2011). By applying these methods (ICA, dipole fitting, time-frequency analysis, Granger-causality), brain network dynamics of sensorimotor control processes can be mapped during the execution of goal-directed movements.

This work represents the first step for subsequent intervention and cohort of cross-sectional studies that can be designed to study the effects of causes like injury or fatigue that lead to impaired precision of goal-directed movements in sports. From neurophysiological correlates of precision and performance that might emerge from these studies, biomarkers for sensorimotor control functioning could be generated. This will help to develop neurophysiological based tools for assessing human performance, optimize training strategies for performance enhancement and injury prevention and rehabilitation (Baumeister, 2013). Hence, the results will be of interest for researchers within the field of behavioral neuroscience but are specifically aimed to serve the application in sports medicine research.

Chapter 2 defines the main terms and subjects of this work by first elucidating the model of sensorimotor control, while the following sections provide an introduction into the anatomy and functions of brain structures that are involved in the processing of goal-directed movements. Moreover, brain connectivity provides the framework to explain network dynamics and is thus introduced in the final section of this chapter. Then, the measures of brain network dynamics are elucidated by explaining the applied methods of data acquisition and signal processing. Thereafter, chapter 3 aims to provide a technical guide for the steps of data analysis. Chapter 4 focuses on the application of these methods in sports and exercise research including a review of which measures have been applied to study sensorimotor control. Based on these applications, chapter 5 elucidates the scientific course of action and specifies the aims of this work. The methodological course of action to address these aims are outlined in chapter 6, including descriptions of the conducted experiments in the laboratory and under real-world conditions, as well as outlining the signal processing procedures. The results of both studies are presented in chapter 7. These are discussed regarding content related findings and a critical rating of the applied methods in chapter 8. Chapter 9 concludes the outcomes of this work. Due to the methodological nature of this work, chapter 10 contains prospects about methodological aspects, as well as the future work regarding the application of these methods in sports and exercise.

---

<sup>1</sup>Interventional approaches typically analyze causality by stimulating or lesioning one part of the nervous system to investigate the impact on a second (Bressler & Seth, 2011).



## 2 Sensorimotor control and goal-directed movements

Sensorimotor control is defined as "a dynamic interaction between sensations of sensory stimuli, the processing and integration of sensory information in the central nervous system (CNS) and motor behavior in voluntary movements and postural control" (from Baumeister (2013), p. 13). In fact, the brain can be seen as the central unit for sensorimotor control of voluntary movements. Different structures, anatomically and functionally well described, are engaged in these partly sequential control processes forming a functional brain network. This chapter aims to provide the neurophysiological background about sensorimotor control of voluntary (goal-directed) movements with focus on related processes that are carried out in the cerebral cortex.

### 2.1 A model of sensorimotor control

Sensorimotor control is modeled as a looping mechanism consisting of three major components (blue boxes in figure 2.1): Motor behavior, sensory reception, as well as cortical and subcortical brain structures (Baumeister, 2013). The following sections detail these components and their interrelations.

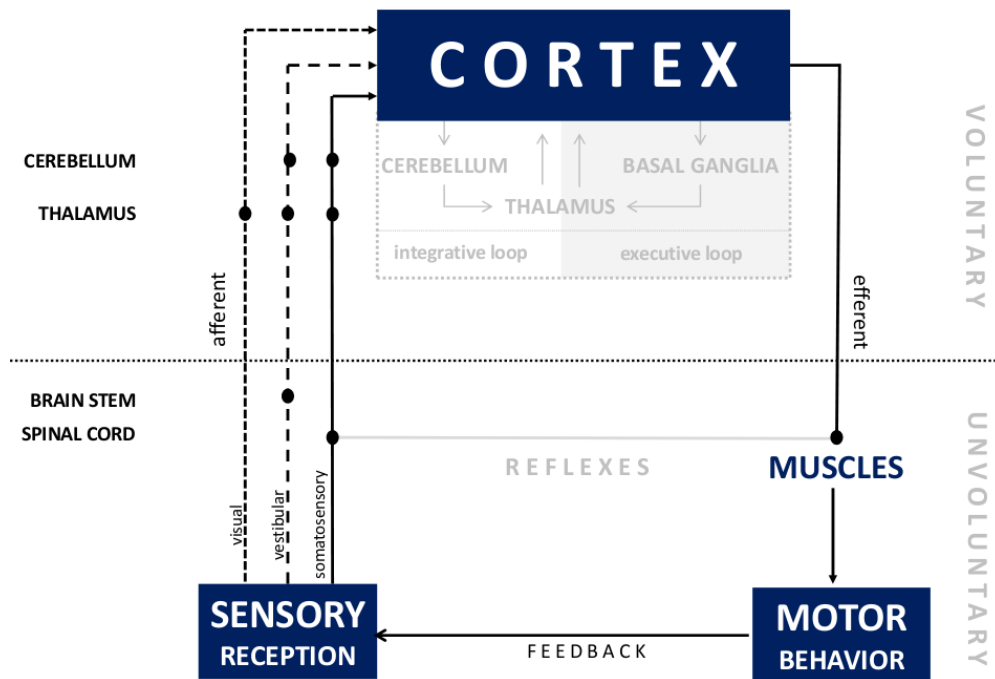


Figure 2.1: Model of sensorimotor control and its different levels of information processing. Source: Baumeister (2013)

### Motor behavior

Motor behavior results from coordinated muscle activation. Muscles are formed by multiple so-called motor units (MU). Each MU consists of a motor neuron and its innervated muscle fibers. Depending on the motor signal (efferent signals), lengthening and shortening of muscle fibers lead to muscle contraction and therewith to joint movements. Motor signals can be caused by spinal reflexes or sent via efferent pathways from higher levels of the CNS (Pearson & Gordon, 2013). The former are involuntary motor responses due to peripheral receptors that directly project to other motor neurons. This neural circuitry is entirely contained within the spinal cord. The latter motor behavior is processed on supraspinal level and is either unconsciously executed, like the control of the gait cycle or keeping balance (postural control), or consciously executed as voluntary movements (Pearson & Gordon, 2013).

The generated muscle force is dependent on the recruitment and discharge rate of the sum of activated MUs. To achieve precise voluntary movements, muscle activation has to be coordinated temporally and with the appropriate amount of force, depending on the number of joints and complexity of the trajectory (Pearson & Gordon, 2013). Movements or phases of movements can be characterized as feedback and feedforward controlled (Wolpert et al., 2013). In feedforward control, a motor command is generated according to a desired final state. During the

movement no sensory feedback is used. Therefore, possible deviations from the planned trajectory cannot be corrected. Feedforward controlled movements are also termed ballistic or open-loop, because no further adjustments can be produced once initiated. Correction can only occur due to monitoring sensory information, available from the movement outcome, and following repetitions. Contrarily, a feedback controller continuously compares the actual state of movement to the desired state based on sensory feedback. Deviations can be corrected by adjustments to the ongoing motor program. Feedback control of motor behavior is a closed-loop process, which allows continuous refinement of behavior (Wolpert et al., 2013).

### **Sensory reception**

The feedback consists of multimodal sensory reception. Each type of receptor is sensitive to one particular kind of stimulus. Once a certain threshold is reached, action potentials are released and form the so-called afferent signal that carries the sensory information. Stimulus intensity is coded by the frequency of action potentials. The modalities of sensory information can be divided into that of visual, vestibular and somatosensory sensation. Information from vision is gathered by observation of position changes of the moving body (parts) relative to the environment, if in the eye's field of view. Vestibular information is provided by sensory organs in the inner ears that react to linear and angular acceleration of the head. Somatosensory information consists of three major modalities: (1) Interoception, the sense of function of the major organ systems (cardiovascular, respiratory, digestive, and renal) is mostly unconscious (Gardner & Johnson, 2013). (2) Exteroception includes thermal senses of heat and cold, pain (nociception), as well as sensation for direct interaction with the environment. Cutaneous and subcutaneous mechanoreceptors (e.g. Meissner corpuscle, Merkel disc receptor, Pacinian corpuscle, Ruffini ending) are distributed throughout the skin to provide sensation for stroking, pressure, vibration, skin stretch, and stroking. (3) Proprioception provides awareness of movements and position of the four limbs and the head even without vision or vestibular information. As such, it allows precise coordinated movements, adapted to the specific task. Receptors for proprioception are located in skeletal muscles, joint capsules, and the skin. Muscle spindles as well as so-called golgi tendon organs provide information of muscle length and speed, stretch and contraction, respectively. Joint capsule receptors detect changes of joint angles according to tension of the capsule (Gardner & Johnson, 2013).

### Cortex

All sensory information is transmitted via afferent pathways into the CNS on different levels. Somatosensory signals travel along the spinal cord towards the brain where they reach subcortical and cortical levels. Sensory information processing culminates in the cortex with the highest degree of information complexity. Amongst other functions, this integration of somatosensory information is particularly important to guide voluntary movements (Amaral, 2013). A central role in the control of voluntary movements fall to so-called cognitive, sensory and motor association cortices within the cerebral cortex and also subcortical brain structures including cerebellum, the thalamus and basal ganglia (Bear et al., 2007). The functions of information integration, motor programming and feedback processing are carried out within these anatomically distinct but interconnected brain areas. The following sections provide a more detailed description about the organization of the CNS with main focus on the involved brain structures in voluntary movement processing.

## 2.2 Neuroanatomy in sensorimotor control

Sensorimotor control processes are carried out on three different levels of the CNS. The most basic form of movement are spinal reflexes, which are carried out in the spinal cord. Conscious voluntary movements however require higher order processing within cerebral cortex. Subcortical brain areas including cerebellum, basal ganglia, and thalamus refine or adjust these motor commands (Baumeister, 2013). The following sections detail these parts of the CNS.

The spinal cord, the most caudal<sup>1</sup> part of the CNS, extends from the base of the skull to the vertebra L1. It receives somatosensory information from and relays motor commands towards the periphery. The inbound and outbound fibers are bundled in 31 spinal nerves, each with an afferent and an efferent division. Higher levels of motor control project onto the motor neurons of the spinal cord. Additionally, interneurons modulate muscle activation patterns and form circuits for spinal reflexes without involvement of brain processes (Amaral & Strick, 2013).

---

<sup>1</sup>Medical terms for describing positions in the CNS are illustrated in appendix A.

The cerebellum holds half of the brain's neurons while only taking about a tenth of its volume. It is located posteriorly to the brain stem, is organized in two hemispheres and consists of internal white matter, three pairs of nuclei, and exterior gray matter, the cerebellar cortex. It can be divided into three functional parts. (a) The vestibulocerebellum receives vestibular and visual inputs and participates in balance, vestibular reflexes, and eye movement. (b) The spinocerebellum receives somatosensory inputs from the spinal cord and also visual, auditory, vestibular, and somatic sensation from the head. It projects to cortical and brain stem regions and is involved in controlling muscles of the body and limbs, governing posture and locomotion as well as eye movements. (c) The cerebrocerebellum is primarily connected with the cerebral cortex. It receives inputs from multiple sensory cortices, while its outgoing connections project to motor, premotor and prefrontal cortices relayed by the thalamus. Through this cerebellar-thalamic-cortical loop (integrative loop in figure 2.1) the cerebrocerebellum participates in the control of motor planning and execution (Lisberger & Thach, 2013).

The basal ganglia consist of four principles hemispheric sets of nuclei distributed within the white matter beneath the cerebral cortex. The striatum is the major input structure of the basal ganglia, receiving information from the cerebral cortex, brain stem and thalamus. Both globus pallidus and parts of the substantia nigra are major output structures transmitting towards the thalamus. Lastly, the subthalamic nucleus also receives projections from the globus pallidus, cerebral cortex, thalamus and brain stem and feeds back to the globus pallidus and substantia nigra. These inputs and outputs form a cortico-basal ganglia-thalamocortical loop, which subserves skeletomotor, oculomotor, associative, and limbic (mostly emotion) functions. The motor circuit originates in frontal sensorimotor regions of the cerebral cortex, pursues into parts of the striatum and substantia nigra and enters the thalamus. The loop is then closed by projections to motor specific cortical regions (executive loop shown in figure 2.1). Hence, the basal ganglia have been found to be involved in motor related functions such as action selection, preparation for movement, movement execution, sequencing of movement, self initiated or remembered movements, the control of movement parameters and reinforcement learning (Wichmann & DeLong, 2013).

The thalamus is composed of about 50 nuclei forming egg shaped structures in each hemisphere, close to the center of the brain. The nuclei are commonly classified into four groups named after their location: The anterior group is thought to be related to memory and emotion and partly connected with parts of the cingulate and frontal cortex. Nuclei of the medial group are also connected to the frontal cortex, receiving input from the basal ganglia and are involved in memory function. The ventral group is important for motor control function and consequently projects to motor and somatosensory areas of the cortex. Lastly, the posterior group is concerned with auditory and visual processing and mediates information to the temporal and occipital lobes, respectively. The thalamus is the one structure through which all sensory information mediates (except olfaction). It is part of both, the cerebellar-thalamic-cortical loop for sensory integration and

the cortico-basal ganglia-thalamocortical loop for executive functions. Notably, it not only relays information, but rather acts as a gatekeeper that enhances or prevents information transmission to the cerebral cortex depending on the behavioral state of the organism (Amaral, 2013).

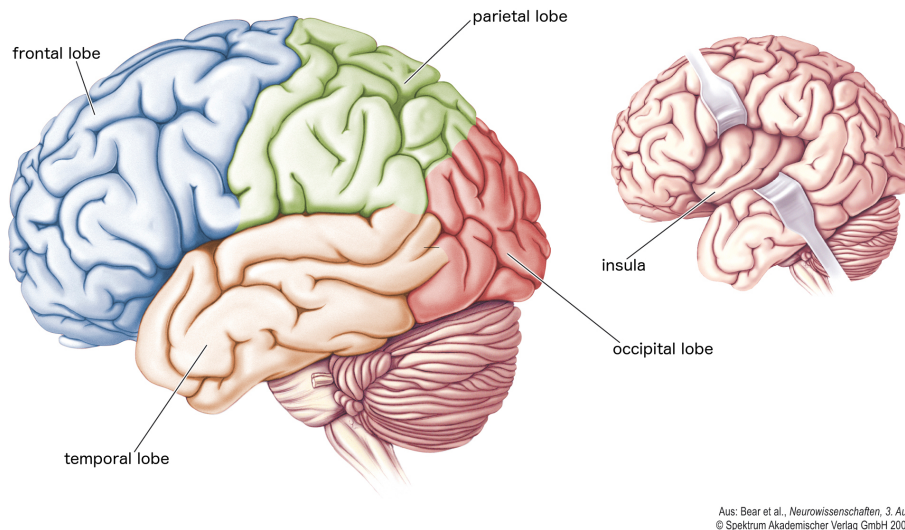


Figure 2.2: Major lobes of the human cerebral cortex. Source: Bear et al. (2007), p. 231, labels translated from German.

The highest level of sensorimotor control processing is carried out in the cerebral cortex. This outer shell of the brain's right and left hemisphere consist of four major lobes (figure 2.2), which are involved in perceptual, motor, and cognitive functions such as emotion and memory (Amaral & Strick, 2013). The frontal lobe is particularly involved in short-term memory, planning actions and movement control. The parietal lobe in contrast is concerned with somatic sensation, forming a body image and relating it to extrapersonal space. Hearing and also learning, functions of memory, and emotion is largely located within the temporal lobe. The occipital lobe holds functions for visual processing (Kandel & Hudspeth, 2013). Two additional lobes are the cingulate cortex, located between the cerebral cortex and corpus callosum (bridge between the two hemispheres) and involved in regulation of emotion and cognition, and the insular cortex (insula), covered by the frontal, parietal and temporal lobes and concerned with the regulation of emotion and homeostasis<sup>2</sup>. Each lobe consists of functional subregions. Korbinian Brodmann identified 47 regions by their cytoarchitectures within layers of the neocortex (most outer part of the cerebral cortex) at the beginning of the 20th century, today known as the Brodmann areas (BA). Based on these findings, the BAs or combinations of those, which are intimately involved in goal-directed movements were identified to be the prefrontal cortex (PFC, BA 9,10,11), the

---

<sup>2</sup>Homeostasis describes the active maintenance of a relatively constant internal environment (Shizgal & Hyman, 2013).

supplementary motor area (SMA, medial BA 6), the premotor area (PMA, lateral BA 6), the primary motor area (M1, BA 4), the primary somatosensory area (S1, BA 1, 2 and 3) and the posterior parietal cortex (PPC, BA 5 and BA 7). Figure 2.3 shows these areas (Bear et al., 2007). Their specific functions in voluntary movements will be outlined in section 2.3.

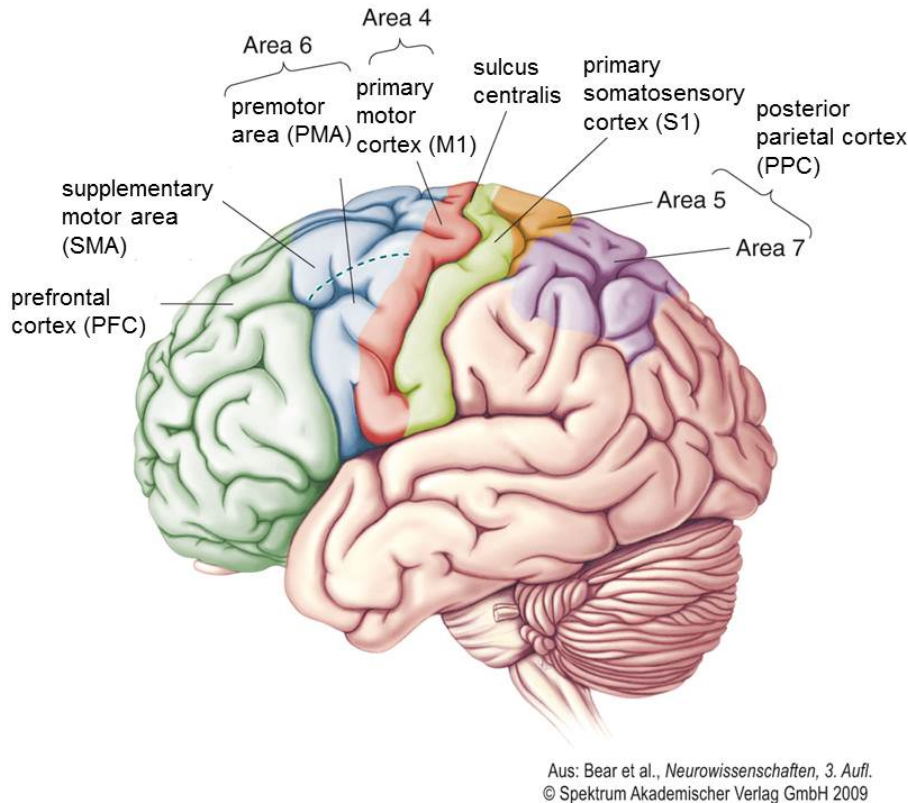


Figure 2.3: Areas of the neocortex involved in planning and execution of movements. Source: Bear et al. (2007), p. 473, labels translated from German.

Each area can be assigned to a certain level of processing. Lower-order processing is carried out in so-called primary association cortices, whereas processing complexity increases in unimodal and finally multimodal association cortices (Amaral, 2013). The primary association cortices (M1 and S1) are organized in functionally specified representation fields of individual parts of the body. Along the precentral gyrus from medial to lateral lie the representative fields of the lower extremities, hip, trunk, areas of the arm, hand, fingers, neck, parts of the face and mouth. This alignment is also called "homunculus". S1 holds four complete neural maps of the body for different modalities of somatic sensation. Stimulating left hemispheric areas cause sensation of, or muscle contraction in right lateral (contralateral) parts of the body and vice versa. This is due to the decussation of nerve fibers within the spinal cord (Amaral & Strick, 2013). The size of the areas

is proportional to the density of innervation such that for example hand and face regions are larger than those of shoulder or trunk (Amaral, 2013).

Unimodal and multimodal association cortices within each lobe receive most of their input from primary association cortices, have larger receptive fields with imprecise maps of the body, and are interconnected by a dense network of pathways. The parietal association cortex is important for guidance of motor behavior based on sensory information and spatial awareness. The temporal association cortex holds functions for sensory stimuli recognition and memory. The organization of behavior and functions of working memory<sup>3</sup> are carried out in the frontal association cortex. Lastly, the limbic association cortex, lying at the medial edge of the cerebral hemisphere, is critical for emotional functions and episodic memory (Olson & Colby, 2013).

Sensorimotor control underlies the hierarchically organization of the CNS from lower to higher-order information processing by parallel and sequential engagement of its components. This includes the realization of voluntary movements from their initiation until execution.

### 2.3 The sequential processing of goal-directed movements

Voluntary movements is defined as the performance of intentional and purposeful action to achieve a goal in the near or distant future (Kalaska & Rizzolatti, 2013). In this sense all voluntary behavior is goal-directed. However, for immediate motor actions in sports, the 'goal' in goal-directed often refers to a specific location to reach (in boxing, a punch towards the opponent's chin) or to an object that needs to be reached (in basketball, the throw towards the basket). This does not only include the generation of a particular sequence of muscle activation, but also involves the conscious control of cognitive, sensory and perceptual processes in the brain (Kalaska & Rizzolatti, 2013; Wolpert et al., 2013).

As mentioned before, higher-order motor functions are localized in areas of the cerebral cortex. Cortical processing of goal-directed movements can be divided

---

<sup>3</sup>The concept of working memory was introduced by A. Baddeley in 1974, who proposed this mechanism as an ongoing combination of current perception, rehearsal and experiences, actions or knowledge. Therewith, working memory holds the function of executive control (Baddeley, 2003, 2012).



into a sequence of movement planning, execution and performance monitoring (Bear et al., 2007). Once the decision has been made to perform a particular movement, sensory information is used to form a unified representation of the extrapersonal space and the individual within it (Kalaska & Rizzolatti, 2013). The processing of somatosensory information in the cerebral cortex begins in the primary receptive fields of S1. These areas project to adjacent secondary or unimodal areas in the anterior parietal lobe and also to the parietal multimodal association cortex (Olson & Colby, 2013). The latter also receives visual and auditory information enabling the integration of somatic sensory information with that from the extrapersonal space (Kandel, 2013). The sequence of information integration is illustrated in figure 2.4.

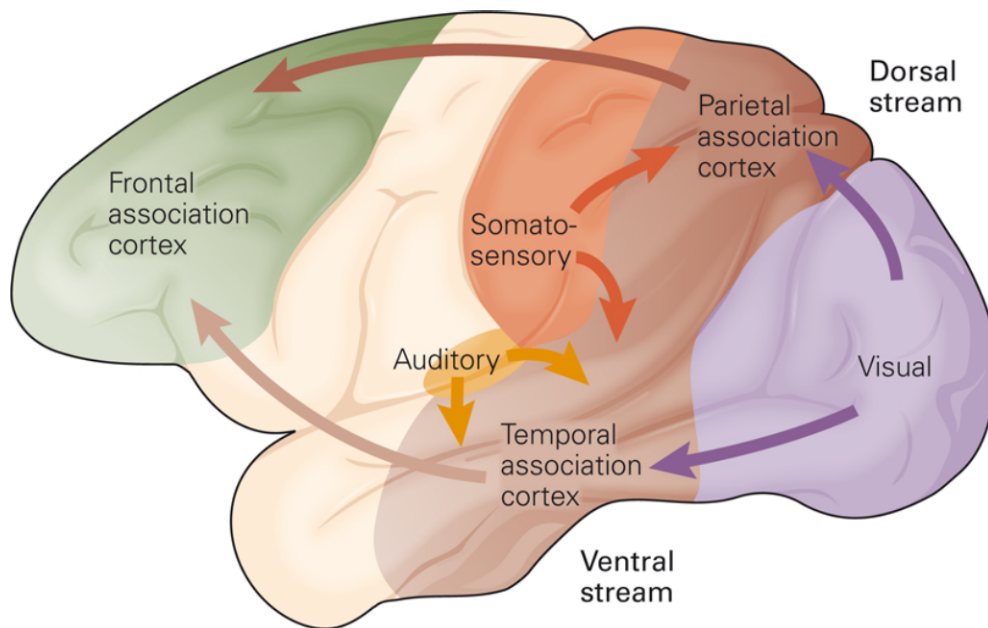


Figure 2.4: Sensory information integration and transmission via dorsal and ventral systems of the cerebral cortex. Source: Olson and Colby (2013), p. 397.

The parietal association cortex projects to both, the temporal and frontal association cortices in parallel. The ventral stream transmits information about the form (texture, shape, color) of an object to the temporal association cortex and then to ventral parts of the PFC. Recognized objects are here assigned to emotional significance. The dorsal stream mediates spatial information directly to SMA and PMA, areas important for motor and executive control functions (Olson & Colby, 2013).

The areas within the frontal cortex, PFC, SMA with PMA and M1 are also functionally connected and organized from higher to lower-order processing. Cognitive control of motor behavior including emotion and executive control is carried out in the PFC. In this context, a central role is thought to be assigned to the anterior

part of the cingulate cortex (ACC). It is densely interconnected with the PFC and PMA and takes part in cognitive control related to motor behavior (Hyman & Cohen, 2013).

PFC then projects to SMA and PMA, where more global motor planning is carried out. This includes the selection of limbs and their sequence of movement for more complex motor behavior (Olson & Colby, 2013). Which of the functionally similar areas is activated depends on the group of muscles involved in the movement. SMA projects to axons that innervate distal, whereas PMA connects to proximal MUs (Bear et al., 2007). Additional adaptations are made through existing motor programs that can be mentally rehearsed by a looping mechanism between PMA and the cerebellum (Lisberger & Thach, 2013). Furthermore, the basal ganglia-thalamocortical motor circuit is involved in motor planning and is thought to influence movement initiation and sequencing of movements (Wichmann & DeLong, 2013). With this information PMA then projects to M1, the lowest order of processing. The motor command information is distributed to the relevant receptive fields of the motor homunculus. M1 has the most direct connections to the efferent neurons in the spinal cord. Hence the activation of these areas leads to the execution of movements of particular parts of the body (Kalaska & Rizzolatti, 2013). M1 activity is greatest just before and during movement execution and modulated by force and direction (Bear et al., 2007). It has to be noted that the organization for motor planning in fact does not follow a strict serial processing. M1 is rather part of a complex network of reciprocal pathways between multiple adjacent pre- and postcentral areas, that allow adjustments to the actual motor command during feedback controlled behavior (Kalaska & Rizzolatti, 2013).

Following the goal-directed movement, sensory information is again fed back into the CNS. Movement execution and whether the intended goal was reached, can thus be monitored. Goal-directed movements, in contrast to reflex movements, are in fact characterized by their improvement of effectiveness (speed, accuracy) over trials (Krakauer & Ghez, 2000). Consequently, every movement execution gains knowledge about motor programming due to performance monitoring (Kalaska & Rizzolatti, 2013). An important structure involved in this is the cerebellum, more precisely, the dentate nucleus. It is particularly activated during the execution of complex motor tasks and conscious evaluation of sensory information and also connected to parts of the PFC (Lisberger & Thach, 2013). It has been shown that also the PFC and ACC are engaged in performance monitoring of goal-directed movements (Wood & Grafman, 2003).

The function of performance monitoring is often left out when describing the sequence of planning and execution of goal-directed movements. However, because the afferent stream is of involuntary nature and the inherent characteristic of goal-directed movements to successfully reach the intended goal, performance monitoring is crucial regarding updating motor programs for execution of future actions. Therefore, it will be included in the sequence of processing goal-directed movements as it completes the cycle of sensorimotor control.

As stated, the realization of goal-directed movements is largely carried out in areas of the cerebral cortex. These can be described by their anatomical localization, linking pathways, as well as their functional engagement during the processes of movement planning, execution and performance monitoring. Amongst these brain areas information is transmitted to perform such complex motor behavior. Although the individual properties do suggest functional interaction between the distributed brain regions, they cannot explain the interaction itself. Thus, besides the description of its components, pathways, and functions, a brain network is characterized by its connectivity in terms of information transmission (Bullmore & Sporns, 2009; Varela et al., 2001). The hierarchic organization and sequential engagement of brain areas throughout the processing of goal-directed movements, indicate transient and therefore dynamic brain network activities.

## 2.4 Brain network dynamics in sensorimotor control

In the former sections it was shown that cortical and subcortical brain regions are interconnected. The so-called neural connectivity in the cerebral cortex ranges in scale from connections between single cortical neurons (local scale, about  $<1$  cm) to the linking of whole brain regions, also described as neural assemblies (large scale, about  $> 1$  cm) (Varela et al., 2001; Sporns & Tononi, 2007). These large scale neural networks are thought to be involved in the implementation of cognitive and motor function of the brain (Breakspear & Jirsa, 2007). Neural assemblies can be spatially identified by their structural properties and/or their specific function. They are often more densely intra-connected on local scale than interconnected on large scale and therefore show highly correlated activity, justifying the concept that spatially distinct areas are also functionally distinguished (Jirsa & McIntosh, 2007). The question of how densely the brain areas are connected with each other and how these connections are used to realize higher brain function can be addressed with the study of neural networks by analyzing the brain connectivity. Brain connectivity consists of three modalities:

a) Structural connectivity forms the anatomical basis for communication between neurons via axons. Before, this was referred to as pathways forming loops between cortical and subcortical structures and also between functional areas within the cerebral cortex. Over long periods (hours to days), synapses can (de)form new connections for example due to learning or development which is why structural connectivity has dynamic properties (Sporns, 2011). However, over the time scale of seconds to minutes, the anatomical connections may be assumed to be static and thus provide a framework for functional and dynamic interactions on a broad

millisecond to second time scale in which motor behavior occurs (Kandel, 1991). This behavior requires dynamic functional coupling between multiple brain regions (Jirsa & McIntosh, 2007).

b) Functional coupling can be described by the deviation from statistical independence of distinct brain regions and has been defined as functional connectivity (Sporns, 2011). Unlike structural connectivity, these functional correlations can be of transient and dynamic nature down to the millisecond time scale, depending on the task or the current state (e.g. arousal, resting) of the brain. Also, functional connectivity can be found between brain regions or cell assemblies that have not been shown anatomically connected. Since no structural model is underlying this concept, the physiologically based transmission of information from one neuronal assembly to another cannot be inferred.

c) Effective connectivity is defined as the causal dependency between the observed neuronal assemblies and interpreted as directional information flow. The estimation of effective connectivity is based on time series analysis, statistical modeling, or experimental perturbations as outlined in section 3.5. Both, approaches that require an explicit description of the structural organization of a network, and approaches that are free of structural models, have been developed. Information flow requires true anatomical pathways, which is why effective connectivity can be seen as a union of structure and function (Sporns, 2011).

In summary, sensorimotor control of goal-directed movements is largely carried out in large scale neural networks within the cerebral cortex. Associated brain regions and their functions indicate transient network dynamics on a subsecond timescale. To fully describe these brain network dynamics during the generation of goal directed movements, the engaged brain region's locations and functions, their activities, but most importantly, the directed information flow by means of effective connectivity between them must be analyzed (Sporns, 2013; Varela et al., 2001).

# 3 Measuring network dynamics in sensorimotor control

The spatial and temporal properties of large scale neural networks, carrying out sensorimotor control, determine the requirements related to the measurement method. Why EEG is currently the best method to measure sensorimotor control processes in various settings is evaluated by a comparison with other functional brain imaging methods in section 3.1. Section 3.2 then provides a more detailed background on signal generation and measurement principle of EEG. As outlined in the previous chapter, functional brain networks are described by their component's individual properties (localization and activity) and their interaction by means of effective connectivity. Corresponding measures can be derived from source reconstructed signals of the brain areas. Section 3.3 explains how ICA is applied to separate EEG channel data into source signals and how to estimate their locations in the brain. Section 3.4 then details how the network component's individual activity can be decomposed into its time and frequency dependent properties. Measures of brain connectivity are explained in section 3.5 with special focus on the estimation of brain effective connectivity.

## 3.1 Choice of method

Methods to measure functional brain activity related to cognition or motor behavior include, amongst others, EEG, magnetoencephalography (MEG), functional magnetic resonance imaging (fMRI), positron emission tomography (PET), and functional near-infrared spectroscopy (fNIRS). EEG and MEG measure electric activity of neuronal populations and according magnetic field changes, respectively. In contrast, fMRI, PET and fNIRS measure indirect metabolic indicators

of neuronal activity.

EEG signals are generated by synchronously firing neurons in the cerebral cortex. The flow of electric currents along their axons generate extracellular fields, which can be detected with surface electrodes placed on the scalp. Due to electric conduction, each electrode receives a summation of subjacent brain areas. The spatial resolution is within centimeters, but with a millisecond time resolution. However, by using EEG-based methods for source localization, the spatial resolution can be increased towards several millimeters (Nunez & Srinivasan, 2006). Nowadays flexible, lightweight, and therefore mobile EEG systems are available (Gramann et al., 2014). The following section 3.2 provides further details about the generation and recording of EEG.

Electric currents induce equivalent magnetic fields (Tipler & Mosca, 2014). The MEG utilizes this effect and detects local field changes according to the electric neuronal activity (da Silva & Van Rotterdam, 2011). One advantage of MEG over EEG is that magnetic fields are unaffected by conduction properties, which allows more realistic head models that are required to estimate the source locations in 3D space, as will be explained in more detail in section 3.3. The temporal and spatial resolution are about equal to that of EEG (Nunez & Srinivasan, 2006). To record the weak magnetic field changes, MEG needs to be recorded in shielded rooms with helium-cooled detector coils (so-called superconducting quantum interference devices - SQUIDS). This makes the recordings costly and less mobile compared to EEG (Bear et al., 2007).

fMRI makes use of the difference in magnetic resonance of oxy- and deoxyhemoglobin. Through direction of magnetic gradient fields, locations of active (oxygen consuming) brain areas can be visualized with a time resolution in the range of hundreds of milliseconds to seconds, but with a spatial accuracy of few millimeters (Bear et al., 2007). The corresponding time course of the blood oxygenation level dependent (BOLD) signal, thus, provides an indication of brain activity in response to a stimulus or as spontaneous fluctuations (Ranjana K Mehta, 2013). For functional brain imaging using PET, a radioactive tracer that emits positrons (e.g. 2-Deoxyglucose (2DG) with a fluorine (FDG) or oxygen isotope) is injected into the blood stream and reaches the brain. Metabolic active neurons absorb the tracer. Positrons react with electrons by emitting photons, which then can be detected by collectors. Because two photons are always emitted at an angle of  $180^\circ$ , the active neuron can be located by coincident detections of photons in opposite collectors. The higher the number of emitted positrons, the higher the metabolic activity level of a brain area's cell population. The temporal resolution here lies between one and several minutes to hours with a spatial resolution within the dozens of the millimeter range and can even be enhanced when combined with MRI (Bear et al., 2007). Both, PET and fMRI, are large stationary and heavy devices, which need the subject/patient to lie between the detectors and only allow very little or no degree of movement. Additionally, PET and fMRI scans are very costly compared to EEG.

A more mobile solution that measures indirect neuronal activity is fNIRS. Cerebral

hemodynamic changes of local differences in oxy and deoxyhemoglobin concentration can also be recorded by illuminating the brain's surface with near infrared light and measuring its absorption. Even though the fNIRS signal and the BOLD signal from cortical regions have been shown to correlate in various motor tasks (reviewed in Steinbrink et al.(2006)), and thus offers mobile measuring of hemodynamic changes, the spatial resolution is lower than with fMRI. Compared to EEG and MEG, the spatial resolution of fNIRS is similar, but the temporal resolution is lower since the measured hemodynamic response (10-15 s) and not the actual neuronal activity is measured (Bear et al., 2007).

Aside from the costs, three main factors are important for the choice of method when analyzing brain activity related to movement in, or outside a laboratory setting: (1) the degree of mobility, (2) the temporal and (3) the spatial resolution (Ranjana K Mehta, 2013). Figure 3.1 shows a comparison of selected methods in terms of these factors.

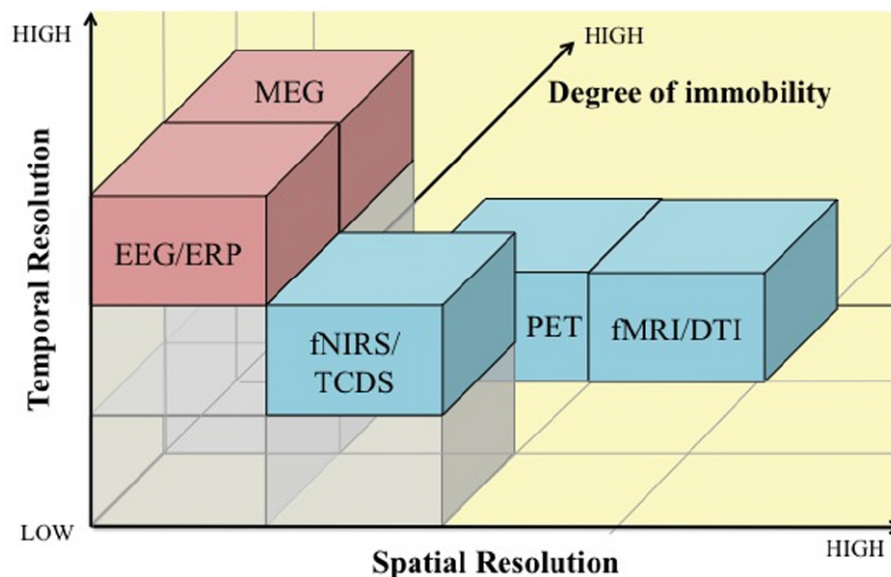


Figure 3.1: Comparison of brain imaging methods regarding temporal and spatial resolution, and system immobility (Ranjana K Mehta, 2013).

Concluding the above remarks, EEG is the only method that measures the true electric neuronal activity on the time scale, in which conscious brain processes occur, while providing the highest degree of mobility. Hence, EEG is currently the best choice for measuring movement related brain processes in the field of sports and exercise. Additionally, it is easy to apply even with a large number of electrodes and by way of comparison to other methods, cost-efficient. This is in line with the reasoning of Thompson et al., who also favors EEG for the applications for sport and performance research (Thompson et al., 2008). Moreover,

Makeig, Gramann, Jung, Sejnowski, and Poizner underline the unique applicability of EEG to study cognition and movement (Makeig et al., 2009). Lastly, EEG was also identified as the method of choice for mobile brain imaging in Gramann et al. (2014). Although, development of EEG devices for mobile application including movements is still an ongoing process (Gramann et al., 2014), high density recording systems, advances in computational neuroscience, especially towards the reliability of source localization, and also compatibility with other brain imaging techniques, have made EEG to become an accepted method for functional brain imaging (C. Michel & Murray, 2012).

## 3.2 Electroencephalography - a brief overview

The first human EEG recordings were described by Hans Berger in 1929 (Berger, 1929), who is known for his discovery of so-called alpha blocking. This effect describes diminishing occipito-parietal EEG oscillations at 10 Hz when subjects open their eyes, indicating desynchronization of neuronal activity in this region. Since then, the measuring principle has not changed dramatically, but recording quality and its applicability has when comparing the early used analogue with currently available digital systems (Maus et al., 2012). Nowadays, EEG counts as one of many brain imaging methods, which is capable of recording brain activity on the time scale of natural motor behavior (Makeig et al., 2009). The generation of the human surface EEG and principles of its recording are described in the following.

Neuronal activity in the cerebral cortex is believed to contribute primarily to the EEG signal. The cortex consists of about  $10^{10}$  highly interconnected neurons that, according to the work of Donald O. Hebb, form cell assemblies of different spatial scales (Nunez & Srinivasan, 2006; Hebb, 1949). These cell assemblies can act as functional units and produce characteristic frequencies in which their activities are synchronized. The oscillating electric potentials propagate through the brain, mainly interfering with the cerebrospinal fluid layer (CSF), skull (also blood vessels, meninges, etc.), to the scalp according to these tissue's conductive properties and can be recorded as the EEG using surface electrodes. Figure 3.2(a) shows the human brain with its three primary divisions brain stem, cerebellum, cerebrum. The cortex itself is the outer part of the cerebrum, of which a patch is shown in figure 3.2(b). It illustrates how propagating action potentials along axons and also synaptic potentials generate an extracellular electric field. In fact,



the main contributors to these fields are inhibitory and excitatory post-synaptic potentials (IPSP and EPSP) (Speckmann et al., 2012). Within layers of the cortex, so-called pyramidal neurons are arranged in parallel and perpendicular to the brain's surface. Due to this name-giving configuration, the field potentials generate electrical current dipoles. When synchronously active, patches of pyramidal cells hence create a dipole layer and cause a summation of local potentials, which propagate to the scalp surface. The resulting EEG signal from between two electrodes is shown in figure 3.2(c). Here underlying cell assemblies produce dominant alpha activity, as can be seen from the 10 Hz peak in the frequency spectrum below.

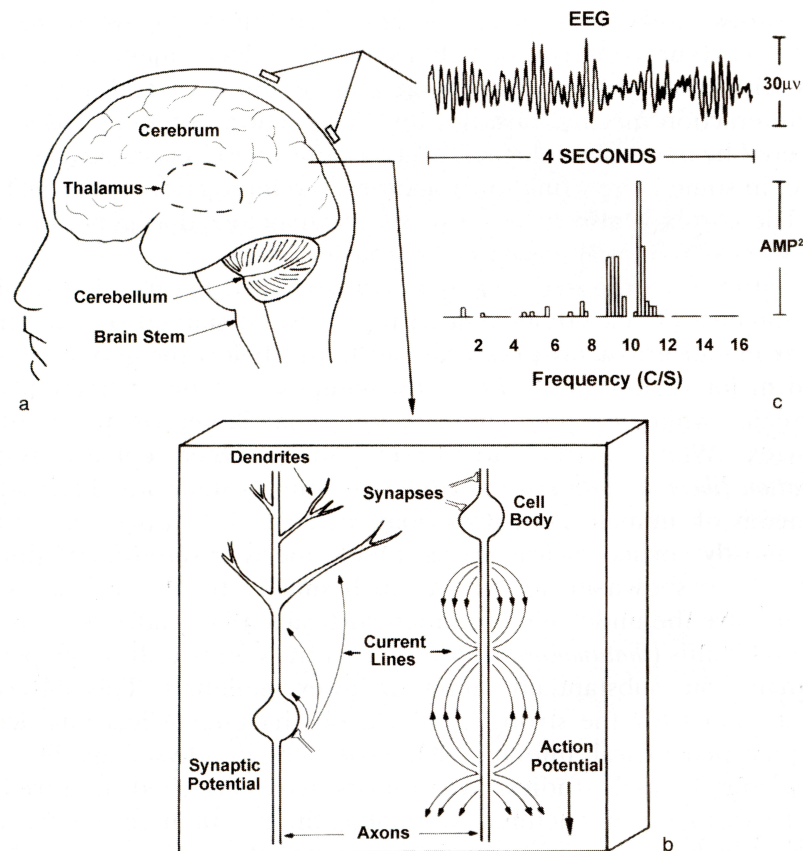


Figure 3.2: (a) The human brain. (b) An illustrated section of cerebral cortex showing microcurrent sources. (c) Segment of EEG recorded between two electrodes. The time course of alpha rhythm and its spectrum is shown. From (Nunez & Srinivasan, 2006) p. 5.

To pick up the EEG oscillations, surface electrodes are placed on the scalp. The most widely used electrode material is silver with a silverchlorid layer ( $\text{Ag}/\text{AgCl}$ ),

which allows stable and low impedances between skin and electrode surface (Cooper et al., 1984). The impedance is additionally lowered using electrolyte paste or gel and should be as low as possible (typically within the lower  $k\Omega$  range). This is however, dependent on the amplifier that is used. In order to distinguish local differences of brain activity, several electrodes are distributed over the head. The 10-20 system has been introduced by Jasper, which separates the head surface in percentiles of 10 and 20 percent, thus defining a distribution of electrode positions that cover the subject's head, independent of subjects' head sizes (Klem et al., 1999). The 10-20 system is illustrated in figure 3.3. Nowadays, this system has been extended to standardize positions for high-density recordings with up to 256 electrodes (Oostenveld & Praamstra, 2001). For a better handling, electrodes can be embedded in flexible electrode-caps. These come in sizes to match different head circumferences.

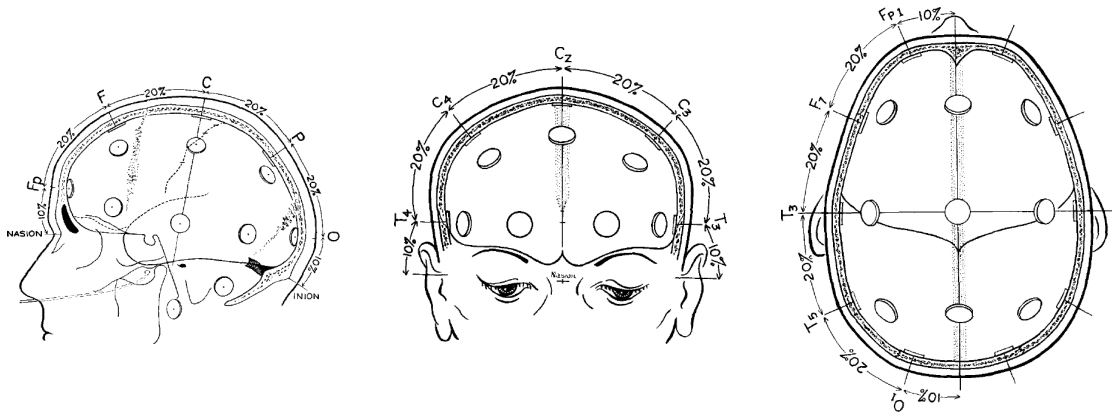


Figure 3.3: The 10-20 electrode system (Klem et al., 1999).

To handle the number of recording sites, electrode cables can be fed into an EEG amplifier. This is not only to ensure simultaneous recordings and simplifies basic functions as impedance measurements and filtering, but also allows to amplify the signals to increase the SNR. By that, the EEG recordings get robust against cross-feed from external electrical fields. These amplifiers also offer recording additional channels for physiological signals like electrocardiogram (ECG), electrooculogram (EOG), electromyogram (EMG). Furthermore they convert the analogue signal to a digital signal which can be saved by a computer (A/D converter).

One essential detail when viewing EEG activity from multichannel recordings is the used reference channel. Raw data is often recorded using an additional reference channel on the scalp (e.g. near FZ or CZ), nose, or ear lobes and mastoids. However digital recorded EEG is easy to re-reference. Unipolar, bipolar, lateral, linked ears, or a Cz reference montage and others have been used for different

purposes of EEG inspection (Fisch, 2012). For high density EEG recordings and for the purpose of source reconstruction (see section 3.3.4) the average reference ( $\frac{1}{N} \sum_{i=1}^N x_i$ ) is typically used. The idea is that by covering the volume of the head with a high number of  $N$  electrodes ( $\geq 60$ ), the averaged sample points  $x_i$  represent the quiet-reference (average of all signals equals zero) (Nunez & Srinivasan, 2006).

The EEG signal is of stochastic nature and represents the sum of all potentials that reach the electrode, generated by the underlying structures. In a homogeneous volume conductor, the signal amplitude decreases quadratically with distance to its origin. Even though the volume between the EEG generators (cell assemblies) and the electrode is not homogeneous, local fluctuations of electric potentials can be localized within centimeters (Cooper et al., 1984). Surface EEG amplitudes typically range between 10 and 100  $\mu V$  with more than 90 % of its energy content between 1 and 30 Hz (Thompson et al., 2008). However, frequencies up to 100 Hz have also been looked at (Ullsperger & Debener, 2010). The spectral distribution of EEG oscillations is typically divided in several frequency bands that can be assigned to different brain structures and functions in particular tasks. A commonly used band division is illustrated in figure 3.4. Predominantly discussed in conjunction with tasks related to cognition and motor behavior are the theta, alpha and beta frequencies, which noteworthy show considerably more specificities than those mentioned in the figure's third column 'State Associated with Bandwidth'.

Due to the  $\mu V$  scale of EEG potentials, the recordings are prone to interferences from a variety of sources, causing these artifacts. Non-biological causes like line noise, cable sway and electrode pops and also biological causes like eye movement, ECG, EMG or transpiration can induce artifactual content, often with higher amplitudes and interfering frequencies compared to the EEG. Non-biological artifacts can be reduced by a good fit of the electrode cap, low impedances and cable fixations. Many of the biological artifacts can be suppressed by offline algorithms or simple filtering techniques. Non-EEG content, which cannot be avoided or reduced, is usually rejected by EEG-experts. The next section provides some more details on how to treat artifactual content during further processing steps. Furthermore, artifacts specific to movements and how they can be reduced will be discussed in the next chapter.

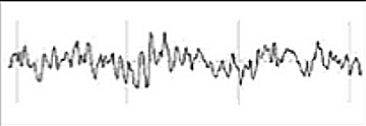

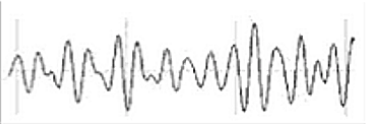
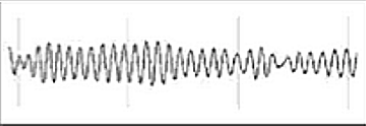

| Frequency Band Name | Frequency Bandwidth | State Associated with Bandwidth | Example of Filtered Bandwidth  |
|---------------------|---------------------|---------------------------------|--|
| Raw EEG             | 0–45 Hz             | Awake                           |  |
| Delta               | 0.5–3.5 Hz          | Deep Sleep                      |  |
| Theta               | 4–7.5 Hz            | Drowsy                          |  |
| Alpha               | 8–12 Hz             | Relaxed                         |  |
| Beta                | 13–35 Hz            | Engaged                         |  |

Figure 3.4: Typical frequency bands of the human EEG (Budzynski et al., 2009).

### 3.3 From channel to source space by ICA

The electrical activity of distinct brain areas is mixed in the electrode signals of the EEG due to volume conduction effects. Thus, the exact localization and individual signal of each source is mathematically undetermined, well-known as the inverse problem of EEG (Nunez & Srinivasan, 2006). The two major approaches to address the inverse problem differ in their assumption of the source distribution. The single dipole approach idealizes each coherently active neural assembly to be one equivalent fixed dipole. The distributed approach does not have restrictions about the spatial distribution of active sources. It rather finds the most probable source current distribution allowing activity from multiple areas (Plummer et al., 2010).

A priori to source localization, the EEG can be spatially filtered which is essentially an attempt to unmix the signal content within the electrode space. Makeig utilized ICA on EEG recordings to reconstruct the brain source signals (Makeig et al., 1996). This technique has evolved over the past years and has been applied to separate artifactual content and noise from the EEG, but more importantly to decompose functional brain source activity. Consequently, source reconstructed

signals have a significantly higher SNR compared to the corresponding electrode signal (Makeig et al., 2000).

ICA is the most widely used method of BBS, which is in general the decomposition of a mixed multivariate signal into its individual components without knowledge (being blind) about the sources or the mixing process (Hyv et al., 2001; Bell & Sejnowski, 1995). It has become a valuable signal processing tool for various applications such as speech separation, processing of radar or sonar signals and multi-sensor biomedical recordings (Bell & Sejnowski, 1995; T. Jung et al., 2000; Stone, 2002). Four assumptions have to be made to apply ICA: (1) Signals need to be mixed linearly, (2) the sources must be spatially fixed, as well as (3) temporally independent, and (4) the component statistical distribution must be non-Gaussian (T. Jung et al., 2000; Hyv et al., 2001; Makeig et al., 1996).

### 3.3.1 The principle of ICA

ICA is commonly introduced by drawing an analogy to the so-called *cocktail-party problem*. Assumed is a cocktail-party setting with, for simplification reasons, two sources  $s = \begin{pmatrix} s_1 \\ s_2 \end{pmatrix}$  of sound, for example two people talking. If one records these sources with two detectors (i.e. microphones), both recorded signals  $x = \begin{pmatrix} x_1 \\ x_2 \end{pmatrix}$  contain portions of both speaking persons. The mixing process can then be expressed by coefficients  $W = \begin{pmatrix} w_{11} & w_{21} \\ w_{21} & w_{22} \end{pmatrix}$ , also called the weight matrix. Including the time dependence of the sampled signals, denoted by  $t$ , and by generalizing the problem to  $m$  sources and detectors, the following equation evolves:

$$\mathbf{x} = \mathbf{W}\mathbf{s} \Leftrightarrow \begin{bmatrix} x_1(t) \\ x_2(t) \\ \dots \\ x_m(t) \end{bmatrix} = \begin{bmatrix} w_{1,1} & w_{1,2} & \dots & w_{1,m} \\ w_{2,1} & \dots & \dots & \dots \\ \dots & \dots & \dots & \dots \\ w_{m,1} & \dots & \dots & w_{i,i} \end{bmatrix} \cdot \begin{bmatrix} s_1(t) \\ s_2(t) \\ \dots \\ s_m(t) \end{bmatrix} \quad (3.1)$$

Equation 3.1 is called the ICA model, which has two unknowns: The true source signals  $x$  and the mixing process denoted by the weight matrix  $W$ . The goal of an ICA is then to estimate  $W$  that best explains the mixing process and calculate its inverse  $W^{-1}$  to obtain the ICs  $s$ :

$$s = W^{-1}x \quad (3.2)$$

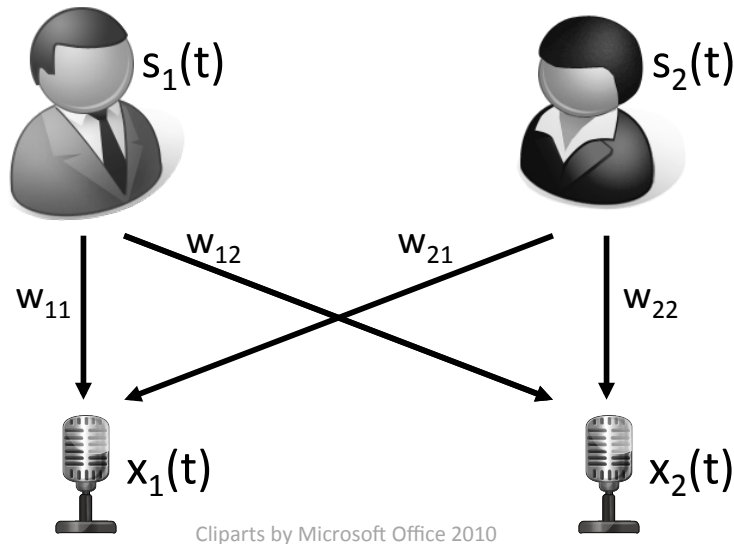


Figure 3.5: The cocktail party-problem

This is implemented by iteratively searching for a weight matrix that makes the ICs maximally independent from each other. Several rules have been applied to quantify statistical independence based on finding maximal non-gaussianity, minimizing mutual information or maximum likelihood estimation (Hyv et al., 2001). Among these, the concept of information maximization, the infomax principle, was the first one that was applied to EEG. This approach maximizes the amount of information transported by the estimated sources, which is equivalent to minimizing their mutual information, because statistically dependent components share information and thus transport a lower amount of overall information. ICs in contrast, transport a maximum amount of information since their mutual information tends towards zero (Bell & Sejnowski, 1995).

### 3.3.2 Application to the EEG

ICA was first applied by Makeig et al. (1996). The four constraints to apply ICA hold for EEG data because: (1) The electrode signal represents a summation of underlying sources and is thus linearly mixed (Nunez & Srinivasan, 2006). (2) During the time of measurement (minutes), the brain is organized in spatially stationary and distinct brain areas and (3) they act independently from each other, which is arguable, but true to some extent as discussed in T. Jung et al. (2000). Lastly (4), non-Gaussianity of the sources can be assumed as also pointed out by

T. Jung et al. (2000).

In ideal ICA results, the IC time courses can be seen as those from distinct brain sources instead of the mixed signals in the electrode space. From equation 3.1 and 3.2 it is obvious that not more ICs than used electrodes can be separated. Thus, the more electrodes were used in the measurement, the more brain components can be found. It has to be noted that the number of true brain sources will most likely exceed the number of electrodes that can be placed on the scalp. However this limitation is also valid for standard analysis in the electrode space.

In addition to functional brain activity, ICA has been shown to be able to isolate so-called stereotypical artifactual content from the EEG (T. P. Jung et al., 2000). These artifacts appear regularly with similar characteristics and have a stationary source location. The most prominent stereotypical artifacts are due to vertical and horizontal eye movements and also EMG, ECG and interspersed external electric fields such as line noise. These are likely to be separated by ICA. Consequently, this has been used to reject artifacts from the EEG to further analyze on clean electrode signals. The unmixing process is a linear transformation and thus completely reversible. Hence, artifact rejection can be done by setting the artifactual IC signal to zero and recalculate the component's time series back into the electrode space. (Makeig et al., 1996; T. P. Jung et al., 2000; Delorme et al., 2012).

In contrast, non-stereotypical artifacts only appear irregularly or with unique characteristics and can either not be decomposed as pure artifactual content or they might be decomposed into several ICs leaving less space for functional components. Typical non-stereotypical artifacts are due to complex and irregular movements, electrode pops, jawing, chewing or teeth clenching (Delorme et al., 2012).

To achieve reasonable ICA results that show clear functional brain and non-brain sources, several steps have to be considered from the recording to the pre-processing.

## Data acquisition

31 channel EEG recordings can bring up five to 15 plausible ICs (Onton & Makeig, 2006). Makeig even used 14 electrodes only in his first work on the application of ICA for EEG decomposition (Makeig et al., 1996). However, further analyzing methods such as source localization require a larger number of channels (Z. Acar & Makeig, 2013). Currently EEG recordings of 64 to 256 electrodes, distributed over the scalp, are called high density EEG and should therefore be considered in planning of data acquisition. Also, the more sensors used, the more sources can be decomposed. Besides that, two further factors play a crucial role for ICA quality:

(1) The number of sample points recorded: According to Onton and Makeig (2006)

this number should be a multiple of the number of electrodes squared. So far no investigation has been made to evaluate this in detail, but factors of 10 to 30 were proposed. For example, for a 64 channel recording  $64^2 \cdot 30 = 122,880$  sample points should be recorded. In theory, when using a sampling rate of 256 Hz, 480 s of artifact-free EEG would be sufficient. However, this also depends on the task, which is carried out. For example, event-related test paradigms with 3 s epochs would require 160 clean trials in the recording (Onton & Makeig, 2006).

(2) The quality of the raw data: Following the universal rule of signal processing, GIGO ('garbage in, garbage out'), ICA results will be poor if the quality of the raw data is poor (Onton & Makeig, 2006). Artifacts use up the limited amount of ICs and thus leaving less space for functional brain components, especially with few channels. Generally, as much data as possible should go into the ICA. Though, decompositions of long recordings or on concatenated recording sessions in different conditions should only be done if EEG source locations can be assumed to be the same (Onton & Makeig, 2006). For example EEG in an awake and a sleep state should not be jointly decomposed.

### **Pre-processing**

Before analyzing EEG data, pre-processing can have a profound impact on the outcome of the ICA. The here described order and parameter settings of EEG pre-processing ought to describe the relevant details.

- **Filtering:**  
Low frequency content ( $< 1$  or  $2$  Hz) may impair the result signal decomposition of ICA. This, aside from true brain activity in some observations like rest and sleep, can be caused by sweat-artifacts and electrode conduction drift. This in return, leads to non-stationary signal content, which then must be seen as non-stationary source locations. To avoid this, 1-2 Hz high pass filters are advisable. This has shown to produce more reliable ICs with more dipolar topographic maps. Note that if low frequency content is investigated, it is advisable to run ICA on the high pass-filtered data and than apply the weights to the unfiltered data (Ullsperger & Debener, 2010).
- **Down sampling:**  
The iterative ICA process of relatively large datasets requires high computer performance or time. Therefore, it is advisable to down-sample. For example a sampling rate of 256 Hz still conserves relevant spectral content without introducing aliasing effects (Shannon, 1949), while keeping the amount of



data manageable. In contrast to intuitive thinking, it has been reported that using higher sampling rates doesn't necessarily produce better ICA results, because the information content relevant for EEG source activity does not increase significantly (Onton & Makeig, 2006).

- **Channel rejection:**  
Artifact contaminated channels should be left out of the ICA at all. Due to bad electrode-skin contact, electrode specific affection of movement or non-stereotypical EMG patterns, individual channels might show artifacts repeatedly. These channels are unlikely to get decomposed by ICA so that they can be of no value for the process or even disrupt the results. An interpolation of missing channels would not be beneficial since the interpolated channels are always a linear combination of the information that is already present. This is also described as a resulting rank inconsistency (Ullsperger & Debener, 2010). Hence, the number of ICs that can be found is reduced by the number of rejected channels.
- **Re-referencing:**  
ICA is unaffected by the choice of reference (Luck & Kappenman, 2011). All re-referencing (linked ears, common average, Cz, etc.) is a linear combination and therefore does not change the mixing process. The channel back-projection, i.e. the topographic maps of IC activation, might change according to the reference, but IC properties and dipole locations will not. However the choice of reference might be crucial for the interpretation of IC activations or for further analysis (such as dipole fitting). Re-referencing has to be done after channel rejection, because in the case of an average reference, artifacts from one channel would spread into all others.
- **Artifact rejection:**  
Non-stereotypical artifacts should be rejected before running the ICA. In contrast, stereotypical artifacts can be left in the data since they may be separated from the EEG content, leaving more data usable for further analysis.

## ICA algorithms

Over the last two decades several ICA and other BSS algorithms have been developed. Delorme et al. (2012) compared 22 ICA algorithms specifically for the use on EEG data. Based on the assumption that EEG signal generators are statistically

independent and project their activity equivalent to that of a single dipole onto the scalp surface (Scherg & Berg, 1991; Z. A. Acar & Makeig, 2010), they measured the performance of the algorithms regarding (1) the amount of mutual information reduction as a measure of independence of ICs compared to the electrode signals, (2) the mean remaining pairwise mutual information, which is a partial measure of the first by comparing pairwise instead of multiple dependencies, and (3) the dipolar characteristics of scalp projections of each component, measured by the residual variance (rv) between the scalp projection of a true dipole set in the head model and the IC's back projection.

As a result, Delorme found all tested algorithm performances to be fairly close in finding near dipolar, biologically plausible EEG and non-EEG components. However, the AMICA algorithm (from adaptive mixture of independent component analyzers, (Palmer et al., 2007)) was found to be the best performing by showing the strongest reduction of mutual information and the most near dipolar scalp maps. For the evaluation 71 channel EEG recordings from 14 subjects performing a modified Sternberg visual working memory task with about 300,000 recorded sample points each was used (Onton et al., 2005). Figure 3.6 shows the superior performance of AMICA regarding the mentioned factors and also the apparent linear relation between information reduction performance and dipolar scalp maps.

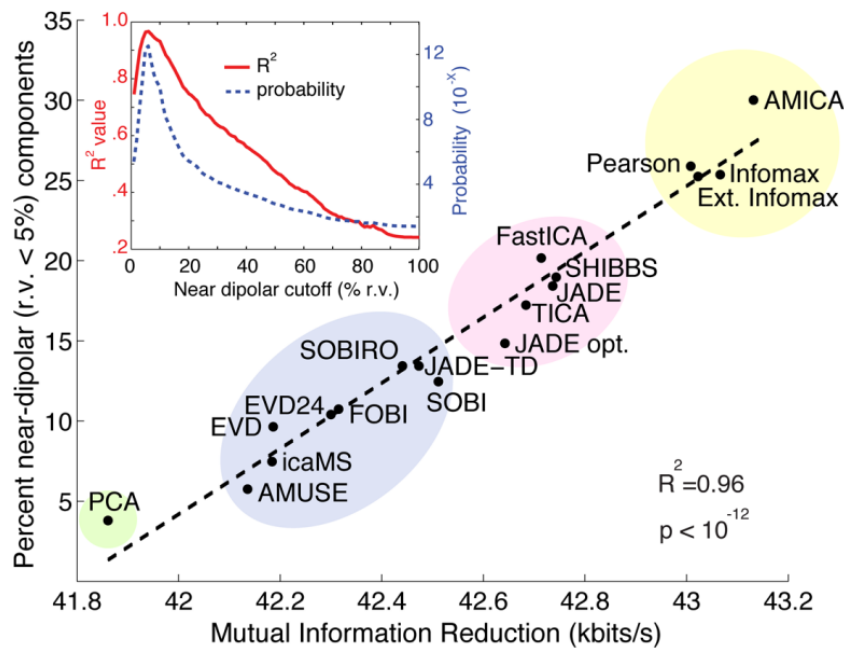


Figure 3.6: Comparison of ICA algorithms (Delorme et al., 2012).

### 3.3.3 Source localization of equivalent single dipoles

Since ICs of brain source activity have been found to show single dipole characteristics, their spatial origin can be estimated by searching a best fit location within a chosen head model, which is co-registered to the electrode positions on the scalp. These head models consist of mathematical descriptions about the conductive and geometrical properties of the head. Scanning through a grid of fixed locations in the model, the so-called forward problem is solved by deriving a single equivalent dipole's back projection on the model's scalp surface. This can be compared to the actual IC's topographic map. The grid location that produces the best matching topographic map is assumed to be the one of the IC's source. The residual variance (rv) is the percent difference between these scalp projections and is an expression of the inverse of how well the estimated dipole explains the data (Groppe et al., 2009). These values can be fairly low and a threshold of less than 10% r.v (Delorme et al., 2012) or 15 % r.v. (Onton et al., 2006) is often used to accept biological ICs. Irregular ICs inherently tend to have high r.v. values because several sources contribute to one component, but fitted with on dipole only. Also, it has to be noted that in some cases bilateral synchronous source activities are present so that a dual-dipole can be fit. This can be the case for ICs that represent activity from occipital brain areas, reflecting visual processing and eye activity itself (Delorme et al., 2012). In general the quality of the dipole fit depends on the quality of the ICA, the chosen head model and the accuracy of the co-registered electrode positions. It has been shown that realistic head models such as boundary element models (BEM) outperform spherical head models. Also 4-shell models, that include the conductivity properties of the brain, CFS, skull and scalp are favored. If no exact 3D electrode locations are available, standard or extended 10-20 system based locations can be used to achieve reasonable results (Onton et al., 2006; Delorme et al., 2012).

### 3.3.4 Component identification

ICA is a data driven approach and thus does not require any a priori assumptions regarding localization, frequency content or temporal patterns (Makeig, Debener, et al., 2004). Consequently, the order of ICs does not consistently relate to the order of channels. Hence, the identification of ICs and their classification into EEG and non-EEG activity represents one major difference compared to the analysis of electrode signals. This is mostly done heuristically by careful inspection of the

IC's topographic maps, equivalent dipole location, frequency spectra, time courses (Onton et al., 2006).

ICs can be categorized into four classes of components as stated by Onton. Firstly, true functional brain sources, secondly, physiological but non-EEG sources such as eye movements and blinks, EMG, ECG, etc. and as a third group, external artifacts including line noise, cable sway, electrode pops, etc. Lastly, spatially irregular ICs of unknown or mixed origin are likely to represent multiple sources not independent enough to be assigned to individual components (Onton et al., 2006). In the following subsections the characteristics of these classes are described for each of the mentioned modalities.

#### **Topographic maps**

Through inversion of the ICA model (eq. 3.1) the projection of each IC into the electrode space can be calculated and thus gives the so-called back projection or topographic scalp distribution. Delorme et al. found that biological plausible ICs are dipolar and such, will have a smooth distribution over the scalp with two separated areas of polarity (Delorme et al., 2012). A very localized back projection into the channel space, possibly attached to a specific channel location, indicates an IC with artifactual signal content. Very diverse or scattered topography with multiple poles is most likely referred to several mixed sources.

#### **Equivalent dipoles**

The equivalent dipole location can be used to assign functional ICs to anatomical brain regions. A first indication is the  $rv$  value. Low values ( $\leq 15\%$ ) are a sign of a good fit and high quality decomposition of the particular IC. Dipole locations also help to determine artifactual ICs such as EOGs, which should be located close to the eyes in the head model, while dipoles of muscle activity appear close to the surface of the scalp. ECG related ICs are most likely located at the very bottom of the head model (closest point to the heart). External artifacts are often located outside the brain structures or even at the very center of the model, because they might appear in all channels with equal magnitude.

## Frequency spectra

Characteristically, the magnitude of spectral power in an EEG frequency spectrum decreases with increasing frequencies. Depending on the location, certain spectral patterns can help to identify ICs. For example, in cognitive tasks, frontal ICs usually show a clear peak in the theta band (4-7 Hz), while more posterior located ICs show prominent alpha (8-12 Hz) activity (Onton & Makeig, 2006). ICs that can be related to motor activity, appear in lateralized central to posterior areas of the scalp and also show a frequency peak around 10 Hz (known as the  $m\mu$  - rhythm) and also beta (13-30 Hz) activity. Also frequency harmonics do appear in the spectra of well decomposed sources (Onton & Makeig, 2006). Artifactual ICs such as eye blinks (EOG) and muscle activity (EMG) usually show considerable different frequency spectra. The EOG spectrum peaks at about 0-3 Hz with a smooth decrease in magnitude. EMG in contrast, shows high power above 20 Hz. External artifacts also differ from the typical EEG spectrum considerably, especially line noise artifacts that show a sharp peak at 50 or 60 Hz, depending on recording location.

## Time courses

To classify ICs by their time course works best for event-related data. Task related activity is present, when averaged or single event-related potentials (ERPs, see section 3.4 for details) show time-locked dynamics relative to the event. However, if these dynamics appear in narrow frequency bands only or even have opposing dynamics in different bands, ERPs will not or only weakly reveal this time-locked activity. Ocular artifacts, ECG and also externally induced artifacts, decomposed as ICs can be investigated by their continuous time course. ECG for example shows regular spikes within the time range of heart rate (approximately around 60/minute).

Recently, Grosse-Wentrup, Harmeling, Zander, Hill, and Scholkopf developed an algorithm which aims to objectify and automate the process of IC selection and identification (Grosse-Wentrup et al., 2013). So far this has most often been done heuristically and was therefore very much depending on the experience of the investigators. However, the new algorithm is based on classification of the topographic maps only. Onton and Makeig (2006) and Shou, Ding, and Dasari (2012) provide more details about the multimodal (maps, dipoles, spectra, ERP) but heuristic approach and how typical functional and artifactual IC are identified.

### 3.3.5 Component clustering

Studying the pre-selected ICs on group-level requires clustering of similar components that represent the same functional brain regions. This issue is not present when working in the electrode space, because electrode locations are equal or assumed to be equal across subjects. This is not the case for the set of selected ICs. One solution for this is to cluster ICs with similar properties. Onton et al. conclude that various IC measures should be incorporated in the clustering process (Onton et al., 2006). This includes spatial measures, such as dipole locations or topographic scalp maps and functional measures like the time course of ERPs, frequency spectra or a combination of these dimensions, that is time-frequency representation (ERSPs, see section 3.4). A multi-measure clustering approach may ensure higher homogeneity of clustered components compared to clustering on single measures. This also raises the question of weighting the individual measures, which has not been evaluated yet. Typically, a distance vector, including a selection of measures with individual weights is created, and for each a pre-selected number of principle components is obtained by principle component analysis (PCA). After that, a k-means algorithm can be utilized to find a specified number of clusters. This approach offers great variability of parameter settings (measure types, weighting, number of principle components per measure and number of clusters) to adjust the clustering to the specific investigation. Several studies have been published in which this approach was applied and described in detail (Onton & Makeig, 2006; Gwin, Gramann, & Ferris, 2010; Gramann, Gwin, et al., 2010).

To bypass the issue of clustering in the first place, so-called group-ICA approaches have been proposed (Congedo et al., 2010; Li et al., 2011; Vía et al., 2011). In principle, these methods concatenate datasets of subjects and then apply the ICA algorithms. However, this procedure was criticized for violating ICA assumptions regarding source stationarity and linearity of the mixing process due to individual differences of brain anatomy and volume conduction (Nunez & Srinivasan, 2006; Bigdely-Shamlo et al., 2013).

## 3.4 Brain activity measures

The analysis of EEG can be classified into measures of spontaneous oscillations on the one hand and evoked or ERP on the other. The former approach investigates

spectral band power in electrode locations or ICs to define brain states related to different conditions such as sleep, rest or during cognitive and motor tasks. This is done by separating the EEG for each condition in epochs of a few hundred milliseconds up to several seconds (depending on the desired frequency resolution), applying a transformation into the frequency domain, such as Fast-Fourier transformation (FFT), and averaging the resulting spectra. This method provides a robust measure for local band power in different conditions, but diminishes the time information, which is one of the EEG's great advantages.

In contrast, ERP analysis offers high time resolution in the order of milliseconds and is thus capable of showing brain processes according to sensory, motor and cognitive events (Bressler, 2011). This requires exact stimulus markers in the data for that epochs can be aligned to the respective events. By averaging these epochs (several dozens or hundreds), spontaneous EEG cancels out while the ERP reveals. According to Bressler (2011), this method represents the principal recording methodology to investigate fine temporal structure of human cognitive processing. Nevertheless, one disadvantage of ERP analysis is that the valuable spectral information is disregarded.

An early approach to combine the functional specificity of frequency bands while maintaining temporal resolution, was introduced by Pfurtscheller and Aranibar (1979a). The basic principle is to apply FFT on short segments of event-related data and average the power value of a chosen frequency band for each segment over all epochs. The resulting measure is called event-related (de-) synchronization (ERD/S) revealing time dependent dynamics for a specific frequency band. Band power throughout a patch of cortex is higher in times when neuronal activity is synchronized and lower when it is desynchronized. ERD/S was developed to investigate functional brain dynamics and their topography related to voluntary self-paced movements with which a better SNR, due to the focus on only relevant spectral properties, was achieved (Pfurtscheller & Aranibar, 1979a). In contrast to the event related potentials, which represent phase-locked activity over the whole frequency spectrum, ERD/S shows time-locked activation in chosen frequency bands in relation to an event (Pfurtscheller & Lopes da Silva, 1999). The measure of event-related spectral perturbation (ERSP), introduced by (Makeig, 1993), is a representation of spectral dynamics in the time-frequency domain. It simultaneously shows the time course of power density for each frequency and therefore generalizes the ERD/S. ERSP images are created by computing the power spectra of overlapping time windows along epochs and average these over trials that are aligned to some event of a specific task (Rosenberg-Katz et al., 2012). To visualize the perturbation, power values are color coded in [dB] and furthermore normalized by the mean baseline log power spectrum (Delorme & Makeig, 2004). Figure 3.7 shows an exemplary ERSP image with distinct alpha and beta band desynchronization, potentially related to motor activity ( $\mu$ -suppression). Additionally, theta ERS appears about 400 ms after the event, which is usually set to time point 0. This figure illustrates that ERSPs reveal more information than time courses of averaged ERPs or ERD/S, which either are not frequency depen-

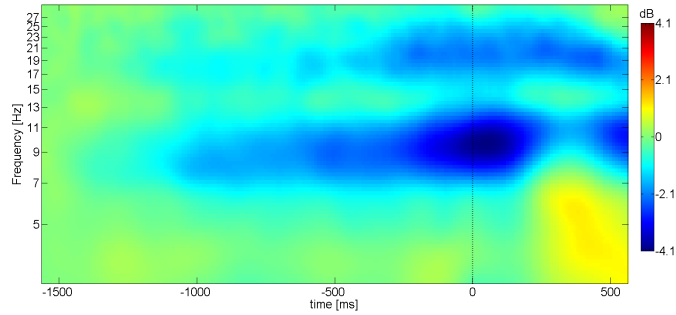


Figure 3.7: An ERSP image denotes time-frequency decomposed dynamics averaged over epochs. Here: Alpha and beta band desynchronization and late theta synchronization.

dent or are limited to one frequency band only (Makeig, 1993). If present, ERSP shows time dependent and distinct multi-band activity patterns, possibly characteristic for distinct functional brain sources (specific frequency band dynamics). Hence, ERSP images can be utilized as a functional measure in the process of IC clustering and also as a comprehensive measure for brain area activity. Using ERSP, T. Jung et al. demonstrated its SNR of task-related ICs to be superior to results obtained from electrode signals (T. Jung et al., 2000).

### 3.5 Brain connectivity measures

The previously described EEG measures allow the simultaneous analysis of locally and functionally distinct brain area activity. The understanding of the brain as a dynamic network has gained the investigation of both, activity and connectivity. As nodes of a functional large scale neural network, engaged brain areas may be structurally and also functionally interconnected. The following builds up on the introduction of the term brain connectivity in section 2.4 and focuses on the estimation of effective connectivity based on the concept of Granger causality, followed by a practical guideline on how to utilize these measures to investigate the causal relations of the nodes of a network that is involved in goal-directed movements.



### 3.5.1 Structural connectivity

Using methods of neuroanatomical tract tracing, regional structural connectivity between brain regions can be analyzed on neuronal level. This is done by placing tracer substances extracellularly to the living tissue, which are then actively incorporated through the neuronal membrane and transported in the cytoplasm, thus localizing the distant but structurally connected cell bodies (Kötter, 2007). Furthermore, to study anatomical structures of the human brain on large scale level, diffusion weighted imaging (DWI) sequences of MRI, in particular diffusion tensor imaging (DTI), has become a widely used method (Kötter, 2007). DTI elicits the orientation of diffusion processes of water molecules in the brain. Since the Brownian motion is constraint by myelinated fiber tract, it allows diffusion along, but not across these structures. Hence, diffusion direction indicates the 3D orientation of anatomical pathways in the brain.

### 3.5.2 Functional connectivity

P. Fries proposed a mechanism for neural assembly communication through coherence, thus justifying the study of coupling of neural assemblies within or even across distinct frequency bands (Fries, 2005).

Other methods to investigate functional connectivity between the nodes of a network (pre-defined as regions of interest (ROIs) or by data driven approaches with or without anatomical presumptions) include covariance, coherency and phase locking (Kötter, 2007). Using fMRI, several functional networks have been detected, including the default mode network (DMN), which is thought to be the most fundamental so-called resting state network (RSN) active in times of no particular task execution (also known as 'rest') (Lee et al., 2013). Among others, a somatomotor, visual, language, dorsal attention, ventral attention and a frontoparietal control network have been identified from the BOLD response, detectable in both resting and task-related conditions. RSNs are believed to provide knowledge about the general functional organization of the brain and thus provide a promising approach with high clinical application e.g. in the future of examining patients with neurodegenerative diseases by detecting irregularities within these networks (Lee et al., 2013; Fox & Raichle, 2007).

RSNs are represented by rather static measures of functional connectivity. Utilizing the high time resolution of EEG and MEG, functional connectivity can

also be derived time and frequency dependent. For example Gevins and Bressler developed event-related covariance, while Rappelsberger, Pfurtscheller, and Filz used coherence on event-related epoched data (ERCoh) to approach the spectral dynamics of functional coupling Gevins and Bressler, (Rappelsberger et al., 1994). However, the informative value of functional connectivity is limited because it does only explain which regions of the brain are engaged simultaneously in a task, but not how these areas effectively share information to function as a network.(Nunez & Srinivasan, 2006; Sporns & Tononi, 2007).

### 3.5.3 Effective connectivity

Numerous methods to calculate effective connectivity have been developed over the past decades. This includes structural equation modeling (McIntosh & Gonzalez-Lima, 1994), dynamic causal modeling (DCM, (K. J. Friston et al., 2003)), transfer entropy (TE, (Schreiber, 2000)), dynamic Bayesian networks (DBN, (Rajapakse & Zhou, 2007; Smith et al., 2006)) and granger causality mapping (GCM, (Goebel et al., 2003)). All of these have been applied to electrophysiological or hemodynamic brain recordings. However, the principle of Granger causality (Granger, 1969) is one of the most widely used methods of effective connectivity estimation and has specifically been used to study large scale sensorimotor networks using EEG and also fMRI data (Sporns & Tononi, 2007). Advantageously, it is a data driven approach and thus can be derived without requiring a model for directed interaction between the observed variables.

Granger causality is based on the principle of statistical predictability (Hesse, 2009) and goes back to the work of N. Wiener (Wiener, 1956). Lacking of practical implementation, Wiener's concept was adapted for bivariate linear stochastic autoregressive (AR) models by the econometrician Granger in (1969). Essentially, it estimates the amount of information that a variable provides to predict another one (Sporns & Tononi, 2007). In other words, two time series A and B were recorded. Now, if B can be predicted more accurately using information from the past of A and B instead of using B's past alone, A is said to granger cause B (at least in parts) (Hesse, 2009; Mullen, Delorme, et al., 2010; Kamiński et al., 2001). For the case of  $n$ -dimensional time series observations, such as the  $n$  channels of an EEG recording, multivariate autoregressive (MVAR) models are fitted to the data, which parameters allow the analysis of coupling between the processes (Schlögl & Supp, 2006). Assuming  $n$  processes, denoted by a time series vector  $x(t) = (x_1(t), \dots, x_n(t))'$  with zero mean, the MVAR model of order  $p$  can

be written as

$$x(t) = \sum_{r=1}^p a(r)x(t-r) + \varepsilon(t) \quad (3.3)$$

where  $x(t)$  contains the modeled time series of each process,  $a(r)$  are the  $n \times n$ -coefficient matrices of the model and  $\varepsilon(t)$  is a white noise process containing the unexplained data of the observation. Elements of the coefficient matrix  $a_{ij}(r)$  contain the values about the contribution of process  $j$  with the time lag  $r > 0$  to process  $i$ . Moreover,  $a_{ij}(r) \neq a_{ji}(r)$  and such provides information about the directional causal relation between the observed processes in terms of Granger-causality (Schlögl & Supp, 2006; Schelter et al., 2009).

Without going into further detail, the first step to fit a MVAR model is to estimate the coefficient matrix so that all processes can be described appropriately without significant residuals. The assumptions for this are that the data  $x(t)$  is stationary and stable. If this is the case, multivariate least squares approaches (MLS) can be used to fit the model. Additional information about model fitting can be found in Schlögl (2000), Kilian (2006) or Schlögl and Supp (2006).

To quantify the causality, either statistical variance, the prediction error or the probability of predictability are used (Hesse, 2009). For looking at causality between two individual processes  $i$  and  $j$ , bivariate case of the Granger causality  $F_{ij}$  can be expressed as:

$$F_{ij} = \ln \left( \frac{\overline{\sum_{ii}}}{\sum_{ii}} \right) = \ln \left( \frac{\text{var}(x_t^{(i)} | x_{(\cdot)}^{(i)})}{\text{var}(x_t^{(i)} | x_{(\cdot)}^{(i)}, x_{(\cdot)}^{(j)})} \right) \quad (3.4)$$

Equation 3.4 expresses the ratio of prediction errors for using process  $i$  ( $\overline{\sum_{ii}}$ ) alone over using  $i$  and  $j$  ( $\sum_{ii}$ ). Here  $\text{var}$  denotes the variate autoregressive model of order  $p$  (VAR[ $p$ ]),  $x_t^{(i)}$  describes the process  $i$  (or  $j$ ) at time point  $t$ , whereas  $x_{(\cdot)}^{(i)}$  expresses the past of process  $i$  (or  $j$ ). The assumptions that have to be fulfilled are (1) the cause must precede the effects in time and (2) the information about the cause must improve the predictability of the effect (Mullen, Delorme, et al., 2010).

Winterhalder et al. compared different linear signal processing techniques to estimate effective connectivity in multivariate neural systems and found the so-called partial directed coherence (PDC) to be best performing over other estimators like directed transfer function (DTF) and the Granger causality index (GCI). In the mentioned work, other techniques were excluded because they were argued to be improper for the use on neural networks (e.g. not frequency dependent or limited to bivariate, not multivariate, observations) (Winterhalder et al., 2005). Further comparisons and reviews of different techniques of effective connectivity estimation can be found in L. Astolfi et al. (2005), Winterhalder et al. (2005), Schlögl and Supp (2006), and Bressler and Seth (2011).

PDC was introduced in Baccalá and Sameshima (2001) and follows the principle of Granger causality for multivariate data. It generalizes the directed coherence by adding frequency dependence to the measure ( $F_{ij}(f)$ ) and therefore reveals the information flow between observed time series decomposed into discrete frequencies. This is done by Fourier transformation of the coefficient matrix. One advantage of PDC is that it allows the observation of interactions regardless of processes that were not included or observed (latent variables). This is because PDC is normalized by taking the ratio of the information outflow of a process  $j$  to  $i$ , relative to all the outflows from  $j$ , not including interfering inflows (Hesse, 2009). Hesse states the PDC as the favored method (amongst DTF and GCI) because it requires less computing time, discriminates direct and indirect interactions and considers multivariate processes. For example, if an information flow from  $i$  to  $j$ , as well as from  $j$  to a third process  $k$  is truly present, PDC will (correctly) return the true information flow from  $i$  to  $k$  and not (incorrectly) sum up both  $F_{ij}(f)$  and  $F_{jk}(f)$  (L. L. Astolfi et al., 2007). The mathematical background and more profound details can be found in Baccalá and Sameshima (2001), Hesse (2009) or L. L. Astolfi et al. (2007). The normalization between 0, no causal influence, and 1, full causal influence, is also one of PDC's pitfalls, because it does not allow comparison of different scales (e.g. different recording units or subjects) or interpretations about the strength of effective connectivity between different processes, within or across frequencies (Schelter et al., 2009). To overcome these disadvantages, Schelter proposed a new renormalization of PDC by the inverse covariance matrix of the VAR[p] process (Schelter et al., 2009). This is denoted by:

$$\lambda_{ij}(f) = Q_{ij}(f) * V_{ij}(f)^{-1} Q_{ij}(f) \quad (3.5)$$

Here,  $\lambda_{ij}(f)$  is the frequency dependent strength of causality, between process  $i$  and  $j$ . The inverse covariance matrix is included in  $V_{ij}(f)$ . For the full mathematical derivation, please refer to (Schelter et al., 2009). With this, renormalized PDC (rPDC) allows the comparison of processes of different scale, eliminates normalization by the number of information outflow and therefore makes statistical testing across observations possible (Schelter et al., 2009; Velu et al., 2014).

### 3.5.4 Estimating effective connectivity - Application to the EEG

EEG based estimation of effective connectivity requires valid MVAR models, which can be fitted to either electrode or IC signals. Ideally, the latter represent

individual brain source signals with none or minimal noise or crosstalk from other sources, and should thus allow better model fittings. For the application to EEG data, effective connectivity estimation consists of four main steps: (1) specific pre-processing, (2) model fitting, (3) model validation and (4) the connectivity estimation itself. T. Mullen gives a comprehensive introduction to these processing steps and therein contained methods (Mullen, Delorme, et al., 2010). The following paragraphs summarizes Mullen's remarks to provide a practical guideline for the steps of effective connectivity estimation.

### Step 1: Pre-processing

- Down sampling:  
The sample rate determines the frequency content that can be analyzed. However, a broader frequency range requires a higher model order to capture the spectral content sufficiently. The problem with high model orders is that those models tend to exhibit higher variability. As a consequence, the sample rate should be chosen as high as necessary to capture the relevant frequency range (following the Nyquist theorem, Shannon,(1949)), but as low as possible according to the relevant frequency content. The sampling rate cannot be less than  $2fHz$ , with  $f$  being the highest frequency of interest. More details about model order  $p$  follows in step 2.
- Detrending and filtering:  
Low frequency content introduces non-stationarity, which can lead to poor model fitting. If present, linear trends/drift can be removed by piecewise subtraction of the temporal mean using a least squares fit approach. Detrending is not causing any changes in the phase relations between processes, which some filter functions might induce. If high-pass filtering is done, a zero-phase shift or acausal filter should be used to avoid corruption of the causal relations between the observed nodes.
- Normalization:  
To further improve local stationarity, two kinds of normalizations can be applied. Temporal normalization subtracts the mean of each epoch and dividing it with the standard deviation. Ensemble normalization is the pointwise subtraction of the mean of all trials divided by the corresponding standard deviation. This basically removes the local mean, ensures a variance of 1 and

therefore removes ERPs from the data, allowing to model causal relations on the remaining, mathematically stationary oscillations (Ding et al., 2000).

## Step 2: Model fitting

- Stationarity:

As stated above data stationarity is required to fit MVAR models. EEG however can be very non-stationary, which is why models are fit to smaller subwindows, which are more likely to be locally stationary. These windows are slid along the epoch with a certain overlap, defined by the step size. Longer windows will smooth the time course of effective connectivity fluctuations, while shorter windows increase time resolution. This technique is named adaptive MVAR modeling (AMVAR) and is illustrated in figure 3.8.

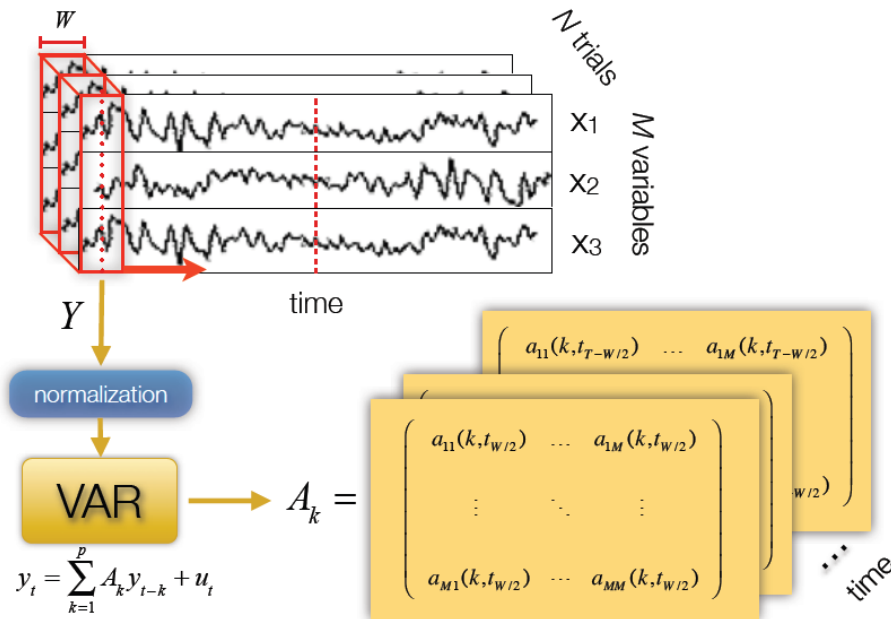


Figure 3.8: Adaptive MVAR (AMVAR) modeling (Mullen, Delorme, et al., 2010).

- Window length:

The window length  $W$  determines the lowest frequency to capture (at least one cycle must fit in) and also the factor of temporal smoothing. The longer

the window, the lower the frequency that can be modeled and the higher its smoothing factor, but the shorter the window, the more likely local stationarity can be achieved. Window length needs to be adjusted to the characteristics of processes and their dynamics intended to investigate.

- Required amount of data:  
The number of coefficients to estimate is given by the number of included channels or ICs  $M$  squared multiplied with the chosen model order  $p$ . Thus, at least  $M^2p$  data samples are needed. Schlögl and Supp (2006) and Korzeniewska, Crainiceanu, and Kuś (2008) suggest ten times as many data points to accurately fit the model in each time window.
- Model order:  
Mullen provides a detailed description of considerations and their dependencies about selecting an appropriate model order (Mullen, Delorme, et al., 2010). In summary  $p$  should be chosen so that it doubles the number of expected relevant frequency peaks in the processes. For EEG data, an order of  $p = 10$  was found to be optimal for a sampling rate of 128 Hz (Jansen et al., 1981; Florian & Pfurtscheller, 1995). Again, the sampling rate  $F_s$  is crucial for the frequency range that can be displayed ( $f_{max} = 0.5F_s$ , (Shannon, 1949)).

### Step 3: Model validation

- Whiteness of residuals:  
Equation 3.3 includes the term  $\varepsilon$  for unexplained data content or the model's residuals. An adequate model fit will have small and uncorrelated (white) residuals. Tests like autocorrelation function (ACF) or Portmanteau can be used to check for significant correlations (non-whiteness) in the residuals. For further information on this and the next validation criteria, please consider Mullen, Delorme, et al. (2010) and cited literature.
- Consistency:  
Whether the model captures the correlation structure between processes of the data can be checked with the so-called percent consistency  $PC$  (Ding et

al., 2000). A value of  $PC > 85\%$  is suggested.

- **Stability:**  
Stability and stationarity were two main assumption for MVAR models. A stable process is also a stationary process and can be checked by utilizing the stability index  $SI = \ln|\lambda_{max}|$ , where  $\lambda_{max}$  denotes the maximal eigenvalue of VAR[p]'s coefficient matrix. If this is less than 0, the model can be confirmed stationary.

#### **Step 4: Connectivity estimation**

The final step is to estimate the connectivity using the fitted and validated MVAR model. This depends on the choice of estimator, of which PDC and rPDC were described in the above section 3.5.3. The result is a time-frequency representation of effective connectivity for each pair of nodes and direction of information flow.

As mentioned, more details about the estimation of effective connectivity on EEG data is given in (Mullen, Delorme, et al., 2010) which represents the manual for the source information flow toolbox (SIFT). In this toolbox, the relevant pre-processing steps are implemented. It also incorporates functions for model fitting, model validation and estimating various effective connectivity measures including PDC and rPDC. Though, it has to be noted that SIFT is in beta state and still under development (date: April 27th, 2015).



## 4 Applying brain network measures in sports and exercise

In the previous chapter, EEG was identified as the method of choice for recording brain activity during movement, despite being prone to artifacts. Even though ICA can be used to separate artifactual signal content from that of brain sources, the amount of stereotypical and especially non-stereotypical artifacts should be kept to a minimum. This can be achieved by (a) considering methodological challenges regarding data acquisition and (b) by choosing suitable movement epochs, as will be outlined in the following section (4.1).

Dipole source localization, event-related power spectral density (ERD/S, ERSP) and effective connectivity (by rPDC) were introduced as measures of brain network dynamics. The current state of research with respect to applying these measures to precise goal-directed movements and the implications drawn from the corresponding parameters is reviewed in section 4.2. This is differentiated between experiments conducted in laboratory settings on the one hand, and measuring more complex movements in real-world settings on the other.

As will be outlined below, complementary mapping of brain network dynamics by means of localization, activation and effective connectivity during the execution of goal-directed movement in sports and exercise has rarely been approached. This research deficit is specified in section 4.3.

### 4.1 Methodological challenges

Inherently, complex movements and real-world measuring settings create challenges regarding data acquisition and its quality with the currently available recording techniques. These problems are often bypassed by either measuring

before or after movement executions, during movement imagination, or by investigating brain activity in simulated sporting environments (Thompson et al., 2008). However, in-task cortical activity, reflecting brain processes during the actual execution of movements, is thought to differ significantly from these conditions, because brain dynamics are directly influenced by active behavior in relation to the environment and actual sensory information in that moment (Gramann et al., 2014). Thus, the aforementioned methodological challenges of EEG measurements during movement must be approached.

### 4.1.1 Challenges in data acquisition

EEG is prone to artifacts even in calm measurement settings, which is exacerbated during motion. Cable sway, electrode shifts and sweating are the most common artifacts that specifically appear in the EEG during movement.

Cable sway artifacts are caused by individually moving cables, which carry the often not yet amplified and therefore interference-prone signals from electrode sites to the amplifier. These artifacts typically appear as high amplitude changes in distinct individual channels. Cable fixations and bundling of cables, as well as minimizing the cable length help to reduce the described interferences. However, the cable fixations must still allow for the range of movement, necessary for the particular task to prevent shifts of electrodes relative to the skin. Otherwise, electrode shifts can cause so-called electrode pops, which are rapid changes of impedance or even a short loss of connection. The affected electrodes' signals show sharp and high amplitude changes. Besides sufficient freedom to move (strain-relief), enough gel and a tight cap fit reduce the occurrence of electrode pops throughout the measurement.

Over time and depending on the physical load of the movement, artifacts caused by perspiration might occur. These are represented by slow ( $< 1$  Hz), high amplitude fluctuations in few, possibly laterally distributed channels as a result of impedance changes due to the sweat. A well-tempered environment according to the physical activity, electrode cap material from breathable textures or with open spaces between electrode positions (electrode nets) reduces heat accumulation. Heavy sweating (and also too much gel/electrolyte) may also cause electrode bridging. Bridged electrodes show identical signals, resulting in loss of spatial information and may lead to erroneous interpretation if undetected.

Impedance changes/drifts can induce non-stationarity due to drying electrodes, which violates the stationarity constraint of ICA. Non-stationarity can in fact be of particular importance in longer recordings in outside conditions and should be controlled by repeatedly checking and readjusting the impedance values through-

out the measurement.

Considering these causes of artifacts and following the recommendations to avoid them should result in better data quality even during limited movements and therewith yield more data for further processing (Thompson et al., 2008; Gramann et al., 2014).

As described in section 3.3, ICA can be used to effectively separate artifactual content arising from stereotypical non-brain sources, such as muscle activity and eye movements, from brain activity. EMG is characterized by high frequency content around 10 - 1000 Hz with higher amplitudes (100 - 1000  $\mu V$ ) compared to EEG (10 - 100  $\mu V$ ) (Thompson et al., 2008). It appears at channel locations overlying or adjacent to muscles. If these muscles are specifically engaged in the task's movement, their activity cannot be suppressed without changing the movement itself. However, muscles represent stationary sources with stereotypical activation patterns when they are movement related. The EMG can therefore be separated as ICs from the EEG (Gwin, Gramann, & Makeig, 2010).

Another stationary source of typical EEG artifacts is the movement of eyes. Each eye forms an electrical dipole with the positively charged cornea and the negatively charged retina (Dworetzky et al., 2012). High amplitude potentials according to eye ball movements are distributed predominantly in frontal and frontocentral electrodes and may or may not be task-related. Eye movement can be reduced by designing the task so that relevant visual information is only presented at a certain location. However, in sports and exercise, aiming for a target or following an object's trajectory is often required. Eye movements are therefore inevitable and often stereotypical for certain movements (e.g. looking back and forth between hole and ball prior to a golf putt). Since the eyes' dipole locations are fixed, eye movement artifacts are likely to be separated by ICA.

Consequently, even though artifacts of all kinds should be avoided, in cases of challenging measurement settings and in studies that involve complex movements, stereotypical artifacts from muscle activity and from the eyes can be accepted. This can also be generalized for any stereotypical and stationary signal content like line noise or even regularly appearing motion artifacts (e.g. during walking) (Gwin, Gramann, & Makeig, 2010). However, the more artifactual ICs are to be decomposed, the less component space is left for ICs representing actual brain sources.

### 4.1.2 Suitable movements

Even when considering the previously outlined causes of movement related artifacts and the possibility to reject some unavoidable non-brain activity, only a limited amount of movement can still be accepted during EEG recordings. To ensure sufficient data quality, studies utilizing EEG in sports have been confined to disciplines involving relatively minimal head movement such as golf, darts, archery, stationary bike cycling and rifle shooting (Thompson et al., 2008; Crews & Landers, 1993). Especially because of motionlessness in the aiming period before the actual movement, the process of taking aim in target shooting sports presents ideal conditions for EEG recordings, (Thompson et al., 2008). Furthermore, such movements can be tracked by external sensors (motion, force, joint angle) to mark important events (onsets, offsets, trigger pull, etc.) so that distinct phases of the movement can be related to the EEG (Makeig et al., 2007).

For example, golf putting has been shown to be suitable and reliable for EEG recordings in both laboratory and real-world settings (Reinecke et al., 2011). Channel power spectral density in both settings revealed comparable patterns during task execution. The golf putt is described as a goal-directed movement, which requires sensory information processing, focused attention and motor planning prior to its execution (Baumeister et al., 2008). Once the motor plan is created, the golf putt itself is described as a self-paced movement, consisting of two phases, the backswing and the downswing towards the ball (Beilock & Gray, 2012). The ball's trajectory depends on the initial velocity, direction and spin that is transferred from the putter head to the ball. The athlete has immediate visual feedback and can evaluate the performance (distance to the hole) once the ball is at rest.

The relatively calm motions, the demands on sensory information integration, the involvement of attentional control and the distinguishable sequences of planning, execution and monitoring of the golf putt create an ideal framework to study sensorimotor control processes during complex goal-directed movements in a real-world setting (Babiloni et al., 2008; Baumeister et al., 2008).

As in golf putting, the given impact force in any ballistic motion determines whether a hit object travels the intended distance (Craig et al., 2000; Urbano et al., 1996). Thus, the process of fine motor control, like precise force generation, largely account for putt performance (Babiloni et al., 2008). In fact, Urbin specifically states that studying ballistic force generation in a controlled condition can be of great value to understand mechanisms underlying more complex multi-joint motor skills. This is because multi-joint movements can be seen as to be largely governed by sets of precise muscular impulses (Urbin et al., 2011). Consequently,

the accuracy of the resulting force pulses account for the variability of limb trajectories in complex movements. In this context, variability has been considered as a consequence of erroneous sensorimotor processes that control muscular impulses and determine the quality of motor skill performance (Newell et al., 1984).

Thus, a simplified force pulse generation task under laboratory conditions can be used to study this key aspect of complex goal-directed movements. Moreover, this reduced model provides a framework to test the methods for mapping brain network dynamics before approaching the more complex tasks and test settings in the real-world condition.

## 4.2 Current state of research

### 4.2.1 Measures of brain dynamics in motor precision tasks in controlled settings

Methodologically, the time dependent analysis of voluntary movements in general began with the introduction of the Bereitschaftspotential (BP), by averaging EEG electrode signals aligned to the onset of voluntary movements (Kornhuber & Deecke, 1965). The BP is a decrease of head surface potentials preceding, for instance, wrist extensions (Kukleta & Lamarche, 2001), thumb adduction (Wheaton, Yakota, & Hallett, 2005) or finger movements (Sochůrková et al., 2006). The early BP starts about 2 s before the movement onset and is generated in the SMA as suggested by EEG based dipole source localization, which were verified by findings from intracranial recordings and fMRI (Praamstra et al., 1996). The early BP is thought to reflect preparatory processes for upcoming movement initiation. It is modulated by the level of intention and by the force to be generated, but not by precision or movement complexity (Shibasaki & Hallett, 2006). The latter two factors modulate the so-called late BP, which is allocated to PMA and contralateral M1, starting approximately 400 ms before the movement onset, as demonstrated by ICA based dipole source localization utilizing a fMRI-constraint approach (Toma et al., 2002).

Additional information about cortical activation during goal-directed movements has been found by calculating the ERD/S. While the BP shows local phase-locked cortical activity, the ERD/S reveals frequency specific dynamics that are time locked to the movement execution. The typical ERD in alpha power in central electrode positions (often referred to as rolandic  $\mu$ -rhythm) has been assigned

to bilateral S1, starting approximately 2 s before movement onset, while a decrease in beta band power appears later and is allocated to M1 with contralateral predominance (Nagamine et al., 1996). After movement termination, ERD recovers for both frequency bands and even shows an increase, also described as post-movement beta rebound (PMBR), on the contralateral side of the movement (Pfurtscheller et al., 1996). This complex pattern of frequency specific dynamics have been analyzed in numerous motor actions including voluntary finger movements (Pfurtscheller et al., 1994; Pfurtscheller & Neuper, 1992; Riva et al., 2012; Houdayer et al., 2012; Visani et al., 2006; Babiloni et al., 2000), button presses, (Pfurtscheller & Aranibar, 1979b; Pfurtscheller, 1989), foot movements (Neuper & Pfurtscheller, 1996; Pfurtscheller et al., 2000; Müller-Putz et al., 2007), motor imagery (Takata et al., 2012), comparison between slow and brisk movements (A. J. Stancák & Pfurtscheller, 1996) and also precise force generations in a go/no-go paradigm (Fukuda & Hiwaki, 2013). The pre-movement alpha and beta ERD, which lasts throughout movement execution is modulated in amplitude and latency by the force that is generated (A. Stancák et al., 1997) and the muscle mass to be activated for the particular movement (Pfurtscheller & Lopes da Silva, 1999). Following movements, the contralateral beta ERS is discussed as a mechanism for information processing or a recovery into the 'idling' state of the motor cortex (Gulyás et al., 2009; Pfurtscheller et al., 1996; Pfurtscheller & Lopes da Silva, 1999). In this regard, Tan et al. found neural correlates of motor error monitoring with the PMBR over the sensorimotor cortex in a joystick operated, targeted reaching task (Tan et al., 2014). Here, beta ERS of the EEG was lower for larger errors.

By means of ERPs, post-movement activity, referred to as the phase of performance evaluation or error monitoring and processing, is represented by the so-called error related negativity (ERN) and is thought to reflect phase-locked activity within the ACC (Ullsperger et al., 2014; Shenhav et al., 2013). It is either modulated by the outcome of an action or by the action prediction error (Ferdinand et al., 2012; Kobza & Bellebaum, 2013). ERS, with spatially and temporally similar dynamics to that of an ERN, is observed in the theta band, appearing as a positive burst following cognitive actions, like decision making (Nigbur et al., 2011) and motor errors in terms of erroneous button presses (Navarro-Cebrian et al., 2013). This theta burst is proposed to reflect a general mechanism of action evaluation (Armbrecht et al., 2012).

BP and ERD/S are used to distinguish time and also frequency dependent signatures of movement planning, execution and monitoring in individual brain regions. However, sensorimotor control requires the interplay of the participating brain regions to achieve precise motor performance. Consequently, individual components need to be observed simultaneously to be able to capture their network dynamics.

Using fMRI, it was found that brain regions including PFC, SMA, PMA, S1, secondary somatosensory area (S2), and PPC are particularly engaged during the production and scaling of fine fingertip forces (Kuhtz-Buschbeck et al., 2001; Ehrsson et al., 2001). In accordance with this, recordings from spontaneous EEG during an air traffic control task, spatially filtered by ICA, identified similar anatomical regions (ACC, PMA, SMA, M1, S2, PPC, and visual cortex). Their appearance and activation patterns throughout the task were discussed towards a participation in both sensorimotor and attentional control functions (Shou et al., 2012). Though, results also showed that not all anatomical regions were found for all subjects and recording sessions. Less reliably detected ICs were those assigned to S2, SMA, and also occipital areas. Clustering was performed based on topographic maps, frequency spectra and dipole localizations. Supporting these findings, source reconstructed EEG and MEG signals were identified to originate from S1, PFC/PMA, SMA and PPC in a finger tapping task (Muthuraman et al., 2014). A comparison of source localization results between both recording techniques showed that EEG has sufficient spatial resolution to localize cortical brain areas during the motor task. However, MEG was able to additionally find subcortical structures (here: the thalamus and cerebellum).

These findings demonstrate that similar sensorimotor control networks during motor tasks, and cognitive tasks, which require motor action, can be localized in fMRI, MEG and also EEG studies and are consistent with the relevant brain areas for carrying out goal-directed movements, as described in chapter 2.

The localization of a brain network and measuring the activation of its components is complemented by the observation of their connectivity by means of structural, functional and effective connectivity. During the execution of goal-directed movements, the structural connectivity can be assumed static (see section 2.4). Nevertheless, due to intensive training in sports and exercise (and/or predisposition), structural differences of the anatomical pathways can be detected in the athletes' brain compared to control subjects. This was shown in professional gymnasts using DTI tractography (Wang et al., 2013). Athletes showed increased structural connection density between brain regions that were assigned to a sensorimotor and an attentional network (categorization of functional networks according to Y. He et al. (2009)). Accordingly, highly-practiced golfers showed increased volume in the gray matter in parts of the attentional frontoparietal network including PMA and parietal areas (Jäncke et al., 2009). Functional connectivity analysis reveals statistically significant coupling of brain areas and is denoted by the coherence between electrodes or source reconstructed signals when applied to EEG or MEG recordings. Using ERCoh as a complementary measure to the ERD/S, Rappelsberger et al. found contralateral increased coupling in the alpha band of premotor (electrodes F3, F4) and motor areas (electrodes C3, CZ, C4) preceding the onset of self-paced index finger movements.

In addition, accompanied by the bilaterization of ERD over sensorimotor areas, inter-hemispheric coupling between C3 and C4 increased (Rappelsberger et al., 1994). These findings were confirmed by Leocani, Toro, Manganotti, Zhuang, and Hallett, who identified a functional network of frontal (assigned to the PFC) and central (overlying SMA, M1, S1) electrode positions engaged during voluntary thumb movements aligned to EMG onsets, indicating a motor planning and movement control mechanisms (Leocani et al., 1997). Likewise, Wheaton, Nolte, Bohlhalter, Fridman, and Hallett used EMG, recorded from the abductor pollicis brevis and flexor carpi ulnaris (muscles of the right upper limb) to calculate ERCoh in relation to onsets of tool-use hand movements and communicative gestures. Contralateral increase of beta band ERCoh between electrodes over motor hand area and parietal cortex, as well as electrodes over SMA to M1 and parietal area was maximal during movement preparation. These findings suggest the critical role of frontoparietal motor networks for the integration of preparatory and motor-related activity for praxis movements (Wheaton, Nolte, et al., 2005). While the previous studies focused on event-related dynamics of functional connectivity during general, non-goal-directed, voluntary movements, Rilk, Soekadar, Sauseng, and Plewnia investigated changes of cortico-cortical coupling during a unimanual visuomotor task and their correlation with performance. The task consisted of continuous tracking of an irregularly fluctuating target on a computer screen using a force sensor. Alpha band coherence was increased during task performance between frontal and central electrode locations. Performance accuracy correlated with higher alpha coherence in occipitocentral (i.e. visuomotor) regions whereas high errors of tracking performance enhanced frontocentral coupling (Rilk et al., 2011). These findings are in line with a recent review of EEG studies, in which performance monitoring and adaption causing processes following goal-directed action were found to be implemented by a frontal network consisting of the ACC, functionally connected with PFC, M1 and S1 (Ullsperger et al., 2014).

The aforementioned investigations demonstrate functional connectivity between electrode signals that were assigned to subjacent brain areas. This can only explain which brain areas might interact, but their causal relations remain indefinite (Jirsa & McIntosh, 2007). To capture the transient dynamics of the information flow, measures of effective connectivity are required (see section 2.4 and 3.5).

In this regard, DCM has been used on fMRI data recorded during simple motor performance tasks to detect the average causality between motor and attentional network areas over the time of observation. Grefkes, Wang, Eickhoff, and Fink showed that enhanced information flow from primary visual cortex (V1) and intraparietal sulcus (IPS) to frontal areas, including frontal eye field, PMA, SMA and M1, optimizes motor behavior in a joystick operated goal-directed movement task (Grefkes et al., 2010). Concordantly, the malfunction of motor behavior in patients with Parkinson's disease is associated with decreased effective connectivity within a network of PMA, SMA, M1 and cerebellum during performance of self-initiated movements compared to healthy controls (Wu et al., 2011). Differences of effective connectivity patterns can also be seen between key areas of the motor



network (SMA, PMA, M1, putamen and cerebellum) depending on handedness and movement of the dominant or non-dominant hand (Pool et al., 2014). In Pool, Rehme, Fink, Eickhoff, and Grefkes (2013), authors investigated motor performance of fist closures related to effective connectivity within the human motor system (M1, SMA, PMA). Results indicated that stronger effective connectivity from contralateral PMA to M1 enables increased motor performance of simple unilateral hand movements. However, here motor performance is referred to as movement speed, rather than accuracy or force generation.

DCM can also be applied to EEG recordings when using a predefined model of a network, allowing a more detailed view of the interplay because of the higher time resolution and frequency information of electrophysiological signals. Herz et al. were able to infer motor task-specific modulations of effective connectivity patterns between the contralateral M1, lateral PMA and SMA, localized by source reconstruction using on 122 channel recordings (Herz et al., 2011). During isometric contraction of the forearm, M1 and SMA showed a strong coupling in the beta frequency (13-30 Hz). In contrast, fast repetitive finger movements were characterized by coupling in the gamma band (31-48 Hz). This method however lacks temporal dynamics related to the single movements, neglecting the major advantage of EEG and MEG recordings.

Korzeniewska et al. introduced event-related causality (ERC) to be able to estimate the direction, intensity, spectral content, and temporal course of brain activity propagation within a cortical network (Korzeniewska et al., 2008). The method was initially applied to subdural electrocortigraphy recordings to study the effective connectivity patterns between the sensors of an electrode array during word productions in a language task (Korzeniewska et al., 2008, 2011). Here MVAR model based direct DTF was used to calculate the time-frequency ERC patterns. Recently, Ewen et al. applied Korzeniewska's ERC approach and investigated the dynamics of effective connectivity within the human cortical motor control network (Ewen et al., 2014). Participants performed praxis hand movements (pantomime of using daily living tools like hammer, scissors, pencil, etc.) with a defined preparation phase including a cue for the tool and a following go signal to indicate movement initiation. Effective connectivity was calculated between four ROIs consisting of six EEG electrodes that showed strongest ERS response during the averaged trials. An increased parietal to frontal information flow during movement preparation, but not during execution, was interpreted as a mechanism for updating motor commands in frontal areas based on integrated sensory information within the parietal cortex. This study captured the effective connectivity dynamics during movement planning and execution, but did not include feedback about the motor performance. Regarding this, Zhang, Chavarriaga, Goel, Gheorghe, and del Millán studied cortical processing during the monitoring of stimuli moving in either correct or incorrect direction. An ERC approach was developed to reveal human somatosensory information processing based on 64 channel EEG data (Zhang et al., 2012). Electrode signal based MVAR models using DTF showed theta band specific causal dependencies between S1 over S2

and S2 over cingulate cortex 200 ms after stimulus presentation. This pattern was highly discriminative for erroneous and correct trials and was discussed to be useful for brain computer interface applications.

### 4.2.2 Measures of complex movements in real-world settings

As elucidated above, measuring EEG during complex movements requires consideration regarding data acquisition, the movement itself, and the environment to carry out the experiments. Although the golf putt may serve as an excellent model to investigate representation of cortical activity during the execution of complex goal-directed movement, only one study under real-world settings has been conducted for this purpose using EEG (Reinecke et al., 2011). Authors reported comparable theta and alpha band power spectral density during golf putting from recordings in a laboratory and in the real-world setting (outside putting green) for most channels. The following work also investigated golf putting, but under laboratory settings and on artificial putting greens.

First cortical representations of sensorimotor processes during indoor putting were observed as early as 5 seconds before a putting stroke (Babiloni et al., 2008; Crews & Landers, 1993). More specifically, Crews and Landers reported hemispheric patterns of alpha band power in temporal and motor cortices during movement preparation that correlated with task error (Crews & Landers, 1993). Concomitantly, Babiloni et al. (2008) found ERD in higher alpha frequencies (10-12 Hz) in electrode positions overlying SMA, PMA and S1. These dynamics also appeared 5 s before the putter head hit the ball and were predictive for the outcome of golf putts (Babiloni et al., 2008).

A different approach was used by Baumeister et al. to study sensorimotor control as quasi-static representations in the EEG (brain states) using average in-task power spectral density without considering event-related dynamics. In this investigation, skilled golfers showed higher focused attention (represented by higher frontal theta power) and less effort for sensory integration processing (higher parietal alpha) during putting than novices (Baumeister et al., 2008).

Previously reviewed golf putt studies demonstrate that spectral power measures (spectral brain state analysis and ERD/S) provide insights in cortical processes of sensorimotor control during the pre-movement period. Especially the correlation of central alpha ERD with putt performance has been utilized in numerous appli-

cations to generate predictive online indices for success probability, implemented in neurofeedback training systems for golfers (Arns et al., 2008; Chen et al., n.d.; Muangjaroen & Wongsawat, 2012; Sakai et al., 2012; Sourina et al., 2012).

As previously mentioned, individual ERD patterns based on electrode signals are not sufficient to gain a mechanistic understanding about the processes of sensorimotor control in goal-directed action. So far, only Babilloni et al. approached connectivity measures during golf putting investigating intra-hemispheric functional coherence between electrode signals in a golf putting task with expert golfers (Babiloni et al., 2011). It was shown that stronger coupling between parietal cortex and frontal located areas in the lower and upper alpha frequencies correlated with putting performance.

Apart from this first functional connectivity approach, neither source localization based analysis have been carried out, nor have effective connectivity measures been applied in golf putting or other kinds of comparable complex goal-directed movements and especially not in a real-world setting.

### **4.3 Summary and Research Deficit**

EEG offers the mobility, time and sufficient spatial resolution to investigate sensorimotor control during goal-directed movements in various settings including selected real-world environments. Nevertheless, methodological challenges regarding the reduction of non-stereotypical artifacts like cable sway, electrode pops, slow potentials due to sweat, and impedance drift have to be overcome, especially in real-world settings. Stereotypical artifacts like EMG, eye movement and even repetitive motion artifacts that induce interferences with the EEG can be separated by spatial filtering like ICA. Moreover, from a methodological point of view, as well as with regards to its content related value, it appears appropriate to first gain clean data from a simple motor task in a controlled laboratory setting. For this, precise ballistic force production was identified as a crucial sub component of skilled motor performance making it ideal to first test the measures of brain network dynamics during goal-directed movements in a controlled setting.

ICA can not only separate artifactual content, but also decomposes surface electrode signals into task-relevant brain sources. Based on these reconstructed source signals, their equivalent dipoles can be estimated and assigned to cortical brain areas as part of a functional sensorimotor control network. In fact, ICs reflecting PFC, ACC, PMA, SMA, M1, S1, S2, and PPC have been reliably decomposed in several motor tasks or tasks that require motor behavior (e.g. button presses). Their individual spectral power density can be captured over time using ERD/S

and even indicate functional connectivity by simultaneous activation patterns in time and frequencies. The phases of goal-directed movements, planning, execution and performance monitoring, have mostly been analyzed in separate investigations by focusing on subsets of brain regions, but have not been observed as a whole. Though, a collective observation of localization and activity patterns of network components is essential to analyze the actual network dynamics. Moreover, most studies did not include performance-oriented aspects in test paradigms, which is often a key aspect of goal-directed behavior in sports and exercise.

Towards a mechanistic understanding of the underlying processes, measures of effective connectivity need to be applied. More specifically, only time resolved effective connectivity estimation (ERC) can distinguish patterns of information flow throughout movement planning, execution and monitoring. In combination with time-frequency analysis and source localization, this would complement the description of the brain network dynamics in sensorimotor control. In summary, the present state of research shows a deficit in simultaneously mapping the brain network dynamics by means of localization, activity and effective connectivity of the brain areas that are involved throughout the phases of goal-directed movements such as precise force generation.

Even less is known about the feasibility of capturing these network dynamics in real-world settings. Even though EEG recordings during complex movements in real-world settings are challenging regarding data quality, reliable recordings seem possible. Sophisticated analyses methods, including ICA based network measures, have not yet been utilized.

The golf putt was identified as an adequate framework to study sensorimotor control processing during complex goal-directed movements in real-world settings. Using EEG, skill level and performance have been distinguished by spectral analysis of data that was recorded during putting. Furthermore, patterns of electrode signal ERD/S in the alpha band during movement planning have even been found to be predictive for performance in golf putting. However, neither source separation for both artifact rejection and source reconstruction respectively has been applied, nor has a collective observation of network dynamics been attempted.

Thus, whether ICA is able to separate artifactual from functional signal content during golf putting on the outside green seems likely, but has not been tested. These ICs are then expected to show characteristic patterns of ERD/S throughout the phases of the movement and, in particular, in the preparatory phase before the movement onset. The literature review provided here revealed only one study that investigated intra-hemispheric functional connectivity during golf putting. An examination of the ERC by means of effective connectivity towards a mechanistic understanding of these couplings has not been done.

## 5 Research strategy and specific aims

In Chapter 2, it was outlined that goal-directed movement is based on sensorimotor control, which is largely carried out in functional networks of the cerebral cortex. To explore functional networks of the brain, measuring brain connectivity and especially effective connectivity adds valuable information as a key characteristic to describe a network. EEG was identified as an optimal tool for the application in sports and exercise research, because it captures electrical brain activity on a millisecond time scale, while being lightweight and mobile. In the field of computational neuroscience, signal processing approaches have been developed that allow for the investigation of brain network dynamics by means of localization, activity and connectivity based on EEG recordings. Probabilistic localization of equivalent dipoles of participating brain areas, as well as time-frequency resolved decompositions of their activation have been applied in various types of goal-directed movement tasks in laboratory settings. However, a deficit exists in complementing these measures by investigating the event-related effective connectivity during goal-directed movements as was outlined in the previous chapter. Furthermore, the transfer to the field of sports medicine research, especially towards the application in real-world environments has not been made.

The main objective of this work is thus to map the processes of sensorimotor control for goal-directed movements regarding the location, activation and effective connectivity of the involved cortical brain regions, hence providing the basis for content related questions towards further investigation of motor performance in sports and exercise.

As a first approach to map the network dynamics during goal-directed movements, a laboratory EEG study was conducted to investigate the generation of precise force pulses produced by the thumb and index finger. In this setting, knowledge about applying measures of localization, activation and effective connectivity of brain areas in the context of precise goal-directed force generation is gained. The second experiment consists of a golf putting task and takes place outside on the green. The signal processing procedure is applied to both the laboratory and real-world conditions to investigate the feasibility and application of these tools

to data sets with potentially problematic quality and lower SNR.

A relatively high amount of trials are necessary to gain sufficient number of data samples for ICA and MVAR modeling. The subjects are highly skilled golfers, thus due to extensive training, they are expected to be able to perform a higher amount of consistent putting strokes in the golf putt experiment than less-skilled golfers. Furthermore this group is supposedly more familiar with the task demands and surroundings on the green. For comparability, the same subjects participate in both experiments.

By conducting a controlled laboratory experiment, this work aims:

**A. To map the activity and effective connectivity of localized brain sources related to precise goal-directed force pulse generation in a laboratory setting.**

Due to the controlled environment and small movements, high data quality is expected so that ICA decomposes the EEG into brain sources that can be further processed by means of localization, activation and effective connectivity. To do so, the following must be accomplished:

**A.1 To define a cortical network by identifying ICs that represent movement-related brain areas and cluster them across subjects.**

*Expectations:* Based on Shou et al. (2012) and Muthuraman et al. (2014), ICs that represent PFC or ACC, bilateral sensorimotor areas, PPC and occipital cortex are expected to be produced from the ICA.

*Endpoint:* Localization of equivalent dipoles and time-frequency images of ERSPs, aligned to movement onsets, are used to cluster manually pre-selected ICs across subjects.

**A.2 To test for movement-related dynamics of power spectral density in each cluster.**

*Expectations:* Based on investigations of cortical ERD/S, pre-movement alpha and beta ERD in sensorimotor and parietal areas followed by post-movement ERS is expected (Neuper & Pfurtscheller, 2001). ICs that may be assigned to PFC and/or ACC are expected to show activity in the theta band but without the assumption of time specific pre-movement-related patterns (Shou et al., 2012). However, processes of performance monitoring, represented by post-movement theta ERD might occur after the movement (Ullsperger et al., 2014).

*Endpoint:* These effects are tested by deriving ERD/S and calculating significant spectral deviations from baseline on group level.

---

### **A.3 To test for movement-related dynamics of effective connectivity between clusters.**

*Expectations:* Only the clusters that contain ICs from the same group of subjects can be used for connectivity analysis. Investigations of ERC during executing praxis hand movements by Ewen et al. (2014) suggest increased parietal to frontal information flow during movement preparation, which may also be observed here prior to the targeted force pulses.

*Endpoint:* ERC is estimated by fitting and validating MVAR models and deriving rPDC between all clusters of the defined network. Significant deviation from baseline on group level denotes frequency dependent dynamics of movement related information flow.

Measuring EEG in a real-world setting (here: the putting green), will not only cause more artifactual data content, but is also assumed to make the task more demanding for subjects. This might influence processing outcomes on the one hand and change patterns of cortical activation on the other. ICA is known for its ability to separate artifactual data from functional brain activity. To test this and to apply the methods used for the controlled condition, the golf putt study is conducted and aims:

### **B. To map the activity and effective connectivity of localized brain sources during golf putting in a real-world setting.**

Due to the less controlled environment and more complex movements, lower data quality is expected from this experiment. Nevertheless, major motion and muscle artifacts during golf putting are assumed to be somewhat stereotypical as has been shown for artifacts that emerge from walking and running (Gwin, Gramann, & Makeig, 2010). Thus, it is expected that ICA decomposes artifactual content from the EEG, even though less ICs and/or a higher drop-out rate of subjects is expected. To map the network dynamics the following sub-aims must be accomplished:

#### **B.1 To define a cortical network by identifying ICs that represent movement-related brain areas and cluster them across subjects.**

*Expectations:* According to the given literature review, no study has applied source localization techniques to EEG recorded during the execution of a complex movement like golf putting. However, both, targeted force pulse generation and golf putting were denoted as goal-directed movement, but with different levels of complexity. Thus, the same brain areas are expected to be engaged in the task as revealed by ICA based localization

(PFC/ACC, sensorimotor, PPC, occipital cortex).

*Endpoint:* Localization of equivalent dipoles and time-frequency images of ERSPs, aligned to the onsets of the putter movement, are used to cluster manually preselected ICs across subjects. For connectivity analysis, only the clusters that contain ICs from the same group of subjects can be used.

### **B.2 To test for movement-related dynamics of power spectral density in each cluster.**

*Expectations:* Pre-movement alpha and beta ERD in sensorimotor and parietal areas is expected as suggested from findings in Babiloni et al. (2008). PFC and/or ACC and parietal clusters are presumed to show activity in the theta and alpha band, respectively (Baumeister et al., 2008).

*Endpoint:* Effects of spectral dynamics are tested by deriving ERSPs and calculating significant spectral deviations from baseline on group level.

### **B.3 To test for movement-related dynamics of effective connectivity between clusters.**

*Expectations:* The literature review revealed no investigation of effective connectivity during golf putting. However, functional connectivity increases between parietal and frontal areas towards the movement initiation in golf putting (Babiloni et al., 2011) and may hence indicate effective connectivity between these areas.

*Endpoint:* ERC is estimated by fitting and validating MVAR models and deriving directional rPDC between all clusters of the defined network. Significant deviations from baseline on group level denotes frequency dependent dynamics of movement related information flow.

By attaining the above outlined specific aims, this work contributes to the application of ICA based EEG analysis of brain network dynamics and therewith depicts a way to map neurophysiological processes related to goal-directed movements. This is done by collectively mapping the individual localization and activity of brain areas and their directed information flow, time-locked to the movement execution. Furthermore, the step towards applying these methods to EEG data, collected during complex movement execution in a real-world setting is made. This work adds to methodological proceedings regarding design and analysis of future studies that investigate group or conditional effects (e.g. of skill level, training, injury, fatigue) on brain network dynamics of sensorimotor control.



## 6 Methods

Two studies using goal-directed precision tasks were conducted to address the previously defined aims. Although both study designs were kept similar, major differences in movement complexity and environmental conditions required specific test procedures. Therefore, both studies are described in individual sections. Due to weather conditions the measurements outside on the putting green, referred to as the golf putt study, was antedated to summer / autumn 2013, followed by the force-pulse study, which took place in January/February 2014. However, the experiments are described from the more controlled laboratory environment of the force-pulse study (section 6.1) to the more complex setting and movement on the golf course (section 6.2). Signal processing as well as statistical procedures are kept similar for both studies and are outlined in sections 6.3 and 6.4 respectively. The studies were conducted according to the Declaration of Helsinki (ethical principles for medical research involving human subjects).

### 6.1 Force pulse study

A force pulse precision task was developed to analyze sensorimotor control processes related to goal-directed movements. More precisely targeted, submaximal, isometric force production in precision grip were assessed in this study. The task demands can be seen as rather low compared to that of a golf putt on the putting green, because it only requires one dimensional movements under a controlled laboratory condition. Except for the movement itself and the setting, the study design was adopted from that of the golf putt study (section 6.2), because acceptable experiment duration in the outside condition was decisive for the number of trials used in both studies.

### 6.1.1 Subject characteristics

For both studies, the same 13 experienced golfers were recruited from two local golf clubs. As this laboratory study was performed after the golf putt study, only ten agreed to participate here. Besides exclusion criteria (records of neurological, physical or mental constraints), the initial inclusion criteria were set as follows:

- gender: male
- handedness: right<sup>1</sup>
- handicap: < 10
- putt direction: left<sup>2</sup>

This ensured sufficient group homogeneity where similar putting skills and therefore well-developed neurophysiological adaptation due to regular training of golf putts can be expected (Jäncke et al., 2009). Due to the combination of handicap, handedness and putt direction, an initially defined range of age was loosened up to be able to recruit more participants. All participants voluntarily agreed to participate in this study and had the right to withdraw from the study at any time without consequences. An overview of the subjects that took part in the force pulse study is listed in table 6.1.

Table 6.1: Force pulse study: Anthropometric description of subjects (N=10).

|                  | min | max | average | standard deviation |
|------------------|-----|-----|---------|--------------------|
| age [a]          | 15  | 62  | 29.5    | 13.26              |
| height [cm]      | 172 | 191 | 184.1   | 5.84               |
| weight [kg]      | 72  | 97  | 82.9    | 7.48               |
| handicap         | 4.8 | 8.7 | 7.26    | 1.32               |
| lateral quotient | 62  | 100 | 83.1    | 12.26              |

---

<sup>1</sup>Handedness is given by the lateral quotient, which ranges from -10 (left handed) to + 10 (right handed) (Oldfield, 1971).

<sup>2</sup>Putting to the left denotes the golfer's positioning to the hole and the resulting direction, in which the ball has to be played. Left means, the golfer's left shoulder faces towards the hole.

### 6.1.2 Task setup

Subjects were seated comfortably in front of a computer screen (19", 640x480 pixel resolution) with a distance of approx. 70 cm. Their right wrist rested on a table, holding a force transducer between thumb and index finger (precision grip). To further standardize the hand posture, a small plastic tube was enclosed by the small, ring and middle finger. Joint angles of the arm and height of the force transducer in relation to the table surface was individually chosen by the subject's statement of comfort. Picture 6.1 illustrates how the force transducer was instructed to be operated.

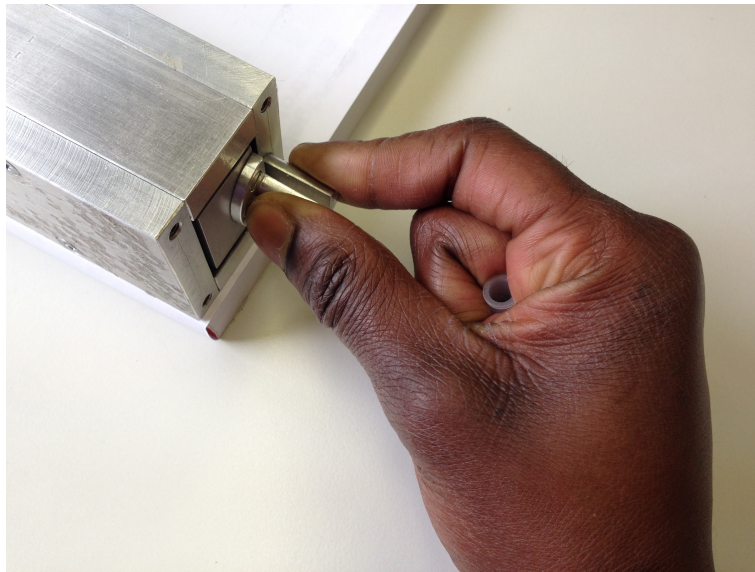


Figure 6.1: The force transducer was operated in precision grip. A small plastic tube was enclosed by small, ring and middle finger to further standardize the hand posture.

### 6.1.3 Task procedure

Prior to test day, all subjects were familiarized with the task environment including laboratory space, the EEG system and the procedure of electrode cap application. The cap size was identified by head circumference. Furthermore, subjects filled out an anthropometric form, as well as the Edinburgh inventory to assess handedness

(Oldfield (1971), see appendix C.1 and C.2). On test day, subjects were first set up with the EEG cap (electrode Cz at center of distance between nasion andinion). After that, the individual maximal voluntary contraction (MVC) was determined to set the target values for the task. This was done in three trials of five seconds with 60 s breaks between each trial. Subjects were instructed to slowly build up the force to prevent irreproducible forces due to initial force pulses. The highest value achieved was taken as 100 %MVC, to which submaximal target forces were related. The whole procedure (force production and breaks) was guided by a rising bar graph on the screen for exact timing. This test was done between EEG cap application and lowering impedances to allow muscular recovery (approx. 30 min) before the actual task began. Subjects then received descriptions of the following procedures. During lowering impedances they were asked to fill out the State-Trait Anxiety Inventory Form (STAI-X1, appendix C.3) to record current mental state (Spielberger et al., 1983). Subsequently, to (1) familiarize subjects with the setup and surroundings, (2) reduce task-specific learning effects and (3) to determine an individual performance level, one block of the actual task was performed. Subjects could then relax for approximately two minutes or ask remaining questions.

The whole task consisted of 10 blocks with 24 trials (8 times each of the 3 forces, = 240 trials) and a 2 min break in-between. The number of trials was chosen according to the limitations of the golf putt study (see details in section 6.2). In each trial, one of three forces, 5, 10 and 15 %MVC, were presented randomly. According to the literature, these forces are common in everyday life, lie in the range of fine motor control (Ehrsson et al., 2001) and should not cause muscle fatigue during the test (Voelcker-Rehage & Alberts, 2005). Each trial starts with the word 'relax' displayed at the center of the black screen for 500 ms to indicate a *relax* period. 2.5 s into the trial, the target force in form of a horizontal line (blue, 3 pixels line width) and the corresponding cue word ('vorne', 'mitte' or 'hinten'; engl. 'short', 'middle' or 'far')<sup>3</sup> was shown (*cue* period). The cue word disappeared after 500 ms. Only the target force remains displayed, centered in either the lower (120 pixels) or upper half (360 pixels) of the screen, or in the absolute center (240 pixels) depending on the current target force (*go* period). Additionally, a target zone of +/- 1 %MVC was marked by two lines under and above the target force. Subjects were then ask to generate a ballistic force pulse to match the target force as exact as possible. The instruction was to generate pulses that could not last for more than 200 ms (onset to peak) and it was explicitly pointed out that forces can be applied at own pace to achieve self-paced motor behavior. Immediate feedback was given in form of another horizontal line (white, 5 pixels line width) that represented the applied force. This line only displays the current highest value detected during each trial, that is, it did not return to lower values when less force was applied during the trial. Triggered by the onset ( $> 0.1N$ ), the force feedback was represented for 3 s. In case the line lay in the target zone, the

---

<sup>3</sup>These were the cues used for the three distances from which subjects had to putt balls in the golf putt study (section 6.2).

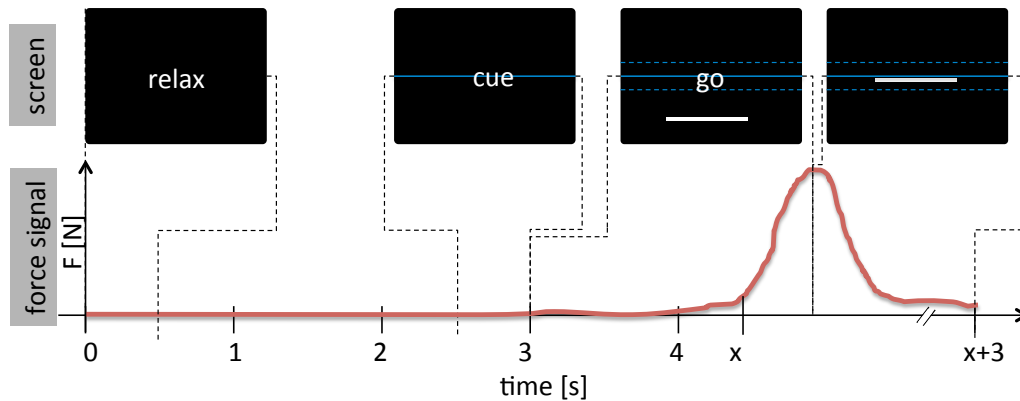


Figure 6.2: Illustration of the force pulse study trial sequence with *relax*, *cue*, and *go* period.

correct force was generated and the trial counted as successful (hit, analogue to a holed golf putt). After that, the screen turned black for 1 s. Figure 6.2 illustrates the sequences (*relax*, *cue*, *go*) and their timing in each trial.

After each block, two visual analogue scales (VAS) were presented, with which the subject was asked to rate his stress level and level of motivation to continue the task (McCormack, Horne, and Sheather (1988), see appendix C.4). Once the last block was completed, the subject was asked to fill out another STAI-X1 questionnaire to record current state of anxiety after the task. The whole task procedure did not exceed more than 90 minutes including cap application (30 minutes), depending on subjects pace in each trial.

#### 6.1.4 Data acquisition and event processing

Figure 6.3 illustrates the principle data acquisition setup used in the force pulse study. Subjects sat in front of a computer screen, holding the force transducer (F), which was positioned on the table. A Field Programmable Gate Array (FPGA, Xilinx XUPV5-LX110T Evaluation Platform) ran the custom-built test software. It read and wrote to and from the weight cell's microcontroller (solid double arrow), ran the MVC test, calculated target forces, and provided visualization of the task procedure (dashed arrow). It also calculated and presented the performance rate at the end of each block. Furthermore, the FPGA send triggers to the EEG system (dotted arrow) at appearance of each cue on the screen so that the time and type of event was available in the EEG data stream. The calibrated force

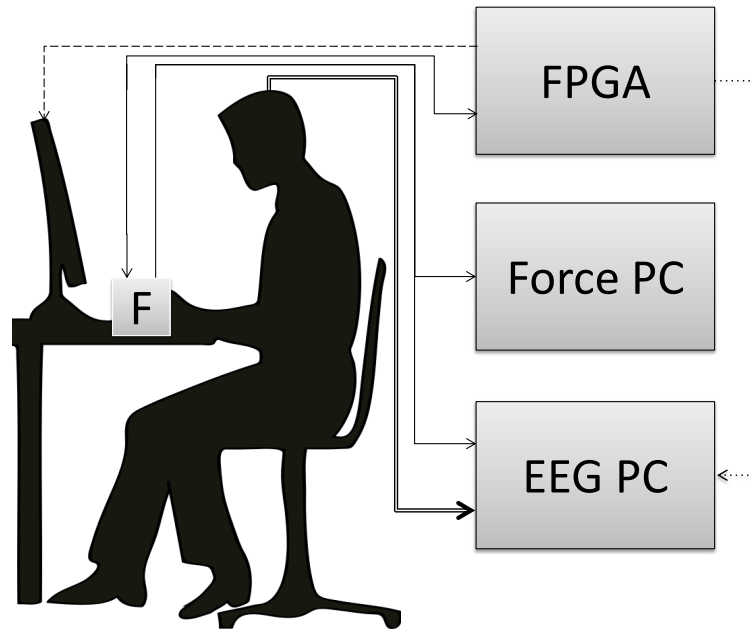


Figure 6.3: Force pulse study: Principle data acquisition setup.

signal (in newtons [N]) was recorded by another computer, while the raw sensor signal was fed into the EEG amplifier (solid right arrows). The double lined arrow in figure 6.3 represents the EEG data stream, picked up by the scalp surface electrodes, amplified, and recorded by the EEG computer. In the following the systems and setting used for force and EEG acquisition are outlined in more detail.

### Force acquisition

A platform load cell (1022-C3-20kg, Soemer), based on the strain gauge measuring principle, was used to detect forces. Its nominal load reaches up to 20 kg with 0.002 % error with a displacement of 0.4 mm, which fulfills the requirements of measuring maximal and submaximal isometric forces produced by humans in precision grip (Mathiowetz et al., 1985). The load cell was attached to a microcontroller (LDU68.1, Soemer) that is used to digitize the signal, convert it to newtons and to perform calibration (tare function). The microcontroller was set to a sample rate of 80 Hz and amplitude resolution was 17 bit with 5 V supply voltage for the strain gauge bridge circuit. No filters were set during recording. Communication to read and write from and to the microcontroller was realized via RS-232 to the FPGA and the additional computer. Technical sheets, with detailed information of each component can be found in appendix D.1 and D.2.

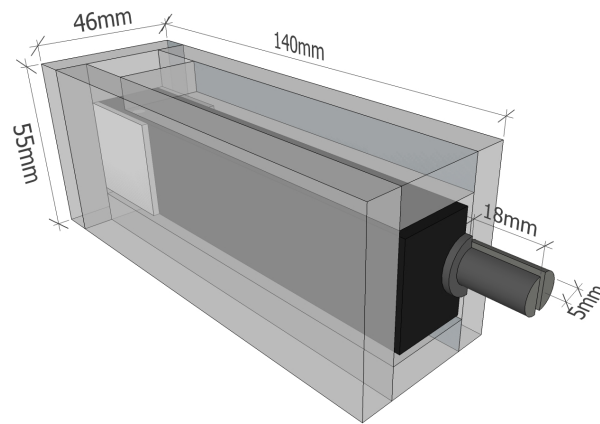


Figure 6.4: Blueprint of the force transducer. The load-cell (black) is mounted on a socket within a steel cage (transparent texture) leaving 2 mm space between the two elements.

The sensor was custom build according to task specific constraints. Figure 6.4 shows the blueprint of the force transducer's buildup, with which one-dimensional forces were registered. The load cell (black) was embedded in an ordinary steel cage (transparent texture), fixed at its rear end (25 mm). This left a 2 mm gap around the load cell. To allow a comfortable pinch grip operation as demonstrated in figure 6.1, the two halves of a pin, 10 mm in diameter, were mounted to the load cell and on the steel case, respectively. The pin's size and the gap between load cell and case added up to a pinch grip width of 12 mm.

## EEG acquisition

EEG acquisition was done using a Neuroscan Synamps RT (Compumedics Neuroscan, USA) amplifier with an extended 10-20-system (Klem et al., 1999) 64 channel electrode cap (QuickCap64, Neuroscan, USA). The electrode's material was sintered Ag/AgCl, which was brought into contact with the skin using Neuroscan's QuickCell system, filled with proprietary liquid electrolyte. Impedances were lowered to  $< 5 \text{ k}\Omega$  at each electrode site. Two additional bipolar channels were used to record horizontal and vertical eye movements. The recording software was SCAN 4.5 (Neuroscan, USA), in which the sampling rate was set to 1 kHz with 24 bit amplitude resolution and a low-pass filter at 200 Hz. The force signal was recorded using a high level input channel without filtering.

### Event processing

In order to synchronize the two force signals, raw force (recorded via the EEG system) and calibrated force (acquired by the additional computer), had to be synchronized. This was done by upsampling the latter to the EEG's sampling rate. Next, the peak of the normalized cross-correlation function of the two signals identified the time lag, with which the signals were shifted. Thus, the calibrated signal with true newton values was aligned with the EEG and imported to the data structure as an additional channel. Two important events of movement were then calculated. The onset of each force pulse was set where the signal reached a value of  $\geq 0.01$  N in each trial and the following maximum was set as the corresponding force peak. It was also checked whether the time from onset to peak was  $\leq 200$  ms. In cases where this time interval was longer, no events were set. These trials did not go into further analysis since they were considered not to be a force pulse, but a rather slow force generation with possible adjustments during execution (Hinder et al., 2010).

## 6.2 Golf putt study

The golf putt study was conducted on a putting green at the golf club Haxterpark<sup>4</sup> GmbH, Paderborn, Germany. It has to be noted that neither subject's that were club members, nor the golf club itself or experimenters gained material or financial benefits from these experiments.

### 6.2.1 Subject characteristics

Table 6.2 characterizes the group subjects that attended the golf putt study. All 13 recruited participants were experienced, male, and right-handed golfers with a handicap of  $< 10$  according to the inclusion criteria outlined in section 6.1.1.

---

<sup>4</sup><http://www.haxterpark.de/>



Table 6.2: Golf putt study: Anthropometric description of subjects (N=13).

|                  | min | max  | average | standard deviation |
|------------------|-----|------|---------|--------------------|
| age [a]          | 15  | 62   | 33.15   | 13.58              |
| height [cm]      | 172 | 194  | 184.31  | 6.02               |
| weight [kg]      | 67  | 100  | 83.23   | 9.38               |
| handicap         | 4.8 | 11.2 | 7.55    | 1.59               |
| lateral quotient | 62  | 100  | 84.77   | 12.23              |

### 6.2.2 Task setup

Depending on the time of the day and sunshine intensity, the specific hole (diameter 108 mm) and putt direction was chosen so that subjects stood faced away from the sun during the task. This was to avoid extreme light changes due to head movements. Similar to the three target forces in the force pulse study, here three putting distances (2.5 m, 3.0 m and 4.0 m from ball to closest edge to the hole) were chosen to avoid habituation (Rankin et al., 2009). The 50% probability to hole-out for professional golfers is at a distance of approx. 7 feet (2.13m, see Figure 6.5) (Fearing et al., 2011). Considering participants performed not one but many putts, longer distances were chosen to presumably achieve an approximate success rate of 50%. In all measurements the same 24 golf balls (Wilson Staff,

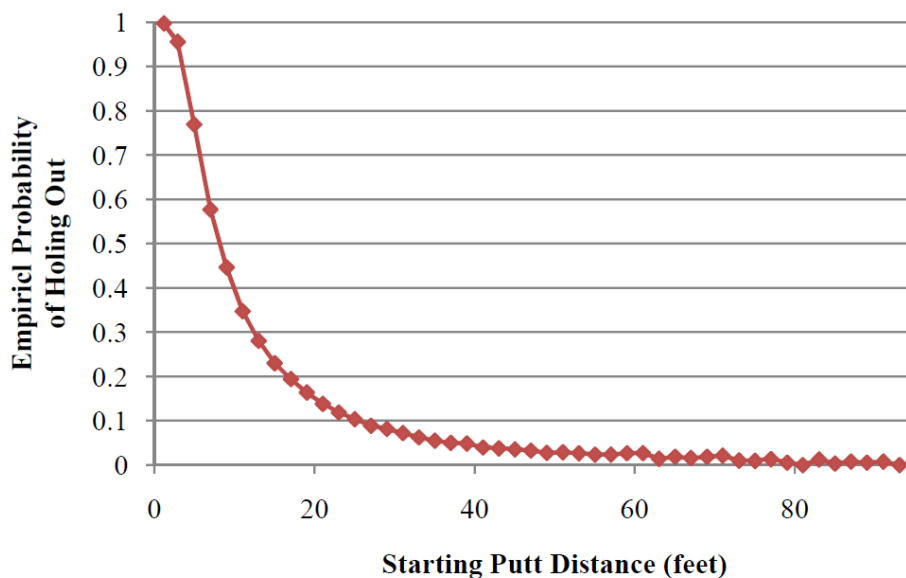
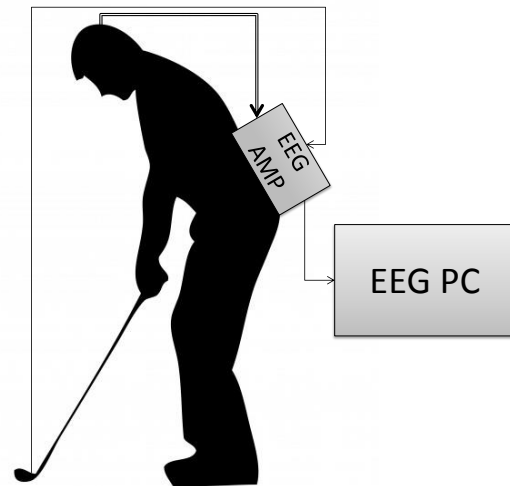


Figure 6.5: Empirical probabilities of holing out plotted over putt distance (Fearing et al., 2011).

DX2 Soft Distance) and putter (Ping Redwood Zing 303ss, 35") were used. An accelerometer was attached to the putter head to track swing phases. Furthermore, the EEG amplifier was positioned at the lower back of subjects, fixated by a belt. From there, one wire (5 m long) connect the amplifier with an EEG recording computer. The investigator and one assistant stayed out of vision during pre-shot routines and putt execution. Figure 6.6(a) shows a picture of the putting situation. Figure 6.6(b) illustrates the principle data acquisition.



(a)



(b)

Figure 6.6: Golf putt study task setup. (a) Exemplary measurement setting. (b) Principle data acquisition setup.

### 6.2.3 Task procedure

At least one day, but not more than a week before test day, subjects were familiarized with test procedures and measurement devices (EEG, putter with accelerometer). EEG cap size was identified by head circumference and an anthropometric form as well as the Edinburgh inventory (Oldfield, 1971) to assess handedness was

filled out. Here, subjects also performed one block of trials without recording. This was done to familiarize subjects with the procedure, reduce task specific learning effects and to establish an initial score of performance.

On test day, subjects were set up with the EEG cap and again received descriptions of the following procedures. During lowering impedances they were asked to fill out the STAI-X1 questionnaire. As in the force pulse study, one block of 24 trials without recordings was performed to accommodate subjects to the specific task. To check signal quality and to allow subjects to get used to the situation, subjects relaxed in a comfortable seating position for five minutes.

Before each putt, one of the three distances was announced randomly. The subject then placed a ball on the specific position (marked by a golf T in the ground, about 20 cm off the supposed trajectories). All subjects were instructed to putt at their own pace and with their individual routines. However, practice swings and green reading (kneeling down) were only allowed between blocks but not before each trial. In case of disruption (noises, gusts of wind, insects, etc.) the trial was aborted and re-initiated. After the ball was putted and came to rest, an assistant measured the distance to the hole in full centimeters and collected the ball from the green.

As in the force pulse study the whole task consists of 10 blocks with 24 trials (8 of each of the 3 distances = 240 trials) and a 2 min break in-between. Following each block two VAS were presented with which the subject was asked to rate his stress level and level of motivation to continue the task (McCormack et al., 1988). Additionally, performance (percentage of successful putts) was presented as feedback of results. Following the test, another STAI-X1 was filled out to record changes of mental state. Including a 30 minute EEG setup procedure and depending on the subjects putting pace, the whole protocol took approximately 150-180 minutes. Pre measurements approved that the total task procedure should not last more than 3 h for several reasons: (1) 240 putts are considerably more than usually performed in a typical training session. Lack of motivation, concentration, physical as well as mental fatigue could affect the results. (2) Depending on the fit, EEG caps may become uncomfortable over time. (3) Depending on weather conditions, electrodes might dry out and introduce impedance drifts. (4) Relatively stable light and weather conditions had to be given throughout each measurement. To ensure enough data for ICA and MVAR model fitting on the one hand, but to avoid the above temporal restrictions on the other, the trial number was set to 240 divided into ten blocks. For comparability, this was transferred to the force pulse study as well.

## 6.2.4 Data acquisition and event processing

The task procedure was not guided or timed by a software as in the laboratory. Therefore, an accelerometer was attached to the putter head to track the stroke patterns and to detect movement onsets. This signal was fed into the EEG amplifier (single arrow in figure 6.6(b)) and recorded along with the EEG (double arrow in figure 6.6(b)). The accelerometer's power supply and wire for signal transmission was routed along the bottom side of the putter's shaft, around the subject's hip into the EEG amplifier. A fixation at the trousers (or belt) ensured disruptive cable sway while leaving enough room for putt movements.

### Acceleration acquisition

The accelerometer (ADLX330, Analogue Devices) was attached to the putter head. The sensor detects static (gravity) and dynamic (motion and shock) acceleration of  $\pm 3$  g in the range of 0.5 Hz up to 1600 Hz with a nonlinearity of  $\pm 0.3$  %. Here, one of three axes was chosen to track the motion. The Y-axis' sensitivity is given with 270 mV/g at its supply voltage of 3 V, which was provided by the EEG amplifier (for more details see D.3). Figure 6.7 shows how the ADLX330's y-axis was aligned with the main putting axis and taped to the putter head to get maximal sensor output caused by the movement. The sensor's position and the color of the tape was chosen, to minimize optical irritation due to unusual appearance. No subject reported major difficulties with this particular setup.

### EEG acquisition

The same EEG system as described in the force pulse study (section 6.1.4) was used here: A SynampsRT with a QuickCap64 and the QuickCell application system (Neuroscan, USA). However, the sampling rate was set to 2 kHz to capture all relevant segments of movement (especially the putter to ball impact) by the accelerometer. Amplitude resolution was also 24 bit and EEG channels were recorded with a low-pass filter at 500 Hz, which was given by the amplifier setup at this sample rate. The high level input channel, to which the accelerometer was attached, was recorded without filtering. Impedances were aimed to be below 5 k $\Omega$  throughout the measurement.



Figure 6.7: Putter-head with ADLX330 accelerometer. Sensor's axis aligned to the main putting direction.

### Event processing

Movement onset and putter to ball impact was determined by processing the accelerometer signal. For this purpose, a semi-automated procedure, based on template matching, was developed. This procedure consists of the following steps:

1. A subject specific time window that covers the putt pattern was chosen as well as the length of the baseline. These adjustments are necessary to handle the variation between subjects.
2. Manual selection of a representative putt pattern with the length of the chosen time window. This was then set as the template.
3. The template was then slid along the acceleration signal and the cross correlation function maximizes where the signals are similar. These template matches were then extracted.
4. Movement onsets were set by sliding a window along each match until the sum of the current mean value and standard deviation was higher than three

- times the baseline's mean. If the standard deviation decreases over time (less acceleration dynamics) the baseline is adapted to the average within this time window.
5. Putter to ball impact was set by determining the highest value within the matching period. The maximal acceleration always occurs when the putter head transfers its energy onto the ball.
  6. Finally, matches were aligned at putter to ball impact and displayed. False positive detections were then deleted manually.

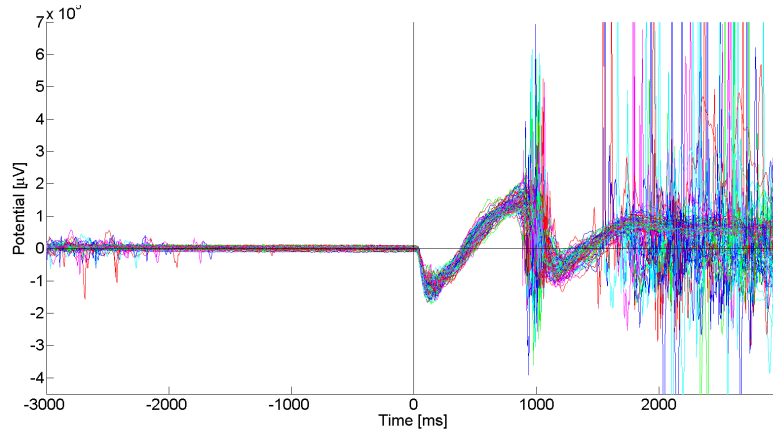


Figure 6.8: Acceleration profiles of 86 putts from one subject aligned to the movement onset. The peaks around 1 s are the putter to ball impacts.

Figure 6.8 shows 86 superimposed acceleration profiles from one subject. The signals are aligned at the movement onset, which was determined by the procedure above. The figure also shows the clear putter to ball impacts around 1 s. The events for onset and time of impact were added to the event structure and saved with the corresponding dataset.

### 6.3 Signal processing

All data processing was done with MATLAB and Statistics Toolbox (Release 2013b, The MathWorks, Inc., Natick, Massachusetts, United States) using functions of the EEGLAB toolbox (vers. 13.1.1) (Delorme & Makeig, 2004) and additional EEGLAB-plugins that are indicated accordingly. Also, study specific differences are pointed out in the corresponding sections. It was stated in section 3.5.3 that ICA and effective connectivity estimation require specific data pre-processing

regarding filter settings. Consequently, signal processing was carried out in two parallel processing streams illustrated in figure 6.9. The ICA specific stream on the left is detailed in the next, the effective connectivity specific stream on the right, in the following section.

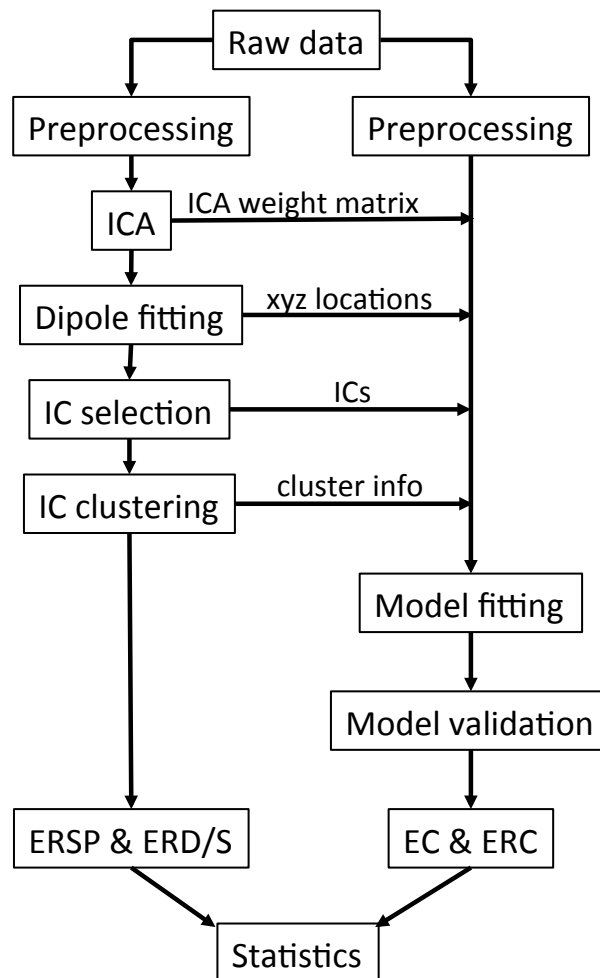


Figure 6.9: The EEG processing pipeline consists of two parallel streams. Left: ICA specific pre-processing. Right: AMVAR modeling specific pre-processing. ICA weights, dipole localizations, IC selection and clustering is derived in the left, but used in both streams.

### 6.3.1 ICA and ERSP specific processing

The following order and parameter settings were specifically adapted for optimal ICA results. Subsequently, ERSP are derived from the resulting ICs.

#### Preprocessing

First, standard locations for the Neuroscan QuickCap64 were loaded for the EEG data. The 3D channel locations, provided by Neuroscan, are listed in D.5. A zero-phase, sinc finite impulse response (FIR) bandpass filter with -6 dB cut-off frequencies at 1 and 49 Hz was then applied to all EEG channels (Widmann & Schröger, 2012; Widmann, 2012). To further remove remaining 50 Hz line noise, an adaptive frequency domain regression technique was applied (Mullen & Miyakoshi, 2011). Subsequently, the data was downsampled to 250 Hz. This was done to save disk space and processing time in the following steps. Artifact contaminated channels, if present, were then identified and deleted by EEG experts. For consistency data was re-referenced to the average reference. Finally, a manual artifact review was carried out, in which segments containing non-stereotypical artifacts were cut out of the time course of the EEG. stereotypical artifacts that can be decomposed by ICA were left in the data.

In the golf putt study, neither the time between trials, nor sequences (*rest*, *cue*, *go*) within each trial could be controlled as in the laboratory. Because of varying duration of pre-shot routines and aborted putts followed by reentering the phase of movement planning, data was segmented from -8 s to 5 s around movement onset after filtering and before ICA. This was done to perform the source separation on EEG content that is related to the task only and undefined periods in between putts could be disregarded.

#### Independent Component Analysis

According to section 3.3.2, AMICA was used to perform source separation. Non-EEG channels (here the imported force signal) were excluded from AMICA processing. Between three and five ICAs were performed until manual artifact rejection didn't improve the decomposition based on judgment of the experienced investigator. Decision criteria included:



- EEG typical frequency content in functional components
- no distinct large amplitude spikes in functional component's time course
- appearance of ICs with dipolar distribution of topographic maps
- consistent IC ranking (in EEGLAB, ICs are in decreasing order of the EEG variance accounted for by each IC)<sup>5</sup>
- no major artifactual activity across several components. That is, no more obvious segments with activity that could not be assigned to a specific source by the algorithm

### Source localization

To assign ICs to an equivalent dipole with 3D coordinates an iterative best-fit procedure was used. For that, a BEM consisting of 3 layers (cortex, skull, skin), derived from the Montreal Neurological Institute (MNI) canonical template brain, was taken as the head model (Oostendorp & van Oosterom, 1989). Channel locations from this model were co-registered with the actual electrode locations that were loaded for the EEG recording. Since the EEG caps were designed according to an extended standard 10-20 system, co-registration could be done by electrode label matching. The used procedures are part of the DIPFIT2-plugin<sup>6</sup> for EEGLAB and are based on a non-linear optimization technique by Scherg (Scherg, 1990): An automated two-step fitting procedure first scans a coarse 3D grid for acceptable starting positions. The consecutive fine fit iteratively finds best fitting equivalent dipoles for each IC. Finally, ICs are manually inspected for bilateral activity distribution and, if present, re-fitted with two symmetric dipoles. An rv-value threshold was set to 15% for ICs to be included in further processing.

### Epoching

Cortical activation in the EEG, related to motor activity, has been reported to be detectable as early as 2 s prior to and 500 ms after the actual movement (see section 4.2.1). Data was segmented -3 s to 2 s relative to the movement onset. This allows time to capture baseline activity, even though epochs will be clipped on both ends due to windowing functions for calculating ERSP and fitting MVAR models. Epochs were then baseline corrected by subtracting the mean value from -3 s to -2 s.

<sup>5</sup>The lower the order of an IC, the more data (neural and/or artifactual) it accounts for.

<sup>6</sup><http://sccn.ucsd.edu/wiki/A08:DIPFIT>, retrieved 8/17/2014

### Component selection

According to the heuristic approaches described in Onton and Makeig (2006) the following modalities of EEG data representation were adducted to identify ICs as either functional or stereotypical artifactual brain components:

- Topographic maps: Functional ICs typically show clear dipolar backprojections onto the scalp as found by (Delorme et al., 2012). In contrast, artifactual IC are often either focally or uniformly distributed over the scalp map.
- Frequency spectra: The clinical relevant frequency range of the EEG lies between 0.3 and 70 Hz (Schomer & Da Silva, 2012). ICs of functional activity show distinct peaks within the frequency bands theta (4-7 Hz), alpha (8-12 Hz) and beta (15-30 Hz) (Shou et al., 2012). The spectrum flattens out towards higher frequencies.
- ERP images (stacking single trial ERPs to obtain a 2D time-trial plot shown in figure 6.10): If event related activity is present, the ERP image reveals whether this is consistent over trials. However, event related dynamics might be frequency specific and thus do not appear as ERP components. Hence, ERP images were an optional criteria, but not necessary.
- Dipole location: The location of equivalent dipoles was used in addition to the previous modalities to approve or enforce the prior set identification.

Figure 6.10 shows the topographic map, the ERP image with ERP and power spectrum of a functional IC from one subject. It shows a smooth dipolar map, event-related activity throughout the trials, but with short artifactual content at the very beginning and around trial 90. The power spectrum shows a clear alpha and beta peak.

### Component clustering

Component clustering was performed on log-transformed mean spectra (3-35 Hz), ERSP images (over the whole epoch time range and also 3-35 Hz) and locations of the equivalent dipoles. The frequency range was chosen to cover the range of theta, alpha and beta frequency bands. In the next step, the chosen measures were reduced to their first ten principle components using PCA. Note, dipole location is inherently limited to three dimensions. In contrast to the default setting

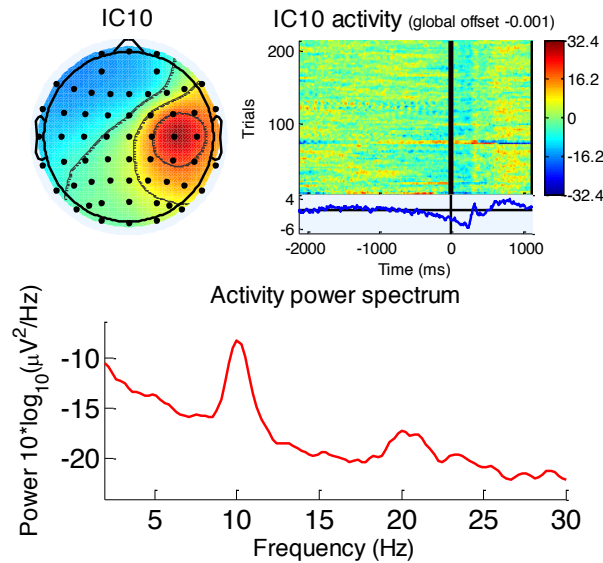


Figure 6.10: Properties of an IC. Top left shows the topographic map by back-projection, top right the ERP image with averaged ERP below (blue line) and bottom graph, the power spectrum.

of EEGLAB's respective clustering function, ERSPs weighting was increased from 1 to a value of 5 whereas dipole location was decreased from 10 to 5. These adjustments were made by considering that (1) a maximum of 64 channels (if not reduced due to artifact contamination) represents a rather sparse coverage of the scalp<sup>7</sup> and (2) neither individual MRIs, nor true electrode locations were available. This can significantly lower the accuracy of source localization, which is why dipole location was downgraded. ERSP is a relatively strong functional measure considering that it combines time and frequency information. The weight for frequency spectra was kept at a value of 1.

With the above described pre-cluster measures, a global distance vector for each component is created, from which an IC-paired distance matrix was constructed. A kmeans algorithm then creates clusters by assigning ICs with distances inside of two standard deviations of the respective cluster. ICs outside this range are assigned to an outlier cluster. The number of clusters to construct was set to the mean number of ICs per subject included in the study, plus the additional outlier cluster. This clustering approach was also used in Gramann, Gwin, et al. (2010), Gramann, Onton, et al. (2010) and T. P. Jung et al. (2001). In cases where two or more ICs from the same subject were assigned in one cluster, a two dimensional correlation (time, frequency) between the ERSP image of each of these ICs with the mean ERSP image of the remaining cluster ICs is calculated. The one IC with the highest correlation within  $\pm 50$  ms and  $\pm 2$  Hz was kept in the cluster. Others

<sup>7</sup>Note: For example, a study of Gramann et. al weighted dipole location with a factor of 25 (Gramann, Gwin, et al., 2010). However, this work was done with 248 channel recordings, which makes dipole location more reliable than it can be assumed here.

were reassigned to the outlier cluster so that at most one IC per subject was left in each cluster. Clusters, to which less than half of the subjects contributed, were left out of further analysis.

### **ERSP and ERD/S**

ERSP was used as one measure to cluster ICs, but it also represents the central measure for time-frequency resolved dynamics of activity in individual brain areas. ERSP was calculated by linearly increasing wavelet cycles with a factor 0.8 from 3 Hz up to the nyquist frequency of 125 Hz. The baseline limits were set to -3 s to -2 s as previously stated. The resulting decomposition dimensions were set to 200 time points (time resolution  $\Delta t = 20$  ms) and 100 frequency values (frequency resolution  $\Delta f = 0.25$  Hz) for the given range.

From investigating the time-frequency distribution of the ERSP images, distinct spectral band dynamics become obvious (Makeig, Delorme, et al., 2004). Averaging the time courses for these bands, generates a single time course to observe classical ERD/S. Frequency bands were calculated as theta from 4-7 Hz, alpha from 8-12 Hz and beta from 15-25 Hz. These were plotted in time-ERD/S graphs allowing the display of data variances.

### **6.3.2 Effective connectivity and ERC specific processing**

The estimation of effective connectivity was done on the selected ICs after clustering by using functions of SIFT (v.1.33, Delorme et al. (2011)). This procedure requires deliberate parameter settings, which will be outlined in the following sections. As mentioned before, the processing stream is parallel to the previous steps and starts from raw data level.

#### **Preprocessing**

Data was high-pass filtered with a zero-phase, sinc FIR filter with -6 dB and 0.1 Hz cut-off frequency (Widmann & Schröger, 2012; Widmann, 2012). Again, 50 Hz line noise was reduced by adaptive frequency domain regression (Mullen & Miyakoshi, 2011). After that, the same artifactual channels and segments of

data that were cut out in the previous described ICA processing stream, were also excluded from each dataset here. Then, the unmixing matrix from the ICA that was obtained before, was applied to the current data to get the same decomposition but applied to the less filtered data. 3D source localization was performed as described above (6.3.1) and epochs were created from -2.125 s to 1.125 s. Next, a least-squares fit detrending method was used to remove slow drifts from each epoch while keeping causal relations intact. Data was also down-sampled to 125 Hz, which still allows frequency observations up to about 60 Hz, while reducing the amount of spectral information to be modeled by a factor of two. Finally, temporal and ensemble normalization was applied.

To analyze network dynamics at group level, only subjects that contributed to all chosen clusters, were included in effective connectivity analysis. This is also important, so that models can be fitted with equal input variables.

### **Model fitting**

MVAR models were estimated using the Viera-Morf algorithm (evaluated in (Schlögl & Supp, 2006)) with a window size of 0.3 s and 0.01 s step size. This window length makes local stationarity more likely, allows a maximum component interaction lag  $\tau$  of 0.3 s and spectral content as low as about 3 Hz can be modeled. To achieve comparable models, the model order was chosen by the mean model order over datasets, which was suggested for each case by the Hannan-Quinn criterion (Mullen & Miyakoshi, 2011). Hence, a model order of  $p=10$  was chosen to fit the MVAR models for each dataset with respective ICs.

### **Model validation**

Model validation consists of three criteria: (1) Check for statistical whiteness of residuals that are not explained by the model, (2) a consistency check and (3) the model stability (see section 3.5.4). The whole data range was tested for whiteness using a significance threshold of  $p \leq 0.05$  with the Ljung-Box, Box-Pierce, and Li-McLeod multivariate portmanteau tests as well as with a test for correlation (ACF). Only datasets with models that passed all three checks for all time windows were included in further analysis.

## Connectivity estimation

rPDC was used to estimate the directional causal influences between all selected ICs. First, this measure is robust against deviances from zero mean within a time window (relevant for time normalization (Mullen & Miyakoshi, 2011)) and second, it allows direct comparison of information flow between time series of different scales (e.g. across subjects) (Mullen, Delorme, et al., 2010; Schelter et al., 2009). By averaging the time courses of specific frequency bands (theta, 4-7 Hz; alpha, 8-12 Hz; beta, 15-25 Hz) from the 2-dimensional connectivity images, a measure of ERC is obtained.

## 6.4 Statistical procedures

Statistical tests were conducted using SPSS Statistics for Windows (Version 22.0. Armonk, NY: IBM Corp.) for task performance and psychometric measures, and MATLAB and Statistics Toolbox (Release 2013b, The MathWorks, Inc., Natick, Massachusetts, United States) for EEG data analysis.

### 6.4.1 Task performance and psychometric measures

Task performance was measured by the success rate in each block by means of correctly produced forces and holed balls respectively in relation to all 24 trials (% hits). Descriptive statistics are given for the group's mean and standard deviation per block and the overall mean for all blocks. Furthermore % hits from block 1 and 10 were tested for difference using a two-sided paired t-test ( $p \leq 0.05$ ). Psychometric measures, STAI-X1 and VAS (for stress and motivation) from before (pre) and after (post) test procedures were analyzed to check for significant changes. To test for normal distribution of variables, the Shapiro-Wilks test was used due to its validity for small sample sizes (Razali & Wah, 2011). In case data were normally distributed, pre and post measurements were tested for significant differences by a two-sided paired t-test. The Wilcoxon signed rank test was applied as a non-parametric test for significances in the case of non-gaussian distribution of variables. The significance level was set to  $p \leq 0.05$ .

T-tests are reported by  $t$ -value with the degrees of freedom ( $df$ ), significance  $p$  and the effect size  $r$  calculated by  $r = \sqrt{\frac{t^2}{t^2 + df}}$ . Results from the Wilcoxon test are presented by the  $z$ -value, significance  $p$  and the effect size  $r$  calculated by  $r = \frac{z}{\sqrt{N}}$ , where  $N$  denotes the number of observations (Field, 2009).

### 6.4.2 EEG data

IC clustering results are displayed by (1) overview of subject's ICs contributing to each cluster, (2) subject's estimated dipole localization and the cluster centroid (mean location) projected into a standard MRI brain scan image, and (3) the cluster ERSP images masked by significant ( $p \leq 0.05$ ) baseline deviations. Using the Tailairach Client software (Lancaster et al., 2000) the nearest structures of gray matter to the dipole locations are identified as BAs. However, the relation to BAs is speculative, because the inverse problem of EEG source reconstruction does not allow definite conclusions about the true origin in 3D coordinates, especially here, where clustering weights for dipoles was reduced and instead patterns in the functional measures ERSP were enhanced. Thus, these assignments can at most be seen as indicators for a possible association with specific brain anatomical structures, but are further verified by functional measures like the ERSP and comparison with according findings from the literature.

To approximate the true distribution of time-frequency representations for both ERSPs and ERC, nonparametric surrogate statistical methods were used. The data of each subject was baseline corrected by subtracting the mean of the pre-defined time period (ERSPs: -3 to -2 s before onset, ERC: -2.125 to -1.5 s before onset). Then a permutational one-sample paired t-test was conducted against zero to test for significant deviations relative to the baseline. The surrogate distribution was generated by 1000 permutations. According to (Manly, 1997), this gives an adequate distribution to test at a significance level of  $p \leq 0.05$ . For each sample of the time-frequency distribution an individual t-test is performed. To correct for multiple comparison,  $p$ -values are adjusted by the BH-FDR procedure (Benjamini & Hochberg, 1995). However, false detection rate (FDR) correction is also known to be rather conservative and might diminish valuable information (Kim & van de Wiel, 2008). For the sake of the exploratory nature of this work, FDR correction was not applied to two-dimensional ERSP and ERC time-frequency images. However, BH-FDR was applied to the 1-dimensional time-courses of ERD/S. In favor of clarity, only significant tests are indicated graphically instead of sample-wise exact  $p$ -value plots. This, along with all relevant information to assess results, will be reported in detail in the following chapter.





# 7 Results

Precondition measures were used in both studies to quantify data quality and drop-out rates, as well as to record psychometric and behavioral data. Firstly, each section outlines these measures. Then, for each study, EEG results are presented according to the specific aims A and B. IC clustering was based on source localization substantiated by ERSPs (specific aims A.1, B.1). This is followed by results of frequency specific ERD/S denoting network activities (specific aims A.2, B.2) and its connectivity, measured by ERC (specific aims A.3, B.3).

## 7.1 Force pulse study

### 7.1.1 Precondition measures

#### Drop-outs

Nine out of ten subjects were included in the ERSP and ERD/S analysis as ICs of one subject did not appear in any of the generated clusters. A detailed inspection found that 74 force pulses were longer than the limit of 200 ms and 92 trials were lost additionally due to artifacts, leaving 74 remaining trials for analysis. Notably, this participant was the group's oldest (62 a, see table 6.1) and was subsequently excluded.

Not all of the nine subjects showed an IC in each of the selected clusters. To maximize the number of observed nodes while retaining as many subjects as possible in the study, one cluster was omitted and two further subjects excluded in this exploratory approach. Subsequently, ERC was estimated for seven subjects.

### Psychometric measures

VAS and STAI-X1 were used to keep track of possible changes of mental states. However, no differences were found for the STAI-X1 ( $t(8) = -1.037$ ,  $p = 0.330$ ,  $r = 0.344$ , two-sided t-test), motivation (VAS,  $t(8) = 0.641$ ,  $p = 0.539$ ,  $r = 0.221$ , two-sided t-test) and stress (VAS,  $z = -0.561$ ,  $p = 0.575$ ,  $r = -0.132$ , Wilcoxon signed rank test), measured before and after the test. Mean STAI-X1 scores were  $32.250 \pm 4.768$  (possible values: 0 - 100), whereas VAS for stress was denoted with  $15.427 \pm 12.629\%$  and for motivation with  $86.827 \pm 9.204\%$  on average over all blocks.

### Task performance

Figure 7.1 provides an overview of the task performance achieved for the force pulse task. The group's mean success rate was  $38.208 \pm 4.415\%$  over all blocks (red line) with no trend for improvement or decrease in performance apparent. No significant changes from first to tenth block were found ( $t(8) = -1.358$ ,  $p = 0.212$ ,  $r = 0.433$ , two-sided t-test).

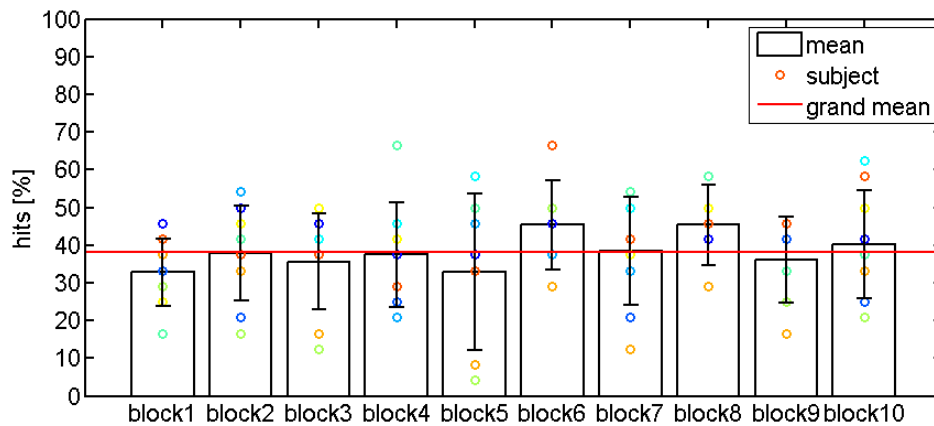


Figure 7.1: Task performance force pulse study (N=9). Circles indicate single subject performance [%hits] in each block. Identical performances are superimposed and may appear as one subject.

## EEG data quality

240 trials were performed by each subject. Due to artifacts and force pulses longer than 200 ms, the number of trials that were used for analysis were reduced (mean:  $18.889 \pm 3.820$ , min=16, max=20 of 24 trials per block). Rejected epochs were evenly distributed throughout the blocks. Consequently, an average of  $188.9 \pm 38.197$  trials from each subject were included for analysis.

The average number of channels left after rejection was  $62 \pm 2.517$  out of the measured 64. Since ICA was performed on continuous data before epoching, the required data points for applying ICA were sufficient for all subjects. For the subject with the lowest number of remaining trials (120) and 406 sample points in each epoch, the available amount of data points were 48720. This exceeded the required number of data points for ICA as well as the suggested  $10M^2p = 10 \cdot 5^2 \cdot 10 = 2500$  sample points for MVAR modeling.

### 7.1.2 Network localization

K-means clustering revealed eight functional clusters. However, only six of these consisted of ICs from six or more subjects (presumably labeled *frontal*, *motorL*, *motorR*, *tempL*, *tempR* and *parietalR*) and were selected for further analysis as can be seen from table 7.1.

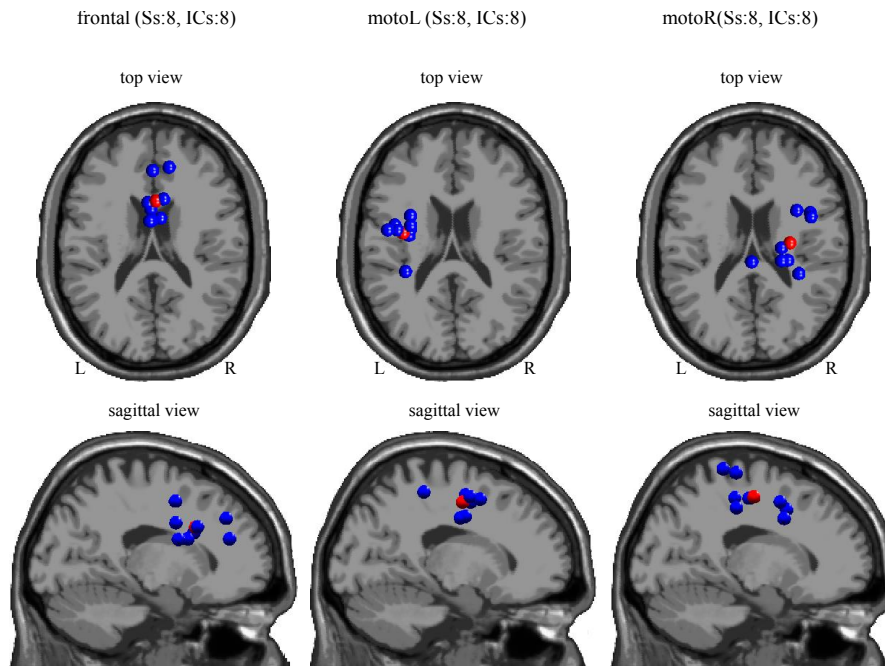
Table 7.1: Force pulse study: Identified independent components of each subject (indicated by x).

| subject | frontal | motoL | motorR | tempL | tempR | parietalR | parietalL | occipital |
|---------|---------|-------|--------|-------|-------|-----------|-----------|-----------|
| 1       | x       | x     | x      | x     | x     | x         | x         | x         |
| 2       | x       | x     | .      | x     | x     | x         | x         | .         |
| 3       | x       | x     | x      | x     | x     | x         | .         | x         |
| 4       | x       | .     | x      | x     | x     | x         | .         | x         |
| 5       | x       | .     | x      | x     | .     | x         | .         | .         |
| 6       | x       | x     | x      | x     | x     | x         | x         | .         |
| 7       | x       | x     | x      | x     | x     | x         | x         | x         |
| 8       | x       | x     | x      | x     | .     | x         | .         | .         |
| 9       | x       | x     | x      | x     | .     | x         | x         | x         |

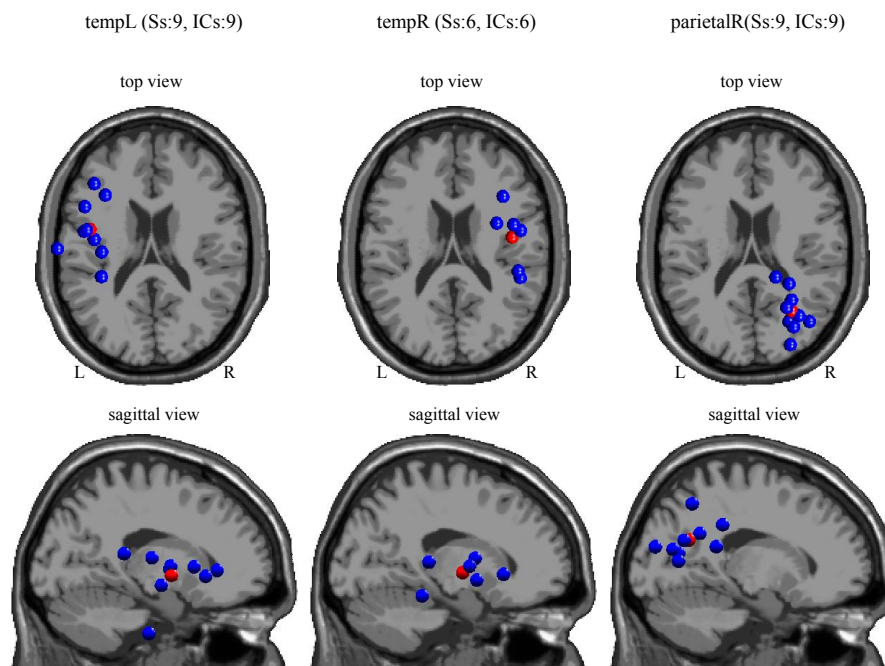
### Equivalent dipole locations

Figure 7.2(a) and 7.2(b) show the equivalent dipole locations of each subject (blue) as well as the respective centroid (mean location in red) for each cluster projected into a standard MRI brain scan image. Clusters were assigned to and labeled after brain lobes according to each cluster centroid's location (frontal, temporal, motor, parietal). An 'R' or 'L' indicates the left or right lateralization. Cluster *frontal*'s mean source origin is located at (x: 2 mm, y: 17 mm, z: 26 mm) of the Talairach head model. This location is closest to BA 24, 32 and 33, which form parts of the ACC. *MotoL* (x:-36 mm, y: -5 mm, z: 44 mm) and *motoR* (x: 27 mm,y: -12 mm, z: 48 mm) clusters are both found to be closest to their lateral counterparts of BA 6 and 4. Both clusters assigned to the lateral temporal lobes (*tempL* - x: -44 mm, y: -2 mm z: -2 mm; *tempR* - x: 43 mm, y: -7 mm, z: -1 mm) can be related to BA 13 (insular) and 22. *TempL* was also found to be close to BA 21 and 38 according to the Talairach client software. The parietal located cluster *parietalR* (x: 29 mm, y: -59 mm, z: 24 mm) lies close to BA 39 in transition to the occipital and temporal lobes.

However, these assignments must be seen in light of the inverse problem of EEG source localization. Thus functional measures by means of ERSP were used in addition.



(a)



(b)

Figure 7.2: Equivalent cluster dipoles in the force pulse study projected into a standard MRI scan (top row: top view, bottom row: sagittal view). In blue: subject dipoles, red: centroids. Labels indicate presumed origin of clusters with number of contributing subjects and ICs.

**ERSP**

Cluster ERSPs showed time and frequency specific dynamics relative to the baseline in all selected clusters (figure 7.3). The dashed line at 0 ms indicates the movement onset, red colors show an increase of power spectral density (in dB) relative to the given baseline, while blue colors show a respective decrease in power. The plots are masked by the significant threshold of  $p \leq 0.05$ . All non-significant values are set to zero (green).

Cluster *frontal* (figure 7.3, top left) is represented by eight subjects consisting of an average of 147 trials. It shows a clear burst peaking approximately at 500 ms after movement onset and a center frequency of 6 Hz (theta band). This activity is also noticeable in all other clusters except *parietalR*.

Both, left and right motor clusters (each from eight subjects and 157/148 trials on average) exhibit ERD starting from about -1500 ms until 500 - 1000 ms around frequencies of 10 and also 20 Hz, reflecting alpha and beta band activity. Furthermore, beta power increases (ERS) at 700 ms in cluster *motoL*.

Lateral temporal cluster's ERSP images differ remarkably: *TempL* (nine subjects with 169 trials on average) shows an increase in power from -1000 ms to 600 ms, peaking at 250 ms after movement onset around 11 Hz (alpha band). In contrast, *tempR* decreases around this frequency from 500 ms onwards. The latter cluster consists of ICs from six subjects with an average of 145 trials.

The main deviations from baseline level for cluster *parietalR* occur in broad alpha frequencies around 10 Hz. Temporally, the desynchronization spans from about 1500 ms before initial force generation throughout the movement until about 1000 ms. Figure 7.3, bottom right shows the right parietal cluster, to which nine subjects contribute with an average of 169 trials.

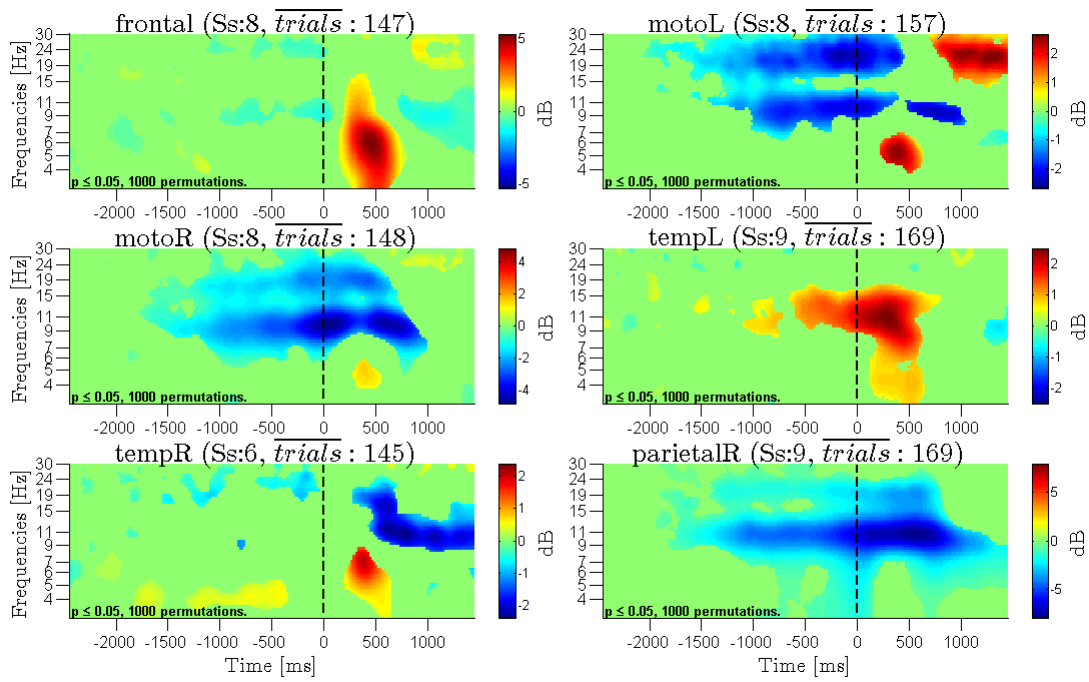


Figure 7.3: Cluster ERSP of the force pulse study. Images show the mean time-frequency plots of each cluster labeled by its presumed origin. Ss denotes the number of contributing subjects, and  $\overline{trials}$  the average number of trials per subject.

### 7.1.3 Network activity

Theta, alpha, and beta ERD/S time courses over the epoch range are plotted in the following figures (averaged time course in blue with standard deviation in light blue). Green bars indicate periods of significant deviations from the baseline. Figures also indicate the number of permutations and BH-FDR corrected  $p$  values. The following reports only significant baseline deviations in time [ms] and amplitude [dB] with a probability of the respective  $p$ -values in each cluster and frequency band.

Theta activity of the frontal cluster (figure 7.4, top left) bursts up to 4.72 dB between 200 and 700 ms. The right temporal cluster (figure 7.4, bottom left) also shows a smaller increase in theta activity by 1.28 dB, which becomes significant between 250 and 540 ms. A decrease down to -0.78 dB and -2.21 dB from -750 to -400 ms and from -260 to -150 ms respectively occurs in the right parietal cluster (figure 7.4, bottom right). After a recovery around movement onset, theta power decreases again from 560 ms onwards until the end of the epoch by up to -1.47 dB.

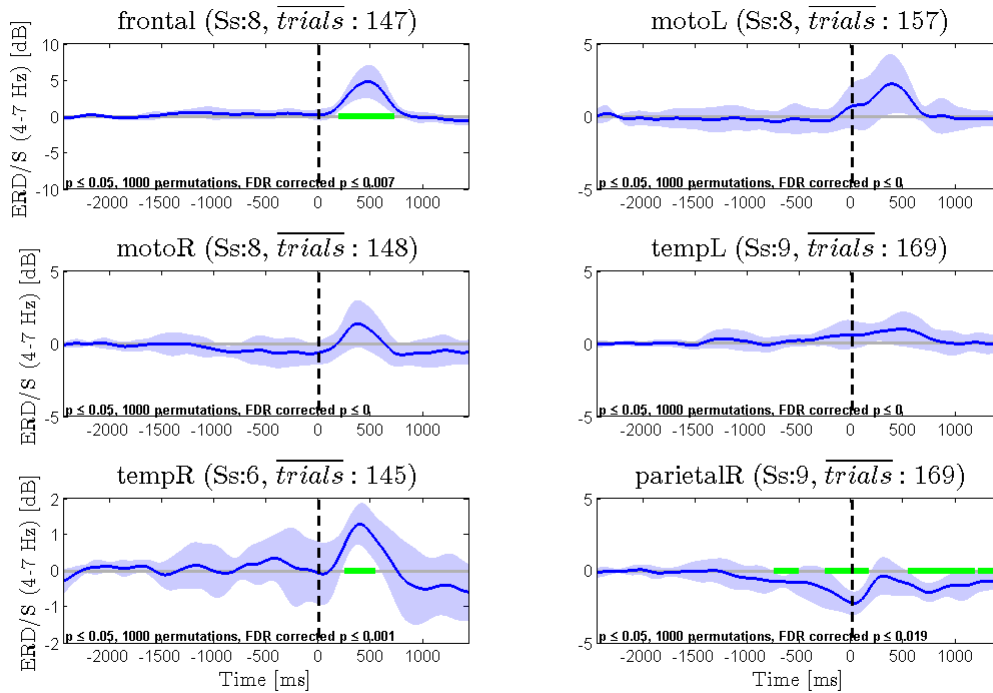


Figure 7.4: Cluster theta ERD/S in the force pulse study. Group mean (blue) with standard deviations (light blue) and significant deviation from baseline (green) with BH-FDR corrected  $p$ -values.



Figure 7.5 shows the dynamics of alpha power in all six clusters. Frontal alpha (top left) increases significantly from 300 to 500 ms, peaking with 2.57 dB and decreases from 900 ms onwards down to -0.94 dB below baseline level. Left and right motor clusters denote a decrease in alpha power. Notably, this is weaker for left lateral (significant with -1.73 dB from -900 to -700 ms and -1.78 dB from -20 to 150 ms) than for the right lateral motor cluster, where the desynchronization becomes significant from as early as -1150 ms prior onset to 850 ms post-movement onset, peaking more than twice as strong as its lateral counterpart with -4.12 dB. In contrast to all other clusters, the left temporal cluster (middle right in figure 7.5) shows an increase of alpha power by up to 2.22 dB between 200 and 500 ms. Right temporal alpha decreases from 700 ms onwards throughout the epoch by up to -1.89 dB. Alpha power in *parietalR* decreases by as much as -6.54 dB at 700 ms. Significant alpha desynchronization starts -1900 ms before onset and recovers to baseline level at 1300 ms (figure 7.5, bottom right).

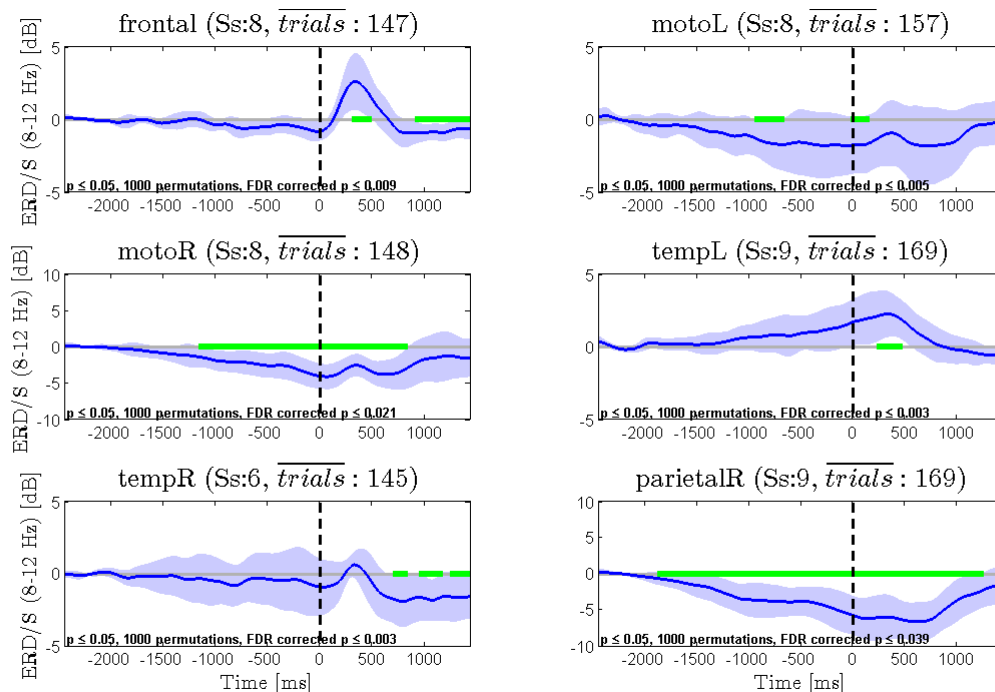


Figure 7.5: Cluster alpha ERD/S in the force pulse study. Group mean (blue) with standard deviations (light blue) and significant deviation from baseline (green) with BH-FDR corrected  $p$ -values.

Beta ERD/S shows significant dynamics in four of the six clusters as shown in figure 7.6. The left motor cluster (top right) shows a decrease in beta power as early as -1900 ms, peaking at movement onset with -1.84 dB and returning to baseline level at 380 ms. After that, beta power increases up to 2.01 dB from 900 until end of the epoch. The right motor cluster also decreases down to -2.12 db relative to the baseline between -1600 and 600 ms. Beta power in the right temporal cluster decreases from -1800 ms, sparsely significant as indicated by the

interrupted green bars in the bottom left plot of figure 7.6, and peaks between 400 and 700 ms with -1.4 dB. Finally, the right parietal cluster, decreases over a time period of -1800 to 800 ms, peaking at 500 - 600 ms after movement onset with -3.25 dB (figure 7.6, bottom right).

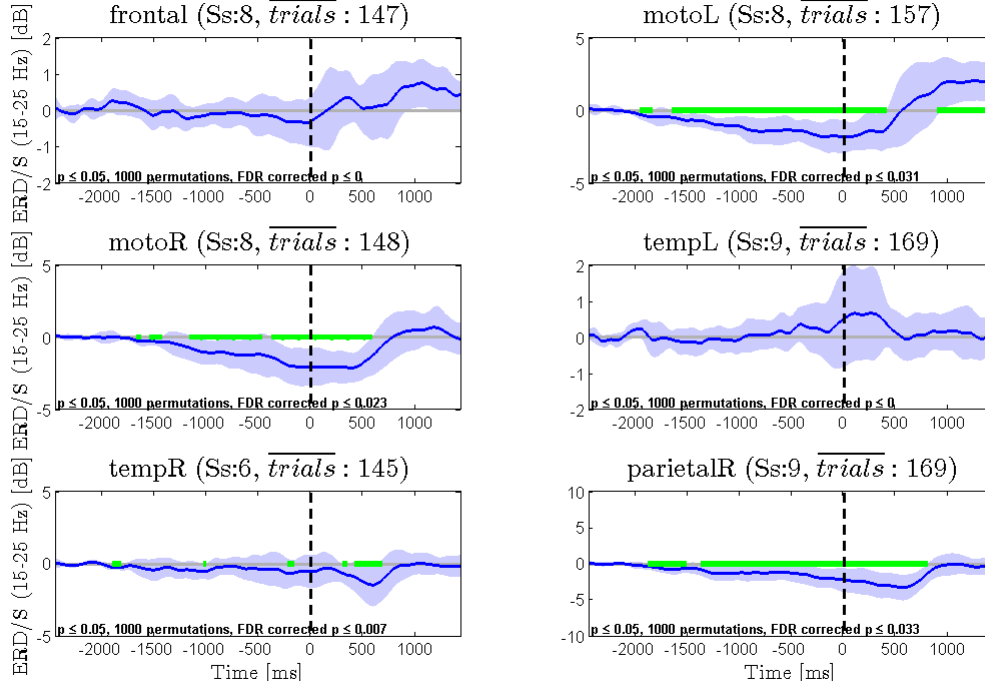


Figure 7.6: Cluster beta ERD/S in the force pulse study. Group mean (blue) with standard deviations (light blue) and significant deviation from baseline (green) with BH-FDR corrected  $p$ -values.

### 7.1.4 Network connectivity

Effective connectivity by means of ERC was estimated using a network of five nodes (*frontal*, *motorR*, *motorL*, *parietalR* and *tempL*) by calculating their rPDC. Figure 7.7 illustrates the whole connectivity grid with the bidirectional time-frequency images for each pair of clusters. From the grid it can be seen that connectivity dynamics between the frontal and both motor clusters exist. However, due to scaling and hence partly weakly colored perturbations, relevant results may be overseen. Frequency bands (theta (4-7 Hz), alpha (8-12 Hz) and beta (15-25 Hz)) were created from the connectivity time-frequency images, providing a measure for frequency specific ERC. Results of node pairs with prominent significant causal dependencies are shown in this section (the whole set of ERC between remaining nodes can be found in appendix B.2). However, using the BH-FDR

correction for multiple comparison (5 nodes, 2 directions and 370 t-tests each), no significant deviations from baseline level were found. Results are shown without FDR correction. The following reports only significant baseline deviations in time [ms] and amplitude [rPDC] with a probability of  $p \leq 0.05$  in each node and frequency band.

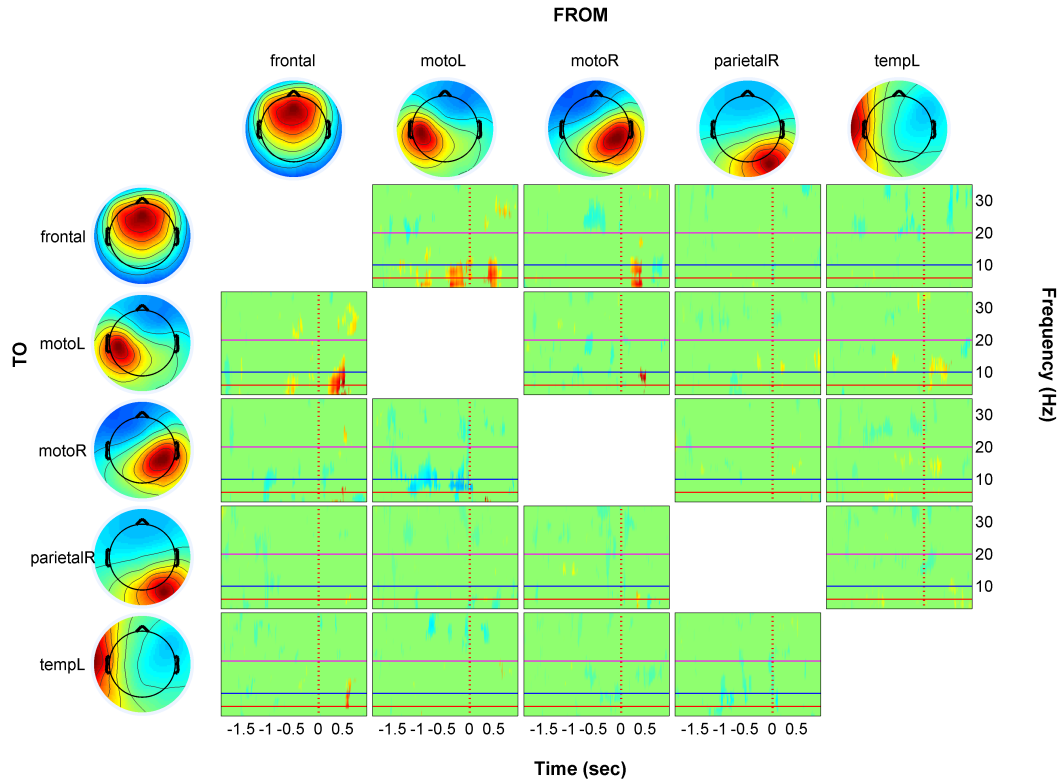


Figure 7.7: Force pulse study time-frequency connectivity grid of rPDC. Information flow from clusters, shown as topographic maps, in the top row to clusters in columns. For each direction and combination of clusters, one time-frequency connectivity image is displayed. Values shown are masked by permutational paired t-tests with 1000 samples for  $p \leq 0.05$ . Warm (yellow, red) colors show increase of rPDC relative to baseline, cold (blue) colors indicate a decrease.

Figure 7.8 shows the time courses of theta ERC from and to the frontal cluster with (a) left motor cluster and (b) right motor cluster. The green bars indicate time-periods of significant deviation from the baseline based on the surrogate statistics, while light blue areas indicate standard deviations. The dashed line at time zero, marks the movement onset. In (a), significant information flow is alternating between frontal and left motor cluster, starting from the latter at -1150 ms before movement onset beginning with causal dependence of *motoL* over *frontal*. Post onset, both clusters show an increase of rPDC between 200 - 700 ms after movement onset. ERC between frontal and right lateral motor clusters also shows

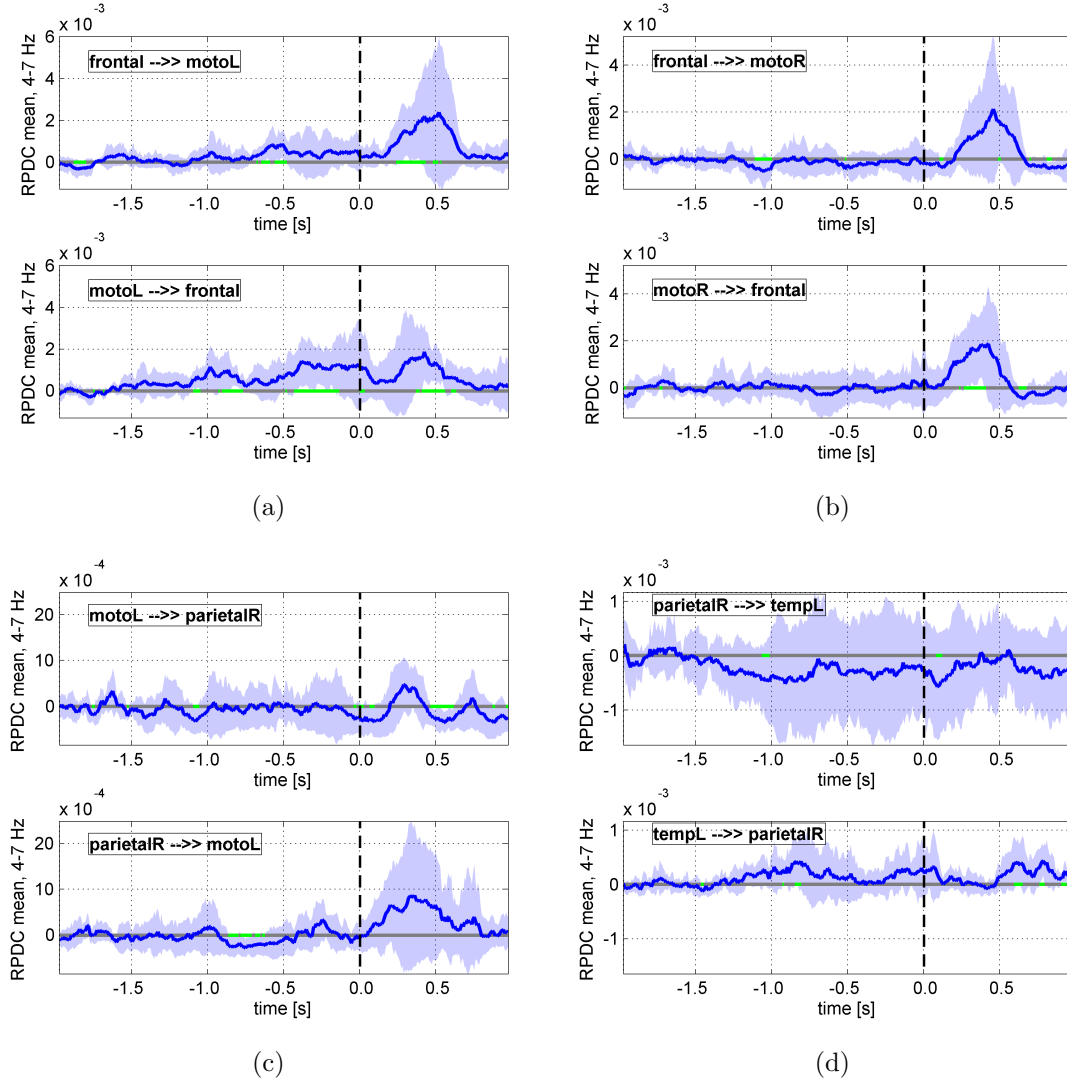


Figure 7.8: Cluster theta ERC [rPDC] in force pulse study. Group mean rPDC (blue) with standard deviation (light blue) and significant deviations from the baseline (green). (a) *frontal* to *motoL*, (b) *frontal* to *motoR*, (c) *motoL* to *parietalR* and (d) *parietalR* to *tempL* and back.

this increase of rPDC in both directions between 200 and 700 ms. A consecutive period of time, where this is significant spans from 250 to 400 ms for the lower subplot (*motoR* to *frontal*, figure 7.8(b)).

Dynamics in information flow from right lateral PPC to left motor area occur between -800 and -600 ms. Following the movement onset, dynamics appear bidirectional but only significant from *motoL* to *parietalR* (figure 7.8(c)). Information flow from right PPC to left temporal cluster appears to decrease from -1500 ms during the pre onset period. However, this is not significant (figure 7.8(d)). In contrast, causal dependencies increase in the counter direction between these nodes

in periods before and after movement onset.

Figure 7.9(a-b) display alpha ERC from frontal to both motor clusters. *Frontal* only shows considerable increase of rPDC following the onset between 250 and 500 ms towards the left motor cluster. Additionally, the opposite direction shows positive valued fluctuations before movement onset, significant between -1400 and -750 ms and from -300 to 20 ms. In (b), an alpha burst around 500 ms is noticeable, but not statistically significant from *frontal* to *motoR*. Instead pre-onset fluctuation decreases in alpha ERC from frontal to right lateral motor cluster from -1050 to -800 ms and shortly after onset around 175 ms. The bottom subplot of (b) reveals a clear increase of rPDC from 200 to 350 ms, which then decreases below baseline level between 700 and 800 ms.

Figure 7.9 denotes alpha ERC between (c) *motoL* and *motoR*, (d) *motoL* and *tempL* and (e) *parietalR* and *tempL*, which showed statistically relevant fluctuations throughout the epochs. The top subplot of (c) denotes a decrease throughout the pre-onset period until 50 ms into the movement, which is significant between -1300 and 0 ms. A following increase above baseline level, cannot be statistically affirmed. Information flow from *motoR* to *motoL* in contrast does show an increase from 200 to 800 ms, becoming significant from 400 - 500 ms. *TempL* shows an increased ERC towards *motoL* from 100 to 500 ms as denoted by (d), but no communication was detected in the opposite direction. Due to large standard deviation within alpha rPDC from *parietalR* to *tempL*, the decrease of information flow throughout pre-onset period and 300 ms post-movement only show sparse significances between -1000 and -500 ms, as well as 0 and 150 ms. The respective bottom subplot, reveals alpha ERC from *tempL* to *parietalR* between 500 and 700 ms.

Within the beta band, only *tempL* showed significant information flow towards the frontal cluster as denoted by figure 7.10(a), bottom subplot. In this direction, rPDC fluctuates around baseline level and becomes significant for less information flow within the time periods from -1500 to -1200 ms and -650 to 100 ms. Even though the opposite direction (top subplot) shows a prominent increase of rPDC from 500 to 800 ms, this cannot be statistically affirmed. Finally, figure 7.10(b) denotes significant periods of bidirectional rPDC decrease between left and right motor clusters relative to baseline level prior to movement onset. No other cluster pairs showed clear significant patterns of ERC.

## 7. RESULTS

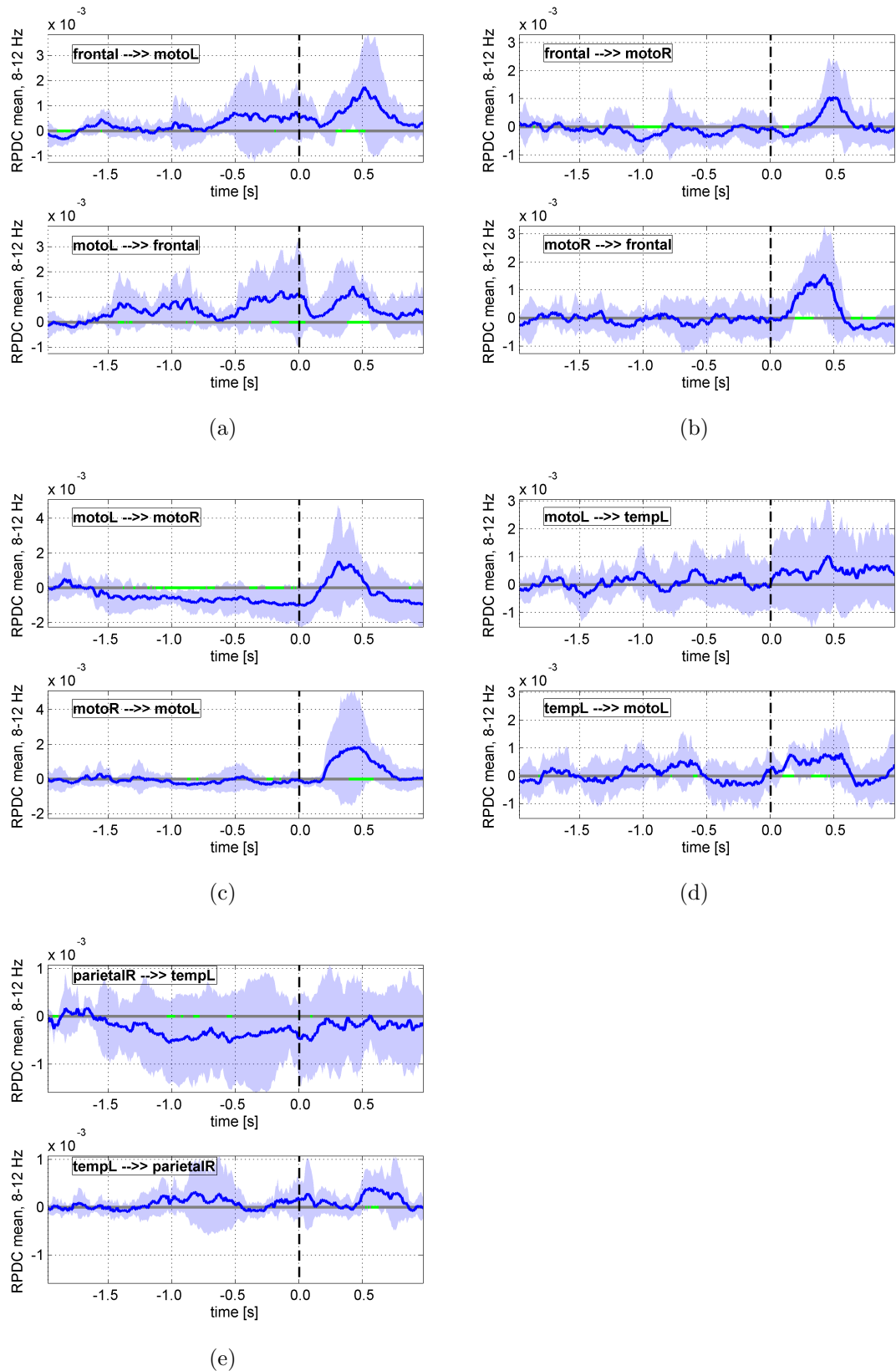


Figure 7.9: Cluster alpha ERC [rPDC] in force pulse study. Group mean rPDC (blue) with standard deviation (light blue) and significant deviations from the baseline (green). (a) *frontal* to *motoL*, (b) *frontal* to *motoR*, (c) *motoL* to *motoR*, (d) *motoL* to *tempL* and (e) *parietalR* to *tempL* and back.

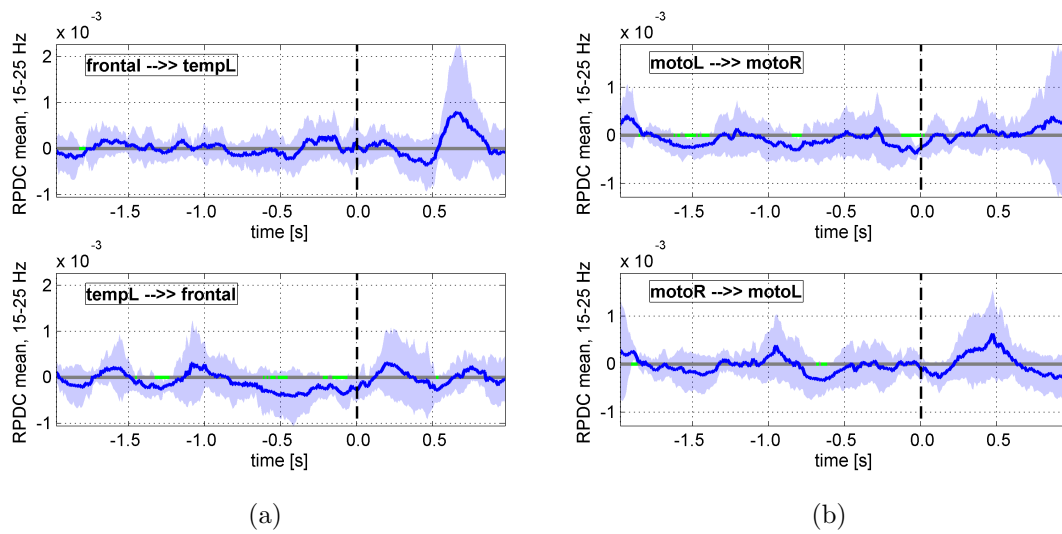


Figure 7.10: Cluster beta ERC [rPDC] in force pulse study. Group mean rPDC (blue) with standard deviation (light blue) and significant deviations from the baseline (green). (a) *frontal* to *tempL* and (b) *motoL* to *motoR* and back.

## 7.2 Golf putt study

### 7.2.1 Precondition measures

#### Drop-outs

In the golf putt study, one subject was excluded from analysis. Here, the back-swing was executed too slow to show a clear pattern of movement onset in the accelerometer signal. Hence, the algorithm, which was developed to find distinct events in the putt pattern (described in section 6.2.4), revealed unstable results. Even though, less trials could be used due to artifact contamination compared to the force pulse study, the remaining twelve subjects were included in further processing steps.

#### Psychometric measures

None of the psychometric measures showed significant changes. Mental state (STAI-X1,  $t(11) = -1.129$ ,  $p = 0.283$ ,  $r = 0.322$ , two-sided t-test), motivation (VAS,  $z = -0.51$ ,  $p = 0.61$ ,  $r = -0.1$ , Wilcoxon signed rank test) and stress (VAS,  $z = -0.306$ ,  $p = 0.76$ ,  $r = -0.06$ , Wilcoxon signed rank test) was measured before and after the task, but no statistically relevant changes can be reported. Mean STAI-X1 scores were  $32.411 \pm 4.93$  (possible values: 0 - 100), whereas VAS for stress was denoted with  $18.76 \pm 11.02\%$  and for motivation with  $89.6 \pm 10.48\%$  on average over all blocks.

#### Task performance

Figure 7.2.1 denotes the group's task performance achieved in the putting task. Performance rate by means of the percentage of holed putts was  $36.509 \pm 3.059\%$  over all blocks (red line). Over blocks, no trend for improvement or decrease in performance was notable from these descriptive statistics. Also, no significant difference from first to tenth block was found ( $z = -1.247$ ,  $p = 0.213$ ,  $r = -0.245$ , Wilcoxon signed rank test).



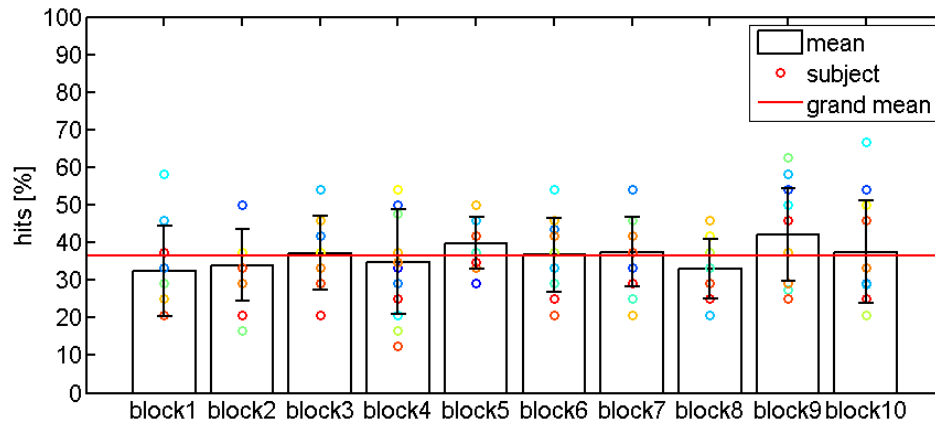


Figure 7.11: Task performance golf putt study (N=12). Circles indicate single subject performance [% hits] in each block. Identical performances are superimposed and may appear as one subject.

### Data quality

240 putts were performed by each subject. Due to artifacts, the number of trials that were used in the analysis was reduced. On group average, 6 - 13 of 24 trials/block (mean:  $10.823 \pm 3.283$ ) were classified as artifact-free from each block. Thus, on average,  $108.23 \pm 32.83$  trials were left after artifact cleaning from each subject. The average number of channels left after rejection was  $55.308 \pm 6.223$  out of the measured 64. Since ICA was performed on the longer pre-epoch data, sufficient sample points were available. After epoching, the lowest number of trials was 75 with 406 sample points each. Considering the suggested amount of data points to use for fitting of MVAR models ( $10M^2p = 10 \cdot 5^2 \cdot 10 = 2500$ ), the here used 30.450 sample points exceeds the number of required amount of data.

## 7.2.2 Network localization

The same clustering settings as described for the force pulse study were applied. Thereby, six clusters that consisted of at least five subjects were found. Table 7.2 provides an overview of the subject's ICs appearing in clusters, which were named by their presumed location or cause of appearance after inspection. Their equivalent dipoles are shown in figure 7.12.

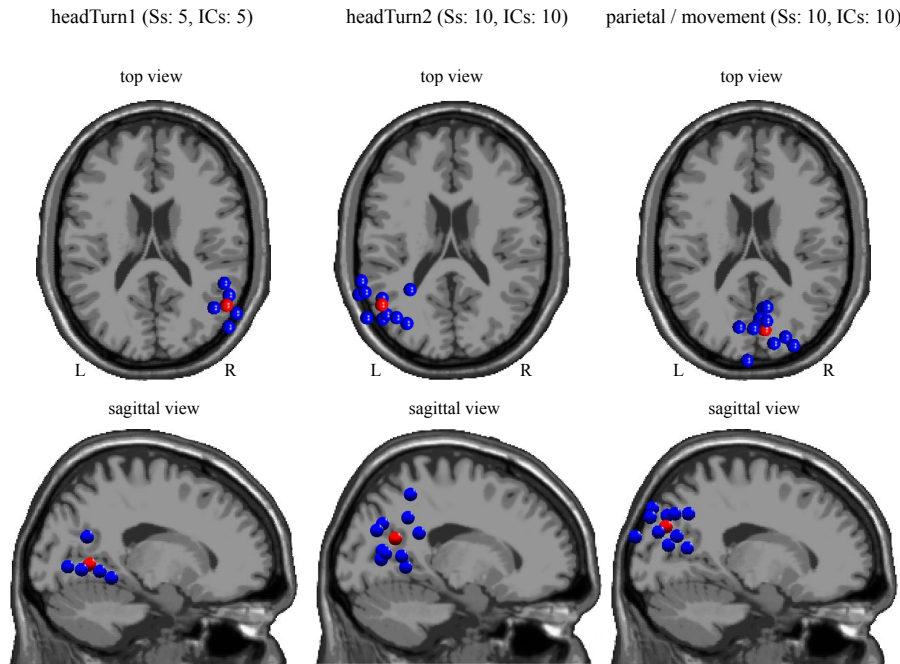
The location of the first cluster (see figure 7.12(a), left column), *headTurn1*, was found to be closest to BA 37 (centroid location:  $x = 53$  mm,  $y = -59$  mm,  $z = 4$  mm), *headTurn2* (middle column) originates from close to BA 39 (centroid

Table 7.2: Golf putt study: Identified independent components of each subject (indicated by x).

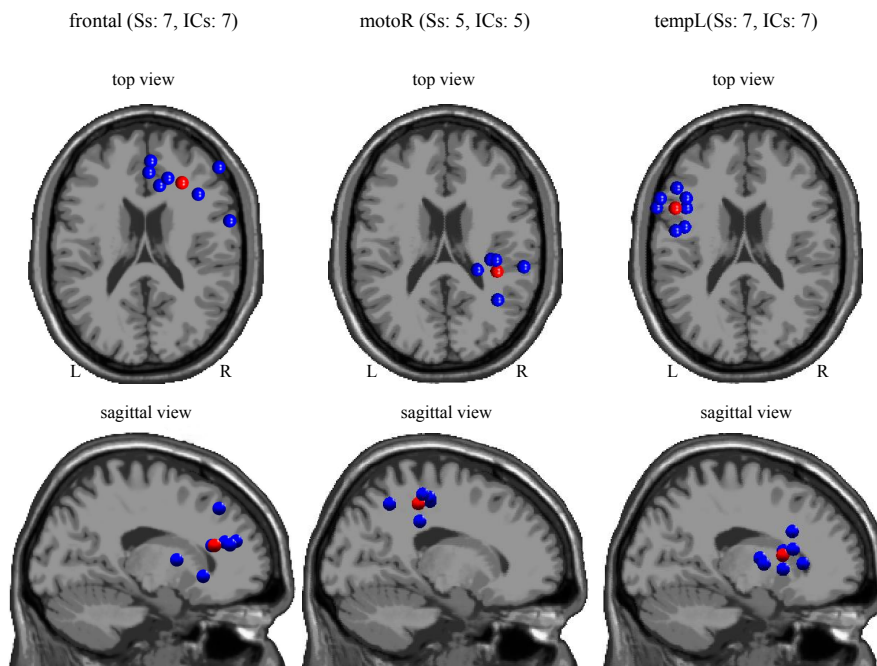
| subject | headTurn1 | headTurn2 | frontal | motoR | tempL | parietal |
|---------|-----------|-----------|---------|-------|-------|----------|
| 1       | .         | x         | x       | .     | .     | x        |
| 2       | .         | x         | x       | x     | .     | x        |
| 3       | x         | x         | x       | x     | x     | x        |
| 4       | x         | .         | x       | x     | x     | x        |
| 5       | .         | .         | .       | x     | x     | .        |
| 6       | x         | x         | x       | x     | .     | .        |
| 7       | .         | x         | .       | .     | x     | x        |
| 8       | .         | x         | x       | .     | x     | x        |
| 9       | x         | x         | .       | .     | x     | .        |
| 10      | .         | .         | .       | .     | .     | .        |
| 11      | x         | x         | .       | .     | x     | x        |
| 12      | .         | x         | x       | .     | .     | x        |

location:  $x = -50$ ,  $y = -58$ ,  $z = 21$ ). However, in both clusters individual dipoles appear to be located close to the skull. The respective ERSP images (figure 7.13, top row) denote a decrease of power from 3 - 6 Hz from just before movement onset until the end of the epoch. Also higher broadband ( $> 12$  Hz) event locked dynamics can be noticed. Note that here the ERSP images are plotted for frequencies up to 126 Hz, allowing the display of cross-feed from EMG or other high frequency content. Besides high frequency content, clusters *headTurn1* and *headTurn2* show narrow-band frequency specific dynamics from 11 - 16 Hz and 7 - 12 Hz, respectively. Cluster *parietal*'s equivalent dipoles (7.12(a), right column) lie inside the head model (centroid location:  $x = 9$  mm,  $y = -75$  mm,  $z = 30$  mm) closest to BA 19. The respective ERSP image (figure 7.13, middle left) also reveals high frequency content, time locked to movement onset. However, narrow-band dynamics within the theta band (4-7 Hz) are also apparent. Showing a scattered distribution of equivalent dipoles, cluster *frontal* (figure 7.12(b), left column) was assigned to the right lateral BA13 (centroid location:  $x = 29$  mm,  $y = 27$  mm,  $z = 12$  mm). Cluster *motoR* (figure 7.12(b), middle column) originates from BA 3, is also close to BA 2, 4 and 40 (centroid location:  $x = 38$  mm,  $y = -31$  mm,  $z = 46$  mm) but consists of five subjects only. The sixth cluster, *tempL* (figure 7.12, right column) was assigned to BA 44 (also 13 and 45) according to its centroid location ( $x = -50$  mm,  $y = 12$  mm,  $z = 9$  mm).

The ERSP image of cluster *frontal* in figure 7.13, middle right, denotes frequency specific dynamics from 4 - 8 Hz. Besides broad-band high frequency decrease around movement onset, *tempL* also shows an increase in theta and a decrease in beta activity. In cluster *motorR* slight beta suppression from movement onset onwards can be observed. Furthermore, a short theta burst between 1000 and 1500 ms is present.



(a)



(b)

Figure 7.12: Equivalent cluster dipoles in the golf putt study projected into an standard MRI scan (top row: top view, bottom row: sagittal view). In blue: subject dipoles, red: centroids. Labels indicate presumable origin of clusters with number of contributing subjects and ICs.

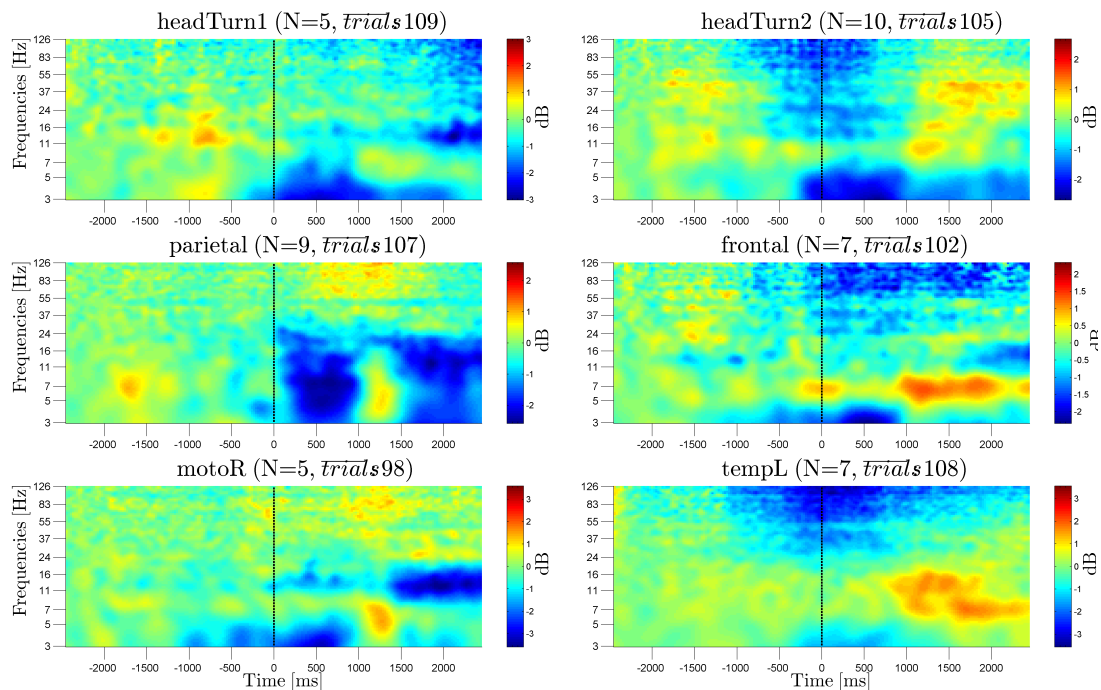


Figure 7.13: Cluster ERSP of the golf putt study. Images show the mean time-frequency plots of each cluster labeled by its presumable origin.  $N$  gives the number of contributing subjects, and  $\overline{trials}$  the average number of trials per subject.

### 7.2.3 Network activity

The clusters that were identified to show functional brain dynamics and consisted of data from at least half of the included subjects (*frontal* and *tempL*), were tested for significant perturbation relative to the baseline. No significant (FDR corrected at  $p \leq 0.05$ ) ERD/S patterns were found in either theta (4-7 Hz), alpha (8-12 Hz) or beta (15-25 Hz) band activity.

## 7.3 Summary

Before analysis of the force pulse study data one and three subjects were excluded from ERD/S and ERC analysis, respectively. Task performance and psychometric measures showed no significant changes throughout the measurement. After artifact reduction, over 78 % of the trials were used for analysis. Six clusters with a minimum of six subjects were identified as functional brain components that showed time and frequency dependent dynamics by significant deviations from the baseline. This includes a frontal brain area, two lateral motor and temporal areas, as well as a right lateral parietal area. Their activation patterns showed time-locked dynamics to the movement onset by means of ERD/S in theta, alpha and beta frequencies. Between five of these six clusters, effective connectivity was estimated, which revealed frequency dependent, directional information flow for between the nodes of this network. Most prominent ERC patterns were found in a frontal to lateral motor network for the theta band which showed bidirectional causal dependencies before and after movement onset. Especially theta bursts around 500 ms were prominent in both, theta ERD/S and ERC measures. Interestingly, causality in the alpha band between left and right motor area decreased before movement onset with their ERD pattern accordingly, but only unidirectional from left to right hemisphere. Though, it has to be noted that the effects of ERC measures did not withstand FDR correction for multiple comparison and are shown without corrected  $p$ -values.

In the golf putt study, data quality was an issue. Here only 45.1 % of trials were usable for ERD/S and effective connectivity analysis. All tested psychometric measures (motivation, stress, anxiety) and also task performance were stable throughout the measurement procedures. However, only a maximum of seven out of twelve subjects contributed to clusters. Two clusters are analyzed by means of ERD/S but did not show significant activation dynamics using BH-FDR corrected surrogate data statistics. Due to the diverse representation of subjects in clusters, no consistent network of nodes could be defined to perform ERC analysis.



## 8 Discussion

The main objective of this work is to map brain network dynamics during sensorimotor control of goal-directed movements by means of the location, activation and effective connectivity of the involved cortical brain regions. This is done by first conducting a controlled laboratory study utilizing a force pulse precision task to gain knowledge about applying measures of network dynamics, especially regarding the estimation of brain effective connectivity. The second experiment consists of a golf putting task and takes place outside on the green in a real-world setting. A signal processing procedure is applied to both the laboratory and real-world condition to investigate the feasibility of these tools to datasets of potentially problematic quality.

Results gained from the force pulse study reveal a five-node network that is described by localization and time-frequency signatures of activity and effective connectivity during movement execution. However, the results presented for data acquired under real-world conditions demonstrate the urge for further methodological research and hardware development. Both studies are discussed in detail in the following sections.

### 8.1 Force pulse study

For the force pulse study, a cortical sensorimotor control network was identified and its activity and effective connectivity was derived from source reconstructed signals. The network consists of a frontal area, lateral areas assigned to those of motor and sensory cortices, as well as a posterior parietal area. According to the findings from ERSP and ERD/S, these nodes of the network show unique spectral spatiotemporal movement-related activity patterns. Furthermore, for the first time, ERC between these brain areas is observed during precise goal-directed

force generation. Amongst others, a prominent pattern of pre- and post-movement information flow between clusters that are assigned to ACC and lateral motor areas was found.

ERC, along with measures of localization and activity, discussed in light of task specific preconditions, yields a complemented description of the brain network dynamics during precise force generations.

### 8.1.1 Precondition measures

#### Drop-outs

Initially, all subjects are included in the EEG data processing of this study. However, ICs of one out of the ten subjects does not appear in any of the generated clusters and is therefore excluded from further analysis. That particular participant was the groups oldest and had difficulties producing force pulses of less than 200 ms from onset to peak as claimed. This is not surprising because finger force coordination has been shown to be slower and less precise in the elderly from 50 years of age and above (Diermayr et al., 2011; Shinohara et al., 2003). Thus only 74 trials (compared to 188 on average) can be used for this subject, which supposedly leads to deviant measures causing the assignment to an outlier cluster. Whether this number is too low per se, or only too low in relation to the others, causing a difference in SNR requires further investigations. Further exclusions were made based on restrictions of group network analysis and are therefore explained in the appropriate sections below.

#### Psychometric measures

Levels of stress and motivation, as well as state anxiety do not show any significant changes from before the task to its completion. Low levels of stress and state anxiety suggest that participants felt comfortable throughout the task procedure, while being motivated to perform well throughout the task. Hence, psychological states can be assumed to be constant during the measurements and did not bias either task performance or EEG measures.



### Task performance

The force pulse study was designed to induce demands on sensorimotor control functions, using a simple force pulse precision task executed with index finger and thumb (pinch grip). The success rate of below 40% denotes the task's difficulty and therewith suggests high demands on sensory motor control functions. Hinder et al. also used ballistic force pulses in a similar precision task (Hinder et al., 2010). Unfortunately, authors did not provide information about the performance to compare the success rates.

Three submaximal forces ( $\leq 15\%$  MVC) were used in random order to prevent muscle fatigue, lower learning effects, and habituation. Constant success rates throughout the measurement indicate that the task did not cause fatigue at these low submaximal forces, as muscle fatigue is expected to induce impaired sensorimotor control denoted by decreased motor precision (Baumeister et al., 2012b). Additionally, learning effects or habituation were not observed in the task performance results, which can be explained by the fact that precise and targeted force generation in pinch grip is a common task of daily-living and thusly already well-developed (Hinder et al., 2010).

### EEG data quality

On average, 52 of 240 trials are rejected before further analysis of the data. This is (1) due to occasional force pulse duration longer than 200 ms and (2) artifacts that mainly originated from facial and neck muscle tension. Only few, if any, channels are excluded and with over 70% of artifact free trials the required amount of data for ICA is obtained. The used trials per block are equally distributed so that no phase of the task procedure is under or over represented in the data.

### 8.1.2 Network localization

Clustering reveals eight clusters (*frontal, lateral medial, temporal, parietal, occipital*), which consist of six to nine individual preselected ICs and are grouped by their dipole locations and ERSP images. This is in line with findings of (Shou et al., 2012) who found 13 similar clusters in a study with eleven participants using a 128 channel EEG system. Considering that amongst these 13, four were denoted as occipital sub clusters the number and also type of reliably found ICs

is comparable to the results presented for this study.

Here, the ERSF images are weighted equally to the estimated location of equivalent dipoles, enhancing functional properties. The weighting of IC properties, as well as how many clusters are generated (here mean of ICs per subject included in the clustering) is assessed heuristically as also described in Onton and Makeig (2006) or Gramann, Onton, et al. (2010). This appears to be common practice until proven otherwise. Furthermore, only clusters that consist of ICs from more than half of the subjects are considered for network analysis. Hence, a left parietal and an occipital cluster are excluded (both contributing with 5 ICs).

In the following, clusters are assigned to anatomical brain areas based on their equivalent dipole centroids and functional ERSF patterns, substantiated by findings from studies using MRI, MEG and EEG in related tasks.

### **Frontal cluster**

The frontal cluster shows predominant theta band activity and its equivalent mean dipole is estimated to be close to BA 24, of which the ACC is part of (Lancaster et al., 2000). Numerous studies, recently reviewed by Shenhav et al., have found ACC activity to be reflected by theta band activity in the EEG. Activation of this region has mostly been related to cognitive control which in turn holds three functions namely regulation, specification and monitoring of both cognitive and motor actions (Shenhav et al., 2013). For exemplifying, using EEG, it was shown that so-called frontal midline theta power during aiming correlates with performance in rifle shooting (Doppelmayr et al., 2008). This activity is assigned to the ACC and discussed towards a reflection of attentional control processes. Furthermore, performance monitoring has specifically been related to frontal theta band activity (Cavanagh et al., 2012; van Driel et al., 2012) and its modulations correlate with the fMRI BOLD signal from the ACC (Debener et al., 2005; Hoffmann et al., 2014). This was found in simultaneous EEG-fMRI studies, substantiating the link of functional measures with anatomical structure. Therefore the frontal cluster is thought to predominantly reflect ACC activity.

### **Motor clusters**

ERSF images of both clusters (motoL, motoR) that are labeled by their apparent location close to the lateral motor areas show distinct alpha and beta band dynamics. This has been extensively studied in the work of Pfurtscheller et al. in which these fluctuations were observed in EEG electrode signals mainly from C3

and C4 locations, representing the motor cortex and adjacent areas (Pfurtscheller & Aranibar, 1979a; Pfurtscheller & Berghold, 1989; Pfurtscheller et al., 2006). Whether the alpha and beta oscillations originate from the same brain areas, or are generated by different areas remains to be determined. According to Sclocco et al. (2014), there is evidence from simultaneous EEG-fMRI recordings that beta rhythm is more likely to originate from M1, while alpha activity is believed to be generated in the somatosensory cortex. Contrary, the PMA and SMA have been assigned to these functional representations of alpha and beta band modulations (Bigdely-Shamlo et al., 2013; Shou et al., 2012). Based on these findings and considering the estimated dipole locations of motoL and motoR to be close to BA 4 and 6 (M1, SMA/PMA) the identified motor clusters might represent a mixture of PMA and M1 activity and is thus identified as an area reflecting general motor area activity, labeled by lMA and rMA, respectively. This is also in line with IC identification in Shou et al. (2012), Huang, Jung, Delorme, and Makeig (2008) and Onton et al. (2005).

### **Temporal clusters**

In addition to the two lateral motor clusters, two more temporally located (close to BA 13, 21, 22, and 38) clusters with prominent alpha band activity are identified. These cluster characteristics are in line with findings from Shou et al. (2012). The authors relate this activity to the secondary sensory cortex. Notably, this assignment to the specific brain area is based on topographic IC back projections and their time-frequency characteristics, only. This has not been found elsewhere and thus remains speculative. However, further interpretation regarding these clusters might benefit from the assumption that its activity can be related to that of the lateral S2, located on the upper bank of the lateral sulcus. The link between functional measures and anatomical location remains to be confirmed, because cited investigations are based on source reconstruction of surface EEG signals only.

### **Parietal cluster**

The one repeatedly decomposed parietal IC across all subjects is a right lateral localized area, which is found to be close to BA 39 and thus likely located within the PPC. It is functionally characterized by sole, but prominent alpha band activity. Ehrsson et al. studied frontoparietal brain regions involved in a precision grip task. It was found that parts of the right posterior parietal cortex (rPPC) are explicitly involved in somatosensory-motor integration to control fine fingertip

forces during an object manipulation task (Ehrsson et al., 2001). Functionally, the rPPC is represented by alpha modulations during the control of visual-spatial attention (Capotosto et al., 2008). Thus the activation and connectivity patterns of the parietal cluster are discussed with regard to the rPPC.

### 8.1.3 Network activity

Based on the identified brain regions, their activation patterns are discussed in the following section. Frequency band dynamics in each individual area allow to draw inferences about their task-specific engagement and how this is modulated in certain times and conditions. Findings from studies that also measured brain activity related to similar motor tasks are discussed in the context of the here reported activation patterns. Because the identified areas now define the variables of a sensorimotor control network, they are referred to as nodes of the network.

#### Frontal node (ACC)

The ERSP image of the frontal cluster (figure 7.4, top left) shows predominant theta band modulation, statistically verified by its respective ERD/S. So-called frontal midline theta has been found as a marker for cognitive inference (Nigbur et al., 2011), attention (Doppelmayr et al., 2008) and mental effort (Sauseng et al., 2007), thereby indicating a central control mechanism in the context of the working memory system (Sauseng et al., 2010). During force pulse productions, Vaillancourt, Yu, Mayka, and Corcos found the ACC and dorsolateral prefrontal cortex (DLPFC) to be involved in the planning of precise motor actions and responsible for selecting the amplitude of precise force pulses (Vaillancourt et al., 2007). This was done in an fMRI study, comparing involvement of the mentioned areas during (a) steady force production, (b) repetitive force pulses and (c) selecting force pulses of different amplitude using a precision grip. In our study, pre-movement ACC theta power does not show any dynamics before the generation of force pulses. In contrast, Doppelmayr et al. for example, did find increasing frontal theta power towards the trigger-pull in rifle shooting (Doppelmayr et al., 2008). Possible reasons for this difference in results may be due to task differences. Doppelmayr interpreted this effect towards a signature of increasing attention, which might be stronger for a task like rifle-shooting rather than in targeted pinch grip force productions. Also, the methodological procedures differed consid-

erably. Results were gained from electrode signals consecutively epoched into 500 ms segments from 3 s before until 500 ms before trigger pull. FFT denotes theta power increase to be significant between the first and last epoch only. Thus, the reference period producing significant results lies outside the time window that was used here.

Looking at the temporal appearance of the theta burst, the main activity increases about 500 ms after movement onset and thus about 300 ms after its termination (onset to peak force was restricted to last less than 200 ms). A very similar pattern was found, though in a cognitive, so-called forced-choice speeded response paradigm, investigating the relation of ERN and frontal midline theta in the EEG (Luu et al., 2004). Beginning just before incorrect button presses, midfrontal theta-band power increased and became partially and transiently phase-locked to the subject's motor response, accounting for 57 % of ERN peak amplitude according to the authors. More comparably, frontal ERN has also been investigated in correct and incorrect choices of force amplitude production (Armbrecht et al., 2012); however, no evidence of a force-error sensitive monitoring mechanism, but rather a general action-evaluation system was found. According to these results, the baseline dynamic is most likely related to performance monitoring and evaluation of generated force pulses, though presumably not discriminative for force levels.

In addition to the theta burst, figure 7.5 also denotes dynamics in the alpha band following the force pulse. Frontal alpha dynamics are mostly discussed in context of depression and emotion denoted by hemispheric alpha asynchrony (Davidson, 1998). A current literature review does not allude to alpha activity arising from the ACC in relation to motor behavior. However, the ACC is known to be one node of the frontoparietal network, which in turn shows short and long range functional connectivity in theta and also alpha frequencies (Sauseng et al., 2005). Thus, the reported frontal (ACC) alpha activity might relate to functional coupling with other brain regions.

### **Motor nodes (MA)**

The clusters most likely representing lateral motor function related activity show obvious ERD within the alpha and beta band. This becomes significant in comparison to the baseline as early as 1.5 - 2 s before movement onset and can be discussed in the context of the well-described rolandic  $\mu$  rhythm ERD preceding voluntary movements (Pfurtscheller & Aranibar, 1979a). This ERD is known to be modulated in time and amplitude by handedness (A. Stancák & Pfurtscheller, 1996), intention and execution of right or left lateral movements (Pfurtscheller

& Aranibar, 1979a; Zaepffel & Brochier, 2011; Masaki et al., 2004; Bozzacchi et al., 2012), task complexity and uncertainty of target location (Tzagarakis et al., 2010).

In this study, participants performed force pulses with their dominant right hand only. As can be seen from figure 7.5 and 7.6 rMA activity is less suppressed towards the movement onset in the alpha band than that of the left-hemispheric counterpart. This is in line with the findings of Pfurtscheller et al. in an early report of the  $\mu$ -ERD prior to voluntary thumb movements, where ipsilateral ERD was also stronger during movement execution than at the contralateral side (Pfurtscheller & Aranibar, 1979a).

Another frequency specific pattern, which is assigned to motor areas, is the contralateral PMBR, investigated in Parkes, Bastiaansen, and Norris (2006). This can also be seen in figure 7.6, in the top right panel. Parkes et al. reports intrasubject correlation between the fMRI BOLD signal amplitude in the sensorimotor cortex during movement and the PMBR strength, measured with EEG, suggesting representations of motor activity itself or that of somatosensory input associated to motor activity. The functional significance of the PMBR remains controversial, as reviewed by Kilavik et al. In summary, PMBR could either reflect active inhibition of a motor network or the recalibration or reset of the motor system after movement execution (Kilavik et al., 2013). Moreover, Tan et al. found neural correlates of motor error monitoring with the PMBR over the sensorimotor cortex in a joystick operated, targeted reaching task (Tan et al., 2014), in which beta ERS of the EEG was lower for larger task errors.

### **Secondary somatosensory nodes (S2)**

The ventral lateral localized S2 is only rarely described in the EEG literature. Shou et al. characterized the lateral topographic scalp projection of respective ICs as part of a functional sensorimotor network (Shou et al., 2012). The authors also reported the prominent spectral activity to lie in the alpha band. The results presented here for left and right S2 support this observation (see figure 7.3, middle right and bottom left). Though, Shou et al. investigated long-term effects over 60 min and thus did not analyze event-related dynamics in these clusters. Due to lacking description of time-frequency representations of S2 areas, only speculations about the different lateral and frequency band specific ERD and ERS can be made.

In general, S2 plays a functional role in sensorimotor integration of tactile stimuli, as investigations of cortical reorganization in S1 and S2 suggest (Pleger et al., 2003). In fact, within the alpha band, a contralateral ERS builds up from the planning phase throughout force pulse generation, followed by ipsilateral ERD. According to Narici, Forss, Jousmäki, Peresson, and Hari this activity might re-

flect the processing of tactile stimuli (here from pressing the force transducer). Activity in frequencies within the alpha band, assigned to S2, were found responsive for afferent nerve stimulation (Narici et al., 2001). Like here, response to the stimulus was bilateral, but stronger on the ipsilateral site in this MEG study. Additionally, a prominent theta burst appears following the force pulse in ipsilateral S2 but is not observed contralaterally. This may refer to a lateral coupling with the ACC based on the similar activation patterns (see figure 7.4), possibly indicating the inclusion of tactile sensory input in the processes of performance monitoring.

### **Right posterior parietal node (rPPC)**

The human PPC is involved in several cognitive functions including sensorimotor information integration during planning and execution of goal-directed movements as found by fMRI investigations (Ehrsson et al., 2001; Teixeira et al., 2014). In the EEG, parietal alpha power inversely correlates with the quantity of sensory information processing as demonstrated by a comparison of spectral EEG signatures during golf putting in a real-world versus virtual environment (Baumeister et al., 2010). Figure 7.5, bottom right, shows the ERD of alpha activity in the rPPC from 2 s before the force pulse lasting until 1 s after the movement. This has also been described in Babiloni et al. (1999) and stated as changes in background oscillatory activity in wide cortical sensorimotor areas preceding goal-directed movements. However, neither Baumeister et al., nor Babiloni et al. related the observed effects to specific (lateral) locations of the PPC. Using fMRI, Ehrsson et al. showed that rPPC is specifically involved in sensorimotor integration required for the control of fine fingertip forces during an object manipulation task (Ehrsson et al., 2001). The region was particularly engaged when subjects used a precision grip to manipulate an object, while its activity was inversely modulated with the amount of force that was applied to the objects. In contrast, Wheaton, Shibasaki, and Hallett (2005) pointed out the predominant role of the left PPC in right hand movements indicated by alpha ERD beginning as early as 3 s before movement onset. However, he also discussed the rPPC as a mediator between left PPC and bilateral PMA. This coupling might be indicated by alpha and/or beta band dynamics, which is synchronously apparent in both rPPC and l/rMA (see figure 7.5 and 7.6). The latter assumption is also supported by Wheaton, who reported beta specific functional connectivity between parietal and motor cortices during the execution of praxis hand movements, demonstrating the critical role of this network for motor preparation and execution (Wheaton, Nolte, et al., 2005). Lastly, figure 7.4 shows significant theta ERD/S before, during and after force pulse generation. As mentioned before, this might account for the theta specific long-range communication within a frontoparietal network (Sauseng et al., 2005).

### 8.1.4 Network connectivity

ERC was estimated for a five node network consisting of ICs that were identified as ACC, IMA, rMA, IS2, rPPC. For all seven included subjects, AMVAR models were fitted with equal parameter settings and were confirmed valid by checking whiteness of residuals, stability and consistency at each time window (appendix B.1). rPDC was calculated so that network dynamics of 3.5 Hz and above could be captured during targeted force pulse generation. The dynamics discussed here failed to be significant using FDR corrected  $p$ -values lower than 0.05 and are presented without correcting for multiple comparison. It has to be noted that even with reducing the tests to one frequency bin only, correction for multiple comparison included the number of time windows and number of nodes ( $371 \cdot 5 = 1855$  t-tests). Even though FDR correction is less conservative than traditional familywise error rates (FWER), it can still be very strict especially when applied to data with a low proportion of false null hypotheses (L. He & Sarkar, 2013). The following discussion should therefore be seen in light of these statistical limitations. ERC has not been investigated in relation to goal-directed movements before. The following remarks attempt to classify the three stronger patterns of directional information flow within the identified network. An expected fronto-parietal or parieto-motor network cannot be affirmed from these results. Possible reasons for this are discussed.

#### **A widespread post-movement fronto-motor signature of performance monitoring**

A predominant pattern of increased information flow dynamics appears between approximately 300 and 700 ms after movement onset across frequency bands. This is strongest between ACC and both MAs, denoting bidirectional information flow in theta and also alpha band frequencies. The involved areas and timing of this effect suggest a relation to functions of performance monitoring, as the ERD/S results also suggested. Mullen et al. reported theta specific information flow between ICs assigned to ACC, motor and somatosensory areas near the latency of an ERN potential in an oddball task with auditory feedback to be modulated by trial performance. This was discussed in terms of updating of attention and motor planning following performance evaluation (Mullen, Onton, & Delorme, 2010). Concordantly, patterns of ERC were also found in a time estimation task with correct and incorrect feedback that was conducted to investigate differences in feedback processing between high- and low-learners (Di Luft et al., 2013). High-learners showed larger theta ERC from left central (electrode C3), associated with



motor activity, to mid-frontal (FCz), associated with performance monitoring, immediately after feedback (0 - 0.3 s), followed by (from 0.3 to 0.6 s after feedback) information flow from mid-frontal to prefrontal (F5), associated with executive functioning. It was suggested that these results reflect cognitive processes related to (1) comparison of obtained versus expected feedback, and (2) updating the feedback history based on this information. The post-movement theta specific communication pattern here may thus indicate similar processes, but in relation to performance monitoring of precise force production.

Simultaneously, unidirectional information flow is present from rMA to IMA and also from S2 to IMA and rPPC in the alpha band. This may indicate a global transmission of information during performance monitoring throughout the nodes of this network. Supporting this, long range connectivity was found to be alpha band specific by Sauseng et al., though, in the frontoparietal network only and denoted by measures of functional, not effective connectivity (Sauseng et al., 2005).

### **A pre-movement pattern of fronto-motor ERC**

Prior to the force pulse onset, theta ERC is present between ACC and mainly IMA. Interestingly, the increase and decrease of bidirectional information flow between these nodes alternates back and forth. Due to the timing and sole contralaterality of this effect, this may indicate a (looping) mechanism related to right-lateral movement selection and planning (see figure 7.8, top left). ERC between ACC and motor areas during movement planning has not been described elsewhere and thus the suggested mechanism remains highly speculative and requires further investigation. Though, Rappelsberger et al., also reported increased contralateral interhemispheric functional coupling between frontal and central electrodes (assigned to premotor and motor areas) towards movement onsets of self-paced finger movements (Rappelsberger et al., 1994). However, it remains questionable whether these results are comparable to the here presented observations, due to severe methodological differences: Functional instead of effective connectivity was calculated on surface electrodes instead of source reconstructed signals with a time resolution of only 125 ms. Also, the task did not involve goal-directed motor action in the sense of reaching a specific target, but voluntary movements that might not have required distinctive target-orientated planning.

**Reduced contra to ipsilateral motor area ERC before the movement onset**

Along with IMA and rMA ERD, rPDC appears to be reduced in the alpha band prior to the movement, but only unidirectional from IMA to the ipsilateral counterpart. Reduced coupling between M1 areas during unilateral fist closures was also found by effective connectivity analysis based on fMRI BOLD signals (Pool et al., 2013). This was interpreted as a mechanism for inhibition of neural activity and found bidirectional, for both right and left hand movements. Additionally, Grefkes, Eickhoff, Nowak, Dafotakis, and Fink found enhanced causal dependencies towards the contralateral M1, while neural coupling towards ipsilateral motor areas was reduced during voluntary hand movements (Grefkes et al., 2008). However, both studies used measures of static effective connectivity throughout the task based on BOLD signals without distinctive periods of movement planning or monitoring. Hence, no effects of ERC can be inferred from these results, which may also explain the different observations.

Furthermore, these results reveal unidirectional ERC from IMA to rMA, while both nodes show similar ERD patterns. This highlights that measures of effective connectivity do not necessarily correlate with individual node activity, but add information about the observed processes.

**No fronto-parietal or parieto-motor ERC during force pulse production**

Based on findings in Ewen et al. (2014), increased parietal to frontal information flow during movement preparation was formulated for the expectations in specific aim A.3. Authors related these dynamics to representations of a mechanism to select appropriate motor sequences before movement execution. However, increased ERC between rPPC and frontal regions (ACC or MAs) cannot be confirmed in this investigation. Instead, rPPC to S2 and IMA ERC rather tend to decrease in the theta and alpha band before movement onset (figures 7.8 and 7.9). Reasons for this may be due to task differences. Ewen et al. used complex motor gestures that required movement sequences. Instead, simple and brisk force pulses do not require the initiation of sequential sub-movements, which might considerably affect the processes of movement planning. Furthermore, the effective connectivity was calculated between averaged electrode signal from left and right frontal and parietal regions according to their magnitude of ERD/S. These signals may not be comparable with the here reconstructed source signals as they reflect EEG from rather large areas and might therefore relate to a different set of brain regions.

In Wheaton, Nolte, et al. (2005) increased synchronization preceding praxis hand movements between parietal cortex and SMA, but not between parietal cortex and M1 were reported. As mentioned above, the identified lateral motor areas (l/rMA) are likely to represent mixed activity from multiple motor related regions

including PMA, SMA, M1. Thus, patterns of ERC from rPPC towards l/rMA might represent a mixture of causal dependencies that cannot be discriminated and therefore differ from other observations.

### 8.1.5 Limitations

Limitations should be taken into account for the presented results and their implications. Even though precise submaximal force generation is a common task in everyday life, the specific group of skilled golfers limits the generalization of the observed network dynamics for a broader population. This is due to extensive training of targeted motor behavior in the participant's sport, suggesting better attentional control (Baumeister et al., 2008) and more experience in movement planning, presumably larger representations of relevant brain areas with pronounced structural connectivity (Jäncke et al., 2009) compared to non-golfers. Furthermore, it should be considered that the generation of short force pulses is characterized by feedforward control mechanisms only (despite post-movement evaluation by the outcome) (Bear et al., 2007). Goal-directed movements, however, also include movements that make use of online feedback control to achieve a certain goal. Thus, the activation and connectivity patterns observed can only be assumed to be representative for these brisk feedforward controlled force productions.

Regarding the methodological aspects, ICA based approaches are data driven and thus do not require a priori information. However, an ICA does not necessarily separate all relevant components for each subject. Ideally, ICs represent a single source, but an IC may also contain a mixture of brain sources, a mixture of brain and non-brain sources, or several ICs may in fact represent one source but with different time-dependent characteristics. This gives rise to statistical questions especially for group analysis: How are multiple ICs from one subject in a cluster handled? And is it possible to adjoin ICs when their origin is proven to be from the same source? Here, only one IC was selected per subject and cluster. Especially, the problem of mixed sources in one IC (here assumed to be present for l/rMAs) can be approached by using more electrodes. For example, Shou et al. found slightly more reliable sources using an infomax ICA algorithm with a 128 channel system in eleven subjects and two sessions (Shou et al., 2012). Additionally, the heuristic approach of IC selection itself and selection of weights for measures in the clustering process is prone to misjudgment of the unexperi-

enced investigator and depends on rather arbitrary parameter settings. The usage of multiple complementary measures with reasoned and described weight settings can only partly come up for this non-objective approach.

Another statistical question is which method can be appropriately used to adjust the  $p$ -value to correct for multiple comparisons. The commonly used BH-FDR is considered to be robust but remains conservative considering the amount of tests due to high resolution time-frequency images and multiple nodes (Kim & van de Wiel, 2008). This mainly affected ERSP and ERC results. Due to reduction in the frequency domain, effects of ERD/S are shown to be robust enough against BH-FDR correction.

In terms of source localization, individualized head models using MRI and digitized electrode positions for each subject would improve dipole fitting (Z. Acar & Makeig, 2013). This would have an effect on clustering settings, as the weights for dipole location could be enhanced so that tight clusters can be achieved. However, the inverse problem of source localization remains present.

### **8.1.6 Concluding the specific aims**

- A. To map the activity and effective connectivity of localized brain sources related to precise goal-directed force pulse generation in a laboratory setting.**

As expected, for the data gained in the force pulse study, ICA decomposes the EEG signals into several similar brain sources across subjects. These sources are identified by their equivalent single dipoles and time-frequency patterns. Besides these localizations, movement-related brain dynamics are mapped regarding activation for a six node network by means of ERD/S and movement-related effective connectivity for a five node network using rPDC estimation on validated AMVAR models.

**A.1 To define a cortical network by identifying ICs that represent movement-related brain areas and cluster them across subjects.**

Clustering reveals brain components that are assigned to the ACC, left and right areas related to motor activity (lMA, rMA), left and right secondary sensory areas (lS2, rS2) and right posterior parietal cortex (rPPC) in at least six out of nine subjects. A left lateral PPC and occipital located cluster are also found, but only contain ICs from half of the subjects. Furthermore rS2 is excluded for connectivity analysis, because not all subjects contribute to this cluster. Notably, lMA and rMA may represent a mixture of SMA/PMA and M1, which suggests an incomplete decomposition of these sources.

**A.2 To test for movement-related dynamics of power spectral density in each cluster.**

Each cluster shows characteristic activation patterns in distinct frequency bands over the time course of goal-directed force pulse generations. As expected, movement-related alpha and beta ERD/S is found in almost all brain regions, but strongest for the sensory and motor areas (l/rSII, l/rMA). rPPC ERD/S is mainly restricted to a broader alpha band. ACC indeed shows increased theta power in a short post-movement period. For each brain area, according brain functions were identified by comparing their spatiotemporal and frequency specific activation patterns with similar findings in existing literature. These include performance monitoring indicated by the post-movement theta burst, sensorimotor information integration by rPPC alpha ERD, and motor output preparation and execution by the pre-movement ERD in S2 and MAs. Furthermore, simultaneous frequency specific activity in multiple nodes may indicate functional coupling between the described brain regions.

**A.3 To test for movement-related dynamics of effective connectivity between clusters.**

rPDC can be used to study ERC of simple goal-directed motor behavior such as targeted force pulse generation in a controlled laboratory condition. The information flow appears to be strongest after the targeted force generation, in a sub-network of ACC, lateral MAs and lS2. This may represent a period of performance monitoring in which the participating brain areas

integrate sensorimotor information to update attention and motor planning for following events. An alternating connectivity pattern before movement onset between ACC and IMA may indicate a looping mechanism for motor adjustments during movement planning, but remains highly speculative. This demonstrates the capability of this approach regarding high time and frequency resolved observation of brain processes. Dynamics of a well described frontoparietal network, cannot be confirmed. This might be due to undetected, or indefinite decomposed brain areas or a more static network activation throughout the task, rather than ERC dynamics relative to a baseline, as analyzed here.

### 8.2 Golf putt study

The golf putt is used exemplary as a framework for studying cortical processes of sensorimotor control during a complex motor precision task in a real-world setting. As outlined before, the signal processing techniques used here are sensitive to artifactual content and non-stationarities in the EEG. The aim was to test the methodological approach, applied in the previous study to map the activity and effective connectivity of localized brain sources during golf putting in a real-world setting.

The main outcome is that the expected lower quality of EEG recordings cannot be compensated by ICA, that is, the number of sources (functional and artifactual) exceeded the number of channels used in this study. Hence, unique multi source ICs were found. Some of these did show activation that are thought to be related to expected brain areas (ACC, lateral MA, and PPC) but were also contaminated with EMG activity. Since all following steps depend on a clean decomposition of sources, the mapping of brain network dynamics during golf putting was unsuccessful. However, results allow a detailed discussion of contributing factors.

## 8.2.1 Precondition measures

### Drop-outs

Twelve out of 13 skilled golfers are included in the data analysis of this study. Except for one subject, movement onsets are estimated by using a semi-automated pattern recognition procedure using the signal from an acceleration sensor attached to the putter head. In one case, a very slow back swing pattern showed an exceptionally flat acceleration profile from which the algorithm could not detect the movement onset. In the future, other phases of the golf/putt swing might be of interest in further investigations, so a more reliable system for motion capturing would be needed. Scientific as well as commercially available systems can be used here and are reviewed elsewhere, for example in Nam, Kang, and Suh (2014), Couceiro, Dias, Mendes, and Araújo (2013) and Blake and Grundy (2008). Generally, these either optical or inertial sensor based systems should not interfere with movement execution (added weight, restriction of range of motion, changed appearance) and should be capable of capturing all signal content, from slow changes to patterns as fast as the putter-to-ball impact.

### Psychometric measures

The subjectively reported low stress and high motivation levels, recorded before and after the ten blocks of putting, do not show statistically significant changes suggesting that subjects felt comfortable throughout the task procedure. This also applies for the state anxiety scores, which were also recorded before and after test procedures. Hence, psychological states can be assumed to be constant during the measurements and thus do not affect task performance and EEG measures.

### Task performance

Results indicate stable performance rates throughout the 10 blocks of 24 trials (240 in total per subject). Even though a single subject (handicap 7.4) achieved a performance rate of 45% in a pilot testing, the number of holed balls was about 10-15% lower than assumed for this study design.

The literature shows rather diverse performance statistics, especially because artificial indoor putting greens were used in different setups. Also, a certain rate of success was predetermined due to adjusted task setups according to partici-

pant's individual skill level. In Babiloni et al. (2008) and Babiloni et al. (2011) expert golfers putted on a standardized flat carpet from 2.1 m. From 100 performed putts, 63.5% were successful, mainly because hole diameter was adjusted in a pre-measurement in which success rates of at least 70 % had to be achieved. This setup was used again in Cooke et al. (2014), but with a putting distance of 2.4 m with 62.67% success rate as again hole diameter was adjusted. Different distances were used in Mathers and Grealy (2014). Here expert golfers (N=6) putted from 1-4 m on an artificial plane green using the standard hole diameter of 10.8 cm. Overall success rate here was 92.3% (80 trials each subject). This setup was adopted from Craig et al. (2000). In other studies error rate was calculated by the average distance of the hole or by a point scale according to a defined grid around the hole (Baumeister et al., 2008; Reinecke et al., 2011). Wilson and Percy asked experienced golfers to putt from 3 m on an artificial green with slope of 1.8° achieving an average of 41.3% successful trials (Wilson & Percy, 2009). This is the closest to the here recorded performance rate and the only study that used a slope angle on the green, suggesting a high comparability to the real-world setting.

In the present study, the goal was to create a putting task with continuous demands on sensorimotor control functions. This was assessed by the success rate over blocks (here: approx. 40 %). Putt distances were varied and naturally given slopes of the green were accepted. Professional Golfers' Association (PGA) Tour statistics report a one-trial chance of 50% for holing out from 2.13 m distance, regardless the green's slope. The assumption was that, overall, 240 putts from 2.5, 3 and 4 m distance in randomized order lead to approximately 50% success rate considering the high amount of trials repeatedly executed. The reasons for the deviation from the expected result may be that (1) the tested group of golfers is highly skilled but not at PGA tour level, (2) the putt routine, which typically includes green reading and test swings, was restricted, (3) even though the putter was accepted to be of sufficient quality, nevertheless, length, weight and shape of the putter head differed from individually used ones and (4) the situation may not have been as competitive as during a tournament from which the cited PGA statistics were gained. Apart from the restricted putt routine, none of these points were verbally expressed by the subjects. Nevertheless, it can be assumed that the EEG procedures (lowering impedances) and equipment (amplifier attached to the belt, accelerometer cable from putter head to the amplifier, data transmission cable from amplifier to recording PC) were suboptimal regarding putt performance; however, the high levels of self-reported motivation (see above) suggests that participants rather tried to push themselves than to let themselves get frustrated.



## EEG-data quality

The key aspect to make use of ICA as an artifact rejection tool is to classify artifacts in the raw data as decomposable (stereotypical) and as the ones, which affect decomposition quality (non-stereotypical). The continuous recordings are pre-epoched so that ICA was performed on task relevant data only. The individual putting routine is typically consistent in experienced golfers (Cotterill et al., 2010). Thus repeatedly observed motion and EMG artifacts, were mostly due to these recurring movements including looking downward towards the ball and repetitive head rotations while aiming for the target prior to the actual putting stroke. The main reasons for non-stereotypical artifacts were electrode pops at lower sites (T, FT, O and CB channels) caused by head movements (up and down, turning) and movement artifacts especially post-stroke during watching the ball rolling or reacting to the performance result. Even after rejecting this artifactual content, the constraints of required number of sample points was met for both ICA and AMVAR model fitting. On average, nine channels had to be rejected from each dataset due to extensive artifact contamination. Consequently, less brain, and non-brain sources can be decomposed into separate ICs, which in turn affects clustering and also time-frequency activity representations.

### 8.2.2 Network localization

For this study, clustering revealed six clusters consisting of ICs from five to ten subjects (see 6.3.1). The first two clusters, shown in figure 7.12(a), left and middle panel, show dipole locations close to the skull and high frequency content. This and time-locked activity, revealed by ERSP, indicate movement related EMG, originating from neck muscles (see figure 7.13, top row). Similar patterns were found in Gwin, Gramann, and Ferris (2010), where neck muscle activity was also detected due to the repetitive movement time-locked to the gate cycle during walking, which was confirmed by dipole locations close to the skull. Considering the golf putt, this activity is assumed to be mainly caused by muscle activity during looking back and forth between ball and hole before the putt and visually following the ball rolling towards the hole. Simultaneous motion tracking of the head might help to verify these observations.

The remaining four clusters were localized in (right) frontal, left temporal, right motor and medial parietal areas (see figure 7.12(a) right and (b)). The locations and narrow low frequency content in distinct bands, in which activity appears, are similar to those found in the force pulse study, but with different temporal patterns. The parietal localized cluster shows broad band theta and alpha band

modulations possibly reflecting brain source activity. In the frontal cluster, the ERSP image shows a distinct theta band activity which has been shown to be related to ACC activity. However, dipole locations appear rather scattered. Few right lateral sources drag the centroid from its expected medial location, if ACC is assumed to be the reflected source. Desynchronization related to motor behavior in higher alpha frequencies could represent the  $\mu$ -rhythmic activity of the right lateral motor cluster as shown in figure 7.13, bottom left. Note, this cluster consists of ICs from five subjects only (figure 7.12(b), middle). Also, the cluster assigned to the left temporal cortex is characterized by broad alpha and lower beta synchronization post-movement onset, which is also observed in the force pulse study (see figure 7.13, bottom right). Hence, this might be related to left S2, even though source locations are estimated as being more anterior.

In addition to these functional, rather low frequency activations, spectral power modulations above 30 Hz are present indicating interference from EMG activity or other movement related artifacts causing high frequency content (see figure 7.13, middle and bottom row). This suggests that ICs contain a mixture of EEG and EMG sources. Here, the number of (brain and non-brain) sources likely exceeds the number of possible components, which is restricted by the channels used for the ICA.

This produces several considerations regarding IC interpretation: Estimation of single equivalent dipoles from an in fact bi- or even multiple source IC will describe some mixture of the true source location, thus making an assignment to brain structures improper. Furthermore, clustering of ambiguous ICs based on both localization and functional measures might lead to clusters with scattered dipoles when functional patterns are similar. On the other hand, ICs can be assigned to a cluster due to similar dipole locations even though their functional measures show profound disparities. The former can be seen for the frontal cluster shown in figure 7.12(b), left. The tuning of weights given for the individual measures for clustering could improve results. When uncertain of dipole estimation, weighting for functional measures like ERP, spectra or ERSP could be increased to obtain cluster ICs with more similar temporal and spectral properties. However, disregarding spatial information may result in clusters of ICs with similar functional properties, which in fact originate from different brain sources. Consequently, clustering of ambiguous ICs is unlikely to group corresponding brain components from different subjects correctly. Consequently, it is concluded that cluster settings cannot compensate for the indefinite source decomposition as found in this study results.

### 8.2.3 Network activity

Baseline statistics showed no significant spectral perturbation or ERD/S for the cluster assigned to the frontal or left temporal cluster. The right lateral motor cluster was excluded from analysis since less than half of the subjects contributed to this group of ICs.

It appears as though golf putting measured on the golf course introduces more non-stereotypical artifacts than could be expected from the reported consistency of movement patterns (Cotterill et al., 2010), along with approaches that were able to separate brain and non-brain sources by ICA in walking and even running (Gwin, Gramann, & Makeig, 2010). Therefore, the method failed to identify brain areas and their spectral activation patterns. As a consequence, with no definite nodes, no network is identified as aimed.

The reasons for poor results of source decomposition can be found by reconsidering the main factors that determine ICA quality in relation to the specific setup of this experiment. These factors are found to be (1) the number of channels and (2) the electrode contact, discussed in the following.

#### **An underestimated number of required channels**

In this study, 64 scalp electrodes were used because application time is acceptable (<30 min) and the number of channels is sufficient for source reconstruction despite being at the lower end according to recommendations (Nunez & Srinivasan, 2006). The repetitive head and body movements during golf putting were assumed to produce stereotypical artifacts that can be decomposed by ICA, while still leaving enough space for functional ICs. In contrast, the data suggests that putt movements show a higher variability in terms of artifactual content than expected. This leads to inconsistent ICs of multiple (non-brain and brain) sources in clusters revealing no statistical relevant baseline dynamics for ERSP and ERD/S. More electrodes can increase decomposition quality because more sources can be separated. This was demonstrated in Gwin, Gramann, and Makeig (2010), where a 248 channel EEG was recorded during walking and slow running. Predominant non-brain sources were successfully decomposed in individual components, while brain related activity could still be described as single source ICs. Main non-brain sources included muscle activity originating from neck muscles compensating for head-displacement or due to head movements (Gramann, Gwin, et al., 2010). In general as many channels as possible (100 - 250) are recommended.

The quest for more electrodes however is only beneficial if preparations remain reasonably quick, no bridge building occurs between closely adjoined electrodes

and skin contact is reliable and durable throughout the measurement (Gramann et al., 2014). Furthermore, a larger number of channels also require significantly more sample points for the ICA resulting in longer recordings. Following suggestions in Onton et al. (2006), using 256 electrodes instead of 64 requires 16 times as many data points. This might create problems (time on task effects, fatigue, etc.) of unstable measurement conditions, particularly with regard to physically or mentally demanding tasks.

### **Approximately 60 % data loss due to movement artifacts**

Results of data quality investigations show that only about 40 % artifact-free trials are used for data analysis. Even though sizes of electrode caps are chosen by head circumference and additionally tightened with chin straps, manual artifact rejection revealed frequent electrode pops presumably caused by head movements.

Such non-stereotypical artifacts, once in the data stream, can only be rejected by automatic (Schlögl et al., 2007; Ghandeharion & Erfanian, 2010; Zou et al., 2014) or manual (deleting artifactual periods by experienced EEG experts) post-processing. One solution to gain better ICA quality, while retaining more data could be to perform ICA on very conservatively cleaned datasets, followed by applying the resulting weight matrix to less strictly cleaned data. Thus, the decomposition is more likely to find brain components, while more data is left to analyze in which remaining artifacts are averaged out (Ullsperger & Debener, 2010). Though this may be useful for ERS and ERD/S measures, it might still affect model fitting for further effective connectivity estimation.

To prevent artifacts that arise from suboptimal electrode contact, flexible cap design, a good fit and a reliable fixation needs to be ensured. Individual electrode application (e.g. cup electrodes), that are only connected to the skin but not embedded in a cap would be ideal, but impractical and time consuming. Considerations of mobile EEG recordings including hardware concerns are reviewed in Gramann et al. (2014).

### **8.2.4 Limitations**

Considering the outcome of this study, major points of methodological criticism have already been discussed in the previous sections. Problems have been identified to arise from signal acquisition to which post-processing can only partly

accommodate for. Furthermore, some consideration regarding the putting task itself shall be mentioned, which can be of use for future studies of this kind.

The putting distances were chosen according to PGA tour statistics and single subject pilot testings to achieve approximately 50 % overall success rate during the task for golfers with handicap lower than 10. Even though individual swing movements are described as consistent and low in variation, the different distances are expected to induce movement variability, which should in fact be avoided when observing cortical activation time-locked to specific phases of complex movements. Also, holes and / or angles to the holes were varied from subject to subject in favor of stable light condition. Therefore, putt difficulty varied. Golfers reported individual preferences for different kinds of putts (shape of the green, upward or downward running green) and also for the particular putter that was used. To which degree each of these points creates variation and therefore influences comparability regarding demands and timing of movement patterns of the single putts remains speculative.

In regard to comparable demands across subjects, individual pre-trials could be used to adjust the distance individually to a certain success rate (Babiloni et al., 2008, 2011; Cooke et al., 2014).

With respect to movement kinetics, motion tracking could be used to capture body and putter movement to be able to relate different phases of these complex movements to one another. The approach of simultaneous so-called brain and body imaging was recently reviewed by Gramann et al. and will be discussed in chapter 10 (Gramann et al., 2014).

### **8.2.5 Concluding the specific aims**

#### **B. To map the activity and effective connectivity of localized brain sources during golf putting in a real-world setting.**

The relatively calm movements and stereotypical routines during golf putting gave rise to the assumption that the methodological approach applied in the force pulse study, could also be used to investigate cortical sensorimotor control processes in this more complex measurement setting and movement. It turns out that problems regarding a stable electrode contact using standard electrode caps and interferences from EMG activity cannot be compensated by ICA. That is, the number of sources (functional and artifactual) exceeded

the number of channels used in this study. Thus, the proposed methodological course of action cannot be used for studying cortical sensorimotor control processes during complex measurement settings and movements like golf putting with this specific setup. The problems appear to originate from suboptimal signal acquisition procedures and not from the applied signal processing approaches in general.

Unique multi source ICs are found as a result of the unbalanced channel to source ratio, but still form six clusters with a considerable number of subjects. Some of these clusters show activation that is thought to be related to expected brain areas (ACC, lateral MA, PPC), but are also contaminated with EMG activity so that these clusters cannot be assigned to brain anatomical regions as with the results of the force pulse study.

All following steps (ICA, IC selection, clustering, ERSP, ERD/S, and model fitting for effective connectivity and ERC estimation) depend on the decomposition quality of sources. Hence, following aims falling under B could not be achieved. This includes the identification of reliable ICs that define a network (B.1), clusters that show individual activity by means of ERSP and ERD/S (B.2) and the fitting of MVAR models to estimate ERC between the nodes of a network (B.3). From these results, suggestions are drawn to improve ICA in future studies in real-world settings dealing with complex movements. Essentially, the aim is to reduce or even avoid the above discussed interferences and acquire reliable ICs that predominantly represent single sources of both artifactual and brain activity. In summary, it is suggested to (1) use more electrodes to capture more sources and (2) electrode caps or fixations that are less prone to shifting due to head movements. For the former, it should be considered that setup time should be kept to a minimum regarding further application in exercise research in general and especially when working with top-class athletes. These problems need to be solved when acquiring EEG data in real-world settings and during complex movements to use ICA for the removal of inevitable biological artifacts and to reconstruct source signals.

## 9 Conclusion

This project was set out to map the brain network dynamics of sensorimotor control during precise goal-directed movements in laboratory and real-world settings. For this, novel approaches in computational neuroscience allowing the observation of network dynamics by means of localization, activity and connectivity were applied. Specifically, measures of brain effective connectivity, interpreted as the information flow between brain areas, is proposed to provide a mechanistic understanding of brain processes underlying sensorimotor control. However, these approaches have not been used to study the brain network dynamics during the execution of precise goal-directed movements, which are crucial in sports and exercise. Towards a future application in sports medicine research, for example as a diagnostic tool for fatigue, or influences on or causes of injuries, it is essential to test these methods not only in a laboratory, but also in a real-world setting.

This work demonstrates that ICA based source localization combined with functional time-frequency measures can be used to identify multiple brain areas predominantly engaged in the execution of precise, goal-directed force pulses. The identified network included the ACC, lateral sensory and motor areas, as well as a right lateral area of the PPC, which are known to be involved in sensorimotor control of voluntary movements in general. Besides characteristic ERD/S patterns of these areas, their effective connectivity by means of ERC was estimated. Predominantly, movement-related patterns of bidirectional theta ERC are found between ACC and motor areas. Patterns of both, activation and communication, were related to specific subperiods of the movement (planning, execution and monitoring), justifying the use of methods with high time resolution. Furthermore, it was highlighted that activation and effective connectivity did not necessarily correlate, hence providing complementary measures. Based on existing literature, the observed effects were related to processes of attentional control, information integration and performance monitoring.

In an attempt to apply the same signal processing procedures to recordings that were acquired in a real-world setting during complex movements (here: golf putting),

ICA did not separate artifact from brain source activity sufficiently to clearly identify engaged brain areas. The main problems arose from unstable electrode contact in combination with an insufficient number of electrodes with respect to the amount of task-related artifacts. This led to revised methodological guidelines for future experiments of this kind. As proposed, data acquisition and therewith ICA results can be improved by an increased number of electrodes and also by improving the stability of electrode to skin contact with hardware adjustments to this admittedly challenging setting. However, consequences include longer preparation and recording times, which represent a trade-off with regards to investigations of movements that might induce physical or mental fatigue over time.

The findings emphasize the importance of studying the brain processes (1) on the time scale on which movements are executed and (2) by simultaneously mapping their localized activation and communication patterns as complementary measures. By incorporating the outlined methodological requirements, the methods presented here are thought to be useful to study conditional effects regarding influencing factors of sensorimotor control, which are decisive for motor performance in sports.

Additionally, this work demonstrates challenges to be addressed in future research. The findings from the golf putt study add to currently discussed problems in mobile functional brain imaging (Gramann et al., 2014) and emphasizes the need for further development regarding hardware solutions, adapted test designs and signal processing techniques. Following the discussion, high-density and quality EEG recordings and simultaneous motion tracking are required to study movement related brain network dynamics in or close to real-world settings. This remains restricted to relatively calm movements that can be consistently repeated.

It must be noted that the presented results do have some general limitations. (1) Inclusion criteria of subjects led to a relatively small, but homogeneous cohort of highly skilled golfers; thus, transferability or generalization to a broader population remains to be evaluated. (2) Statistical procedures for high resolution time-frequency images based on source signals gained from data driven approaches appear to be strict and require further clarification. (3) The results from the force pulse study are confined to goal-directed movements that require feed-forward control without online feedback integration. (4) It should once more be emphasized that ERC does not denote static causal dependencies, which may or may not be constantly present throughout the task. ERC rather measures increased and decreased information flow, denoted by positive or negative deviations from a chosen baseline.



---

Although it is well known that information integration and processing for sensorimotor control of goal-directed movements is largely carried out in a network of cortical brain areas, actual measures of information flow have rarely been applied to gain mechanistic understanding of these processes. Here, it was shown that brain network dynamics can be analyzed during the execution of goal-directed force precision tasks by means of localization, activity and connectivity. For the latter, ERC provides the central measure of directed information flow between participating brain areas. Thereby, this work sets the basis for investigations regarding altered performance of goal-directed movements due to factors that influence sensorimotor control function like injury or fatigue.



# 10 Prospects

In chapter 8, some limitations in the methodology as well as requirements for real-world measurements were identified. Due to the procedural nature of this work this final chapter aims to briefly outline some aspects of ongoing research in computational neuroscience and ways to overcome some of the identified problems. In section 10.1, methodological approaches are presented, while section 10.2 considers future work towards reliably recording EEG in sports and exercise to study task-specific brain dynamics. Lastly, future research is proposed that might benefit from applying the methods demonstrated here.

## 10.1 Methodological future work

### IC selection and clustering

A critical point of ICA based investigation is the selection of ICs, because the used methods are heuristic and prone to subjective decisions. Currently this is addressed by incorporating a variety of EEG measures (topographic maps, dipole localization, frequency spectra, ERP and ERSP) to increase certainty for correctly selecting task-relevant brain components (Onton, 2009; Onton & Makeig, 2006). Regarding clustering of ICs, the number of clusters to generate, as well as which measures to use and weights to apply to them is also based on heuristic evaluations. Bigdely-Shamlo et al., recently proposed measure projections analysis (MPA), which can be used with ICA decomposed data. MPA is a probabilistic approach which uses different measures of EEG to group selected brain sources and delivers estimates of the statistical reliability of the formed clusters. This is done in the voxel space of a head model and therewith puts EEG into the framework of other brain imaging methods like fMRI (Bigdely-Shamlo et al., 2013).

This method does not solve the problem of initial IC selection, but provides a statistical measure to classify the quality of IC clustering.

### **Source localization**

Source localization based on scalp electrode data remains restricted to the ill-posed inverse problem. Besides dipole source localization, several other techniques have been proposed: The Minimum Norm (Hämäläinen & Ilmoniemi, 1984), Weighted Minimum Norm (Charles & Richard, 1974), Laplacian Weighted Minimum Norm (LORETA, Pascual-Marqui, Michel, and Lehmann (1994)), Local autoregressive Average (LAURA, de Peralta and Andino (2002)), EPIFOCUS (de Peralta & Andino, 2002), Beamformer (Gross et al., 2001), or Bayesian approaches (Schmidt et al., 1999). A comprehensive review can be found in C. M. Michel et al. (2004). It is common sense that if several of these approaches reciprocally verify each other's results, certainty about the true localization of the observed activity, can be increased. This should be incorporated in future studies. Moreover, accuracy of source localization results can be increased by deriving realistic head-models from individual structural MRI scans and exact measurements of electrode positions in each recording (Z. Acar & Makeig, 2013). However, since the inverse problem remains, simultaneous EEG - fMRI studies can be used to verify the former approaches. Correlating the EEG source with the BOLD signals can be used to find the link between the modalities of electric activity and hemodynamic responses (Ullsperger & Debener, 2010; C. Michel & Murray, 2012).

### **Multimodel ICA**

The routing of information along the communication pathways in the brain is proposed to be flexible to bring about cognitive dynamics (Fries, 2005). Thus, in different conditions or periods during a task the functional organization of distributed neural assemblies varies. Single model ICA, as currently used, is not able to capture these non-stationary effects. One solution would be to incorporate several ICA models of which each may be superior for a certain period of time. Estimating a given number of models is already implemented in Palmer's AMICA algorithm (Palmer et al., 2008), but how to deal with this added complexity of time varying decomposition models remains a question of current research.

### **Time-frequency ICA**

ICA is a data driven approach for which no prior assumption about the underlying sources is necessary. However, for the case of EEG, it is well known that the mixed source signals have characteristic spectral content such as predominant theta, alpha and beta band activity. This information can be used to optimize the source reconstruction by ICA. This was addressed with so-called time-frequency ICA (tfICA) introduced by Shou et al. (2012). Essentially, ICA is performed on predefined dominant frequency bins, based on PCA of time-frequency distributions of the data, thus disregarding less informative or non-characteristic spectral content. The authors argue that more reliable functional ICs can be found during real-world, less controlled tasks. tfICA was proposed as a method for studying long-term effects like mental fatigue in cognitively demanding work environments. However, estimating causal relation between time series require intact phase relations among signals. Whether the preceding preprocessing steps towards tfICA conserve phase relations has yet to be evaluated.

### **Cross-frequency effective connectivity**

The methods applied here are measures of frequency specific ERC amongst brain sources, based on the proposed mechanism of information transmission through neuronal coherence (Fries, 2005). However, networks of different spatial and temporal scales exist (Sporns & Tononi, 2007). For example RSNs represent large scale networks of higher brain functions (Canolty & Knight, 2010). A sensorimotor control network is also spatially large scale, but the mechanisms to provide sensory integration and adapted motor control act on faster time scales (Sporns, 2013). It was proposed that coupling mechanisms must exist that link neuronal interactions at multiple spatial and temporal scales (Engel et al., 2013). One promising idea is to analyze cross-frequency functional and effective connectivity to capture coupling between multiscale networks. Cross-frequency coupling could build the basis for further investigations as reviewed in Engel et al. (2013), Canolty and Knight (2010) and Jensen and Colgin (2007).

## 10.2 Towards the application of effective connectivity measures in sports and exercise

### Improving data acquisition

In the golf putt study the main problem was signal quality and the number of channels used to record the EEG. Even though the latter was chosen deliberately for the sake of applicability (temporal costs), the results suggest that this issue must be overcome differently. Consequently, future studies should use well-chosen electrode caps with a tight fit even in motion so that electrodes are less likely to shift or lose contact. Thus, more electrodes will increase accuracy of source reconstruction and quality of ICA so that data is decomposed into more sources, both artifactual and functional. Very recently, Gramann et al. developed a concept of mobile brain and body imaging (MoBI) and proposed requirements for measuring brain activity in motion and in real-world conditions (Gramann et al., 2014). In short: Gel electrodes are found to provide the best signal quality, but are at a disadvantage because the application can be time consuming, abrasion of outer skin layers might induce discomfort or skin irritations. Short circuits are likely with very high density recordings and because they are hard-wired, artifacts from cable sway may occur. Dry electrodes are favored in principle, but their development was found to be immature for reliable recordings of good quality at this stage. In conclusion, dry and even non-contact wireless sensors are stated to be essential for the future in MoBI.

To be able to move freely during measurements, lightweight wireless systems are necessary. Several mobile solutions are on the market, but mainly for the purpose of entertainment or for monitoring sleep status, for which only few electrodes are sufficient. High density mobile EEG systems would be ideal for future investigations in this field.

### Shortening recording times

Another issue is the amount of data that is required for both ICA and MVAR model fitting. With more electrodes, the number of sample points needed increases quadratically (Onton et al., 2006). However, long time recordings can not only induce problems related to stable recording conditions but might also be biased by effects of mental or physical fatigue or learning. The suggested number of data points for ICA (about 30 times the number of channels squared) is a rule of thumb, but has not been evaluated yet. Shorter recordings would be less prone

to biases caused by fatigue, learning or habituation, less time consuming for the participant and allow shorter intervention times with more flexible measurement protocols. In this regard an online version of ICA, the recursive ICA proposed by Akhtar, Jung, Makeig, and Cauwenberghs (2012), could be useful in future investigations.

Regarding effective connectivity estimation, Mullen, Kothe, Chi, and Ojeda recently reported advances in providing a real-time data extraction, preprocessing, artifact rejection, source reconstruction, multivariate dynamical system analysis and 3D visualization and classification of EEG brain recordings (Mullen et al., 2013). However connectivity estimation was shown on channel data only, but not on source signals so far.

Nevertheless, these methodological approaches illustrate the extensive amount of research carried out at this stage and indicate ongoing advances in the field.

### **Dealing with inter-trial and inter-individual variability**

In the attempt to map sensorimotor control processes during complex movements, it was important to be able to identify particular phases of movements to relate the EEG activity to. This was done by recording the force and acceleration signals respectively. However, considering the time resolution which EEG offers, it should also be noted that inter-trial variability as well as inter-individual differences of movement and thus cortical activation patterns could be significant. In the process of averaging over trials, brain activity dynamics of short duration and at specific points in time could be diminished. Measuring, additional modalities, like the EMG and more biomechanical data (ground reaction forces, motion tracking in time and space) could help to identify correlation with the neuronal activation. This can be done by deriving several trigger events throughout each movement pattern and time-warping each trial to an averaged pattern. This method has been applied to the neuronal correlates of the human gait-cycle in Gwin, Gramann, and Ferris (2010).

### **Following research questions**

In this work, it was shown that it is possible to map the transient brain dynamics of parts of the sensorimotor network during goal-directed movement. The next step is to apply these methods to content related research questions in sports medicine research.

1) In Baumeister et al. (2012a) sensorimotor control was affected by induced fa-

tigue which was expressed by impaired task performance (precision of knee angle reproduction) and by altered spectral signatures in the EEG. Changes of power density in frontal and parietal regions were related to altered processes of attentional control, alertness and somatosensory information integration. Further insights might be gained by conducting an intervention study to compare network dynamics during sensorimotor control in a fatigue and a non-fatigue condition. The force pulse study conducted here could be used in such an investigation.

2) The shown representations of performance monitoring should also be investigated in more detail. Based on the concepts of error processing (Ullsperger et al., 2014) conditional changes for successful and unsuccessful motor behavior can be expected within the fronto-motor network. Brain network dynamics of performance monitoring by means of ERC have been investigated in cognitive tasks but not related to precise motor performance (Mullen, Onton, & Delorme, 2010; Di Luft et al., 2013).

3) Considering performance monitoring as a mechanism for motor learning and adaption of motor programs (Ullsperger et al., 2014), this network activity could be a possible marker for the ability of skill acquisition in sports. This is indicated by recent findings in Di Luft et al. (2013), where high-learners present larger central to mid-frontal theta connectivity in response to incorrect performance feedback compared to low-learners. However, this was tested in a time estimation task, in which some subjects showed higher performance increase (high-learners) than others. Whether this is similar for motor skill acquisition or discriminative for motor skill level (between groups) remains to be investigated.



# References

- Acar, Z., & Makeig, S. (2013). Effects of Forward Model Errors on EEG Source Localization. *Brain topography*, 1–19.
- Acar, Z. A., & Makeig, S. (2010, July). Neuroelectromagnetic Forward Head Modeling Toolbox. *Journal of neuroscience methods*, 190(2), 258–270.
- Akhtar, M. T., Jung, T.-P., Makeig, S., & Cauwenberghs, G. (2012). Recursive independent component analysis for online blind source separation. *Circuits and Systems (ISCAS), 2012 IEEE International Symposium on*, 2813–2816.
- Amaral, D. G. (2013). The functional organization of perception and movement. In *Principles of neural science* (pp. 356–369). McGraw-Hill Education.
- Amaral, D. G., & Strick, P. L. (2013). The Organization of the Central Nervous System. In *Principles of neural science* (pp. 337–355). McGraw-Hill Education.
- Amzica, F., & Lopes da Silva, F. H. (2012, January). Cellular Substrates of Brain Rhythms. In *Niedermeyer's electroencephalography: Basic principles, clinical applications, and related fields*.
- Armbrecht, A.-S., Gibbons, H., & Stahl, J. (2012, January). Monitoring force errors: medial-frontal negativity in a unimanual force-production task. *Psychophysiology*, 49(1), 56–72.
- Arns, M., Kleinnijenhuis, M., Fallahpour, K., & Breteler, R. (2008, August). Golf Performance Enhancement and Real-Life Neurofeedback Training Using Personalized Event-Locked EEG Profiles. *Journal of Neurotherapy*, 11(4), 11–18.
- Astolfi, L., Cincotti, F., Mattia, D., de Vico Fallani, F., Lai, M., Baccala, L., . . . Babiloni, F. (2005). Comparison of different multivariate methods for the estimation of cortical connectivity: simulations and applications to EEG data. *IEEE Engineering in Medicine and Biology Society. Conference*, 5, 4484–4487.
- Astolfi, L. L., Cincotti, F. F., Mattia, D. D., Marciani, M. G. M., Baccala, L. A. L., de Vico Fallani, F. F., . . . Babiloni, F. F. (2007, January). Comparison of different cortical connectivity estimators for high-resolution EEG recordings. *Hum Brain Mapp*, 28(2), 143–157.
- Babiloni, C., Babiloni, F., Carducci, F., Cincotti, F., Del Percio, C., De Pino,

- G., ... Rossini, P. M. (2000, August). Movement-related electroencephalographic reactivity in Alzheimer disease. *NeuroImage*, *12*(2), 139–146.
- Babiloni, C., Carducci, F., Cincotti, F., Rossini, P. M., Neuper, C., Pfurtscheller, G., & Babiloni, F. (1999). Human movement-related potentials vs desynchronization of EEG alpha rhythm: A high-resolution EEG study. *NeuroImage*, *10*(6), 658–665.
- Babiloni, C., Del Percio, C., Iacononi, M., Infarinato, F., Lizio, R., Marzano, N., ... Eusebi, F. (2008, January). Golf putt outcomes are predicted by sensorimotor cerebral EEG rhythms. *The Journal of Physiology*, *586*(1), 131–139.
- Babiloni, C., Infarinato, F., Marzano, N., Iacononi, M., Dassù, F., Soricelli, A., ... Del Percio, C. (2011, December). Intra-hemispheric functional coupling of alpha rhythms is related to golfer's performance: a coherence EEG study. *International Journal of Psychophysiology*, *82*(3), 260–268.
- Baccalá, L. A., & Sameshima, K. (2001, June). Partial directed coherence: a new concept in neural structure determination. *Biological Cybernetics*, *84*(6), 463–474.
- Baddeley, A. (2003, January). Working memory: Looking back and looking forward. *Nature reviews Neuroscience*, 1–11.
- Baddeley, A. (2012, January). Working memory: theories, models, and controversies. *Annual review of psychology*.
- Baumeister, J. (2013). *Sensorimotor Control and associated Brain Activity in Sports Medicine Research*. University of Paderborn.
- Baumeister, J., Reinecke, K., Cordes, M., Lerch, C., & Weiss, M. (2010, August). Brain activity in goal-directed movements in a real compared to a virtual environment using the Nintendo Wii. *Neuroscience Letters*, *481*(1), 47–50.
- Baumeister, J., Reinecke, K., Liesen, H., & Weiss, M. (2008, November). Cortical activity of skilled performance in a complex sports related motor task. *European journal of applied physiology*, *104*(4), 625–31.
- Baumeister, J., Reinecke, K., Schubert, M., Schade, J., & Weiss, M. (2012a). Effects of induced fatigue on brain activity during sensorimotor control. *European journal of applied physiology*, *112*(7), 2475–2482.
- Baumeister, J., Reinecke, K., Schubert, M., Schade, J., & Weiss, M. (2012b, July). Effects of induced fatigue on brain activity during sensorimotor control. *European journal of applied physiology*, *112*(7), 2475–2482.
- Baumeister, J., Reinecke, K., Schubert, M., & Weiss, M. (2011, September). Altered electrocortical brain activity after ACL reconstruction during force control. *Journal of orthopaedic research : official publication of the Orthopaedic Research Society*, *29*(9), 1383–1389.
- Bear, M. F., Connors, B. W., & Paradiso, M. A. (2007). *Neuroscience*.
- Beilock, S. L., & Gray, R. (2012, December). From attentional control to attentional spillover: a skill-level investigation of attention, movement, and performance outcomes. *Human movement science*, *31*(6), 1473–1499.
- Bell, A., & Sejnowski, T. (1995). An Information-Maximization Approach to

- Blind Separation and Blind Deconvolution. *Neural Computation*, 7(6), 1129–1159.
- Benjamini, Y., & Hochberg, Y. (1995, January). Controlling the false discovery rate: a practical and powerful approach to multiple testing. *Journal of the Royal Statistical Society Series B*, –.
- Berger, P. D. H. (1929, December). Über das Elektrenkephalogramm des Menschen. *Archiv für Psychiatrie und Nervenkrankheiten*, 87(1), 527–570.
- Bigdely-Shamlo, N., Mullen, T., Kreutz-Delgado, K., & Makeig, S. (2013, May). Measure projection analysis: a probabilistic approach to EEG source comparison and multi-subject inference. *NeuroImage*, 72, 287–303.
- Blake, A., & Grundy, C. (2008). Evaluation of motion capture systems for Golf Swings: Optical vs. gyroscopic. *30th International Conference on Information Technology Interfaces (ITI)*, 409–414.
- Bozzacchi, C., Giusti, M. A., Pitzalis, S., Spinelli, D., & Di Russo, F. (2012, January). Awareness affects motor planning for goal-oriented actions. *Biological psychology*, 89(2), 503–514.
- Breakspear, M., & Jirsa, V. K. (2007, January). Neuronal Dynamics and Brain Connectivity. In *Handbook of brain connectivity* (pp. 3–64). Berlin, Heidelberg: Springer Berlin Heidelberg.
- Bressler, S. L. (2011, January). Event-Related Potentials of the Cerebral Cortex. In *Electrophysiological recording techniques* (pp. 169–190). Totowa, NJ: Humana Press.
- Bressler, S. L., & Seth, A. K. (2011, January). Wiener–Granger causality: a well established methodology. *NeuroImage*, 1–7.
- Budzynski, T. H., Budzynski, H. K., Evans, J. R., & Abarbanel, A. (2009). *Introduction to Quantitative EEG and Neurofeedback*. Academic Press.
- Bullmore, E., & Sporns, O. (2009). Complex brain networks: graph theoretical analysis of structural and functional systems. *Nature reviews Neuroscience*, 10(3), 186–198.
- Canolty, R. T., & Knight, R. T. (2010, November). The functional role of cross-frequency coupling. *Trends in Cognitive Sciences*, 14(11), 506–515.
- Capotosto, P., Babiloni, C., & Romani, G. L. (2008). Posterior parietal cortex controls spatial attention through modulation of anticipatory alpha rhythms. *Nature*.
- Cavanagh, J. F., Figueroa, C. M., Cohen, M. X., & Frank, M. J. (2012, November). Frontal theta reflects uncertainty and unexpectedness during exploration and exploitation. *Cerebral cortex (New York, N.Y. : 1991)*, 22(11), 2575–2586.
- Charles, L. L., & Richard, J. H. (1974). *Solving least squares problems*. Preutice-Hall Series.
- Chen, L. C., Huang, J. K., Huang, C. J., & Hung, T. M. (n.d.). Effects of Central Alpha Neurofeedback Training on Golf Putting. *ntnu.edu.tw*.
- Congedo, M., John, R. E., De Ridder, D., & Prichep, L. (2010, November). Group independent component analysis of resting state EEG in large normative

- samples. *International Journal of Psychophysiology*, 78(2), 89–99.
- Cooke, A., Kavussanu, M., Gallicchio, G., Willoughby, A., McIntyre, D., & Ring, C. (2014, April). Preparation for action: Psychophysiological activity preceding a motor skill as a function of expertise, performance outcome, and psychological pressure. *Psychophysiology*, 51(4), 374–384.
- Cooper, R., Osselton, J. W., & Shaw, J. C. (1984). *Elektroenzephalographie: Technik und Methoden*. Fischer.
- Cotterill, S. T., Sanders, R., & Collins, D. (2010, January). Developing Effective Pre-performance Routines in Golf: Why Don't We Ask the Golfer? *Journal of Applied Sport Psychology*, 22(1), 51–64.
- Couceiro, M. S., Dias, G., Mendes, R., & Araújo, D. (2013). Accuracy of pattern detection methods in the performance of golf putting. *Journal of motor behavior*, 45(1), 37–53.
- Craig, C. M., Delay, D., Grealy, M. A., & Lee, D. N. (2000). Guiding the swing in golf putting. *Nature*.
- Crews, D. J., & Landers, D. M. (1993, January). Electroencephalographic measures of attentional patterns prior to the golf putt. *Journal of the American College of*, 1–11.
- da Silva, F., & Van Rotterdam, A. (2011). *Biophysical aspects of EEG and MEG generation*. Electroencephalography.
- Davidson, R. J. (1998, September). Anterior electrophysiological asymmetries, emotion, and depression: conceptual and methodological conundrums. *Psychophysiology*, 35(5), 607–614.
- Debener, S., Ullsperger, M., Siegel, M., Fiehler, K., von Cramon, D. Y., & Engel, A. K. (2005, December). Trial-by-trial coupling of concurrent electroencephalogram and functional magnetic resonance imaging identifies the dynamics of performance monitoring. *The Journal of neuroscience : the official journal of the Society for Neuroscience*, 25(50), 11730–11737.
- Delorme, A., & Makeig, S. (2004, March). EEGLAB: an open source toolbox for analysis of single-trial EEG dynamics including independent component analysis. *Journal of neuroscience methods*, 134(1), 9–21.
- Delorme, A., Mullen, T., Kothe, C., Akalin Acar, Z., Bigdely-Shamlo, N., Vankov, A., & Makeig, S. (2011). EEGLAB, SIFT, NFT, BCILAB, and ERICA: New Tools for Advanced EEG Processing. *Computational Intelligence and Neuroscience*, 2011, 1–12.
- Delorme, A., Palmer, J., Onton, J., Oostenveld, R., & Makeig, S. (2012, January). Independent EEG sources are dipolar. *PLoS ONE*, –.
- de Peralta, R. G., & Andino, S. G. (2002). *Comparison of algorithms for the localization of focal sources: evaluation with simulated data and analysis of experimental data*. *Int J Bioelectromagn*.
- Diermayr, G., McIsaac, T. L., & Gordon, A. M. (2011). Finger force coordination underlying object manipulation in the elderly - a mini-review. *Gerontology*, 57(3), 217–227.
- Di Luft, C. B., Nolte, G., & Bhattacharya, J. (2013, January). High-learners

- present larger mid-frontal theta power and connectivity in response to incorrect performance feedback. *The Journal of neuroscience : the official journal of the Society for Neuroscience*, 33(5), 2029–38.
- Ding, M., Bressler, S. L., Yang, W., & Liang, H. (2000, June). Short-window spectral analysis of cortical event-related potentials by adaptive multivariate autoregressive modeling: data preprocessing, model validation, and variability assessment. *Biological Cybernetics*, 83(1), 35–45.
- Doppelmayr, M., Finkenzeller, T., & Sauseng, P. (2008, April). Frontal midline theta in the pre-shot phase of rifle shooting: differences between experts and novices. *Neuropsychologia*, 46(5), 1463–1467.
- Dworetzky, B., Herman, S., & Tatum IV, W. O. (2012, January). Artifacts of recording. In *Niedermeyer's electroencephalography: Basic principles, clinical applications, and related fields*. . . .
- Ehrsson, H. H., Fagergren, A., & Forssberg, H. (2001, June). Differential frontoparietal activation depending on force used in a precision grip task: an fMRI study. *Journal of neurophysiology*, 85(6), 2613–23.
- Engel, A. K., Gerloff, C., Hilgetag, C. C., & Nolte, G. (2013, November). Intrinsic Coupling Modes: Multiscale Interactions in Ongoing Brain Activity. *Neuron*, 80(4), 867–886.
- Ewen, J. B., Lakshmanan, B. M., Hallett, M., Mostofsky, S. H., Crone, N. E., & Korzeniewska, A. (2014, September). Dynamics of functional and effective connectivity within human cortical motor control networks. *Clinical neurophysiology : official journal of the International Federation of Clinical Neurophysiology*.
- Fearing, D., Acimovic, J., & Graves, S. C. (2011). How to catch a Tiger: Understanding putting performance on the PGA Tour. *Journal of Quantitative Analysis*, 7(1).
- Ferdinand, N. K., Mecklinger, A., Kray, J., & Gehring, W. J. (2012, August). The processing of unexpected positive response outcomes in the mediofrontal cortex. *The Journal of neuroscience : the official journal of the Society for Neuroscience*, 32(35), 12087–12092.
- Field, A. (2009, January). *Discovering Statistics Using SPSS*. SAGE.
- Fisch, B. J. (2012, January). Polarity and Field Determinations. In *Niedermeyer's electroencephalography: Basic principles, clinical applications, and related fields* (pp. 143–151).
- Florian, G., & Pfurtscheller, G. (1995, November). Dynamic spectral analysis of event-related EEG data. *Electroencephalography and clinical neurophysiology*, 95(5), 393–396.
- Fox, M. D., & Raichle, M. E. (2007, September). Spontaneous fluctuations in brain activity observed with functional magnetic resonance imaging. *Nature reviews. Neuroscience*, 8(9), 700–711.
- Fries, P. (2005). A mechanism for cognitive dynamics: neuronal communication through neuronal coherence. *Trends in Cognitive Sciences*, 9(10), 474–480.
- Friston, K., Moran, R., & Seth, A. K. (2012, January). Analysing connectivity

- with Granger causality and dynamic causal modelling. *Current opinion in neurobiology*, 1–7.
- Friston, K. J., Harrison, L., & Penny, W. (2003, August). Dynamic causal modelling. *NeuroImage*, 19(4), 1273–1302.
- Fukuda, H., & Hiwaki, O. (2013, October). Brain activity evoked by motor inhibition before volitional finger movement. *Neuroreport*, 24(14), 791–796.
- Gardner, E. P., & Johnson, K. O. (2013). The Somatosensory System: Receptors and Central Pathways. In *Principles of neural science* (pp. 475–497).
- Gevins, A. S., & Bressler, S. L. (1988). *Functional topography of the human brain*. Functional brain imaging.
- Ghandeharion, H., & Erfanian, A. (2010, September). A fully automatic ocular artifact suppression from EEG data using higher order statistics: Improved performance by wavelet analysis. *Medical Engineering & Physics*, 32(7), 720–729.
- Goebel, R., Roebroeck, A., Kim, D.-S., & Formisano, E. (2003, December). Investigating directed cortical interactions in time-resolved fMRI data using vector autoregressive modeling and Granger causality mapping. *Magnetic Resonance Imaging*, 21(10), 1251–1261.
- Gramann, K., Ferris, D. P., Gwin, J., & Makeig, S. (2014, January). Imaging natural cognition in action. *International Journal of Psychophysiology*, 91(1), 22–29.
- Gramann, K., Gwin, J. T., Bigdely-Shamlo, N., Ferris, D. P., & Makeig, S. (2010, January). Visual evoked responses during standing and walking. *Frontiers in Human Neuroscience*, 4, 202.
- Gramann, K., Onton, J., Riccobon, D., Mueller, H. J., Bardins, S., & Makeig, S. (2010, December). Human brain dynamics accompanying use of egocentric and allocentric reference frames during navigation. *Journal of Cognitive Neuroscience*, 22(12), 2836–2849.
- Granger, C. W. J. (1969). Investigating causal relations by econometric models and cross-spectral methods. *Econometrica: Journal of the Econometric Society*, 424–438.
- Grefkes, C., Eickhoff, S. B., Nowak, D. A., Dafotakis, M., & Fink, G. R. (2008). Dynamic intra- and interhemispheric interactions during unilateral and bilateral hand movements assessed with fMRI and DCM. *NeuroImage*, 41(4), 1382–1394.
- Grefkes, C., Wang, L. E., Eickhoff, S. B., & Fink, G. R. (2010, April). Noradrenergic modulation of cortical networks engaged in visuomotor processing. *Cerebral cortex (New York, N.Y. : 1991)*, 20(4), 783–797.
- Groppe, D., Makeig, S., & Kutas, M. (2009, May). Identifying reliable independent components via split-half comparisons. *NeuroImage*, 45(4), 1199–1211.
- Gross, J., Kujala, J., Hämäläinen, M., Timmermann, L., Schnitzler, A., & Salmelin, R. (2001, January). Dynamic imaging of coherent sources: Studying neural interactions in the human brain. *Proceedings of the National Academy of Sciences*, 98(2), 694–699.

- Grosse-Wentrup, M., Harmeling, S., Zander, T., Hill, J., & Scholkopf, B. (2013). How to Test the Quality of Reconstructed Sources in Independent Component Analysis (ICA) of EEG/MEG Data. *2013 International Workshop on Pattern Recognition in Neuroimaging (PRNI)*, 102–105.
- Gulyás, S., Szirmai, I., & Kamondi, A. (2009, January). Post-movement beta synchronisation after complex prosaccade task. *Clinical neurophysiology : official journal of the International Federation of Clinical Neurophysiology*, *120*(1), 11–17.
- Gwin, J. T., Gramann, K., & Ferris, D. P. (2010, January). Electro cortical brain activity is coupled to gait cycle phase during treadmill waking. *Abstr 3rd Int*, 1–8.
- Gwin, J. T., Gramann, K., & Makeig, S. (2010, January). Removal of movement artifact from high-density EEG recorded during walking and running. *Journal of*.
- Hämäläinen, M. S., & Ilmoniemi, R. J. (1984). *Interpreting measured magnetic fields of the brain: estimates of current distributions*. Helsinki University of Technology.
- He, L., & Sarkar, S. K. (2013). On improving some adaptive BH procedures controlling the FDR under dependence. *Electronic Journal of Statistics*, *7*(0), 2683–2701.
- He, Y., Wang, J., Wang, L., Chen, Z. J., Yan, C., Yang, H., . . . Evans, A. C. (2009). Uncovering intrinsic modular organization of spontaneous brain activity in humans. *PLoS ONE*, *4*(4), e5226.
- Hebb, D. O. (1949). *The Organization of Behaviour: A Neuro-psychological Theory*. Wiley.
- Herz, D. M., Christensen, M. S., Reck, C., Florin, E., Barbe, M. T., Stahlhut, C., . . . Timmermann, L. (2011). Task-specific modulation of effective connectivity during two simple unimanual motor tasks: A 122-channel EEG study. *NeuroImage*, 1–7.
- Hesse, W. (2009). *Untersuchung gerichteter Interaktionen multivariater biomedizinischer Signale auf der Basis des Vorhersagbarkeitsprinzips nach Granger*. Technische Universität Ilmenau.
- Hinder, M. R., Schmidt, M. W., Garry, M. I., & Summers, J. J. (2010, March). The effect of ballistic thumb contractions on the excitability of the ipsilateral motor cortex. *Experimental Brain Research*, *201*(2), 229–238.
- Hoffmann, S., Labrenz, F., Themann, M., Wascher, E., & Beste, C. (2014, March). Crosslinking EEG time–frequency decomposition and fMRI in error monitoring. *Brain Structure and Function*, *219*(2), 595–605.
- Houdayer, E., Degardin, A., Salleron, J., Bourriez, J. L., Defebvre, L., Cassim, F., & Derambure, P. (2012, June). Movement preparation and cortical processing of afferent inputs in cortical tremor: an event-related (de)synchronization (ERD/ERS) study. *Clinical neurophysiology : official journal of the International Federation of Clinical Neurophysiology*, *123*(6), 1207–1215.
- Huang, R.-S., Jung, T.-P., Delorme, A., & Makeig, S. (2008, February). Tonic and

- phasic electroencephalographic dynamics during continuous compensatory tracking. *NeuroImage*, *39*(4), 1896–1909.
- Hyman, S. E., & Cohen, J. D. (2013). Disorders of Mood and Anxiety. In *Principles of neural science* (pp. 1402–1424). McGraw-Hill Education.
- Hyv, A., Karhunen, J., & Oja, E. (2001). Independent component analysis. *Wiley-Interscience*, –.
- Jäncke, L., Koeneke, S., Hoppe, A., Rominger, C., & Hänggi, J. (2009). The architecture of the golfer’s brain. *PLoS ONE*, *4*(3), e4785.
- Jansen, B. H., Bourne, J. R., & Ward, J. W. (1981). Autoregressive Estimation of Short Segment Spectra for Computerized EEG Analysis. *IEEE Transactions on Biomedical Engineering, BME-28*(9), 630–638.
- Jensen, O., & Colgin, L. L. (2007, July). Cross-frequency coupling between neuronal oscillations. *Trends in Cognitive Sciences*, *11*(7), 267–269.
- Jirsa, V. K., & McIntosh, A. R. (2007). *Handbook of Brain Connectivity*. Springer-Verlag Berlin Heidelberg.
- Jung, T., Makeig, S., Lee, T., & McKeown, M. (2000, January). Independent component analysis of biomedical signals. *Component Analysis*, –.
- Jung, T. P., Makeig, S., Humphries, C., Lee, T. W., McKeown, M. J., Iragui, V., & Sejnowski, T. J. (2000, March). Removing electroencephalographic artifacts by blind source separation. *Psychophysiology*, *37*(2), 163–178.
- Jung, T. P., Makeig, S., Westerfield, M., Townsend, J., Courchesne, E., & Sejnowski, T. J. (2001, November). Analysis and visualization of single-trial event-related potentials. *Human Brain Mapping 2010*, *14*(3), 166–185.
- Kalaska, J. F., & Rizzolatti, G. (2013). Voluntary Movement: The Primary Motor Cortex. In *Principles of neural science* (pp. 835–864). McGraw-Hill Education.
- Kamiński, M., Ding, M., Truccolo, W. A., & Bressler, S. L. (2001). Evaluating causal relations in neural systems: Granger causality, directed transfer function and statistical assessment of significance. *Biological Cybernetics*, *85*(2), 145–157.
- Kandel, E. R. (1991). Nerve cells and behavior. *Principles of neural science*, 18–32.
- Kandel, E. R. (2013). From Nerve Cells to Cognition: The Internal Representations of Space and Action. In *Principles of neural science* (pp. 370–391). McGraw-Hill Education.
- Kandel, E. R., & Hudspeth, A. J. (2013). The brain and behavior. In *Principles of neural science*. McGraw-Hill Education.
- Kilavik, B. E., Zaepffel, M., Brovelli, A., MacKay, W. A., & Riehle, A. (2013, July). The ups and downs of  $\beta$  oscillations in sensorimotor cortex. *Experimental neurology*, *245*, 15–26.
- Kilian, L. (2006, October). New introduction to multiple time series analysis by Helmut Lütkepohl, Springer, 2005. *Econometric theory*, *22*(05), 961–967.
- Kim, K. I., & van de Wiel, M. A. (2008). Effects of dependence in high-dimensional multiple testing problems. *BMC bioinformatics*, *9*(1), 114.



- Klem, G. H., Lüders, H. O., Jasper, H. H., & Elger, C. (1999). *The ten-twenty electrode system of the International Federation. The International Federation of Clinical Neurophysiology.*
- Kobza, S., & Bellebaum, C. (2013, May). Mediofrontal event-related potentials following observed actions reflect an action prediction error. *The European journal of neuroscience*, *37*(9), 1435–1440.
- Kornhuber, H. H., & Deecke, L. (1965, March). Hirnpotentialänderungen bei Willkürbewegungen und passiven Bewegungen des Menschen: Bereitschaftspotential und reafferente Potentiale. *Pflüger's Archiv für die gesamte Physiologie des Menschen und der Tiere*, *284*(1), 1–17.
- Korzeniewska, A., Crainiceanu, C. M., & Kuś, R. (2008). Dynamics of event-related causality in brain electrical activity. *Human brain . . .*
- Korzeniewska, A., Franaszczuk, P. J., Crainiceanu, C. M., Kuś, R., & Crone, N. E. (2011, June). Dynamics of large-scale cortical interactions at high gamma frequencies during word production: event related causality (ERC) analysis of human electrocorticography (ECoG). *NeuroImage*, *56*(4), 2218–2237.
- Kötter, R. (2007, January). Anatomical Concepts of Brain Connectivity. In *Handbook of brain connectivity* (pp. 149–167). Berlin, Heidelberg: Springer Berlin Heidelberg.
- Krakauer, J., & Ghez, C. (2000). Voluntary movement. In *Principles of neural science*. Principles of neural science.
- Kuhtz-Buschbeck, J. P., Ehrsson, H. H., & Forssberg, H. (2001, July). Human brain activity in the control of fine static precision grip forces: an fMRI study. *European Journal of Neuroscience*, *14*(2), 382–390.
- Kukleta, M., & Lamarche, M. (2001). Steep early negative slopes can be demonstrated in pre-movement Bereitschaftspotential. *Clinical Neurophysiology*, *112*(9), 1642–1649.
- Lancaster, J. L., Woldorff, M. G., Parsons, L. M., Liotti, M., Freitas, C. S., Rainey, L., . . . Fox, P. T. (2000, July). Automated Talairach Atlas labels for functional brain mapping. *Human Brain Mapping 2010*, *10*(3), 120–131.
- Lee, M. H., Smyser, C. D., & Shimony, J. S. (2013, October). Resting-state fMRI: a review of methods and clinical applications. *AJNR. American journal of neuroradiology*, *34*(10), 1866–1872.
- Leocani, L., Toro, C., Manganotti, P., Zhuang, P., & Hallett, M. (1997, May). Event-related coherence and event-related desynchronization/synchronization in the 10 Hz and 20 Hz EEG during self-paced movements. *Electroencephalography and clinical neurophysiology*, *104*(3), 199–206.
- Li, X.-L., Adali, T., & Anderson, M. (2011, October). Joint blind source separation by generalized joint diagonalization of cumulant matrices. *Signal processing*, *91*(10), 2314–2322.
- Lisberger, S. G., & Thach, W. T. (2013). The cerebellum. In *Principles of neural science* (pp. 960–981). McGraw-Hill Education.
- Luck, S. J., & Kappenman, E. S. (2011). *Oxford handbook of event-related potential components: Chapter 3: ERP Features and EEG Dynamics: An ICA*

- Perspective*. Oxford: Oxford University Press.
- Luu, P., Tucker, D. M., & Makeig, S. (2004, August). Frontal midline theta and the error-related negativity: neurophysiological mechanisms of action regulation. *Clinical Neurophysiology*, *115*(8), 1821–1835.
- Makeig, S. (1993, January). Auditory event-related dynamics of the EEG spectrum and effects of exposure to tones. *Electroencephalography and clinical neurophysiology*, 1–20.
- Makeig, S., Bell, A., & Jung, T. (1996, January). Independent component analysis of electroencephalographic data. *Advances in neural*, –.
- Makeig, S., Debener, S., Onton, J., & Delorme, A. (2004, May). Mining event-related brain dynamics. *Trends in Cognitive Sciences*, *8*(5), 204–210.
- Makeig, S., Delorme, A., Westerfield, M., Jung, T.-P., Townsend, J., Courchesne, E., & Sejnowski, T. J. (2004, June). Electroencephalographic brain dynamics following manually responded visual targets. *PLoS biology*, *2*(6), e176.
- Makeig, S., Enghoff, S., Jung, T. P., & Sejnowski, T. J. (2000, June). A natural basis for efficient brain-actuated control. *IEEE transactions on rehabilitation engineering : a publication of the IEEE Engineering in Medicine and Biology Society*, *8*(2), 208–211.
- Makeig, S., Gramann, K., Jung, T.-P., Sejnowski, T. J., & Poizner, H. (2009, August). Linking brain, mind and behavior. *International Journal of Psychophysiology*, *73*(2), 95–100.
- Makeig, S., Onton, J., Sejnowski, T. J., & Poizner, H. (2007). Prospects for mobile, high-definition brain imaging: EEG spectral modulations during 3-D reaching. *target*.
- Manly, B. (1997). *Randomization, Bootstrap and Monte Carlo Methods in Biology*. 2nd Editon. Chapman and Hall.
- Masaki, H., Wild-Wall, N., Sangals, J., & Sommer, W. (2004, March). The functional locus of the lateralized readiness potential. *Psychophysiology*, *41*(2), 220–230.
- Mathers, J. F., & Greal, M. A. (2014, January). Motor control strategies and the effects of fatigue on golf putting performance. *Frontiers in psychology*, *4*, 1005.
- Mathiowetz, V., Kashman, N., Volland, G., Weber, K., Dowe, M., & Rogers, S. (1985, February). Grip and pinch strength: normative data for adults. *Archives of physical medicine and rehabilitation*, *66*(2), 69–74.
- Maus, D., Epstein, C. M., & Herman, S. T. (2012, January). Digital EEG. In *Niedermeyer's electroencephalography: Basic principles, clinical applications, and related fields*.
- McCormack, H., Horne, D., & Sheather, S. (1988, January). Clinical applications of visual analogue scales: a critical review. *Psychol Med*.
- McIntosh, A. R., & Gonzalez-Lima, F. (1994). Structural equation modeling and its application to network analysis in functional brain imaging. *Human Brain Mapping 2010*, *2*(1-2), 2–22.

- Michel, C., & Murray, M. (2012, January). Towards the utilization of EEG as a brain imaging tool. *NeuroImage*, 1–15.
- Michel, C. M., Murray, M. M., Lantz, G., Gonzalez, S., Spinelli, L., & Grave de Peralta, R. (2004, October). EEG source imaging. *Clinical Neurophysiology*, 115(10), 2195–2222.
- Muangjaroen, P., & Wongsawat, Y. (2012, January). Real-time index for predicting successful golf putting motion using multichannel EEG. *IEEE Engineering in Medicine and Biology Society. Conference, 2012*, 4796–9.
- Mullen, T., Delorme, A., Kothe, C., & Makeig, S. (2010). An Electrophysiological Information Flow Toolbox for EEGLAB [Computer software manual]. San Diego.
- Mullen, T., Kothe, C., Chi, Y. M., & Ojeda, A. (2013). Real-time modeling and 3D visualization of source dynamics and connectivity using wearable EEG. *Conf Proc IEEE Eng . . .*
- Mullen, T., & Miyakoshi, M. (2011, January). CleanLine Plugin.
- Mullen, T., Onton, J., & Delorme, A. (2010). Analysis and visualization of theta-band information flow dynamics in an ERN-producing task. In *Human brain mapping 2010*. Barcelona, Spain.
- Müller-Putz, G. R., Zimmermann, D., Graimann, B., Nestinger, K., Korisek, G., & Pfurtscheller, G. (2007, March). Event-related beta EEG-changes during passive and attempted foot movements in paraplegic patients. *Brain research*, 1137(1), 84–91.
- Muthuraman, M., Hellriegel, H., Hoogenboom, N., Anwar, A. R., Mideksa, K. G., Krause, H., . . . Raethjen, J. (2014). Beamformer source analysis and connectivity on concurrent EEG and MEG data during voluntary movements. *PLoS ONE*, 9(3), e91441.
- Nagamine, T., Kajola, M., Salmelin, R., Shibasaki, H., & Hari, R. (1996, September). Movement-related slow cortical magnetic fields and changes of spontaneous MEG- and EEG-brain rhythms. *Electroencephalography and clinical neurophysiology*, 99(3), 274–286.
- Nam, C. N. K., Kang, H. J., & Suh, Y. S. (2014, April). Golf Swing Motion Tracking Using Inertial Sensors and a Stereo Camera. *Instrumentation and Measurement, IEEE Transactions on*, 63(4), 943–952.
- Narici, L., Forss, N., Jousmäki, V., Peresson, M., & Hari, R. (2001, April). Evidence for a 7- to 9-Hz "sigma" rhythm in the human SII cortex. *NeuroImage*, 13(4), 662–668.
- Navarro-Cebrian, A., Knight, R. T., & Kayser, A. S. (2013, July). Error-monitoring and post-error compensations: dissociation between perceptual failures and motor errors with and without awareness. *The Journal of neuroscience : the official journal of the Society for Neuroscience*, 33(30), 12375–12383.
- Neuper, C., & Pfurtscheller, G. (1996, September). Post-movement synchronization of beta rhythms in the EEG over the cortical foot area in man. *Neuroscience Letters*, 216(1), 17–20.

- Neuper, C., & Pfurtscheller, G. (2001, December). Event-related dynamics of cortical rhythms: frequency-specific features and functional correlates. *International Journal of Psychophysiology*, *43*(1), 41–58.
- Newell, K. M., Carlton, L. G., & Hancock, P. A. (1984, July). Kinetic analysis of response variability. *Psychological bulletin*, *96*(1), 133–151.
- Nigbur, R., Ivanova, G., & Stürmer, B. (2011, November). Theta power as a marker for cognitive interference. *Clinical neurophysiology : official journal of the International Federation of Clinical Neurophysiology*, *122*(11), 2185–2194.
- Nunez, P. L., & Srinivasan, R. (2006). *Electric Fields of the Brain*. Oxford University Press, USA.
- Oldfield, R. C. (1971). The assessment and analysis of handedness: the Edinburgh inventory. *Neuropsychologia*, *9*(1), 97–113.
- Olson, C. R., & Colby, C. L. (2013). The Organization of Cognition. In *Principles of neural science* (pp. 392–411). McGraw-Hill Education.
- Onton, J. (2009). High-frequency broadband modulation of electroencephalographic spectra. *Front Hum Neurosci*, *3*, –.
- Onton, J., Delorme, A., & Makeig, S. (2005, August). Frontal midline EEG dynamics during working memory. *NeuroImage*, *27*(2), 341–356.
- Onton, J., & Makeig, S. (2006). Information-based modeling of event-related brain dynamics. *Progress in brain research*, *159*, 99–120.
- Onton, J., Westerfield, M., Townsend, J., & Makeig, S. (2006). Imaging human EEG dynamics using independent component analysis. *Neuroscience and biobehavioral reviews*, *30*(6), 808–822.
- Oostendorp, T. F., & van Oosterom, A. (1989, March). Source parameter estimation in inhomogeneous volume conductors of arbitrary shape. *IEEE Transactions on Biomedical Engineering*, *36*(3), 382–391.
- Oostenveld, R., & Praamstra, P. (2001, January). The five percent electrode system for high-resolution EEG and ERP measurements. *Clinical Neurophysiology*, –.
- Palmer, J. A., Kreutz-Delgado, K., Rao, B. D., & Makeig, S. (2007, January). Modeling and Estimation of Dependent Subspaces with Non-radially Symmetric and Skewed Densities. In *Independent component analysis and signal separation* (pp. 97–104). Berlin, Heidelberg: Springer Berlin Heidelberg.
- Palmer, J. A., Makeig, S., Delgado, K. K., & Rao, B. D. (2008). Newton method for the ICA mixture model. In *Acoustics, speech and signal processing, 2008. icassp 2008. ieee international conference on* (pp. 1805–1808). IEEE.
- Parkes, L. M., Bastiaansen, M. C. M., & Norris, D. G. (2006, February). Combining EEG and fMRI to investigate the post-movement beta rebound. *NeuroImage*, *29*(3), 685–696.
- Pascual-Marqui, R. D., Michel, C. M., & Lehmann, D. (1994, October). Low resolution electromagnetic tomography: a new method for localizing electrical activity in the brain. *International Journal of Psychophysiology*, *18*(1), 49–65.

- Pearson, K., & Gordon, J. (2013). Spinal reflexes. In *Principles of neural science* (pp. 790–811). McGraw-Hill Education.
- Pfurtscheller, G., Neuper, C., & Berger, J. (1994). Source localization using event-related desynchronization (ERD) within the alpha band. *Brain topography*, *6*(4), 269–275.
- Pfurtscheller, G. (1989, January). Functional topography during sensorimotor activation studied with event-related desynchronization mapping. *Journal of Clinical Neurophysiology*, *6*(1), 75–84.
- Pfurtscheller, G., & Aranibar, A. (1979a, February). Evaluation of event-related desynchronization (ERD) preceding and following voluntary self-paced movement. *Electroencephalography and clinical neurophysiology*, *46*(2), 138–146.
- Pfurtscheller, G., & Aranibar, A. (1979b, February). Evaluation of event-related desynchronization (ERD) preceding and following voluntary self-paced movement. *Electroencephalography and clinical neurophysiology*, *46*(2), 138–146.
- Pfurtscheller, G., & Berghold, A. (1989, March). Patterns of cortical activation during planning of voluntary movement. *Electroencephalography and clinical neurophysiology*, *72*(3), 250–258.
- Pfurtscheller, G., Brunner, C., Schlögl, A., & Lopes da Silva, F. H. (2006, May). Mu rhythm (de)synchronization and EEG single-trial classification of different motor imagery tasks. *NeuroImage*, *31*(1), 153–159.
- Pfurtscheller, G., & Lopes da Silva, F. H. (1999, November). Event-related EEG/MEG synchronization and desynchronization: basic principles. *Clinical Neurophysiology*, *110*(11), 1842–1857.
- Pfurtscheller, G., & Neuper, C. (1992). Simultaneous EEG 10 Hz desynchronization and 40 Hz synchronization during finger movements. *Neuroreport*, *3*(12), 1057–1060.
- Pfurtscheller, G., Neuper, C., & Krausz, G. (2000, October). Functional dissociation of lower and upper frequency mu rhythms in relation to voluntary limb movement. *Clinical neurophysiology : official journal of the International Federation of Clinical Neurophysiology*, *111*(10), 1873–1879.
- Pfurtscheller, G., Stancák, A., & Neuper, C. (1996, April). Post-movement beta synchronization. A correlate of an idling motor area? *Electroencephalography and clinical neurophysiology*, *98*(4), 281–293.
- Pleger, B., Foerster, A. F., Ragert, P., Dinse, H. R., Schwenkreis, P., Malin, J. P., . . . Tegenthoff, M. (2003, October). Functional imaging of perceptual learning in human primary and secondary somatosensory cortex. *Neuron*, *40*(3), 643–653.
- Plummer, C., Wagner, M., Fuchs, M., Harvey, A. S., & Cook, M. J. (2010, June). Dipole Versus Distributed EEG Source Localization for Single Versus Averaged Spikes in Focal Epilepsy. *Journal of Clinical Neurophysiology*, *27*(3), 141–162.
- Pool, E.-M., Rehme, A. K., Fink, G. R., Eickhoff, S. B., & Grefkes, C. (2013,

- January). Network dynamics engaged in the modulation of motor behaviour in healthy subjects. *NeuroImage*, 1–9.
- Pool, E.-M., Rehme, A. K., Fink, G. R., Eickhoff, S. B., & Grefkes, C. (2014, October). Handedness and effective connectivity of the motor system. *NeuroImage*, *99*, 451–460.
- Praamstra, P., Stegeman, D. F., Horstink, M. W., & Cools, A. R. (1996, June). Dipole source analysis suggests selective modulation of the supplementary motor area contribution to the readiness potential. *Electroencephalography and clinical neurophysiology*, *98*(6), 468–477.
- Rajapakse, J. C., & Zhou, J. (2007, September). Learning effective brain connectivity with dynamic Bayesian networks. *NeuroImage*, *37*(3), 749–760.
- Ranjana K Mehta, R. P. (2013). Neuroergonomics: a review of applications to physical and cognitive work. *Frontiers in Human Neuroscience*, *7*, 889.
- Rankin, C. H., Abrams, T., Barry, R. J., Bhatnagar, S., Clayton, D. F., Colombo, J., . . . Thompson, R. F. (2009, September). Habituation revisited: an updated and revised description of the behavioral characteristics of habituation. *Neurobiology of learning and memory*, *92*(2), 135–138.
- Rappelsberger, P., Pfurtscheller, G., & Filz, O. (1994, January). Calculation of event-related coherence—a new method to study short-lasting coupling between brain areas. *Brain topography*, *7*(2), 121–7.
- Razali, N. M., & Wah, Y. B. (2011). Power comparisons of shapiro-wilk, kolmogorov-smirnov, lilliefors and anderson-darling tests. *Journal of Statistical Modeling and Analytics*, –.
- Reinecke, K., Cordes, M., Lerch, C., Koutsandr eou, F., Schubert, M., Weiss, M., & Baumeister, J. (2011, December). From lab to field conditions: a pilot study on EEG methodology in applied sports sciences. *Applied psychophysiology and biofeedback*, *36*(4), 265–271.
- Rilk, A. J., Soekadar, S. R., Sauseng, P., & Plewnia, C. (2011, November). Alpha coherence predicts accuracy during a visuomotor tracking task. *Neuropsychologia*, *49*(13), 3704–9.
- Riva, N., Falini, A., Inuggi, A., Gonzalez-Rosa, J. J., Amadio, S., Cerri, F., . . . Leocani, L. (2012, August). Cortical activation to voluntary movement in amyotrophic lateral sclerosis is related to corticospinal damage: electrophysiological evidence. *Clinical neurophysiology : official journal of the International Federation of Clinical Neurophysiology*, *123*(8), 1586–1592.
- Rosenberg-Katz, K., Jamshy, S., Singer, N., Podlipsky, I., Kipervasser, S., Andelman, F., . . . Hendler, T. (2012, January). Enhanced functional synchronization of medial and lateral PFC underlies internally-guided action planning. *Frontiers in Human Neuroscience*, *6*, 79.
- Sakai, Y., Yagi, T., & Ishii, W. (2012, January). EEG analysis of mental concentration in golf putting. *Biomedical Engineering International*.
- Saper, C. B., Iversen, S., & Frackowiak, R. (2000). Integration of Sensory and Motor Function: The Association Areas of the Cerebral Cortex and the Cognitive Capabilities of the Brain. In *Principles of neural science*. McGraw-

- Hill Education.
- Sauseng, P., Griesmayr, B., Freunberger, R., & Klimesch, W. (2010, June). Control mechanisms in working memory: a possible function of EEG theta oscillations. *Neuroscience and biobehavioral reviews*, *34*(7), 1015–1022.
- Sauseng, P., Hoppe, J., Klimesch, W., Gerloff, C., & Hummel, F. C. (2007, January). Dissociation of sustained attention from central executive functions: local activity and interregional connectivity in the theta range. *European Journal of Neuroscience*, *25*(2), 587–593.
- Sauseng, P., Klimesch, W., Schabus, M., & Doppelmayr, M. (2005). Fronto-parietal EEG coherence in theta and upper alpha reflect central executive functions of working memory. *International Journal of Psychophysiology*, *57*(2), 97–103.
- Schelter, B., Timmer, J., & Eichler, M. (2009). Assessing the strength of directed influences among neural signals using renormalized partial directed coherence. *Journal of neuroscience methods*, *179*(1), 121–130.
- Scherg, M. (1990, January). Fundamentals of dipole source potential analysis. *Auditory evoked magnetic fields and*, –.
- Scherg, M., & Berg, P. (1991, December). Use of prior knowledge in brain electromagnetic source analysis. *Brain topography*, *4*(2), 143–150.
- Schlögl, A. (2000). *The electroencephalogram and the adaptive autoregressive model: theory and applications*.
- Schlögl, A., Keinrath, C., Zimmermann, D., Scherer, R., Leeb, R., & Pfurtscheller, G. (2007, January). A fully automated correction method of EOG artifacts in EEG recordings. *Clinical Neurophysiology*, *118*(1), 98–104.
- Schlögl, A., & Supp, G. (2006). Analyzing event-related EEG data with multivariate autoregressive parameters. *Progress in brain research*, *159*, 135–147.
- Schmidt, D. M., George, J. S., & Wood, C. C. (1999). Bayesian inference applied to the electromagnetic inverse problem. *Human Brain Mapping 2010*, *7*(3), 195–212.
- Schomer, D., & Da Silva, F. (2012). *Niedermeyer's electroencephalography: Basic principles, clinical applications, and related fields*.
- Schreiber, T. (2000, July). Measuring Information Transfer. *Physical review letters*, *85*(2), 461–464.
- Sclocco, R., Tana, M. G., Visani, E., Gilioli, I., Panzica, F., Franceschetti, S., . . . Bianchi, A. M. (2014). EEG-informed fMRI analysis during a hand grip task: estimating the relationship between EEG rhythms and the BOLD signal. *Frontiers in Human Neuroscience*, *8*, 186.
- Shannon, C. E. (1949, January). Communication in the Presence of Noise. *Proceedings of the IRE*, *37*(1), 10–21.
- Shenhav, A., Botvinick, M. M., & Cohen, J. D. (2013, July). The expected value of control: an integrative theory of anterior cingulate cortex function. *Neuron*, *79*(2), 217–240.
- Shibasaki, H., & Hallett, M. (2006). What is the Bereitschaftspotential? *Clinical Neurophysiology*, *117*(11), 2341–2356.

- Shinohara, M., Li, S., Kang, N., Zatsiorsky, V. M., & Latash, M. L. (2003, January). Effects of age and gender on finger coordination in MVC and submaximal force-matching tasks. *Journal of Applied Physiology*, *94*(1), 259–270.
- Shizgal, P. B., & Hyman, S. E. (2013). Homeostasis, Motivation, and Addictive States. In *Principles of neural science* (pp. 1095–1115).
- Shou, G., Ding, L., & Dasari, D. (2012, July). Probing neural activations from continuous EEG in a real-world task: time-frequency independent component analysis. *Journal of neuroscience methods*, *209*(1), 22–34.
- Smith, V. A., Yu, J., Smulders, T. V., Hartemink, A. J., & Jarvis, E. D. (2006, November). Computational Inference of Neural Information Flow Networks. *PLoS Computational Biology*, *2*(11), e161.
- Sochůrková, D., Rektor, I., Jurák, P., & Stancák, A. (2006, September). Intracerebral recording of cortical activity related to self-paced voluntary movements: a Bereitschaftspotential and event-related desynchronization/synchronization. SEEG study. *Experimental Brain Research*, *173*(4), 637–649.
- Sourina, O., Wang, Q., Liu, Y., & Nguyen, M. K. (2012, July). EEG-Enabled Human–Computer Interaction and Applications. In *Biological and medical physics, biomedical engineering* (pp. 251–268). Berlin, Heidelberg: Springer Berlin Heidelberg.
- Speckmann, E.-J., Elger, C. E., & Gorji, A. (2012, January). Neurophysiological Basis of EEG and DC Potential. In *Niedermeyer’s electroencephalography: Basic principles, clinical applications, and related fields* (pp. 17–31).
- Spielberger, C., Gorsuch, R., Lushene, R., & Vagg, P. (1983, January). State-Trait Anxiety Inventory (STAI). *BiB 2010*.
- Sporns, O. (2011). *Networks of the Brain*. MIT Press.
- Sporns, O. (2013, September). Structure and function of complex brain networks. *Dialogues in clinical neuroscience*, *15*(3), 247–262.
- Sporns, O., & Tononi, G. (2007, January). Structural Determinants of Functional Brain Dynamics. In *Handbook of brain connectivity* (pp. 117–148). Berlin, Heidelberg: Springer Berlin Heidelberg.
- Stancák, A., & Pfurtscheller, G. (1996, August). The effects of handedness and type of movement on the contralateral preponderance of mu-rhythm desynchronization. *Electroencephalography and clinical neurophysiology*, *99*(2), 174–182.
- Stancák, A., Riml, A., & Pfurtscheller, G. (1997, June). The effects of external load on movement-related changes of the sensorimotor EEG rhythms. *Electroencephalography and clinical neurophysiology*, *102*(6), 495–504.
- Stancák, A. J., & Pfurtscheller, G. (1996, April). Mu-rhythm changes in brisk and slow self-paced finger movements. *Neuroreport*, *7*(6), 1161.
- Steinbrink, J., Villringer, A., Kempf, F., Haux, D., Boden, S., & Obrig, H. (2006, May). Illuminating the BOLD signal: combined fMRI-fNIRS studies. *Magnetic Resonance Imaging*, *24*(4), 495–505.



- Stone, J. V. (2002, February). Independent component analysis: an introduction. *Trends in Cognitive Sciences*, 6(2), 59–64.
- Takata, Y., Kondo, T., Saeki, M., Izawa, J., Takeda, K., Otaka, Y., & It, K. (2012). Analysis of extrinsic and intrinsic factors affecting event related desynchronization production. *IEEE Engineering in Medicine and Biology Society. Conference, 2012*, 4619–4622.
- Tan, H., Jenkinson, N., & Brown, P. (2014, April). Dynamic neural correlates of motor error monitoring and adaptation during trial-to-trial learning. *The Journal of neuroscience : the official journal of the Society for Neuroscience*, 34(16), 5678–5688.
- Teixeira, S., Machado, S., Velasques, B., Sanfim, A., Minc, D., Peressutti, C., ... Silva, J. G. (2014, March). Integrative parietal cortex processes: neurological and psychiatric aspects. *Journal of the neurological sciences*, 338(1-2), 12–22.
- Thompson, T., Steffert, T., Ros, T., Leach, J., & Gruzelier, G. (2008, January). EEG applications for sport and performance. *Methods*, 1–10.
- Tipler, P. A., & Mosca, G. (2014). *Physik*. Springer Spektrum.
- Toma, K., Matsuoka, T., Immisch, I., Mima, T., Waldvogel, D., Koshy, B., ... Hallett, M. (2002, September). Generators of movement-related cortical potentials: fMRI-constrained EEG dipole source analysis. *NeuroImage*, 17(1), 161–173.
- Tzagarakis, C., Ince, N. F., Leuthold, A. C., & Pellizzer, G. (2010, August). Beta-band activity during motor planning reflects response uncertainty. *The Journal of neuroscience : the official journal of the Society for Neuroscience*, 30(34), 11270–7.
- Ullsperger, M., & Debener, S. (2010). *Simultaneous EEG and fMRI*. Oxford University Press.
- Ullsperger, M., Fischer, A. G., Nigbur, R., & Endrass, T. (2014, May). Neural mechanisms and temporal dynamics of performance monitoring. *Trends in Cognitive Sciences*, 18(5), 259–267.
- Urbano, A., Babiloni, C., Onorati, P., & Babiloni, F. (1996, December). Human cortical activity related to unilateral movements. A high resolution EEG study. *Neuroreport*, 8(1), 203–6.
- Urbin, M. A., Stodden, D. F., Fischman, M. G., & Weimar, W. H. (2011, May). Impulse-Variability Theory: Implications for Ballistic, Multijoint Motor Skill Performance. *Journal of motor behavior*, 43(3), 275–283.
- Vaillancourt, D. E., Yu, H., Mayka, M. A., & Corcos, D. M. (2007). Role of the basal ganglia and frontal cortex in selecting and producing internally guided force pulses. *NeuroImage*.
- van Driel, J., Ridderinkhof, K. R., & Cohen, M. X. (2012, November). Not all errors are alike: theta and alpha EEG dynamics relate to differences in error-processing dynamics. *The Journal of neuroscience : the official journal of the Society for Neuroscience*, 32(47), 16795–16806.
- Varela, F., Lachaux, J.-P., Rodriguez, E., Martinerie, J., & Rodriguez, J. M. (2001,

- April). The brainweb: Phase synchronization and large-scale integration. *Nature reviews Neuroscience*, 2(4), 229–239.
- Velu, P. D., Mullen, T., Noh, E., Valdivia, M. C., Poizner, H., Baram, Y., & de Sa, V. R. (2014). Effect of visual feedback on the occipital-parietal-motor network in Parkinson's disease with freezing of gait. *Frontiers in neurology*, 4, 209.
- Vía, J., Anderson, M., Li, X. L., & Adali, T. (2011). Joint blind source separation from second-order statistics: Necessary and sufficient identifiability conditions. *Acoustics*.
- Visani, E., Agazzi, P., Canafoglia, L., Panzica, F., Ciano, C., Scaioli, V., ... Franceschetti, S. (2006). Movement-related desynchronization-synchronization (ERD/ERS) in patients with Unverricht-Lundborg disease. *NeuroImage*, 33(1), 161–168.
- Voelcker-Rehage, C., & Alberts, J. L. (2005, September). Age-related changes in grasping force modulation. *Experimental brain research. Experimentelle Hirnforschung. Expérimentation cérébrale*, 166(1), 61–70.
- Wang, B., Fan, Y., Lu, M., Li, S., Song, Z., Peng, X., ... Huang, R. (2013, January). Brain anatomical networks in world class gymnasts: a DTI tractography study. *NeuroImage*, 65, 476–487.
- Wheaton, L. A., Nolte, G., Bohlhalter, S., Fridman, E., & Hallett, M. (2005). Synchronization of parietal and premotor areas during preparation and execution of praxis hand movements. *Clinical neurophysiology : official journal of the International Federation of Clinical Neurophysiology*, 116(6), 1382–1390.
- Wheaton, L. A., Shibasaki, H., & Hallett, M. (2005, May). Temporal activation pattern of parietal and premotor areas related to praxis movements. *Clinical Neurophysiology*, 116(5), 1201–1212.
- Wheaton, L. A., Yakota, S., & Hallett, M. (2005). Posterior parietal negativity preceding self-paced praxis movements. *Experimental Brain Research*, 163(4), 535–539.
- Wichmann, T., & DeLong, M. R. (2013). The basal ganglia. In *Principles of neural science* (pp. 982–998). McGraw-Hill Education.
- Widmann, A. (2012). firfilt plugin for EEGLAB. *University of Leipzig*.
- Widmann, A., & Schröger, E. (2012, January). Filter effects and filter artifacts in the analysis of electrophysiological data. *Frontiers in psychology*, –.
- Wiener, N. (1956). *The theory of prediction*. Modern mathematics for engineers.
- Wilson, M. R., & Percy, R. C. (2009, October). Visuomotor control of straight and breaking golf putts. *Perceptual and motor skills*, 109(2), 555–562.
- Winterhalder, M., Schelter, B., Hesse, W., Schwab, K., Leistriz, L., Klan, D., ... Witte, H. (2005, November). Comparison of linear signal processing techniques to infer directed interactions in multivariate neural systems. *Signal processing*, 85(11), 2137–2160.
- Wolpert, D., Pearson, K., & Ghez, C. (2013). The Organization and Planning of Movement. In *Principles of neural science* (pp. 743–767). McGraw-Hill

- Education.
- Wood, J. N., & Grafman, J. (2003, February). Human prefrontal cortex: processing and representational perspectives. *Nature reviews. Neuroscience*, 4(2), 139–147.
- Wu, T., Wang, L., Hallett, M., Chen, Y., Li, K., & Chan, P. (2011, March). Effective connectivity of brain networks during self-initiated movement in Parkinson’s disease. *NeuroImage*, 55(1), 204–215.
- Zaepffel, M., & Brochier, T. (2011, September). Planning of visually guided reach-to-grasp movements: Inference from reaction time and contingent negative variation (CNV). *Psychophysiology*, 49(1), 17–30.
- Zhang, H., Chavarriaga, R., Goel, M. K., Gheorghe, L., & del Millán, J. R. (2012, January). Improved recognition of error related potentials through the use of brain connectivity features. *IEEE Engineering in Medicine and Biology Society. Conference, 2012*, 6740–3.
- Zou, Y., Nathan, V., & Jafari, R. (2014, November). Automatic Identification of Artifact-related Independent Components for Artifact Removal in EEG Recordings. *IEEE journal of biomedical and health informatics*, 1–1.



# **Appendix A**

## **Major axes of the CNS**

# A. MAJOR AXES OF THE CNS

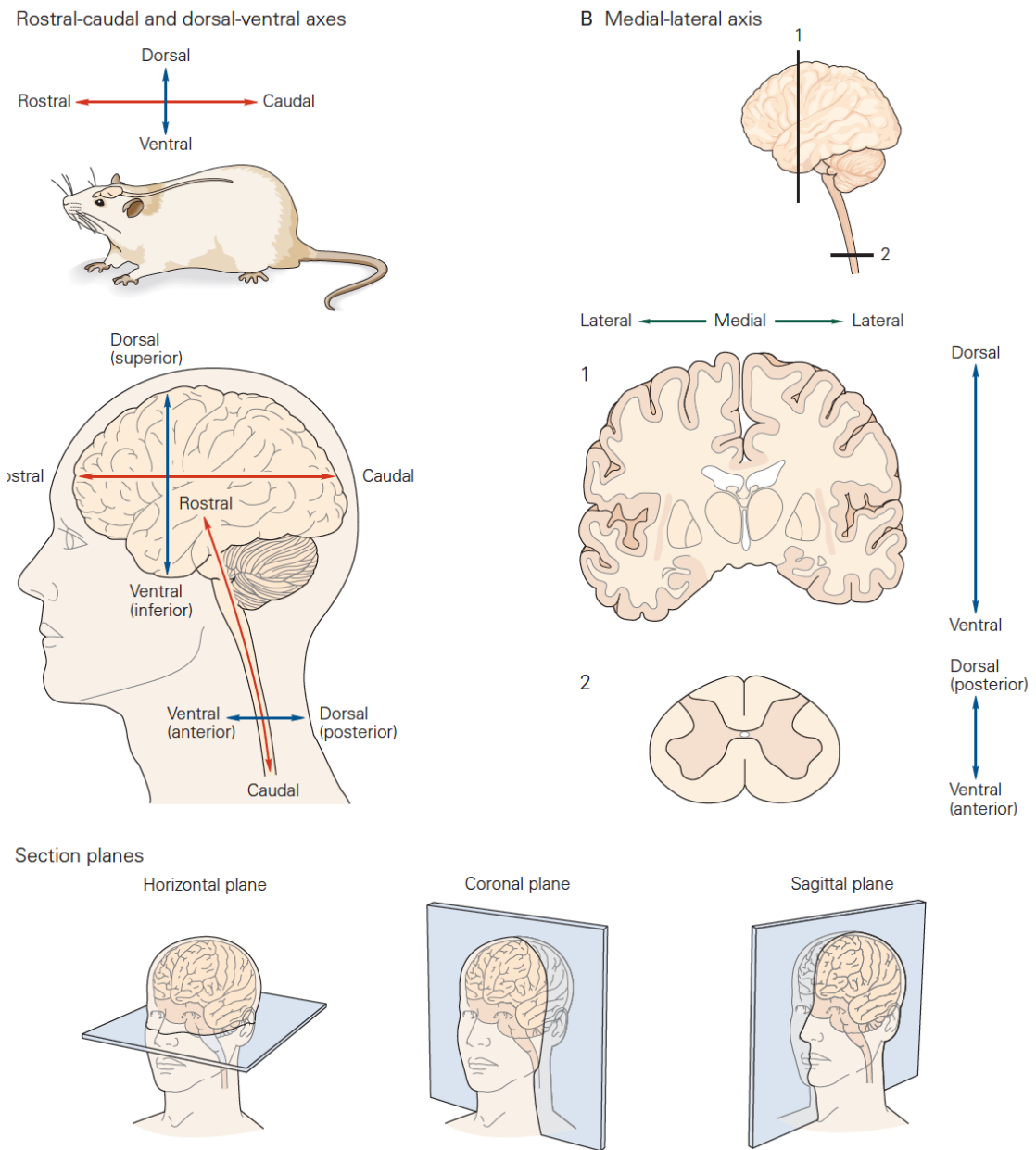


Figure A.1: From Amaral and Strick (2013), p. 339.

# **Appendix B**

## **Model validation and connectivity estimation**

### **B.1 Force pulse study: Model validation results**

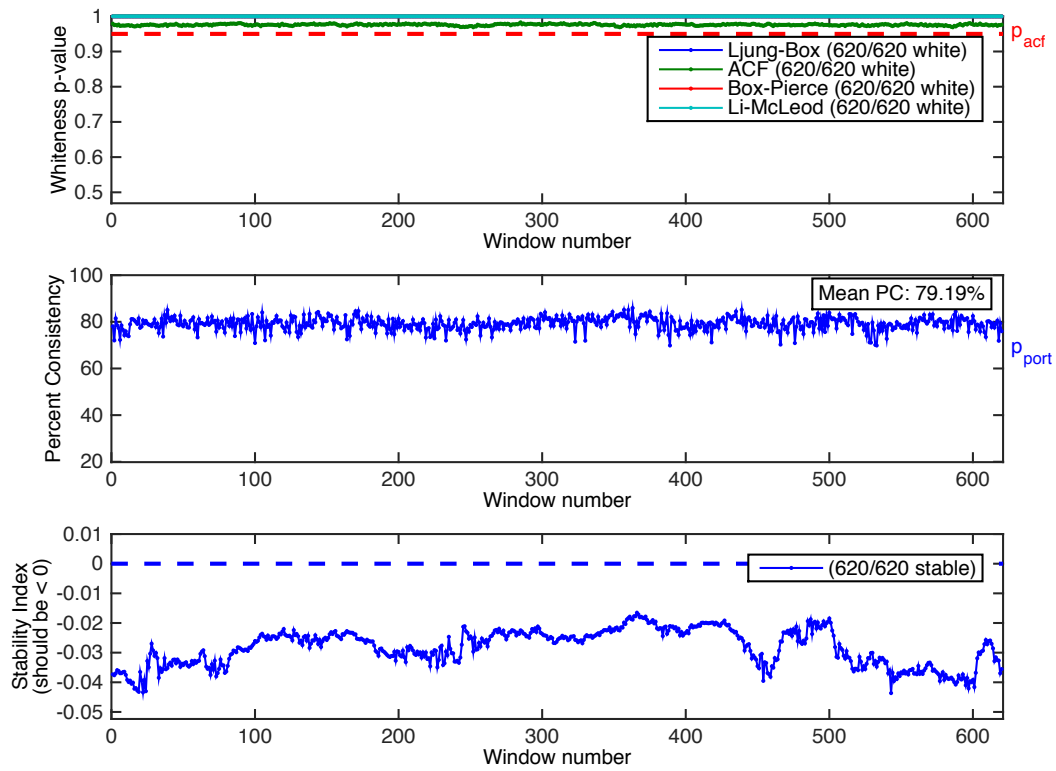


Figure B.1: Model validation subject 1

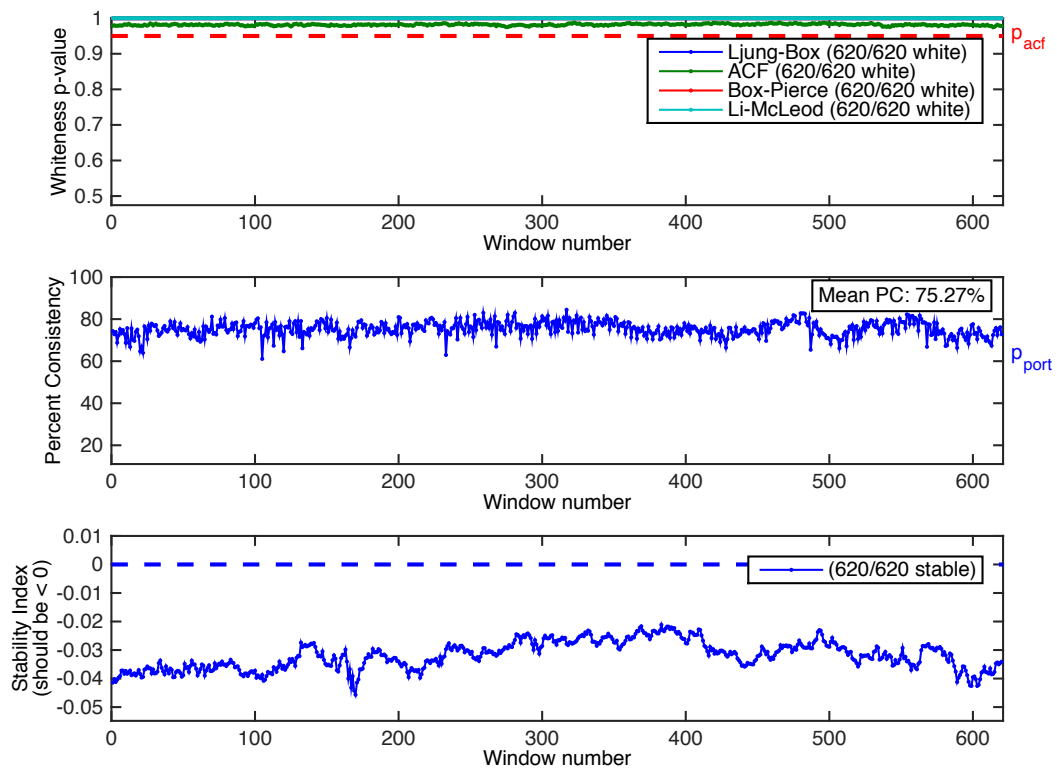


Figure B.2: Model validation subject 2



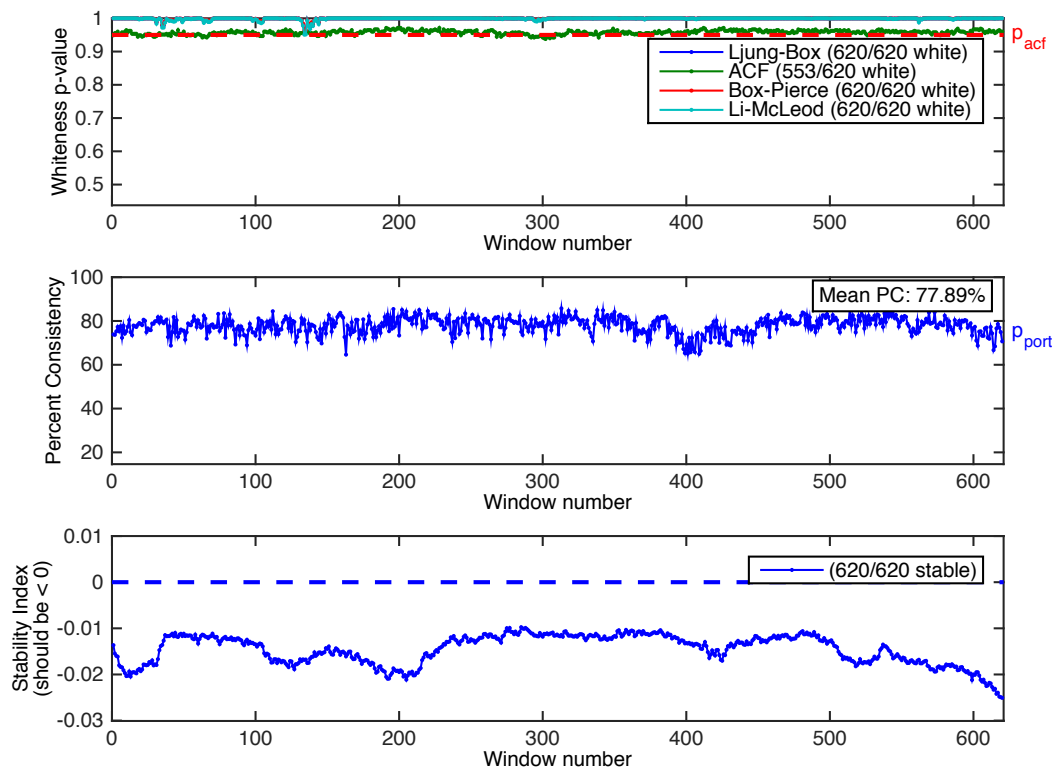


Figure B.3: Model validation subject 3

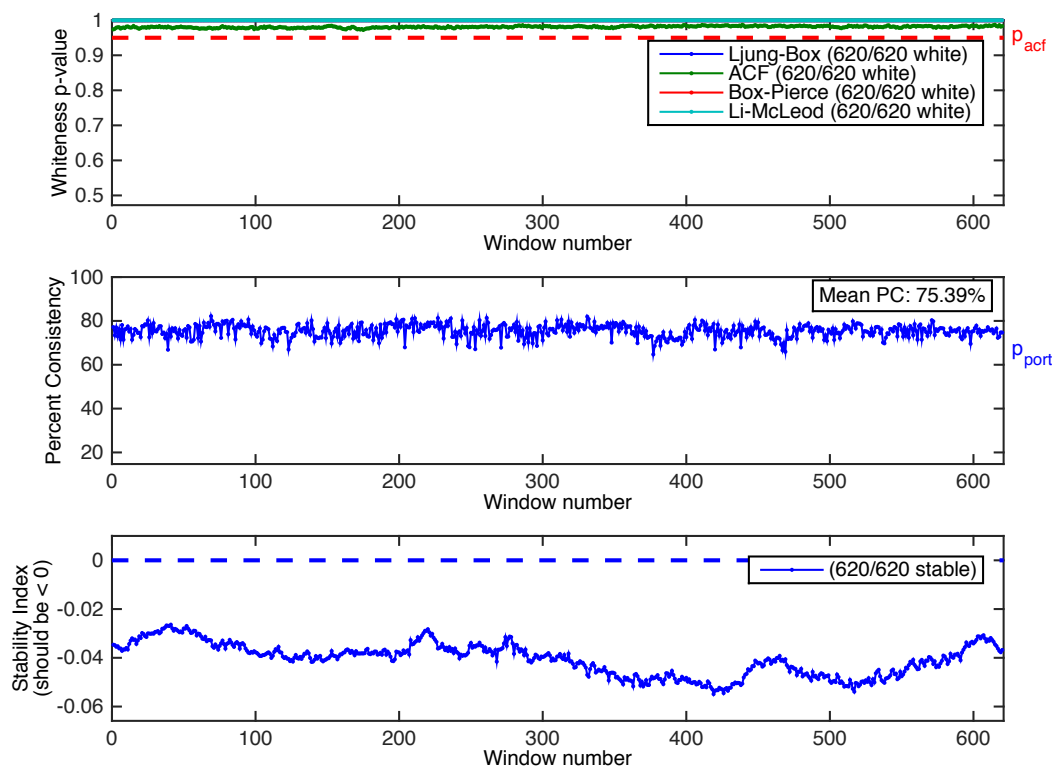


Figure B.4: Model validation subject 4

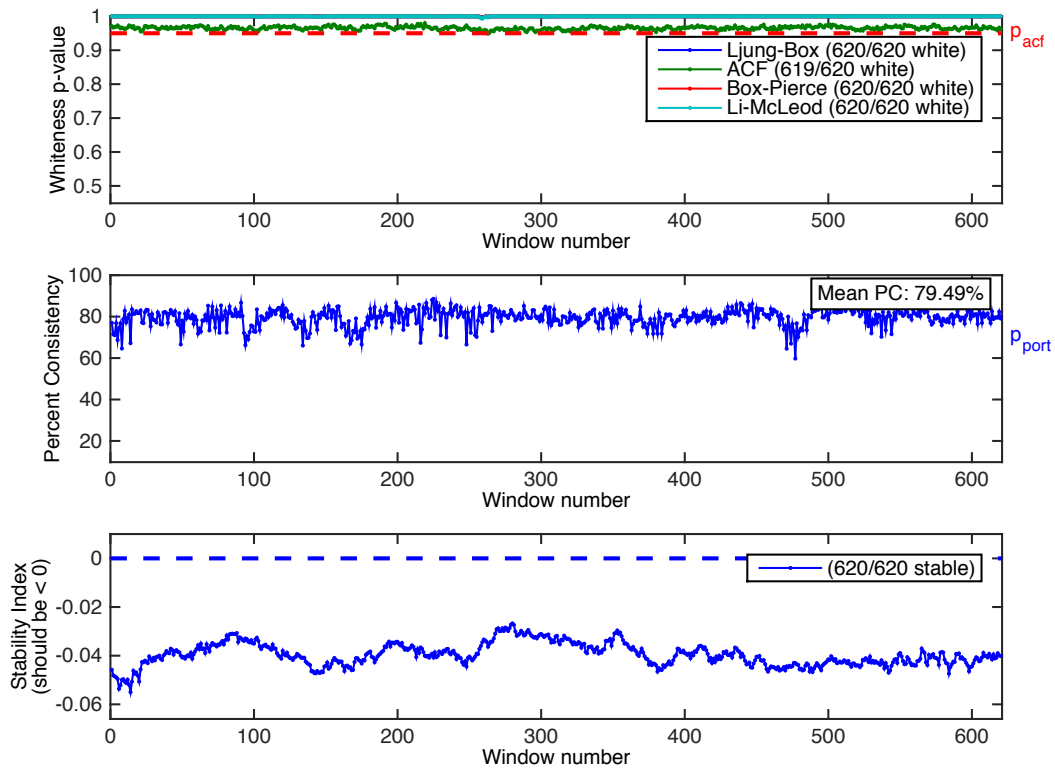


Figure B.5: Model validation subject 5

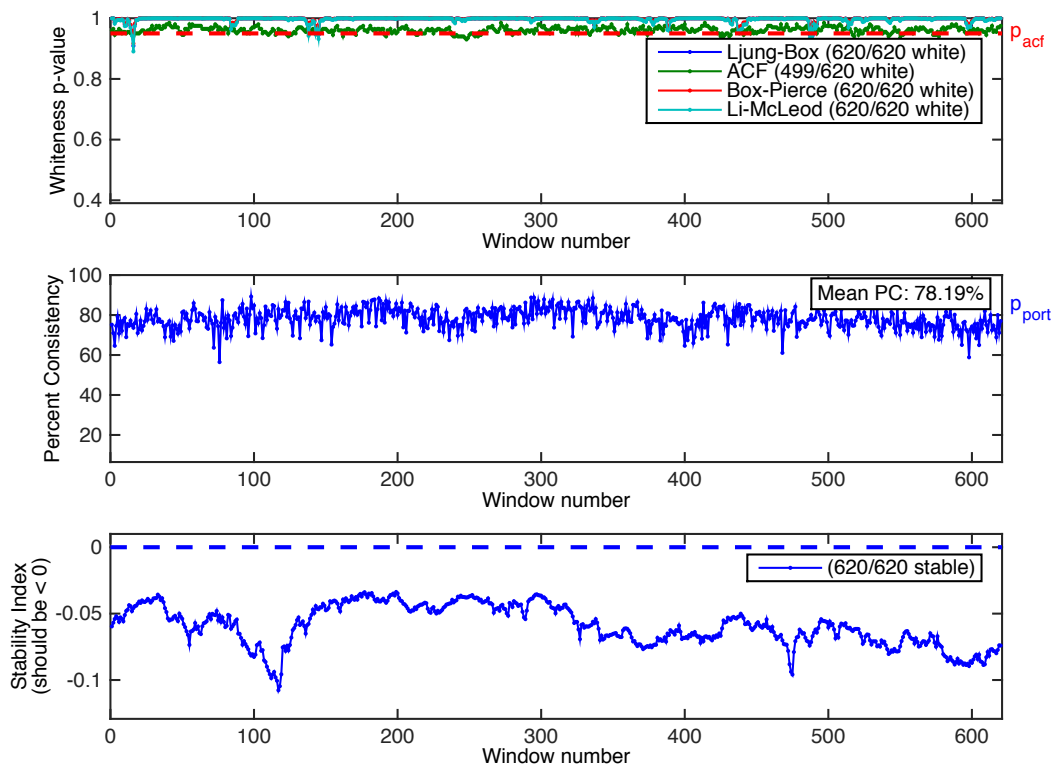


Figure B.6: Model validation subject 6

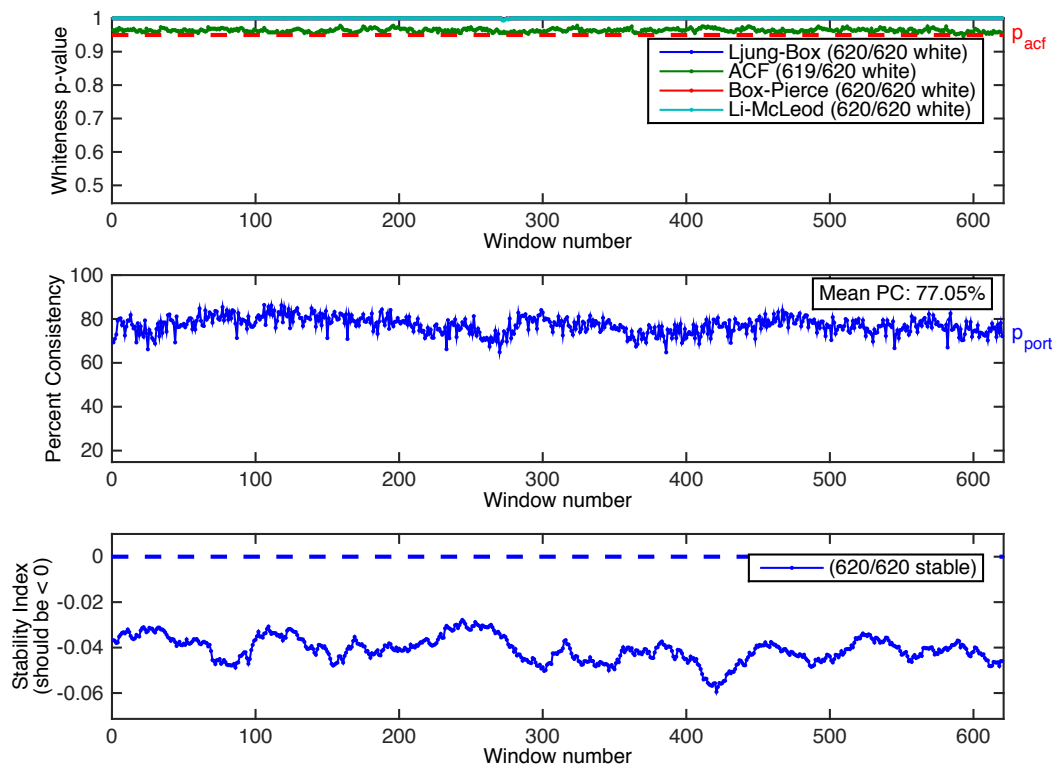
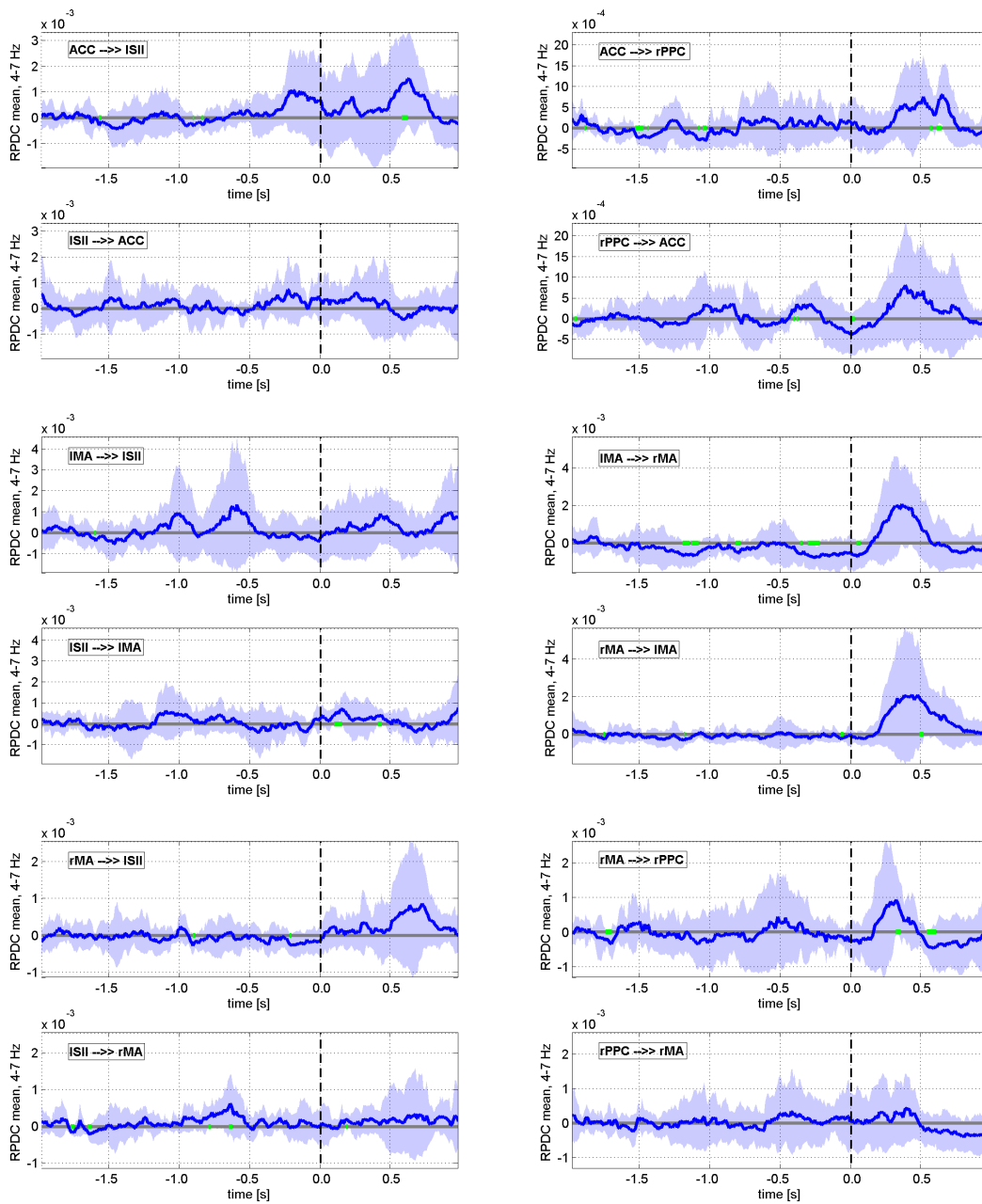


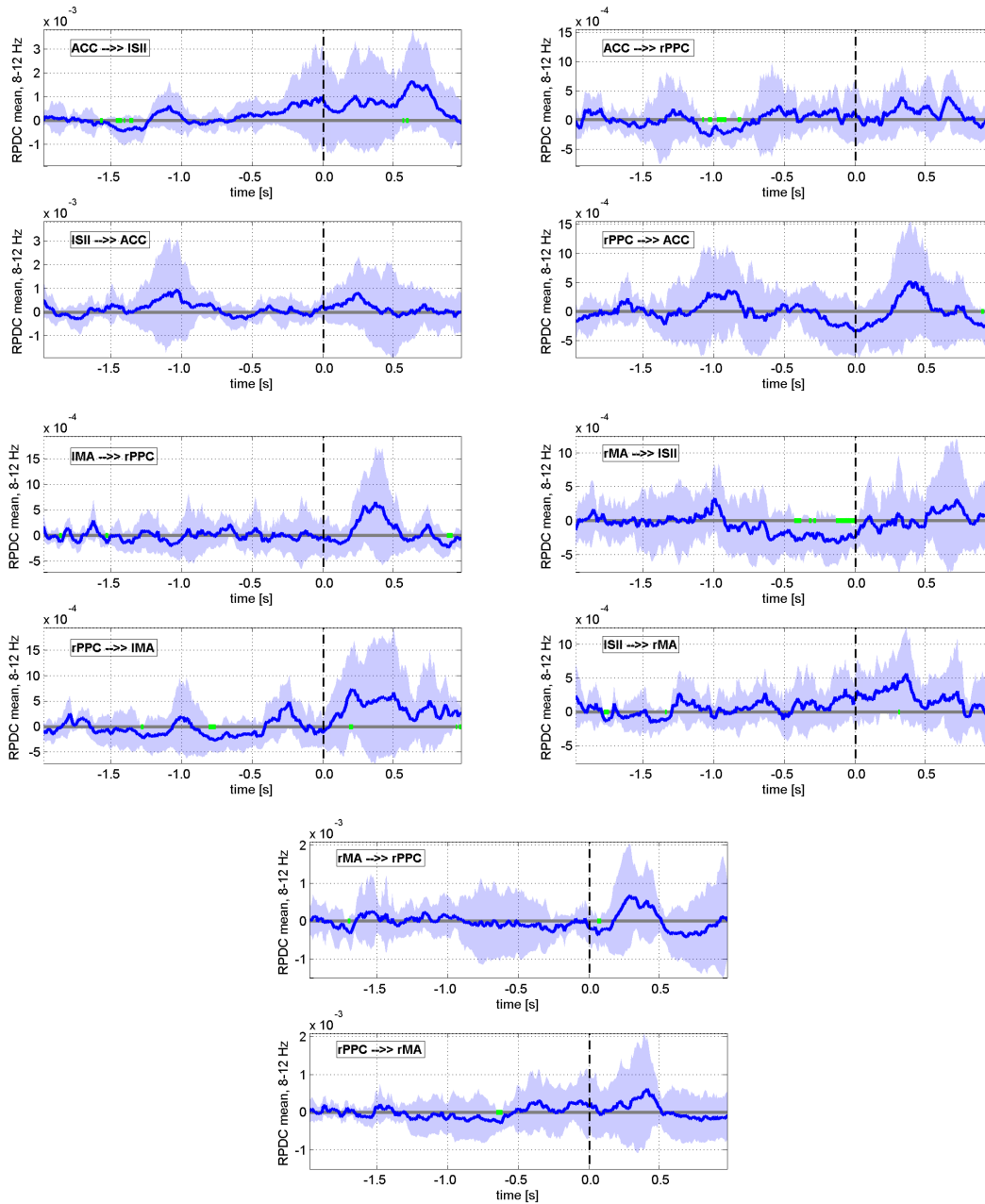
Figure B.7: Model validation subject 7

## B.2 Force pulse study: Additional ERC results force pulse study

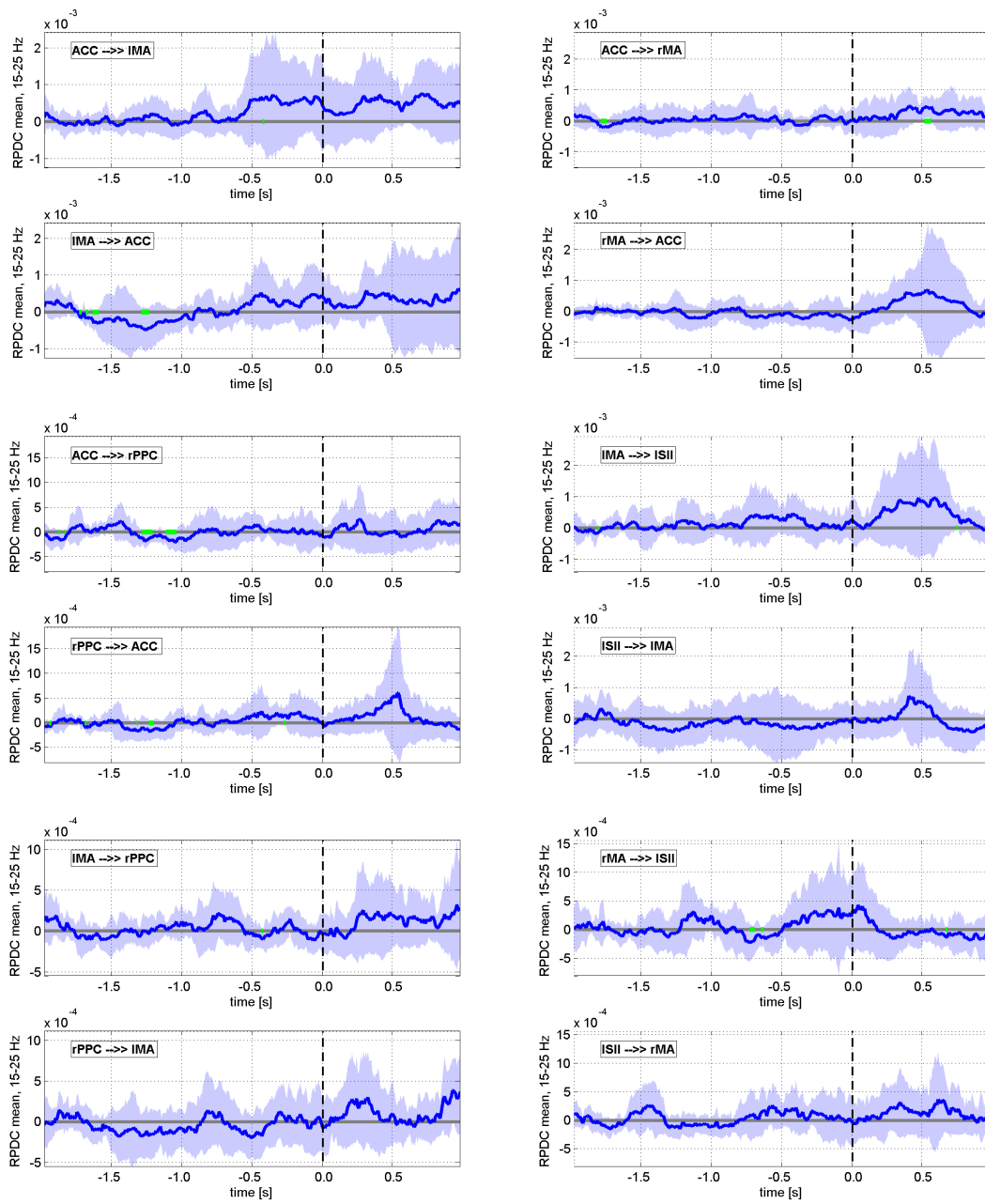
### Theta band ERC



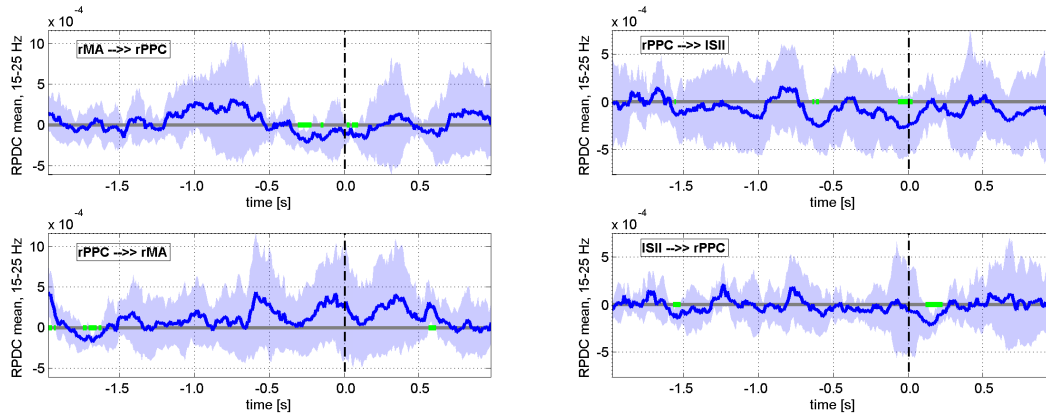
### Alpha band ERC



Beta band ERC



B.2 Force pulse study: Additional ERC results force pulse study



# **Appendix C**

## **Questionnaires**

### **C.1 Anthropometric forms**



**Anthropometric form - force pulse study**

| <b>Anamnese</b>  |                          |   |
|--|--------------------------|---|
| Name: _____  | Vorname: _____           |   |
| Geburtsdatum: _____ Adresse: _____                         |                          |   |
| Größe: ___ cm  | Gewicht: ___ kg          | Kopfumfang: ___ cm Nasion-Inion: ___ cm                 |
| Handicap: _____  |                          |   |
| <b>• Eignungskriterien</b>                                 |                          |   |
| <b>Sie</b>   | <b>Ja</b>                | <b>Nein</b>   |
| • sind im Alter von 20-40 Jahren                           | <input type="checkbox"/> | <input type="checkbox"/>                                |
| • sind Rechtshänder  | <input type="checkbox"/> | <input type="checkbox"/>                                |
| • putten nach links (Standard-Ausrichtung)                 | <input type="checkbox"/> | <input type="checkbox"/>                                |
| • sind männlich  | <input type="checkbox"/> | <input type="checkbox"/>                                |
| • fühlen sich gesund                                       | <input type="checkbox"/> | <input type="checkbox"/>                                |
| wenn nicht, geben sie nachfolgend Ihre Probleme an:        |                          |   |
| <br>   |                          |   |
| <b>• Ausschlußkriterien</b>                                |                          |   |
| Leiden oder litten Sie an                                  | Ja                       | Nein  |
| Nerven- oder Gemütskrankheiten, Epilepsie o.ä.             | <input type="checkbox"/> | <input type="checkbox"/>                                |
| Schlafstörungen  | <input type="checkbox"/> | <input type="checkbox"/>                                |
| Testrelevante körperliche Einschränkungen / Beschwerden    | <input type="checkbox"/> | <input type="checkbox"/>                                |
| Wenn ja, welche:   |                          |   |
| <br><br><br>   |                          |   |
| Aufgenommen in die Probandenliste unter der Probanden-Nr.: |                          | <input style="width: 40px; height: 20px;" type="text"/> |

**Probandenaufklärung und Einverständnis-Erklärung**

Name: \_\_\_\_\_ Vorname: \_\_\_\_\_ Datum: \_\_\_\_\_

**Vorwort**

Es ist wichtig, dass Sie die folgenden Erläuterungen lesen und verstehen, bevor Sie sich bereit erklären, an der Studie teilzunehmen. Wenn Sie irgendwelche unvermeidlichen Fachausdrücke nicht verstehen fragen Sie bitte nach.

**Zweck der Studie**

Mit der Studie werden die neuronalen Mechanismen im Zusammenhang mit zielorientierten motorischen Bewegungen am Beispiel einer Kraft-Puls-Generierung untersucht. Dazu sollen verschiedene Ziel-Kräfte durch drücken eines Kraftsensors zwischen Daumen und Zeigefinger möglichst präzise, impulsartig generiert und die Gehirnaktivität mittels EEG aufgezeichnet. Die Ergebnisse werden Aufschluss über die neuronalen Mechanismen eines der bedeutsamsten Parameter – der Kraft-Impuls-Planung- beim Golf-Putt geben.

**Studienablauf**

Männliche Probanden im Alter von 20 – 40 Jahren, werden an der Studie teilnehmen. Am Ende sollen 10 Personen in die Auswertung übernommen werden können. Teilnehmen werden ausschließlich ambitionierte Golfer, welche an der vorangegangenen Put&Brain2-Studie erfolgreich teilgenommen haben. Die Tests finden an einem Termin über einen Zeitraum von maximal 2 Stunden statt. Zu dem vereinbarten Termin kommen Sie pünktlich in gut ausgeruhtem Zustand zu uns. Sie sollten am Vortag kein Alkohol, Drogen oder andere Stimulantien eingenommen haben. Falls sie eine Sehhilfe benötigen sollten, tragen sie diese bitte unbedingt auch während des Tests. Sie sollten trockene, gewaschene Haare haben, aber keine Pflege oder Stylingprodukte benutzen. Während der Vorbereitung (applizieren einer EEG-Haube, Ausfüllen von Fragebögen), wird ihnen der Testablauf erläutert woraufhin eine kurze Übungsphase folgt.

**Risiken**

*Betreffend EEG*

Über eine Elektrodenhaube wird ähnlich wie beim EKG an der Oberfläche des Kopfes die elektrische Aktivität des Gehirns gemessen. Die Apparaturen sind hoch abgesichert, so dass keine Hochspannung auf den Körper übergehen kann.

**Datensicherheit und Datenverwendung**

Sämtliche Angaben werden vertraulich behandelt. Es gilt die ärztliche Schweigepflicht für das gesamte an der Studie involvierte Personal und bei der Übertragung auf Datenträger werden alle persönlichen Daten anonymisiert. Mit Ihrer Unterschrift stimmen Sie jedoch dem Gebrauch der anonymisierten Daten für wissenschaftliche Zwecke zu.

**Freiwilligkeit**

Ihre Teilnahme an der Studie ist freiwillig. Sie können auch jederzeit aus der Studie auf eigenen Wunsch hin ausscheiden. Ein Rückzug Ihrer Zusage während der laufenden Studie ist nicht mit Nachteilen für Sie verbunden.

**Einverständniserklärung**

Name: \_\_\_\_\_ Vorname: \_\_\_\_\_ Datum: \_\_\_\_\_

Ich habe die Probanden-Informationen und die aufklärenden Hinweise gelesen. Die aufklärenden Informationen habe ich verstanden bzw. hatte auch die Gelegenheit, Fragen jeglicher Art zu stellen. Die Auskunft auf meine Fragen war zufriedenstellend.

Die Risiken sind mir bewusst. Auch willige ich in die Datenverwendung in der Form ein, wie sie in der Probandenaufklärung erläutert wurde.

Meine Teilnahme ist nach der somit erfolgten Aufklärung freiwillig und ich kann ohne Nachteile meinen Rückzug aus der Studie erklären.

Ich habe das Aufklärungsblatt zum Mitnehmen erhalten.

Unterschrift Proband:

Gegenzeichnung Studienleiter:

**Anthropometric form - golf putt study**

| <b>Anamnese</b>   |                          |   |
|---|--------------------------|---|
| Name: _____   | Vorname: _____           |   |
| Geburtsdatum: _____ Adresse: _____  |                          |   |
| Größe: ____ cm  | Gewicht: ____ kg         | Kopfumfang: ____ cm Nasion-Inion: ____ cm |
| Handicap: ____  |                          |   |
| <ul style="list-style-type: none"> <li>• <b>Eignungskriterien</b></li> </ul>  |                          |   |
| <b>Sie</b>  | <b>Ja</b>                | <b>Nein</b>                               |
| • sind im Alter von 20-40 Jahren  | <input type="checkbox"/> | <input type="checkbox"/>                  |
| • sind Rechtshänder   | <input type="checkbox"/> | <input type="checkbox"/>                  |
| • putten nach links (Standard-Ausrichtung)  | <input type="checkbox"/> | <input type="checkbox"/>                  |
| • sind männlich   | <input type="checkbox"/> | <input type="checkbox"/>                  |
| • fühlen sich gesund  | <input type="checkbox"/> | <input type="checkbox"/>                  |
| wenn nicht, geben sie nachfolgend Ihre Probleme an:   |                          |   |
| <ul style="list-style-type: none"> <li>• <b>Ausschlußkriterien</b></li> </ul>   |                          |   |
| Leiden oder litten Sie an   | Ja                       | Nein                                      |
| Nerven- oder Gemütskrankheiten, Epilepsie o.ä.<br>Schlafstörungen   | <input type="checkbox"/> | <input type="checkbox"/>                  |
| Testrelevante körperliche Einschränkungen / Beschwerden<br>Wenn ja, welche:   | <input type="checkbox"/> | <input type="checkbox"/>                  |
| <div style="display: flex; justify-content: flex-end; align-items: center; gap: 20px;"> <div>Aufgenommen in die Probandenliste unter der Probanden-Nr.:</div> <input style="width: 40px; height: 30px; border: 1px solid black;" type="text"/> </div> |                          |   |

**Probandenaufklärung und Einverständnis-Erklärung**

Name: \_\_\_\_\_ Vorname: \_\_\_\_\_ Datum: \_\_\_\_\_

**Vorwort**

Es ist wichtig, dass Sie die folgenden Erläuterungen lesen und verstehen, bevor Sie sich bereit erklären, an der Studie teilzunehmen. Wenn Sie irgendwelche unvermeidlichen Fachausdrücke nicht verstehen fragen Sie bitte nach.

**Zweck der Studie**

Mit der Studie werden die neuronalen Mechanismen im Zusammenhang mit zielorientierten motorischen Bewegungen am Beispiel des Golf-Putts untersucht. Dazu werden Golf-Putts aus verschiedenen Abständen (2,5 m, 3 m und 4 m) durchgeführt und die Gehirnaktivität mittels EEG aufgezeichnet.

**Studienablauf**

Männliche Probanden im Alter von 20 – 40 Jahren, werden an der Studie teilnehmen. Am Ende sollen 10 Personen in die Auswertung übernommen werden können. Die Teilnahme erfolgt abhängig von der Bestätigung der Rechtshändigkeit durch einen Fragebogen. Die Tests finden an einem Termin über einen Zeitraum von etwa 2 - 3 Stunden statt. Zu dem vereinbarten Termin kommen Sie pünktlich in gut ausgeruhtem Zustand zu uns. Sie sollten am Vortag kein Alkohol, Drogen oder andere Stimulantien eingenommen haben. Falls sie eine Sehhilfe benötigen sollten, tragen sie diese bitte unbedingt auch während des Tests. Sie sollten trockene, gewaschene Haare haben, aber keine Pflege oder Stylingprodukte benutzen. Während der Vorbereitung (applizieren einer EEG-Haube, Ausfüllen von Fragebögen), wird ihnen der Testablauf erläutert woraufhin eine kurze Übungsphase folgt.

**Risiken**

*Betreffend EEG*

Über eine Elektrodenhaube wird ähnlich wie beim EKG an der Oberfläche des Kopfes die elektrische Aktivität des Gehirns gemessen. Die Apparaturen sind hoch abgesichert, so dass keine Hochspannung auf den Körper übergehen kann.

**Datensicherheit und Datenverwendung**

Sämtliche Angaben werden vertraulich behandelt. Es gilt die ärztliche Schweigepflicht für das gesamte an der Studie involvierte Personal und bei der Übertragung auf Datenträger werden alle persönlichen Daten anonymisiert. Mit Ihrer Unterschrift stimmen Sie jedoch dem Gebrauch der anonymisierten Daten für wissenschaftliche Zwecke zu.

**Freiwilligkeit**

Ihre Teilnahme an der Studie ist freiwillig. Sie können auch jederzeit aus der Studie auf eigenen Wunsch hin ausscheiden. Ein Rückzug Ihrer Zusage während der laufenden Studie ist nicht mit Nachteilen für Sie verbunden.

**Einverständniserklärung**

Name: \_\_\_\_\_ Vorname: \_\_\_\_\_ Datum: \_\_\_\_\_

Ich habe die Probanden-Informationen und die aufklärenden Hinweise gelesen. Die aufklärenden Informationen habe ich verstanden bzw. hatte auch die Gelegenheit, Fragen jeglicher Art zu stellen. Die Auskunft auf meine Fragen war zufriedenstellend.

Die Risiken sind mir bewusst. Auch willige ich in die Datenverwendung in der Form ein, wie sie in der Probandenaufklärung erläutert wurde.

Meine Teilnahme ist nach der somit erfolgten Aufklärung freiwillig und ich kann ohne Nachteile meinen Rückzug aus der Studie erklären.

Ich habe das Aufklärungsblatt zum Mitnehmen erhalten.

Unterschrift Proband:

Gegenzeichnung Studienleiter:

## C.2 The Edinburgh-Inventory - German translation

### Die Einschätzung und Analyse der Händigkeit

(The Edinburgh Inventory)

Name: \_\_\_\_\_

Geburtsdatum: \_\_\_\_\_

Geschlecht: \_\_\_\_\_

Hatten sie jemals eine Tendenz zur Links-Händigkeit?

Ja

Nein

Bitte zeigen sie Ihre Bevorzugung im Gebrauch der Hände bei den folgenden Aktivitäten an, indem sie + in die entsprechende Spalte einfügen. Wo die Bevorzugung so stark ist, daß sie niemals versuchen würden, die andere Hand zu benutzen, außer sie sind dazu gezwungen, tragen sie ++ ein. Sollten sie in einem Fall keine eindeutige Entscheidung treffen können, setzen sie + in beide Spalten.

Einige der Aktivitäten erfordern beide Hände. In diesen Fällen ist der Teil der Aufgabe, oder Sache, für den die Vorzugshand anzugeben ist, in den Klammern angezeigt.

Bitte versuchen sie, alle Fragen zu beantworten und lassen sie nur eine Lücke, wenn sie überhaupt keine Erfahrung mit der Sache oder Aufgabe haben.

C. QUESTIONNAIRES

|    |   | R | L |
|----|---|---|---|
| 1  | schreiben   |   |   |
| 2  | zeichnen  |   |   |
| 3  | werfen  |   |   |
| 4  | Schere  |   |   |
| 5  | Kamm  |   |   |
| 6  | Zahnbürste  |   |   |
| 7  | Messer (ohne Gabel)   |   |   |
| 8  | Löffel  |   |   |
| 9  | Hammer  |   |   |
| 10 | Schraubenzieher   |   |   |
| 11 | Tennisschläger  |   |   |
| 12 | Messer (mit Gabel)  |   |   |
| 13 | Kricketschläger (untere Hand)                                   |   |   |
| 14 | Golfschläger (untere Hand)                                      |   |   |
| 15 | Besen (obere Hand)  |   |   |
| 16 | Harke (obere Hand)  |   |   |
| 17 | Streichholz anzünden (Streichholz)                              |   |   |
| 18 | Schachtel öffnen (Deckel)                                       |   |   |
| 19 | Karten geben (Karte, die gegeben wird)                          |   |   |
| 20 | Nadel einfädeln (Nadel oder Faden je nachdem, was bewegt wird). |   |   |
|    |   |   |   |
| 40 | Welchen Fuß bevorzugen sie, um damit zu treten?                 |   |   |
| 41 | Welches Auge benutzen sie, wenn sie nur eines benutzen?         |   |   |

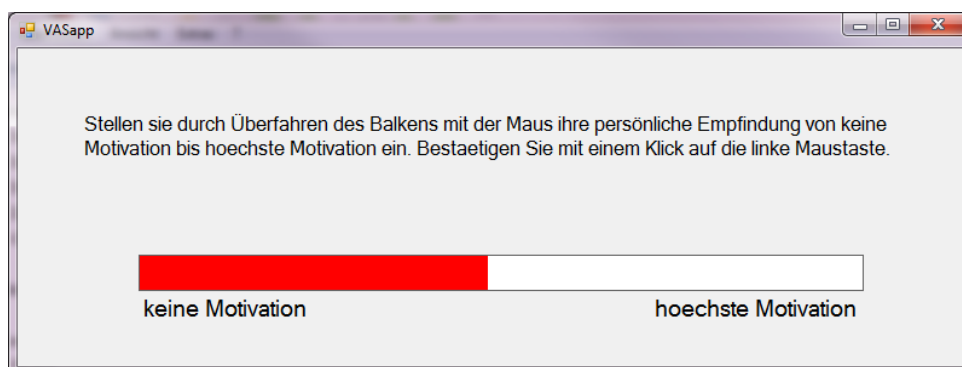
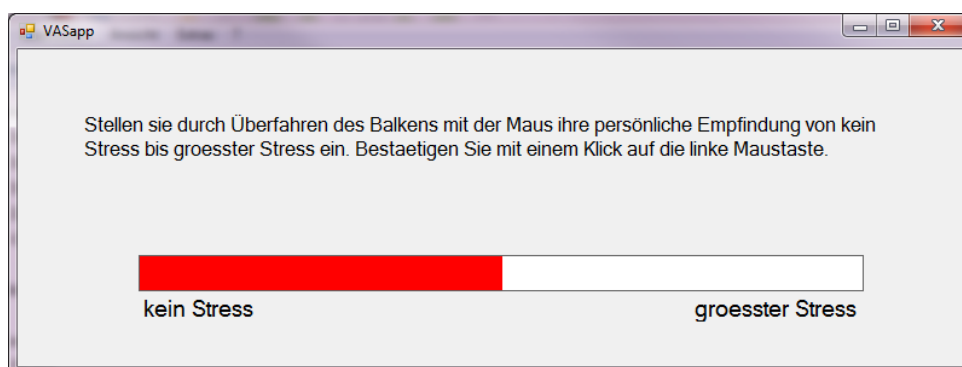
LQ  Lassen sie diese Felder bitte frei Decile



## C.3 The strait anxiety test X1 (STAI-X1) - German translation

| <b>Fragebogen zur Selbstbeschreibung</b>  | <b>STAI-G Form X 1</b>  |           |                 |           |          |      |
|---|---|-----------|-----------------|-----------|----------|------|
| Name _____ Mädchenname _____  |   |           |                 |           |          |      |
| Vorname _____ Geburtsdatum _____ Alter _____ Jahre  |   |           |                 |           |          |      |
| Beruf _____ Geschlecht m/w  |   |           |                 |           |          |      |
| Datum _____ Institution _____   |   |           |                 |           |          |      |
| Uhrzeit _____   |   |           |                 |           |          |      |
| <p><b>Anleitung:</b> Im folgenden Fragebogen finden Sie eine Reihe von Feststellungen, mit denen man sich selbst beschreiben kann. Bitte lesen Sie jede Feststellung durch und wählen Sie aus den vier Antworten diejenige aus, die angibt, wie Sie sich <b>jetzt</b>, d. h. <b>in diesem Moment</b>, fühlen. Kreuzen Sie bitte bei jeder Feststellung die Zahl unter der von Ihnen gewählten Antwort an.</p> <p>Es gibt keine richtigen oder falschen Antworten. Überlegen Sie bitte nicht lange und denken Sie daran, diejenige Antwort auszuwählen, die Ihren <b>augenblicklichen</b> Gefühlszustand am besten beschreibt.</p> | <table border="1" style="width: 100%; border-collapse: collapse;"> <thead> <tr> <th style="width: 10%;"></th> <th style="width: 15%;">ÜBERHAUPT NICHT</th> <th style="width: 15%;">EIN WENIG</th> <th style="width: 15%;">ZIEMLICH</th> <th style="width: 15%;">SEHR</th> </tr> </thead> </table> |           | ÜBERHAUPT NICHT | EIN WENIG | ZIEMLICH | SEHR |
|   | ÜBERHAUPT NICHT   | EIN WENIG | ZIEMLICH        | SEHR      |          |      |
| 1. Ich bin ruhig  | 1 2 3 4   |           |                 |           |          |      |
| 2. Ich fühle mich geborgen  | 1 2 3 4   |           |                 |           |          |      |
| 3. Ich fühle mich angespannt  | 1 2 3 4   |           |                 |           |          |      |
| 4. Ich bin bekümmert  | 1 2 3 4   |           |                 |           |          |      |
| 5. Ich bin gelöst   | 1 2 3 4   |           |                 |           |          |      |
| 6. Ich bin aufgeregt  | 1 2 3 4   |           |                 |           |          |      |
| 7. Ich bin besorgt, daß etwas schiefgehen könnte  | 1 2 3 4   |           |                 |           |          |      |
| 8. Ich fühle mich ausgeruht   | 1 2 3 4   |           |                 |           |          |      |
| 9. Ich bin beunruhigt   | 1 2 3 4   |           |                 |           |          |      |
| 10. Ich fühle mich wohl   | 1 2 3 4   |           |                 |           |          |      |
| 11. Ich fühle mich selbstsicher   | 1 2 3 4   |           |                 |           |          |      |
| 12. Ich bin nervös  | 1 2 3 4   |           |                 |           |          |      |
| 13. Ich bin zappelig  | 1 2 3 4   |           |                 |           |          |      |
| 14. Ich bin verkrampft  | 1 2 3 4   |           |                 |           |          |      |
| 15. Ich bin entspannt   | 1 2 3 4   |           |                 |           |          |      |
| 16. Ich bin zufrieden   | 1 2 3 4   |           |                 |           |          |      |
| 17. Ich bin besorgt   | 1 2 3 4   |           |                 |           |          |      |
| 18. Ich bin überreizt   | 1 2 3 4   |           |                 |           |          |      |
| 19. Ich bin froh  | 1 2 3 4   |           |                 |           |          |      |
| 20. Ich bin vergnügt  | 1 2 3 4   |           |                 |           |          |      |

## C.4 Visual Analogue Scale



# **Appendix D**

## **Spec sheets**

## D.1 Force transducer - Soemer - Load cell 1022

### Plattform-Wägezelle **1022**



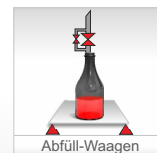
Besonders in flachbauenden Waagen mit hohen Genauigkeitsansprüchen hat sich diese standardisierte **Plattform-Wägezelle 1022** etabliert. Der niedrige Preis und die außergewöhnliche Präzision dieses Modells liefert ideale Voraussetzungen für den Einsatz in preiswerten Plattform-, Zähl-, Gasflaschen- und Personen-Waagen. Auch in industriellen Abfüll- und Dosiersystemen, sowie pharmazeutischen und medizinischen Prozessanlagen hat sich diese Wägezelle bestens bewährt.

Die Wägezelle 1022 hat wie jede Plattform-Wägezelle ein mechanisches Doppel-Lenker-System, auch Parallelogramm genannt, um Torsionskräfte bei exzentrischer Kräfteinleitung auszugleichen. Jede einzelne Wägezelle wird auf Eckenlastempfindlichkeit geprüft und durch eine aufwendige mechanische Bearbeitung optimiert. Dadurch entstehen auch dann keine Messfehler, wenn die zu messende Masse einseitig, bspw. in einer Ecke, auf der Plattform liegt. Der Aufbau einer Plattform-Waage mit dieser Wägezelle ist denkbar einfach. Über die beiden Anschraubflächen oben vorne bzw. hinten unten am Kabelausgang werden zwei Stahl- oder Aluminiumplatten von bis zu 350 x 350 mm angeschraubt und ein entsprechendes DMS-Messgerät oder ein Messverstärker angeschlossen und fertig ist die Waage.

Standardmäßig wird die Wägezelle 1022 mit einem abgeschirmten 4-Leiter-Anschlusskabel geliefert. Sonderkabel und -längen sind auf Anfrage möglich.

Die Wägezelle ist optional in Ex-Schutz Ausführung gemäß Richtlinie 94/9/EG (ATEX 95) lieferbar. Einsetzbar im Gas-Ex-Bereich Zone 1 mit der Kennzeichnung: II 2G EEx ia IIC T4.

- Messbereiche von 3 ... 200 kg
- niedrige Bauhöhe max. 22 mm
- für Plattformgrößen bis zu 350 x 350 mm
- Wägezelle aus hochfester Aluminiumlegierung
- eichfähig nach OIML R60 für bis zu 4.000 d
- bewährt in Plattform- und Zählwaagen
- als Option in ATEX-Ausführung lieferbar
- Parallel-Lenker-System mit hoher Eigenfrequenz





**Technische Daten**

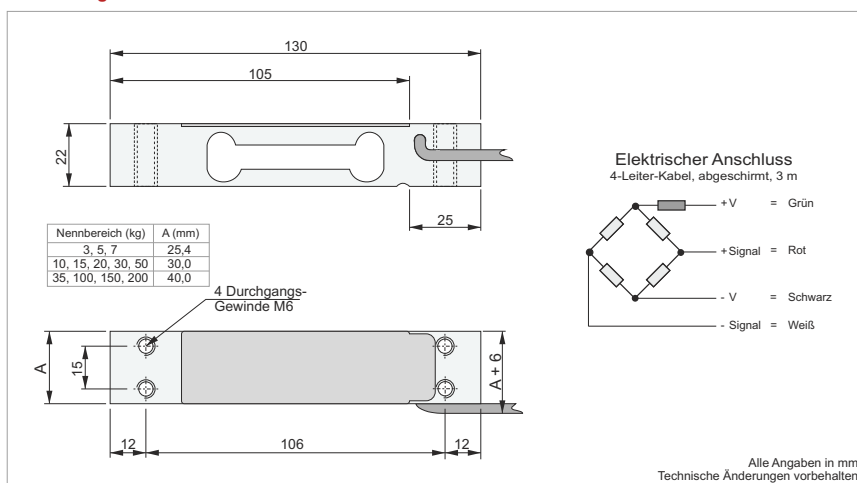
**Modell 1022**

| Genauigkeitsklasse                            |               | G   | C3                        | C4     |
|---|---------------|---|---------------------------|--------|
| Max. Anzahl der Teilungswerte                 | $n_{LC}$      | -   | 3.000                     | 4.000  |
| Mindestanwendungsbereich                      | % v. Nennlast | -   | 50                        | 40     |
| Mindestteilungswert ( $v_{min} = E_{max}/Y$ ) | Y             | -   | 6.000                     | 10.000 |
| Zusammengesetzter Fehler                      | % v. Nennlast | 0,050   | 0,020                     | 0,015  |
| Kriechfehler / DR (30 min.)                   | % v. Nennlast | 0,050   | 0,017                     | 0,013  |
| Temperaturkoeffizient Kennwert                | %/10 °C       | 0,030   | 0,010                     | 0,008  |
| Temperaturkoeffizient Nullpunkt               | %/10 °C       | 0,100   | 0,023                     | 0,014  |
| Nennkennwert (RO)                             | mV/V          |   | 2,00                      |        |
| Nennkennwerttoleranz                          | %             |   | +/-10                     |        |
| Eingangswiderstand                            | Ohm           |   | 415 +/-15                 |        |
| Ausgangswiderstand                            | Ohm           |   | 350 +/-3                  |        |
| Empf. Versorgungsspannung                     | V             |   | 5 ... 10                  |        |
| Nenntemperaturbereich                         | °C            |   | -10 ... +40               |        |
| Gebrauchstemperaturbereich                    | °C            |   | -20 ... +70               |        |
| Nennmessweg                                   | mm            |   | -0,4                      |        |
| Überlastbereich                               | % v. Nennlast |   | 150                       |        |
| Grenzlast                                     | % v. Nennlast |   | 200                       |        |
| Bruchlast                                     | % v. Nennlast |   | 300                       |        |
| Kabellänge                                    | m             |   | 3                         |        |
| Plattformgröße                                | mm            |   | 350 x 350                 |        |
| Werkstoff / Schutzart                         |               |   | Aluminium - 3.1355 / IP66 |        |
| Nennlasten                                    | kg            | 3**, 5**, 7, 10, 15, 20, 30, 35, 50, 100, 150, 200* |                           |        |

NMI Prüfschein TC-2792, \* nur in G-Genauigkeit lieferbar, \*\* nicht in C4-Genauigkeit lieferbar

D-1022-080114

**Abmessungen**



Alle Angaben in mm  
Technische Änderungen vorbehalten

## D.2 Force transducer - Soemer - digitizing unit LDU 68.1

### LDU 68.1 Digitaler DMS-Meßverstärker

**SOEMER**  
MESSTECHNIK GMBH

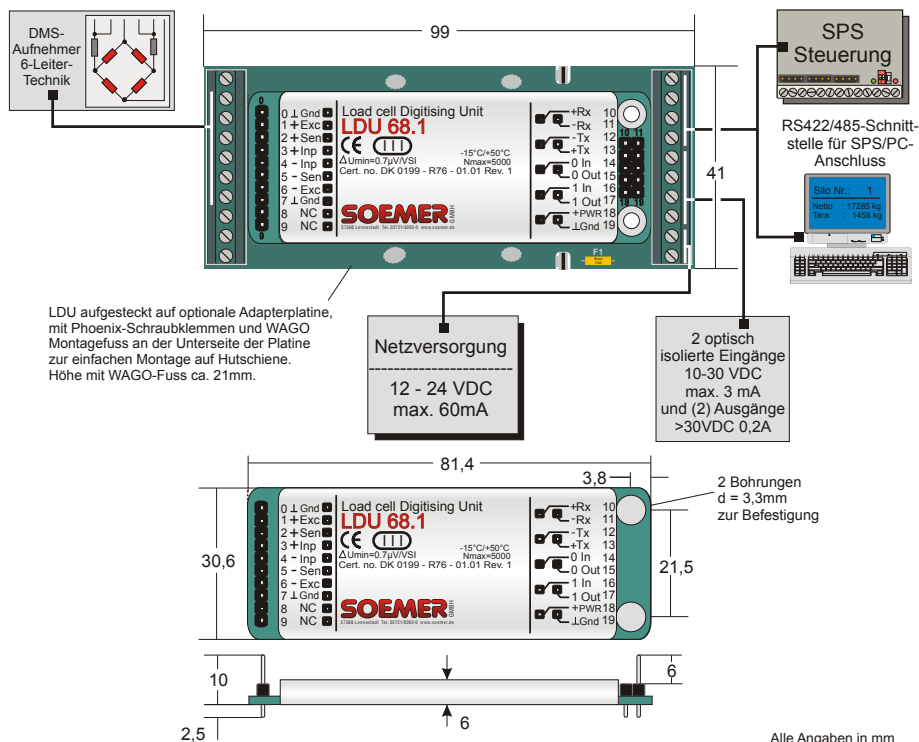


### Digitaler-DMS-Messverstärker LDU 68.1

- eichfähig nach OIML R76 bis 5000D, EMV und CE geprüft
- 90 Digitalisierungen pro Sekunde, 19-bit-Auflösung
- Linearität besser als 0,002 %, Auflösung 100 nV
- Versorgungsspannung von 12-24 VDC +/- 10 %
- RS-422 oder RS-485 Computer-Schnittstelle
- Baudrate von 9600 Baud bis 115,2 kBaud einstellbar
- 2 optisch isolierte Logikein- und Ausgänge
- sehr einfacher und logischer ASCII-Befehlssyntax
- volle bidirektionale Steuerung über die Schnittstelle
- steckbar über integrierte Anschlussleiste
- komplett in SMD-Technik aufgebaut
- optional auf Platine mit Phoenix-Klemmen lieferbar

Technische Daten

Modell LDU 68.1



Spezifikationen

|                              |   |
|------------------------------|---|
| Linearität vom Nennwert      | : < 0,002%  |
| Brückenversorgung            | : 5 VDC, dimensioniert für 1 DMS-Aufnehmer mit 250-2000 Ohm                               |
| Eingangssignalbereich        | : +/-2,2 mV/V, entspricht +/- 11mVDC, Auflösung 100nV                                     |
| Eingangspolarität            | : bipolar, für Wägenwendungen, Kraft- und Drehmomentapplikationen                         |
| A/D-Auflösung                | : bis zu +/-260.000 d, 19-Bit-A/D-Wandler, Ausgabe max. +/- 99.999 D                      |
| A/D-Geschwindigkeit          | : 90 Messungen/Sekunde, unabhängig von Filtereinstellungen                                |
| Digital-Filter               | : von 0,02Hz bis 5Hz in 8 Stufen einstellbar  |
| Kalibrierung                 | : per Software über ASCII-Kommandos, sehr einfach durchführbar                            |
| Computer-Schnittstelle       | : RS-485 oder RS-422, full duplex, 9600...115.200 Baud, busfähig bis zu 32 Einheiten      |
| Schreib- und Lesemöglichkeit | : Brutto, Tara, Netto, Filter, Kalibrieren, Trieren, Nullsetzen, Auflösung usw.           |
| Logik-Eingänge               | : 2 Logik Eingänge 10 - 30VDC 1-3 mA, Minus an Gerätemasse Status über Software auslesbar |
| Logik-Ausgänge               | : 2 Logik Ausgänge <30VDC 0,2A, Minus an Gerätemasse, Status über Software auslesbar      |
| Temperatur-Effekte           | : <10ppm/°C auf den Nullpunkt und <5ppm/°C auf die Verstärkung                            |
| Temperatur-Bereich           | : -15°C bis +50°C (Betrieb); -20°C bis +60°C (Lagerung)                                   |
| Gehäuse                      | : verzinnertes Metallgehäuse, Schutzart IP 40   |
| Abmessungen                  | : 81,3 x 30,6 x 5,6 mm, Gewicht ca. 30 g; mit Adapterboard 99 x 41 x 12 mm, ca. 50g       |
| Versorgungsspannung          | : 12...24 VDC +/-10 %, < 60mA, nicht galvanisch getrennt                                  |

D-LDU-280205

**SOEMER** GMBH  
57368 Lennestadt Tel. 02721/9262-0 Fax 9262-50

Präzisions - Wägezellen  
Zubehör und Einbauhilfen  
Messgeräte und -systeme

## D.3 Accelerometer - Analog Devices - ADXL330



### Small, Low Power, 3-Axis $\pm 3 g$ *i*MEMS<sup>®</sup> Accelerometer

#### ADXL330

#### FEATURES

- 3-axis sensing
- Small, low-profile package  
4 mm × 4 mm × 1.45 mm LFCSP
- Low power  
180  $\mu$ A at  $V_S = 1.8$  V (typical)
- Single-supply operation  
1.8 V to 3.6 V
- 10,000 g shock survival
- Excellent temperature stability
- BW adjustment with a single capacitor per axis
- RoHS/WEEE lead-free compliant

#### APPLICATIONS

- Cost-sensitive, low power, motion- and tilt-sensing applications
- Mobile devices
- Gaming systems
- Disk drive protection
- Image stabilization
- Sports and health devices

#### GENERAL DESCRIPTION

The ADXL330 is a small, thin, low power, complete 3-axis accelerometer with signal conditioned voltage outputs, all on a single monolithic IC. The product measures acceleration with a minimum full-scale range of  $\pm 3 g$ . It can measure the static acceleration of gravity in tilt-sensing applications, as well as dynamic acceleration resulting from motion, shock, or vibration.

The user selects the bandwidth of the accelerometer using the  $C_X$ ,  $C_Y$ , and  $C_Z$  capacitors at the  $X_{OUT}$ ,  $Y_{OUT}$ , and  $Z_{OUT}$  pins. Bandwidths can be selected to suit the application, with a range of 0.5 Hz to 1600 Hz for X and Y axes, and a range of 0.5 Hz to 550 Hz for the Z axis.

The ADXL330 is available in a small, low profile, 4 mm × 4 mm × 1.45 mm, 16-lead, plastic lead frame chip scale package (LFCSP\_LQ).

#### FUNCTIONAL BLOCK DIAGRAM

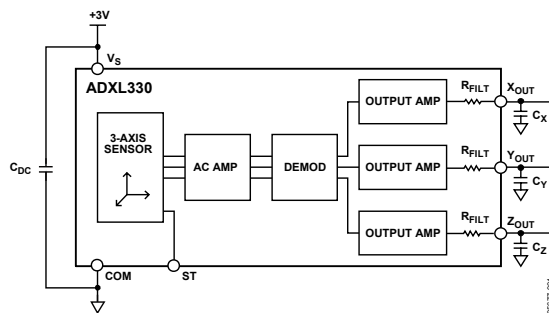


Figure 1.

Rev. A  
Information furnished by Analog Devices is believed to be accurate and reliable. However, no responsibility is assumed by Analog Devices for its use, nor for any infringements of patents or other rights of third parties that may result from its use. Specifications subject to change without notice. No license is granted by implication or otherwise under any patent or patent rights of Analog Devices. Trademarks and registered trademarks are the property of their respective owners.

One Technology Way, P.O. Box 9106, Norwood, MA 02062-9106, U.S.A.  
Tel: 781.329.4700 [www.analog.com](http://www.analog.com)  
Fax: 781.461.3113 ©2007 Analog Devices, Inc. All rights reserved.



**ADXL330**

## SPECIFICATIONS

$T_A = 25^\circ\text{C}$ ,  $V_S = 3\text{ V}$ ,  $C_X = C_Y = C_Z = 0.1\ \mu\text{F}$ , acceleration = 0 g, unless otherwise noted. All minimum and maximum specifications are guaranteed. Typical specifications are not guaranteed.

**Table 1.**

| Parameter  | Conditions                      | Min     | Typ           | Max | Unit                               |
|--|---------------------------------|---------|---------------|-----|------------------------------------|
| <b>SENSOR INPUT</b>                                |                                 |         |               |     |                                    |
| Measurement Range                                  | Each axis                       | $\pm 3$ | $\pm 3.6$     |     | g                                  |
| Nonlinearity                                       | % of full scale                 |         | $\pm 0.3$     |     | %                                  |
| Package Alignment Error                            |                                 |         | $\pm 1$       |     | Degrees                            |
| Interaxis Alignment Error                          |                                 |         | $\pm 0.1$     |     | Degrees                            |
| Cross Axis Sensitivity <sup>1</sup>                |                                 |         | $\pm 1$       |     | %                                  |
| <b>SENSITIVITY (RATIOMETRIC)<sup>2</sup></b>       |                                 |         |               |     |                                    |
| Sensitivity at $X_{OUT}$ , $Y_{OUT}$ , $Z_{OUT}$   | Each axis<br>$V_S = 3\text{ V}$ | 270     | 300           | 330 | mV/g                               |
| Sensitivity Change Due to Temperature <sup>3</sup> | $V_S = 3\text{ V}$              |         | $\pm 0.015$   |     | %/°C                               |
| <b>ZERO g BIAS LEVEL (RATIOMETRIC)</b>             |                                 |         |               |     |                                    |
| 0 g Voltage at $X_{OUT}$ , $Y_{OUT}$ , $Z_{OUT}$   | Each axis<br>$V_S = 3\text{ V}$ | 1.2     | 1.5           | 1.8 | V                                  |
| 0 g Offset vs. Temperature                         |                                 |         | $\pm 1$       |     | mg/°C                              |
| <b>NOISE PERFORMANCE</b>                           |                                 |         |               |     |                                    |
| Noise Density $X_{OUT}$ , $Y_{OUT}$                |                                 |         | 280           |     | $\mu\text{g}/\sqrt{\text{Hz}}$ rms |
| Noise Density $Z_{OUT}$                            |                                 |         | 350           |     | $\mu\text{g}/\sqrt{\text{Hz}}$ rms |
| <b>FREQUENCY RESPONSE<sup>4</sup></b>              |                                 |         |               |     |                                    |
| Bandwidth $X_{OUT}$ , $Y_{OUT}$ <sup>5</sup>       | No external filter              |         | 1600          |     | Hz                                 |
| Bandwidth $Z_{OUT}$ <sup>5</sup>                   | No external filter              |         | 550           |     | Hz                                 |
| $R_{\text{FILTER}}$ Tolerance                      |                                 |         | $32 \pm 15\%$ |     | k $\Omega$                         |
| Sensor Resonant Frequency                          |                                 |         | 5.5           |     | kHz                                |
| <b>SELF TEST<sup>6</sup></b>                       |                                 |         |               |     |                                    |
| Logic Input Low                                    |                                 |         | +0.6          |     | V                                  |
| Logic Input High                                   |                                 |         | +2.4          |     | V                                  |
| ST Actuation Current                               |                                 |         | +60           |     | $\mu\text{A}$                      |
| Output Change at $X_{OUT}$                         | Self test 0 to 1                |         | -150          |     | mV                                 |
| Output Change at $Y_{OUT}$                         | Self test 0 to 1                |         | +150          |     | mV                                 |
| Output Change at $Z_{OUT}$                         | Self test 0 to 1                |         | -60           |     | mV                                 |
| <b>OUTPUT AMPLIFIER</b>                            |                                 |         |               |     |                                    |
| Output Swing Low                                   | No load                         |         | 0.1           |     | V                                  |
| Output Swing High                                  | No load                         |         | 2.8           |     | V                                  |
| <b>POWER SUPPLY</b>                                |                                 |         |               |     |                                    |
| Operating Voltage Range                            |                                 | 1.8     |               | 3.6 | V                                  |
| Supply Current                                     | $V_S = 3\text{ V}$              |         | 320           |     | $\mu\text{A}$                      |
| Turn-On Time <sup>7</sup>                          | No external filter              |         | 1             |     | ms                                 |
| <b>TEMPERATURE</b>                                 |                                 |         |               |     |                                    |
| Operating Temperature Range                        |                                 | -25     |               | +70 | °C                                 |

<sup>1</sup> Defined as coupling between any two axes.

<sup>2</sup> Sensitivity is essentially ratiometric to  $V_S$ .

<sup>3</sup> Defined as the output change from ambient-to-maximum temperature or ambient-to-minimum temperature.

<sup>4</sup> Actual frequency response controlled by user-supplied external filter capacitors ( $C_X$ ,  $C_Y$ ,  $C_Z$ ).

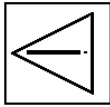
<sup>5</sup> Bandwidth with external capacitors =  $1/(2 \times \pi \times 32\text{ k}\Omega \times C)$ . For  $C_X$ ,  $C_Y = 0.003\ \mu\text{F}$ , bandwidth = 1.6 kHz. For  $C_Z = 0.01\ \mu\text{F}$ , bandwidth = 500 Hz. For  $C_X$ ,  $C_Y$ ,  $C_Z = 10\ \mu\text{F}$ , bandwidth = 0.5 Hz.

<sup>6</sup> Self-test response changes cubically with  $V_S$ .

<sup>7</sup> Turn-on time is dependent on  $C_X$ ,  $C_Y$ ,  $C_Z$  and is approximately  $160 \times C_X$  or  $C_Y$  or  $C_Z + 1\text{ ms}$ , where  $C_X$ ,  $C_Y$ ,  $C_Z$  are in  $\mu\text{F}$ .

## D.4 EEG amplifier - Neuroscan - Synamps RT

### Device Classification



#### **ATTENTION: CONSULT ACCOMPANYING DOCUMENTS BEFORE USING**

The *SynAmps<sup>2</sup>*™ Model 8050 EEG amplifier and data acquisition system is a line-powered instrument designed to meet the applicable requirements of IEC601-1:1988. The *SynAmps<sup>2</sup>* should be used only according to the manufacturer's instructions. Replacement parts and accessories may be obtained from the manufacturer.

#### Manufacturer:

#### **Compumedics Neuroscan USA Ltd.**

6605 West W.T. Harris Blvd., Suite F  
 Charlotte, NC 28269  
 Phone: 877-717-3975 (8am – 5pm EST)  
 E-mail: [techsup@neuroscan.com](mailto:techsup@neuroscan.com)  
 Web: [www.neuroscan.com](http://www.neuroscan.com)

This equipment has been tested and found to comply with the limits and requirements for a Class A device per EN60601-1-2. These limits and requirements are designed to provide reasonable protection under conditions of normal use from interference with and by other devices. There is, however, no guarantee that interference will not result from operation of this device in proximity or connected to some other device. If interference occurs, the user or operator is encouraged to try to correct the interference by one or more of the following measures: (1) Change the orientation of the two devices relative to one another;

(2) Increase the separation between the two devices; (3) Check the power source and grounding for the two devices; and Consult the dealer, Neuroscan Technical Support, or an experienced technician for help.

The safety and electromagnetic compatibility of this system was tested with the following accessories, parts, and associated devices. The user or operator is cautioned to ensure that when using accessories, parts, or associated devices other than those listed, that the safety and electromagnetic compatibility of the system is maintained.

- 1) Neuroscan SCAN Computer P/N 0010915 or 0010914
- 2) Headbox Cable P/N 00080586
- 3) Deblock Interface Cable P/N 00081300

Classification per IEC601-1:1988

The device is ordinary equipment not protected against ingress of water and should not be used in the presence of any spilled liquids. It is not designed to be suitable for use in the presence of a flammable anesthetic mixture of air and oxygen or nitrous oxide. The device is capable of continuous operation.

Class and degree of protection against electrical shock is Class 1, Type CF.

#### Technical Description

|                |                             |
|----------------|-----------------------------|
| Input:         | 120-230VAC, 50/60Hz, 10/5A  |
| Fuses:         | T5A 250V (2 each, 5 X 20mm) |
| <i>Headbox</i> |                             |
| Weight:        | 1.5 kg                      |
| Dimensions:    | Height: 4.5 cm              |
|                | Width: 18.7 cm              |
|                | Depth: 21.8 cm              |

**SynAmps2** Copyright © 2007 CM/NS  
Document Number 8065, Revision B

- 6 -

*System Unit*

Weight: 4.3kg  
 Dimensions  
 Height: 23.0 cm  
 Width: 11.6 cm  
 Depth: 32.5 cm

*Power Unit*

Weight: 12.5kg  
 Dimensions  
 Height: 23.0 cm  
 Width: 11.6 cm  
 Depth: 32.5 cm

**Shipping and Storage Maximum Limits**

-20° C to +70° C, 10% to 100% humidity, non-condensing RH, 500 hPa to 1060 hPa. After unpacking, allow devices to adjust to room temperature for at least two hours prior to interconnection and application of power.

**Operational Limits**

+15°C to +30°C, 25% to 95% humidity, non-condensing RH, 700hPa to 1060hPa pressure.

**Warnings and Precautions**

Instructions  
 Read instructions before operating the device.

**Symbols**

The following symbols are found on the *SynAmps<sup>2</sup>*:

## D.5 Channel locations - Neuroscan - QuickCap64

|    |          |          |        |
|----|----------|----------|--------|
| 1  | -15.53   | 0.62188  | FP1    |
| 2  | -0.38119 | 0.60988  | FPZ    |
| 3  | 14.807   | 0.61976  | FP2    |
| 4  | -20.413  | 0.47739  | AF3    |
| 5  | 18.276   | 0.49144  | AF4    |
| 6  | -47.145  | 0.58868  | F7     |
| 7  | -44.183  | 0.46892  | F5     |
| 8  | -34.853  | 0.38112  | F3     |
| 9  | -20.069  | 0.31704  | F1     |
| 10 | -0.73326 | 0.31706  | FZ     |
| 11 | 18.789   | 0.32585  | F2     |
| 12 | 34.377   | 0.37894  | F4     |
| 13 | 43.102   | 0.46641  | F6     |
| 14 | 46.602   | 0.58276  | F8     |
| 15 | -65.259  | 0.54812  | FT7    |
| 16 | -63.602  | 0.41102  | FC5    |
| 17 | -55.355  | 0.29072  | FC3    |
| 18 | -35.375  | 0.20269  | FC1    |
| 19 | -1.3372  | 0.17387  | FCZ    |
| 20 | 34.786   | 0.20644  | FC2    |
| 21 | 53.55    | 0.29257  | FC4    |
| 22 | 62.826   | 0.40869  | FC6    |
| 23 | 65.959   | 0.55259  | FT8    |
| 24 | -88.294  | 0.52583  | T7     |
| 25 | -86.932  | 0.37223  | C5     |
| 26 | -82.895  | 0.24749  | C3     |
| 27 | -73.442  | 0.12242  | C1     |
| 28 | 0.31801  | 0.039163 | CZ     |
| 29 | 71.607   | 0.12412  | C2     |
| 30 | 81.788   | 0.24425  | C4     |
| 31 | 84.582   | 0.36951  | C6     |
| 32 | 86.586   | 0.51412  | T8     |
| 33 | -91.444  | 0.82083  | M1     |
| 34 | -110.36  | 0.52642  | TP7    |
| 35 | -110.39  | 0.37831  | CP5    |
| 36 | -114.28  | 0.25301  | CP3    |
| 37 | -128.9   | 0.14528  | CP1    |
| 38 | 179.86   | 0.086948 | CPZ    |
| 39 | 126.44   | 0.14639  | CP2    |
| 40 | 111.54   | 0.24842  | CP4    |
| 41 | 108.11   | 0.36905  | CP6    |
| 42 | 108.05   | 0.51505  | TP8    |
| 43 | 91.466   | 0.80844  | M2     |
| 44 | -130.86  | 0.52822  | P7     |
| 45 | -132.83  | 0.40773  | P5     |
| 46 | -139.21  | 0.30397  | P3     |
| 47 | -153.64  | 0.2354   | P1     |
| 48 | 179.94   | 0.21519  | PZ     |
| 49 | 153.55   | 0.23559  | P2     |
| 50 | 137.72   | 0.30531  | P4     |
| 51 | 131.26   | 0.40407  | P6     |
| 52 | 127.88   | 0.51753  | P8     |
| 53 | -147.54  | 0.54127  | PO7    |
| 54 | -150.57  | 0.46061  | PO5    |
| 55 | -156.91  | 0.39193  | PO3    |
| 56 | 179.26   | 0.34988  | POZ    |
| 57 | 154.78   | 0.38673  | PO4    |
| 58 | 148.36   | 0.4486   | PO6    |
| 59 | 146.38   | 0.53309  | PO8    |
| 60 | -164.85  | 0.63704  | CB1    |
| 61 | -164.63  | 0.53131  | O1     |
| 62 | 179.49   | 0.50805  | OZ     |
| 63 | 162.99   | 0.5268   | O2     |
| 64 | 162.39   | 0.62944  | CB2    |
| 65 | -0.63183 | 0.80802  | HEO    |
| 66 | -42.853  | 0.71807  | VEO    |
| 67 | 0        | 0        | sensor |

# Acknowledgments

This work would not have been possible without the great support of so many people that I would like to thank:

My main mentor and principle supervisor Prof. Dr. Jochen Baumeister initiated this project and introduced me to the fascinating and future-oriented field of *exercise & brain research*. His inspiration, previous work and ongoing research, allowed me to participate in a number of national and international projects, which all led to the completion of this work.

Prof. Dr. Jens Bongartz, University of Applied Science Koblenz, RheinAhrCampus Remagen, promoted me for this project and was a permanent person of contact in many regards for which I am especially grateful.

Prof. Dr. Dr. Claus Reinsberger, head of the sports medicine institute, University of Paderborn, supported me throughout the final stages of this work enhancing many fundamental aspects due to his great expertise.

A big thank you goes to Dr. Christina Lavallee, Anna-Maria Tregoning, Dr. Nicholas Tam, and Ian Lay for their great effort in proof reading on such short notice.

Of course, I want to thank the study participants, willing to spare their valuable time to attend in either one or both of the experiments. They all uncomplainingly accepted the time-consuming study proceedings and were flexible when weather conditions did not allow measurements as scheduled. In this regard, thanks to Tim Lehmann and Arnd Gebel for assisting during the measurements and Helmut Böhmer as head of Haxterpark GmbH allowing me to perform the experiments on the club's putting green.

Thanks to my colleagues and friends at the sports medicine institute, University Paderborn, Reinhard Schnittker, Silke von Detten, Flora Koutsandréou and especially Rasmus Jakobsmeier and Kirsten Reinecke, for their constructive crit-

---

icism, valuable discussions and productive coffee breaks. Also I want to thank Prof. Michael Weiß for his support as former head of the institute ensuring the research environment needed to pursue my project.

Last but not least, thank you to all my friends and family, especially to my parents, Maria and Detlef Schubert, as well as my sisters Heike and Katrin for supporting me throughout the whole process of this work. You were always understanding in times of absence and helpful and inspiring when encouragement was needed. This also includes my uncle Prof. Dr. Gerhard Jorch and grandpa Heinrich Jorch for inspiring me to take on this path.